Understanding the role of the tumour microenvironment in chemoresistance and tumour progression

Thesis submitted in accordance with the requirements of the University of Liverpool for the degree of Doctor in Philosophy

By

Lucy Victoria Ireland

September 2018

DECLARATION

This thesis is the result of my own work. The material contained within this thesis has not been presented, nor is currently being presented, either wholly or in part for any other degree or qualification.

Lucy Victoria Ireland

This research was carried out in the Department of Molecular and Clinical Cancer Medicine, Institute of Translational Medicine, University of Liverpool, UK.

CONTENTS

ACKNOWLEDGEMENTS

An enormous and unbridled thank you is deserved by my supervisor Dr Ainhoa Mielgo for all support, time and encouragement which has been put into my PhD and my scientific career. A massive thanks is also deserved by Dr Michael Schmid, who also provided support and scientific insight. I must also thank North West Cancer Research for funding my PhD and the Wellcome trust who also provided funding. Another acknowledgement must be made of all the facilities used at the University of Liverpool, the Centre for Proteome Research, Biomedical services unit and MARIAC FACS facility and to all the colleagues who provided support in these facilities.

All my colleagues in the Mielgo and Schmid labs (past and present) have provided daily comradery, academic support and who would all make time to assist with experimental design or hands on work during large *in vivo* studies. So thank you to Andrea, Peppy, Seb, Valeria, Carolyn, Almudena, Carlos, Shamsher and Meirion.

A huge appreciation for all my fellow PhD candidate peers who have made the long hours and experimental woes appear normal; Sammie Jones, Amy Ball, James Waddington, Joel Watkinson, Georgia Greaves, Nirajh Shah and Lucia Livoti. You guys have been there through the ups and downs which we have all shared at some point throughout our 3 years. You guys rock!

A big and humble thank you is required for Lawrence Howell. Not only a PhD peer but a supportive boyfriend who has had to deal with both scientific and personal crises and elations. Thank you for your daily encouragement and pep talks when things got hectic.

Heartfelt appreciation must also go out to my whole family who have supported my studies and proudly printed my papers despite not understanding a word. A special mention must go out to my Nanny Dorothy who succumbed to pancreatic cancer triggering my passion for cancer research.

PUBLICATIONS

(* joint publications)

- **Ireland L** and Mielgo A 'Macrophages and fibroblasts, key players in cancer chemoresistance' *Frontiers in Cell and Developmental Biology*. 2018 October; doi: 10.3389/fcell.2018.00131

- Figueiredo CR, Azevedo RA, Mousdell S, Resende-Lara PT, **Ireland L**, Santos A, Girola N, Cunha RL, Schmid MC, Polonelli L, Travassos LR, Mielgo A 'Interfering with MIF-CD74 signalling on macrophages and dendritic cells with a peptide-based approach restores the immune response against metastatic melanoma' *Frontiers in Immunology*. 2018 May; doi: 10.3389/fimmu.2018.01132

- **Ireland L**, Santos A, Campbell F, Figueiredo C, Hammond D, Ellies LG, Weyer-Czernilofsky U, Bogenrieder T, Schmid M, Mielgo A 'Blockade of insulin-like growth factors increases efficacy of paclitaxel in metastatic breast cancer' *Oncogene.* 2017 Nov; doi: 10.1038/s41388-017-0115-x

- Howell LS, **Ireland L**, Park BK, Goldring GE 'MiR-122 and other microRNAs as potential circulating biomarkers of drug-induced liver injury' *Expert Review of Molecular Diagnostics.* 2017 Dec 18:1, 47-54, DOI: 10.1080/14737159.2018.1415145

- **Ireland L***, Santos A*, Ahmed MS, Rainer C, Nielsen SR, Quaranta V, Weyer-Czernilofsky U, Engle DD, Perez-Mancera PA, Coupland SE, Taktak A, Bogenrieder T, Tuveson DA, Campbell F, Schmid MC, Mielgo A 'Chemoresistance in Pancreatic Cancer Is Driven by Stroma-Derived Insulin-Like Growth Factors' *Cancer Research.* 2016 Dec 1;76(23):6851-6863. doi: 10.1158/0008-5472.CAN-16-1201.

- Nielsen SR, Quaranta V, Linford A, Emeagi P, Rainer C, Santos A, **Ireland L**, Sakai T, Sakai K, Kim YS, Engle D, Campbell F, Palmer P, Ko JH, Tuveson DA, Hirsch E, Mielgo A, Schmid MC 'Macrophage-secreted granulin supports pancreatic cancer metastasis by inducing liver fibrosis' *Nature Cell Biology.* 2016 May; 18(5):549-60. doi: 10.1038/ncb3340.

ABSTRACT

Cancer resistance to therapies and metastasis remain two of the biggest challenges in the cancer field. Solid tumours are characteristically surrounded by a stroma. The tumour stroma is composed of non-malignant stromal cells and extracellular matrix proteins. Tumour-associated macrophages (TAMs) and cancer-associated fibroblasts (CAFs) are the most abundant cell types in the tumour stroma and can affect cancer resistance to therapies and metastasis. However, how exactly TAMs and CAFs confer chemoresistance towards tumour cells and support metastasis is only partly elucidated.

Two solid tumours which acquire resistance to their standard therapies and exhibit high rates of metastasis are pancreatic ductal adenocarcinoma (PDAC) and invasive breast cancer. Both tumour types possess a rich tumour microenvironment (TME) which partakes in bi-directional signalling with tumour cells to confer survival as well as promote metastasis and growth. However, the exact mechanisms by which TAMs and CAFs promote resistance to therapies and metastasis in these cancers are not fully understood.

The aims of this thesis were 1) to elucidate how TAMs and CAFs in the TME of PDAC and invasive breast cancer promote tumour cell survival and resistance to chemotherapy. 2) To investigate the effect of blocking the mechanisms of therapy resistance identified, in combination with standard chemotherapy, in preclinical PDAC and breast cancer mouse models recapitulative of the human disease. 3) To identify factors supporting PDAC metastasis identification of factors mediating tumour progression.

Using primary isolated macrophages and pancreatic stellate cells (PaSCs) *in vitro* identified insulin-like growth factor 1 and 2 (IGF-1/2) as secreted factors which activate insulin and IGF-1 receptors on tumour cells on both PDAC and breast cancer cells. Isolation of tumour cells, non-immune stromal cells and macrophages from orthotopic PDAC and TNBC-like invasive breast cancer models revealed non-immune stromal cells and macrophages as the main sources of IGF-1 and IGF-2 activating insulin/IGF-1R on tumour cells *in vivo*. Blockade of IGF signalling using an IGF-blocking antibody in combination with standard chemotherapy resulted in a decrease in tumour cell proliferation in PDAC and a decrease in primary breast tumour size and reduction in total metastatic burden in an invasive breast cancer model. These studies

provide the rationale to trial IGF-blocking antibodies in combination with chemotherapy in PDAC and breast cancer patients.

Investigation into the metastatic potential of three PDAC cell lines, FC1199, FC1242 and FC1245, derived from the genetically engineered KPC (Kras LSL.G12D/+; p53R172H/+; PdxCretg/+) mouse model showed that these cells possessed varied aggressiveness and metastatic propensity. Implantation of FC1245 cells resulted in mice having a severely reduced quality of life and reduced life expectancy to around 20 days after implantation. FC1245-tumour bearing mice exhibited both spontaneous liver and lung metastasis at higher levels compared to the other implanted mice. Stable isotope labelling with amino acids in cell culture (SILAC) proteomic analysis of the three cell lines revealed nineteen consistently upregulated proteins from FC1245 cells, of which mesothelin was identified as one of the top candidates upregulated in the highly metastatic FC1245 cells. Immunohistochemical analysis of PDAC tissues revealed that mesothelin expression was limited to the tumour tissue. Mesothelin expression by FC1245 cells was also confirmed by immunoblotting analysis.

Overall, this work has identified new therapeutic targets IGF-1 and IGF-2 to combat chemoresistance in both PDAC and breast cancer which trialled in preclinical models, in combination with chemotherapy, has shown a more favourable outcome compared to standard chemotherapy alone. This work has also identified mesothelin as a potential protein of interest in metastatic PDAC.

ABBREVIATIONS

µL	Microlitre
µm	Micrometre
µM	Micromolar
5-FU	5-fluorouracil
Ab	Antibody
AKT	Protein kinase B
Ambic	Ammonium bicarbonate
ANOVA	Analysis of variance
αSMA	Alpha smooth muscle actin
BCA	Bicinchoninic acid
BSA	Bovine serum albumin
C	Centigrade
CAF	Cancer associated fibroblast
Cg	Cage
cm	Centimetre
CO_2	Carbon dioxide
CSF-1	Colony stimulating factor 1
CTGF	Connective tissue growth factor
CXCL7	C-X-C motif chemokine ligand 7
DAB	Diamino-benzidine
dH_2O	Distilled water
DMEM	Dulbecco's modified eagle medium
DTT	Dithiothreitol
ECM	Extracellular matrix
EDA-FN	Extradomain A-fibronectin
EDTA	Ethylenediaminetetraacetic acid
EGF	Epidermal growth factor
ER	Estrogen receptor

FACS	Fluorescence-activated cell sorting
FBS	Foetal bovine serum
FDR	False detection rate
FFPE	Formalin fixed paraffin embedded
FSP-1	Fibroblasts specific protein-1
g	*g* force
g	Grams
GBSS	Gey's balanced salt solution
Gem	Gemcitabine
GEMM	Genetically engineered mouse model
GO	Gene ontology
H&E	Hematoxylin and eosin
HER2	Human epidermal growth factor receptor 2
HBSS	Hanks balanced salt solution
HR	Hormone receptor
Hr	Hours
IFNγ	Interferon gamma
IGF-1/2	Insulin-like growth factor1/2
IGF-1R	Insulin-like growth factor receptor 1
IL-X	Interleukin X
IMDM	Iscove's modified Dulbecco medium
InsR	Insulin receptor
i.p.	Intraperitoneally
IRS1/2	Insulin receptor substrate 1/2
kg	Kilogram
KPC	LSL-KRasG12D; LSL-Trp53R172H; Pdx1-Cre
L	Litre
LC-HRMS	Liquid chromatography- high resolution mass spectrometry
LC-MS MS	Liquid chromatography tandem mass spectrometry
LTR	Long terminal repeat
Luc/zsGreen	Luciferase/zsGreen
MAM	Metastasis-associated macrophage

MAF	Metastasis-associated fibroblast
mCSF-1	Macrophage colony stimulating factor
MCM	Macrophage conditioned media
Mg	Milligram
Min	Minutes
mL	Millilitres
mm	Millimetre
MMPs	Matrix metalloproteases
mMSLN	Mature mesothelin
MMTV	Mammary tumour virus
Mol	Molar
MPF	Megakaryocyte potentiating factor
mRNA	messenger RNA
MSCs	Mesenchymal stem cells
Muc16	Mucin 16
MyoCM	Myofibroblast conditioned media
NFDM	Non-fat dried milk
NF-kB	Nuclear factor-kB
ng	Nanograms
No.	Number
OCT	Optimal cutting temperature
PanIN	Pancreatic Intraepithelial Neoplasia
PaSC	Pancreatic stellate cell
PBS	Phosphate buffered saline
PCA	Principal component analysis
PDAC	Pancreatic Ductal Adenocarcinoma
PGE_2	Prostaglandin E_2
PI	Propidium iodide
PI3K	phosphoinositide 3- kinase
PR	Progesterone receptor
pRTK	Phospho-receptor tyrosine kinase
PyMT	Polyomavirus middle T-antigen
PVDF	Polyvinylidene fluoride

qPCR	quantitative polymerase chain reaction
R0K0	Carbon 12 containing arginine and lysine
R6K6	Carbon 13 containing arginine and lysine
R10K8	Carbon 13 and nitrogen 15 containing arginine and lysine
recIGF	Recombinant insulin-like growth factor
RBC	Red blood cell
RNA	Ribonucleic acid
ROI	Region of interest
ROS	Reactive oxygen species
Rpm	Rotations per minute
RPMI	Roswell Park Memorial Institute
RT	Room temperature
RTK	Receptor Tyrosine kinase
SILAC	Stable isotope labelling using amino acids in cell culture
SEM	Standard error of the mean
SPARC	Secreted protein acidic and rich in cysteine
TAM	Tumour associated macrophage
TBS-T	Tris-buffered saline with tween 20
TFA	Trifluoroacetic acid
TGFß	Transforming growth factor beta
TIMP	Tissue inhibitors of metalloproteases
TME	Tumour microenvironment
TNBC	Triple negative breast cancer
TNFα	Tumour necrosis factor alpha
Tx	Treatment
VEGF	Vascular endothelial growth factor

Designation of statistical significance:

$p \leq 0.05$ = *

$p \leq 0.01$ = **

$p \leq 0.001$ = ***

ns = non-significant

LIST OF FIGURES

Chapter 1

Chapter 3

Chapter 4

Chapter One:

General Introduction

CONTENTS

1.1 Hallmarks of cancer

Cancer is a group of diseases categorised by abnormal cell growth and spread throughout the body. Cells become neoplastic through a stepwise accumulation of genetic aberrations which ultimately disrupt regulated cell growth. The genetic alterations accumulated may include deletions, amplifications, point mutations, translocations and epigenetic modifications which ultimately alter the function or expression of afflicted genes (Iengar, 2012). However, when these alterations occur in proto-oncogenes or tumour suppressor genes, cancer is more likely to develop. Proto-oncogenes are present in normal parenchymal cells and upon mutation become oncogenes, resulting in either hyperactivity of the encoded protein, increased levels of transcription/translation or expression by inappropriate cell types (Lee and Muller, 2010). Tumour suppressor genes act to prevent tumourigenesis through the control of proliferation and survival. In cancer, tumour suppressor genes become inactivated through mutation resulting in the uncontrolled proliferation of neoplastic cells (Lee and Muller, 2010).

Heterogeneity of tumour cells was acknowledged as early as 1958 (Huxley, 1958). Advancements in technology has now led us to understand that tumours function as complex tissues comprising of cells with varying genetic aberrations, performing diverse functions and displaying phenotypes which are described as hallmarks of cancer (summarised in Fig 1.1). The first hallmark of cancer is the ability to sustain proliferative signalling. Cancer cells can evade the usually tight mitogenic controls that act during homeostasis to limit unchecked proliferation resulting in an escape from regulation of cell numbers. This phenomenon can be mediated by hypersensitivity to available growth factors through upregulated expression of receptors, self-production of growth factors promoting autocrine activation, stimulation of cells in the surrounding tumour microenvironment (TME) to produce growth factors

or constitutive activation of downstream signalling components (Fedi et al., 1997, Hanahan and Weinberg, 2000).

Another underlying hallmark of cancer is the evasion of growth suppressor signals. Tumour suppressor genes or contact inhibition produce signals which force cells to enter a quiescent or post-mitotic state however, these are both overcome by neoplastic cells (Weinberg, 1995, Hanahan and Weinberg, 2011). Normal parenchymal cells are capable of proliferating for a restricted number of times, known as their Hayflick limit (Hayflick, 1965). This limit is determined by telomere length and the eventual uncapping of chromosomes which triggers cellular senescence. Cancer cells bypass this barrier through the reactivation of telomerase meaning telomeres can be regenerated escaping crisis and senescence resulting in reproductive immortality (Hayflick, 1997).

Another key attribute acquired by cancer cells is the resistance of cell death. Tumour cells actively resist apoptosis through various mechanisms. The most common mechanism is the loss or inactivation of tumour protein 53 (P53) tumour suppressor gene preventing the detection of DNA damage and the subsequent onset of apoptosis (Rivlin et al., 2011). Alternatively, increased expression of survival factors and anti-apoptotic regulators can also circumvent established means of prompting cell death (Hanahan and Weinberg, 2000).

As tumour cells increase in number, the size of the tumour mass becomes limited due to an inadequate supply of nutrients and inefficient removal of waste products. To bypass this problem, tumour cells acquire the ability to induce angiogenesis. Tumour-mediated angiogenesis creates blood vessels with enlarged diameters, leaky branches and a more tortuous structure (Bergers and Benjamin, 2003).

An important hallmark in invasive cancers is the ability to effectively metastasise to distant organs. Cancer cells gain the ability to invade their basement membrane through downregulation of cytostatic-associated adhesion molecules and upregulation of adhesion molecules promoting cell movement such as those associated with embryogenesis and inflammation (Christofori and Semb, 1999, Hanahan and Weinberg, 2000).

More recently, enabling characteristics have been described which serve to facilitate neoplastic transition. Genomic instability and increased frequency of mutations are characteristics which govern the acquisition of several other hallmarks and therefore can confer a selective advantage to cells during multistep tumour progression (Hanahan and Weinberg, 2011). Tumour-promoting inflammation was identified as an enabling characteristic. Tumours are infiltrated by immune cells due to innate and adaptive immune responses which contribute to tumour-associated inflammation (Hanahan and Weinberg, 2011). This inflammation can serve to promote tumour progression through the supply of growth, survival and proangiogenic factors along with extracellular matrix modifying enzymes (DeNardo et al., 2010, Qian and Pollard, 2010, Grivennikov et al., 2010).

Advancements in cancer research have recognised two emerging hallmarks (Hanahan and Weinberg, 2011). Tumour cells have been shown to both deregulate their cellular energetics and to actively avoid immune destruction. Tumour cells must adapt their metabolism to support elevated levels of proliferation and cell growth. This metabolic alteration is called the Warburg effect, where cancer cells shift their metabolism towards aerobic glycolysis even in the presence of oxygen (House et al., 1956, Warburg and Dickens, 1930). Tumours have also developed methods to avoid immune destruction through bi-directional signalling with immune components as well

as upregulation of immune checkpoint markers which result in the exhaustion of CD8 cytotoxic T lymphocytes (Juneja et al., 2017).

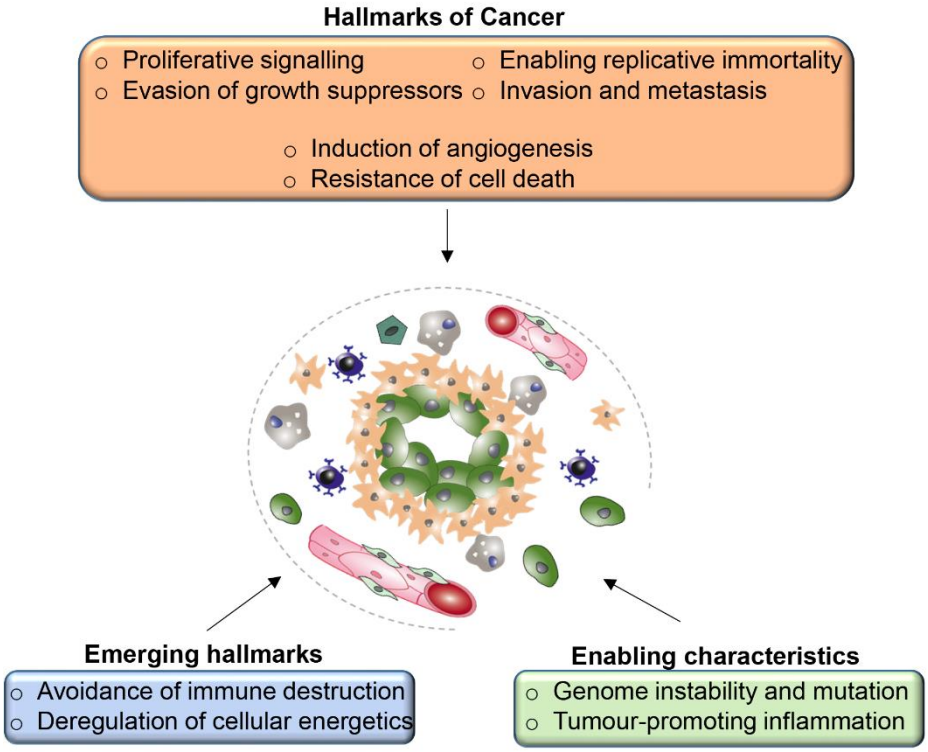

Figure 1.1 The hallmarks of cancer

Cancer cells have been shown to develop a number of hallmark characteristics which promote neoplasia. These include evasion of growth suppressors, enabling replicative immortality, activation of invasion and metastasis, induction of angiogenesis, resistance of cell death and proliferative signalling. Emerging hallmarks include deregulation of cellular energetics and avoidance of immune destruction. Enabling characteristics have been identified as genome instability and mutation and tumour-promoting inflammation. (Adapted from Hanahan and Weinberg, 2011)

1.2 Chemotherapy

The treatment of cancer with chemical substances, known as chemotherapy, is routinely used for cancer treatment. A benefit of chemotherapy is as it circulates throughout the body it targets not only the primary tumour site but disseminated

tumour cells present in distant organs which are often missed with surgical intervention or radiotherapy treatment (Eguchi et al., 2008).

The birth of chemotherapy came after the first world war, using nitrogen mustard as an anti-cancer agent in non-Hodgkin's lymphoma (Gilman, 1963). This agent was non-specific and showed limited effectiveness as patients experienced relapse after a few weeks of treatment. However, this discovery prompted investigation into the mechanism of action leading to the development of other alkylating agents (Haddow et al., 1948). Targeted chemotherapy was developed in the late 1980's after the elucidation of a few signalling pathways aberrantly regulated in tumours. Targeted chemotherapy included pharmacological targeting of cell cycle regulating proteins, growth factors and angiogenesis mediators (Hanahan and Weinberg, 2000, Chabner and Roberts, 2005).

Since its beginning, chemotherapy has provided a plethora of benefits for many cancer patients (Gebski et al., 2007, Klastersky and Paesmans, 2001, Benedetti-Panici et al., 2003). Chemotherapeutic agents given before surgery as 'neoadjuvant' therapy are used to reduce the tumour mass before surgical resection. This has many benefits as a reduction in tumour size may decrease the level of invasiveness required for resection and often improves the distinction between healthy and neoplastic tissue (Hayes and Schott, 2015). Adjuvant administration of chemotherapy occurs post-surgery with the purpose of minimising the chance of recurrence. Adjuvant therapy is effective in two ways: firstly, against micro or macro-metastasis which are already seeded but were not detectable at the time of surgery, and secondly, against micro-metastasis created as a by-product of resection due to tissue regeneration-promoting cytokine storms released after invasive surgery (Hayes and Schott, 2015).

Despite the development of targeted agents with improved toxicity profiles, unfortunately in some cancers chemotherapeutic agents only provide a minimal improvement in overall survival (Burris et al., 1997, Marquette and Nabell, 2012). Drug resistance has become one of the largest hurdles in effective cancer treatment causing the relapse of the majority of cancer patients (Holohan et al., 2013, McMillin et al., 2013). Tumour resistance mechanisms in patients, can be either tumour cell autonomous and/or mediated by the tumour surrounding non-malignant cells present in the TME (Joyce and Pollard, 2009, Mielgo and Schmid, 2013, De Palma and Lewis, 2013, Zheng, 2017).

1.3 Tumour microenvironment (TME)

The TME describes the complete tumour milieu including the malignant tumour cells and the surrounding stroma. The tumour stroma is comprised of non-malignant cells including immune cells (macrophages, neutrophils, T cells), fibroblasts, cells from the vasculature (pericytes and endothelial cells) and extracellular matrix proteins (Hanahan and Weinberg, 2011). Accumulating evidence shows that the stroma develops with the tumour and interacts with the neoplastic cells, participating in bi-directional tumour-stroma signalling which supports tumour progression, metastasis and resistance to therapy (Hanahan and Coussens, 2012, Quail and Joyce, 2013). The most abundant non-cancerous cell types present in the tumour stroma are tumour associated macrophages (TAMs) and cancer associated fibroblasts (CAFs).

1.4 Origin of macrophages and fibroblasts

1.4.1 Macrophages

Tissue resident macrophages are a diverse population of cells which perform tissue-specific functions in tissue homeostasis, repair, immunity and angiogenesis (Davies et al., 2013b). Macrophages can originate from three independent sources. Embryonic macrophage populations have been mapped back to two sources: foetal

liver-derived monocytes or precursor cells found in the yolk sac (Yona et al., 2013, Mass et al., 2016). In adult tissue, macrophage populations differentiate from hematopoietic stem cells in the bone marrow (Orkin and Zon, 2008).

Once established in adult tissue, macrophages maintain their population via self-renewal in the steady state but increase their rate of proliferation in response to stimuli such as interleukin 4 (IL-4) and colony stimulating factor 1 (CSF-1) (Davies et al., 2013b, Jenkins et al., 2011, Jenkins et al., 2013). During inflammation, bone marrow-derived monocytes are recruited into the tissue and mature into macrophage populations which act alongside tissue resident macrophages (Shi and Pamer, 2011). These converted monocytes display cell surface markers associated with resident macrophages increasing their responsiveness to IL-4 and IL-3 (Dal-Secco et al., 2015, Yona et al., 2013).

Bone marrow derived macrophages (BM-DMs) and tissue resident macrophages appear to intermingle and work together to resolve inflammation and promote tissue repair. However, it is currently undetermined if BM-DMs play the exact same role as tissue resident macrophages (Davies et al., 2013a). Bone marrow transplant studies have shown that BM-DMs and tissue resident macrophages share similar characteristics (van de Laar et al., 2016). Nevertheless, transcriptome analysis of lung alveolar resident macrophages has revealed different genes expressed in BM-DMs compared to tissue resident macrophages (Gibbings et al., 2015).

1.4.2 Fibroblasts

Fibroblasts are predicted to be of mesenchymal origin and possess a distinct transcriptional profile dependent on their tissue of origin (Chang et al., 2002). Fibroblasts have never been identified in embryonic tissue but are hypothesised to arise during the epithelial-to-mesenchymal transition (EMT) of the epiblast during gastrulation, along with the generation of mesoderm tissue (Kalluri, 2016). Virchow

identified cells in adult tissue that produced collagen, were resistant to apoptosis, and reverted to quiescence upon the completion of tissue development. These cells were later called fibroblasts (Virchow, 1858). Due to the inability to identify fibroblasts in embryonic tissue it remains unknown whether the majority of activated fibroblasts originate from fibrocytes or mesenchymal stem cells (MSCs) in adult tissue (Kalluri, 2016).

Stellate cells are found in the pancreas, liver, lung and kidney. Although stellate cells are similar to fibroblasts, they display some distinctly different functions such as vitamin A storage as retinol droplets in their cytoplasm that is required for cellular homeostasis (Erkan et al., 2010, Liu, 2006, Keane et al., 2005). Quiescent stellate cells usually constitute <10 % of the organ where they reside and are found in peri-vascular and peri-parenchymal regions (Apte et al., 1998, Bachem et al., 1998, Wake and Sato, 1993). Like fibroblasts, the origin of stellate cells is still debated. Neuroectoderm is suggested as a potential origin of pancreatic stellate cells (PaSCs) and hepatic stellate cells (hStCs) (Friedman, 2000). Lineage tracing studies have shown that hStCs can originate from mesoderm in mice, however lineage-tracing studies are currently lacking for PaSCs (Asahina et al., 2009, Asahina et al., 2011).

Activated fibroblasts (also known as myofibroblasts) can originate from several different cell types that include quiescent fibroblasts from normal parenchyma, endothelial cells, MSCs, and stellate cells (Kalluri, 2016, LeBleu et al., 2013). Assorted origins may play a role in generating myofibroblast populations with diverse phenotypes and functions. Recent studies have described heterogeneous populations of myofibroblasts present in both pancreatic and breast tumours (Ohlund et al., 2017, Costa et al., 2018) and understanding the functions of these different myofibroblast populations in cancer is currently an intensive field of research.

1.5 Physiological functions of macrophages and fibroblasts

Macrophages represent a heterogeneous population of cells that are highly plastic and which adapt to their surroundings to perform a variety of functions in tissue homeostasis, repair and immunity (Wynn et al., 2013). Macrophages are responsive to tissue-derived or external stimuli adapting their phenotype and function accordingly (Biswas and Mantovani, 2010). A spectrum of macrophage subsets with diverse phenotypes and functions co-exist in tissues and the subsets at the extremes of this spectrum are known as M1 (or classically-activated) and M2 (or alternatively-activated) macrophages (Mills, 2012, Murray and Wynn, 2011). Macrophage polarisation into M1-like or M2-like depends on the stimulating cytokine and the length of their exposure (Gordon and Martinez, 2010). However, the nomenclature and understanding of macrophage subtypes and functions is still evolving.

M1-like macrophages are generated in response to interferon gamma (IFNγ) and lipopolysaccharide (LPS) stimulation, factors produced by infiltrating bacteria and pathogens. M1-like macrophages are pro-inflammatory and secrete factors to promote inflammation, microbicidal activity and immunostimulation, such as cytokines IL-12, IL-6, IL-1ß, tumour-necrosis factor alpha (TNFα) as well as reactive oxygen species (ROS) and nitric oxide (NO) (Gordon and Martinez, 2010, Biswas et al., 2013) (Fig 1.2).

In contrast, M2-like macrophages are polarised by IL-4 and IL-13 produced by invading parasites and in response release anti-inflammatory cytokines IL-10, arginase I and transforming growth factor beta (TGF-β), as well as vascular endothelial growth factor (VEGF), promoting the remodelling of their surrounding tissue. Concurrently, macrophages upregulate expression of scavenging receptors while downregulating receptors and markers associated with antigen presentation (Biswas and Mantovani, 2010, Mantovani and Sica, 2010) (Fig 1.2).

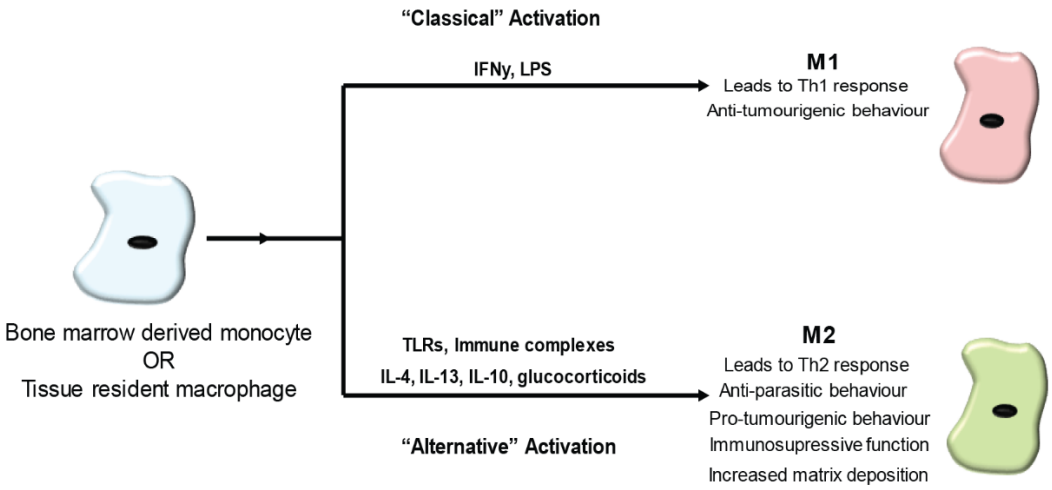

Figure 1.2 Macrophage polarisation

Bone marrow derived monocytes or tissue derived macrophages can be polarised towards either an M1 or M2 phenotype. Classical activation towards M1 polarisation occurs in response to interferon gamma (IFNγ) and lipopolysaccharide (LPS) leading to a Th1 response associated with bacteria and viruses as well as possessing anti-tumourigenic properties. Alternative activation towards an M2 phenotype is triggered in response to toll-like receptors (TLRs), immune complexes, IL-4, IL-13, IL-10 and glucocorticoids. M2 macrophages lead to a Th2 response and exhibit anti-parasitic behaviour. In cancer, M2-like macrophages promote tumour progression.

Tissue resident macrophages play a variety of roles in a tissue context-dependent manner. Largely, they perform functions usually associated with an M2 phenotype including mediating resolution of inflammation, maintaining tissue homeostasis via the removal of debris, supporting angiogenesis and partaking in immune surveillance (Davies et al., 2013b).

Angiogenesis occurs as part of homeostasis and is tightly regulated by macrophages (Fantin et al., 2010, Outtz et al., 2011). In mouse embryos, microglia (central-nervous system specific macrophages) migrate to the brain and assist in developmental angiogenesis (Arnold and Betsholtz, 2013). In the central nervous system,

macrophages promote endothelial tip cell fusion by acting as a chaperone for endothelial cells in vascular development (Fantin et al., 2010). However, it appears that the actions undertaken by macrophages are tissue-dependent as, conversely, macrophages mediate the regression of blood vessels in the developing retina (Lobov et al., 2005, Fantin et al., 2010).

Another homeostatic function of macrophages is the removal of apoptotic and excess cell debris. This function is extremely important in the regulation of haematopoiesis in which macrophages phagocytose excess erythrocytes and neutrophils (Klei et al., 2017, Gordy et al., 2011). When this process was interrupted in mice they suffered severe neutrophilia, splenomegaly, extramedullary haematopoiesis and decreased body weight (Gordy et al., 2011). Macrophages also regulate immune responses through the ingestion of apoptotic cells preventing leakage of cell-death related factors which could promote inflammation (Savill et al., 2002).

In the event of injury or infection, pro-inflammatory M1-like macrophages are recruited to the afflicted area and secrete factors including IL-1ß, NO and TNFα as a defence mechanism to kill invading pathogens (Murray and Wynn, 2011). The release of these factors can also result in secondary damage to host tissue. To limit the impact of this damage, macrophages either undergo apoptosis or reprogram towards an anti-inflammatory M2-like phenotype (Murray and Wynn, 2011). However, when this process goes awry, and macrophages maintain their pro-inflammatory functions, chronic inflammation occurs and becomes the basis of some auto-immune diseases such as crohn's disease, rheumatoid arthritis and autoimmune hepatitis (Sindrilaru et al., 2011, Navegantes et al., 2017). Along with mediating the immunity side of wound healing, macrophages alter their secretory phenotype after inflammation subsides to promote tissue regeneration. To promote the closure of the wound, macrophages

attract and activate fibroblasts through the secretion of TGF-ß (Murray and Wynn, 2011, Khalil et al., 1989).

In healthy tissue, fibroblasts and stellate cells exist in a quiescent state within the extracellular matrix (ECM) making few cell-cell or cell-basement membrane connections. They are usually found as single cells, elongated and spindle-like in morphology situated in the interstitial space between the functional tissues of adult organs (Tarin and Croft, 1969). Quiescent fibroblasts and stellate cells produce very little ECM components such as collagen 1 and fibronectin and secrete a few factors including pigment epithelium-derived factor (PEDF) and thrombospondin-2, although their actual role whilst quiescent is yet to be fully elucidated (Tarin and Croft, 1969, Pollina et al., 2008). Specific markers for fully quiescent fibroblasts are not yet known, however, fibroblasts specific protein-1 positive (FSP1+) cells are often considered as quiescent (Strutz et al., 1995) (Fig 1.3).

The activation of fibroblasts and stellate cells is triggered in response to stress factors produced during tissue stress and damage, including TGF-β and reactive oxygen species (ROS) (Kalluri and Zeisberg, 2006). Activated fibroblasts acquire smooth muscle-like properties with increased contractility, motility, proliferation and a stellate morphology, and are known as myofibroblasts (Ronnovjessen and Petersen, 1993, Sappino et al., 1988). Upon activation, stellate cells also acquire a myoblastic phenotype but lose their cytoplasmic retinol lipid droplets (Blaner et al., 2009). Common markers of myofibroblasts include alpha-smooth muscle actin (αSMA), platelet derived growth factor receptor beta (PDGFRβ), PDGFRα, fibroblast activated protein (FAP), vimentin, desmin and discoidin domain-containing receptor 2 (DDR2) (Ronnovjessen and Petersen, 1993, Quail and Joyce, 2013, Kalluri, 2016, Sugimoto et al., 2006, Jiang et al., 2017) (Fig 1.3).

Myofibroblasts classically function in acute wound healing, becoming ‘reversibly’ activated and deposit ECM proteins, collagens and fibronectin to close the wound (Darby and Hewitson, 2007, Dvorak et al., 1986). Myofibroblasts also modulate ECM consistency by secreting matrix metalloproteases (MMPs) and tissue inhibitor of metalloproteinase (TIMPs) (Tampe and Zeisberg, 2014). Activated myofibroblasts also possess an altered secretory phenotype producing factors such as TGFβ, VEGF, C-X-C motif chemokine ligand 10 (CXCL10), CXCL12, IL- 6 and epidermal growth factor (EGF) to promote proliferation and mediate recruitment of other cell types to the damaged tissue (Dvorak et al., 1986) (Fig 1.3).

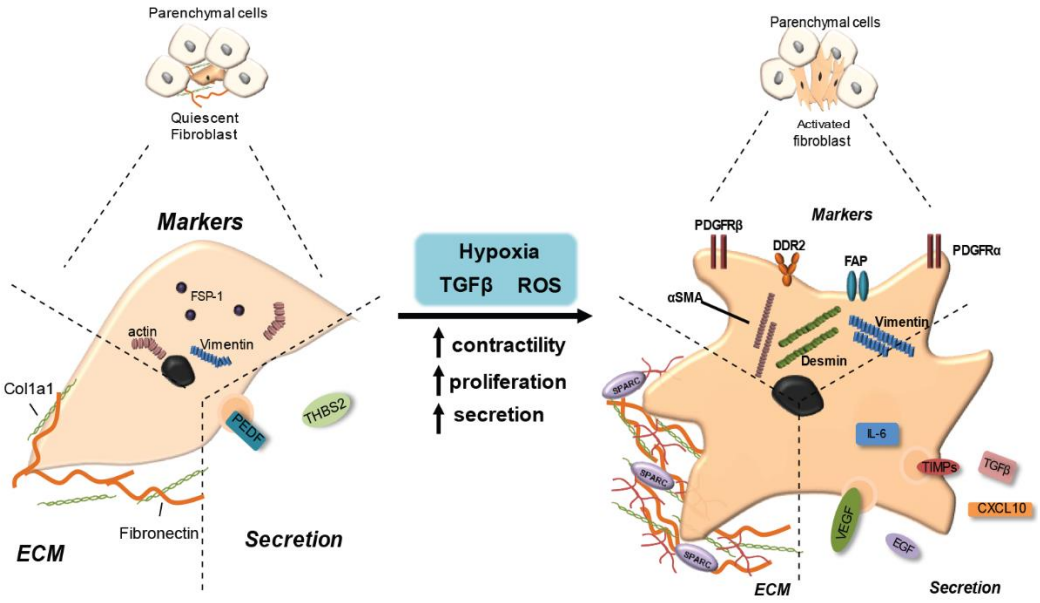

Figure 1.3 Fibroblast activation

Quiescent fibroblasts produce fibronectin and collagen type 1 (Col1a1) extracellular matrix (ECM) components, express fibroblasts specific protein-1 (FSP-1), actin and vimentin and secrete pigment epithelium-derived factor (PEDF) and thrombospondin-2 (THBS2). Stimulation by transforming growth factor beta (TGFß), reactive oxygen species (ROS) or hypoxia, quiescent cells become activated increasing their contractility, proliferation and secretion. Activated myofibroblasts produce larger volumes of fibronectin and collagen along with tenascin-c and secreted protein acidic and rich in cysteine (SPARC). Increased secretion includes IL-6, tissue inhibitor of metalloproteinase (TIMPs), TGFß, vascular endothelial growth factor (VEGF), epidermal growth factor (EGF) and C-X-C motif chemokine ligand 10 (CXCL10). Upregulated receptors/markers include alpha smooth muscle actin (αSMA), platelet derived growth factor receptor alpha/beta (PDGFRα/ß), fibroblast activation protein (FAP), Discoidin domain-containing receptor 2 (DDR2), desmin and vimentin.

Chronic activation of fibroblasts and stellate cells occurs in response to prolonged stimulation including toxins or autoimmune disorders. This results in chronic tissue fibrosis with myofibroblasts continuing to aberrantly perform their wound healing functions without resolution. These myofibroblasts become fibrosis-associated fibroblasts (FAFs), are irreversibly activated and exhibit enhanced proliferation and survival (Zeisberg and Zeisberg, 2013, Rock et al., 2011, Kalluri, 2016).

1.6 Tumour-associated macrophages (TAMs) and cancer-associated fibroblasts (CAFs)

Macrophages and fibroblasts are the two most abundant non-cancerous cells in tumours. Tumours become infiltrated with BM-DMs that are attracted to the tumour via the secretion of damage associated molecular patterns (DAMPs) and specific macrophage chemoattractants CSF-1 and chemokine (C-C motif) ligand 2 (CCL2). M1-like macrophages derived from the bone marrow and tissue resident macrophages are recruited to and activated in the tumour site in response to antigen presentation and inflammatory responses (Zhu et al., 2017). Once the tumour is established, tumour cells secrete cytokines IL-4, IL-10, IL-13 and lactic acid, and along with the presence of CD4+ Th2 cells, cause the polarisation of TAMs towards an M2-like phenotype. The M2 TAMs no longer serve to destroy the tumour but rather support cancer growth, metastasis and resistance to therapies (Ruffell et al., 2012, Colegio et al., 2014, Qian and Pollard, 2010, Gocheva et al., 2010). M2 TAMs support tumour progression by directly stimulating the growth of cancer cells through the production of growth factors, including EGF, TNFα, IL-6 (Grivennikov et al., 2010).

Solid tumours can undergo periods of hypoxia as its growing size limits the disposal of waste products and nutrient delivery becomes limited as simple diffusion can longer provide sufficient levels, triggering the angiogenic switch (Hanahan and Weinberg, 2011, Bergers and Benjamin, 2003). The activation of the angiogenic switch in tumours triggers dysregulated angiogenesis resulting in leaky vasculature with abnormal branching and enlarged diameter (Bergers and Benjamin, 2003). Macrophages are a source of VEGF and are known to support angiogenesis under normal physiological conditions (Fantin et al., 2010, Outtz et al., 2011). However, tumours depleted of myeloid-derived VEGF have a normalised vasculature with increased pericyte coverage and reduced vessel length and this accelerates tumour

progression (Stockmann et al., 2008). Conversely, another study showed that hypoxia-related TAMs possess reduced mTOR activation, and that stimulation of mTOR activity in TAMs resulted in normalised vasculature with decreased vessel leakiness, hypoxia and metastasis (Wenes et al., 2016). TAMs are attracted to areas of tumour hypoxia through the release of Semaphorin 3A by cancer cells and TAMs promote angiogenesis via the phosphorylation of VEGF-receptor on endothelial cells (Casazza et al., 2013). CSF-1 stimulation has been shown to upregulate Tie2 expression on macrophages (Forget et al., 2014). Once inside the tumour, Tie2+ macrophages bind to angiopoietin-2 (Ang-2) expressed by endothelial cells and stimulate the growth of blood vessels promoting tumour growth and metastasis (Mazzieri et al., 2011, De Palma et al., 2005).

Metastatic spread of tumour cells to distant organs involves a multi-step process that requires local tissue invasion, intravasation, circulation through the blood stream, extravasation and successful colonisation of the distant organ by the cancer cells (Hanahan and Coussens, 2012, Massague and Obenauf, 2016). Macrophages play a role in each of these stages of the metastatic cascade. Macrophages help tumour cell invasion into the basement membrane (Wyckoff et al., 2007, Condeelis and Pollard, 2006). In the PyMT breast cancer mouse model, CSF-1 produced by tumour cells and EGF secreted by TAMs results in the migration of both macrophages and cancer cells along collagen fibres and intravasation into the blood vessels (Wyckoff et al., 2007, Goswami et al., 2005). This phenomenon was also seen in glioblastoma, resulting in enhanced cancer cell invasion (Coniglio et al., 2012). TAMs can also promote tumour cell migration and invasion through the secretion of MMPs, secreted protein acidic and rich in cysteine (SPARC) and cathepsins which degrade and remodel the ECM (Bergers et al., 2000, Gocheva et al., 2006) as well as through the secretion of TGF-ß which promotes EMT of tumour cells and increased tumour cell migration (Bonde et al., 2012).

As outlined earlier, fibroblasts are activated in response to tissue damage. After resolution of the insult, fibroblasts will reprogram back to quiescence or undergo apoptosis (Tomasek et al., 2002). However, tumours are referred to as “wounds that do not heal” (Dvorak et al., 1986). Persistent activation signals, in the context of cancer, maintain fibroblasts in a chronically activated state triggering a desmoplastic reaction and generating a dense fibrotic stroma which envelopes the tumour mass. Fibroblast activation signals are tumour-specific and determine the phenotype and function of the resulting myofibroblast. In the TME, a myofibroblast will exert a pro- or anti-tumourigenic response depending upon which chemokines/cytokines it encounters (Tampe and Zeisberg, 2014). TGF-ß is a common activating factor released by tumours which increases the expression of PDGF receptors on activated PaSCs (Apte et al., 1999). Sonic hedgehog (Shh) signalling in pancreatic ductal adenocarcinomas (PDAC) tumours has been reported to promote fibroblast activation and fibrosis in the pancreas (Bailey et al., 2008, Yauch et al., 2008). Other common factors involved in CAF activation include fibroblast growth factor (FGF), platelet derived growth factor (PDGF) and monocyte chemotactic protein (MCP1) (Kalluri and Zeisberg, 2006, Marsh et al., 2013).

Concurrent with their activated state, CAFs express an altered secretory phenotype, compared to quiescent fibroblasts, including ECM proteins and ECM modulating factors such as tenascin C, periostin, SPARC and extradomain A-fibronectin (EDA-FN); and tumour promoting factors such as nuclear factor-kB (NF-kB), IL-8, Prostaglandin E2 (PGE2), connective tissue growth factor (CTGF) and CXCL7 (Kalluri, 2003, Hanahan and Coussens, 2012).

Recent advances in the field of CAF research has shown that different subsets of CAF populations with different functions co-exist within tumours (Costa et al., 2018, Ohlund

et al., 2017, Costea et al., 2013, Brechbuhl et al., 2017). For example, in PDAC a specific subset of CAFs expressing high levels of αSMA but low levels of IL-6 was found in the fibrotic area juxtaposed to cancer cells and was called the myofibroblast CAF subset (myCAFs) (Ohlund et al., 2017). A different subset of CAFs, expressing low levels of αSMA but high levels of IL-6 was found at the periphery of the tumour and was termed the inflammatory CAF subset (iCAFs) (Ohlund et al., 2017). Öhlund et al., showed that the proximity of the myofibroblasts to the PDAC tumour cells, and the concentration of tumour-secreted factors alters the phenotype of the CAFs and the proteins they secrete (Ohlund et al., 2017). Another recent study performed with luminal A, human epidermal growth factor receptor 2 + (HER2+) and triple negative breast cancer (TNBC) patient samples revealed the co-existence of four different CAF subsets in breast tumours (Costa et al., 2018). TNBC samples predominantly had two types of myofibroblast-like CAFs; CAF-S1 and CAF-S4 identified by their high expression of αSMA. However, only CAF-S1 defined as $CD29^{Med}$, FAP^{Hi}, $FSP1^{Low-Hi}$, $aSMA^{Hi}$, $PDGFRb^{Med-Hi}$ and $CAV1^{Low}$; showed an immunosuppressive role by attracting T lymphocytes and promoting their survival and differentiation into immunosuppressive T regulatory cells (Costa et al., 2018). Thus, CAFs, like TAMs, are a heterogeneous population of cells and uncovering the different CAF populations and their functions in cancer is currently an important area of research.

TAMs and CAFs take part in a complex interplay and can regulate each other's functions. For example, cancer cells and myofibroblasts are known sources of VEGF which promotes the accumulation of immune cells including macrophages at the site of fibrosis (Fukumura et al., 1998). VEGF-dependent recruitment and activation of macrophages promotes tumourigenesis, angiogenesis and invasion in skin cancer (Linde et al., 2012). Reciprocally, in liver metastasis of pancreatic cancer, macrophages recruited to the metastatic liver secrete granulin and activate resident

quiescent hStCs which subsequently produce periostin supporting the growth of metastatic cancer cells in the liver (Nielsen et al., 2016).

1.7 Mechanisms of chemotherapy resistance driven by TAMs and CAFs

Chemotherapy is used as a treatment for many different cancer types and is used either alone or in combination with surgical resection or radiation. Chemotherapy targets tumour cells at both the primary tumour site and the metastatic site. However, a common problem encountered with the treatment of many tumours is an acquired resistance to chemotherapeutic agents. Chemoresistance can be mediated by tumour cell-autonomous mechanisms, including changes in tumour cell epigenetics, drug inactivation, EMT, activation of alternative survival and proliferative pathways, and/or selection of drug-resistant cancer cell clones (Housman et al., 2014). However, many solid tumours such as breast cancer and PDAC have a rich stroma which contains, as described before, a plethora of non-malignant cell types that influence cancer progression and response to therapy in various ways. In fact, these non-malignant stromal cells are not simple bystanders but engage in bi-directional tumour- stroma signalling which can result in impaired therapeutic efficacy. For instance, the attraction of TAMs in a MCF-7 breast cancer xenograft model, via CSF-1 signalling, reduces the efficacy of a combination treatment with cyclophosphamide, methotrexate and 5-fluorouracil (CMF) (Paulus et al., 2006) (Fig 1.4 A). The presence of TAMs in the genetic MMTV-PyMT mouse model of breast cancer makes tumours more resistant to paclitaxel therapy (DeNardo et al., 2011). Another study revealed TAM-derived cathepsins B and S as responsible for mediating chemoresistance to taxol in the MMTV-PyMT mouse model (Shree et al., 2011) (Fig 1.4 B). In a subcutaneous mouse model of colorectal cancer, IL-6 released by TAMs mediates chemoresistance to 5-FU via activation of the IL-6R/STAT3 signalling axis (Yin et al., 2017). IGF-1 was also shown to be secreted by TAMs in glioblastoma multiforme and to mediate resistance

to a CSF-1R small molecule inhibitor through activation of phosphoinositide 3- kinase (PI3K) signalling (Quail et al., 2016).

TAMs can also regulate the delivery of chemotherapy to tumour cells. In the MMTV-PyMT transgenic breast cancer mouse model, doxorubicin administration causes necrosis of cancer cells with the release of CCL2, a chemokine that attracts monocytes/macrophages. MMP-9 secretion by the recruited myeloid cells was shown to decrease vasculature leakiness and to impair doxorubicin delivery into the tumours (Nakasone et al., 2012). In fact, MMP-9 null mice showed an improved response to doxorubicin that correlated with increased vascular leakage (Nakasone et al., 2012) (Fig 1.4 C). Conversely, in a Lewis lung carcinoma subcutaneous isograft model, myeloid derived VEGF promotes resistance to cyclophosphamide treatment by promoting the formation of abnormal vessels with reduced pericyte coverage, tortuosity and vessel density (Stockmann et al., 2008).

CAFs also play a role in tumour chemoresistance. In fact, a dense fibrotic stroma correlates with a poor response to neoadjuvant treatment with 5-fluorouracil, epirubicin and cyclophosphamide (FEC) in breast cancer and with gemcitabine in PDAC (Farmer et al., 2009, Pandol et al., 2009, Olive et al., 2009). One way fibrosis promotes chemoresistance in PDAC is through CAF secretion of hyaluronan, generating high interstitial pressure within the tumour, causing the collapse of blood vessels supplying the tumour mass and impairing drug delivery (DuFort et al., 2016) (Fig 1.4 D).

In oesophageal squamous cell carcinoma, CXCR7 expression is upregulated in tumour cells through STAT3/NF-kB signalling stimulated by CAF-derived IL-6, ultimately promoting resistance against cisplatin and 5-fluorouracil (Qiao et al., 2018) (Fig 1.4 E). IL-6 has pleiotropic effects in the tumour microenvironment and also

mediates chemoresistance by promoting EMT of cancer cells (Shintani et al., 2016). TGFß secretion by CAFs was shown to confer resistance of oesophageal squamous cell carcinoma against cisplatin, taxol, irinotecan (CPT-11), 5-fluorouracil (5-FU), carboplatin, docetaxel, pharmorubicin, and vincristine (Zhang et al., 2017) (Fig 1.4 F).

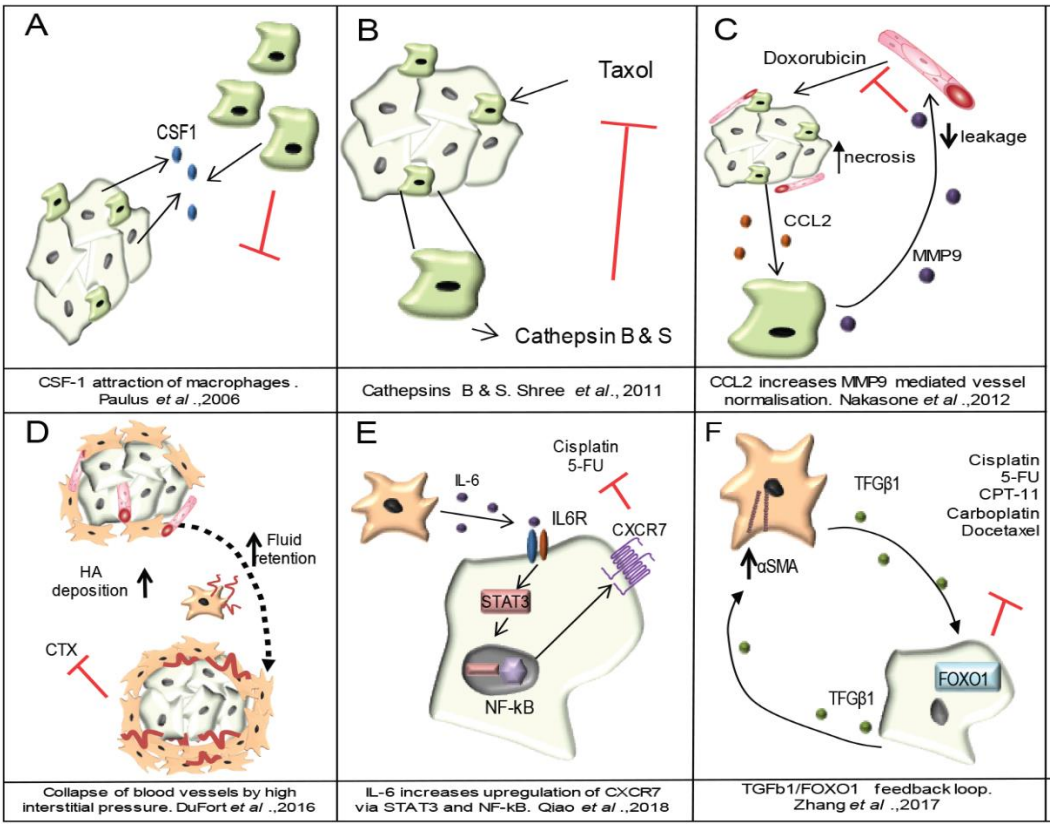

Figure 1.4 Mechanisms of chemoresistance mediated by TAMs and CAFs

A) Cancer cells attract TAMs via CSF-1. TAMs confer resistance of MCF-7 breast cancer cells towards cyclophosphamide, methotrexate and 5-fluorouracil (Paulus et al., 2006). **B)** Cathepsins B and S secreted by TAMS mediate resistance of breast cancer cells to taxol in MMTV-PyMT mouse model (Shree et al., 2011). **C)** In the MMTV-PyMT transgenic mouse model, cancer cell necrosis caused by doxorubicin treatment stimulates cancer cells to release the monocyte chemoattractant CCL2. Recruited TAMs produce MMP-9 which promotes leakiness of blood vessels and reduction in doxorubicin delivery (Nakasone et al., 2012). **D)** In PDAC, CAFs increase deposition of hyaluronan (HA) creating an increase in fluid retention and subsequently interstitial pressure in the tumour rises causing the collapse of blood vessels and limiting the delivery of chemotherapeutic agents (DuFort et al., 2016). **E)** CAF secreted IL-6 stimulates the upregulation of CXCR7 through STAT3/NF-kB signalling promoting resistance of oesophageal squamous cell carcinoma cells against cisplatin and 5-fluorouracil (Qiao et al., 2018). **F)** CAF-derived TGFß upregulates FOXO1 expression in oesophageal squamous cell carcinoma cells triggering reciprocal TGFß secretion which in turn increases the levels of αSMA expression in CAFs and resistance to cisplatin, taxol, irinotecan (CPT-11), 5-fluorouracil (5-FU), carboplatin, docetaxel, pharmorubicin, and vincristine (Zhang et al., 2017).

1.8 Targeting TAMs and CAFs in cancer.

Currently, approaches are being undertaken to block macrophage recruitment to the tumour site, to repolarize TAMs back into an M1-like anti-tumourigenic phenotype, and to target specific tumourigenic functions of TAMs. Preventing recruitment of macrophages to the tumour site has been achieved through targeting macrophage chemoattractants such as CSF-1 and CCL2 or their corresponding receptors: CSF-1 receptor (CSF-1R) and C-C chemokine receptor type 2 (CCR2). Anti-CSF-1R agents have been shown to be effective against recruitment of M2-like macrophages in breast cancer models, and anti-CSF1R inhibitors used in combination with paclitaxel decreased tumour growth and pulmonary metastasis (DeNardo et al., 2011). CSF-1R and CCR2 antagonists have been reported to prevent infiltration of TAMs into the tumour mass increasing response to gemcitabine treatment in mouse models of PDAC (Mitchem et al., 2013). CCL2 inhibition in combination with docetaxel has shown increased efficacy, compared to docetaxel treatment alone, resulting in decreased tumour growth and metastatic spread in prostate cancer (Loberg et al., 2007). This combination has also shown promise in lung cancer, breast cancer metastasis and PDAC (Lu and Kang, 2009, Kalbasi et al., 2017, Fridlender et al., 2011). Due to these successes CSF-1, CCL2 and CSF-1R targeting agents are being investigated in clinical trials in combination with chemotherapy in a range of solid tumours (ClinicalTrial.gov identifiers: NCT01596751, NCT01525602, NCT02435680, and NCT01204996). However, the targeting of chemokines and cytokines has limitations due to their redundant and promiscuous nature. In fact, chemokines and cytokines can often bind to more than one receptor, and at the same time different cytokines/chemokines can bind to the same receptor and activate the same signalling pathway (O'Shea and Murray, 2008, Turner et al., 2014). In addition, to add more complexity, certain cytokine receptors are expressed by several cell types and as a result, inhibiting the cytokine/receptor affects all cell populations expressing the receptor. This is the case with CSF-1R which is not exclusively expressed by M2-like

macrophages but is also expressed by M1-like macrophages, neutrophils, myeloid-derived suppressor cells (MDSCs) and dendritic cells (Cannarile et al., 2017).

Repolarizing macrophages back into an M1-like tumoricidal phenotype appears an attractive approach as the M2 TAMs are already present in the tumour and repolarization could therefore provide an effective strategy to restore the tumoricidal function of macrophages and prevent cancer progression. This has been investigated using an anti-CD40 antibody in combination with gemcitabine in a PDAC genetically engineered mouse model (GEMM) KPC (Kras LSL.G12D/+; p53R172H/+; PdxCretg/+) and in PDAC patients (Beatty et al., 2011). The administration of an agonist CD40 antibody repolarised TAMs back into an M1-like phenotype leading to an increased response to gemcitabine and reduced tumour burden (Beatty et al., 2011). A phase 1 clinical trial has recently been completed for the use of dacetuzumab (human anti-CD40 mAb) with bortezomib chemotherapy in patients with relapsed or refractory multiple myeloma, however results have yet to be published (ClinicalTrial.gov identifier: NCT00664898).

Since TAMs can act as a double edge sword in cancer, with M1-like TAMs exerting anti-tumourigenic functions and M2-like TAMs exerting pro-tumourigenic functions, targeting TAMs pro-tumourigenic functions seems a more promising approach compared to ablation therapies targeting all TAMs. As previously mentioned, TAMs are known to facilitate the intravasation of tumour cells and promote angiogenesis (Wyckoff et al., 2007). Therefore, targeting TAMs role in pathological angiogenesis is an attractive therapeutic opportunity. In MMTV-PyMT mammary carcinomas and RIP1-Tag2 pancreatic insulinomas, an Ang-2 neutralising antibody administration did not reduce the recruitment of Tie-2+ TAMs but instead, prevented their binding to Ang-2 on activated endothelial cells subsequently decreasing angiogenesis and tumour progression (Mazzieri et al., 2011). CSF-1R inhibition increased the efficacy

of anti-VEGFR-2 anti-angiogenic therapy in a mouse model of Lewis lung carcinoma (Priceman et al., 2010). M2 TAMs produce IL-10 at the tumour site leading to resistance of breast cancer to paclitaxel treatment and this resistance can be abrogated with the administration of an IL-10 neutralising antibody (Yang et al., 2015) (Fig 1.5). TAMs in glioblastoma have been shown to regulate resistance to CSF-1R inhibition through the production of IGF upregulating PI3K signalling in tumour cells, however this effect was abrogated through the blockade of IGF-1 receptor signalling with IGF-1R inhibitors (Quail et al., 2016) (Fig 1.5).

It is currently unclear whether CAFs play a supportive or restrictive role in tumour progression. Based on the correlation between a large desmoplastic reaction and poor patient outcome it was hypothesised that ablation of the myofibroblasts would improve therapy response and decrease tumour growth. Shh is overexpressed by neoplastic PDAC cells (Thayer et al., 2003), stimulating Gli activity in surrounding fibroblasts and triggering their activation (Tian et al., 2009). Therefore, Shh became a target to inhibit fibroblast activation and Shh inhibition initially showed promising results in a preclinical PDAC mouse models. Shh inhibition reduced fibrosis and increased tumour vascularization, improving the delivery of gemcitabine to PDAC tumours (Olive et al., 2009). However, a clinical trial of Saridegib, a Shh inhibitor, with gemcitabine, in metastatic PDAC patients, failed at phase II as patients had reduced survival (Madden, 2012). Further investigation into fibroblast function in PDAC in longer-term experiments with mouse PDAC models showed that fibroblast ablation using smoothened inhibitor or genetic depletion of Shh or αSMA+ myofibroblasts, in fact showed that the stroma restrained tumour growth and metastasis (Rhim et al., 2014, Oezdemir et al., 2014). These conflicting results, combined with the emerging evidence that different CAF populations co-exist in tumours, suggest that different CAF populations may have different and possibly opposing effects in cancer progression (Ohlund et al., 2017, Costa et al., 2018). Despite these results, a phase

3 trial in medulloblastoma, using an oral sonidegib (smoothened inhibitor) in combination with temozolomide showed promising results with an objective response rate of 18.8 % (ClinicalTrial.gov identifier: NCT01708174).

One approach which warrants further investigation is the reprogramming of the activated CAFs back into their quiescent state. This approach has seen some success in PDAC mouse models using calcipotriol (vitamin D analogue) which reverts myofibroblasts to quiescence, reducing the desmoplastic reaction which in turn improves gemcitabine delivery (Sherman et al., 2014). In 3D models and genetic mouse models of PDAC the use of all-trans retinoic acid to restore the quiescence of stellate cells increased vascularity, resulting in increased response to gemcitabine and reduced tumour growth (Carapuca et al., 2016). In estrogen receptor positive breast cancer, CAF-derived FGF-2 promotes resistance to anti-estrogens which is abrogated with administration of an FGF-2 neutralising antibody (Shee et al., 2018) (Fig 1.5).

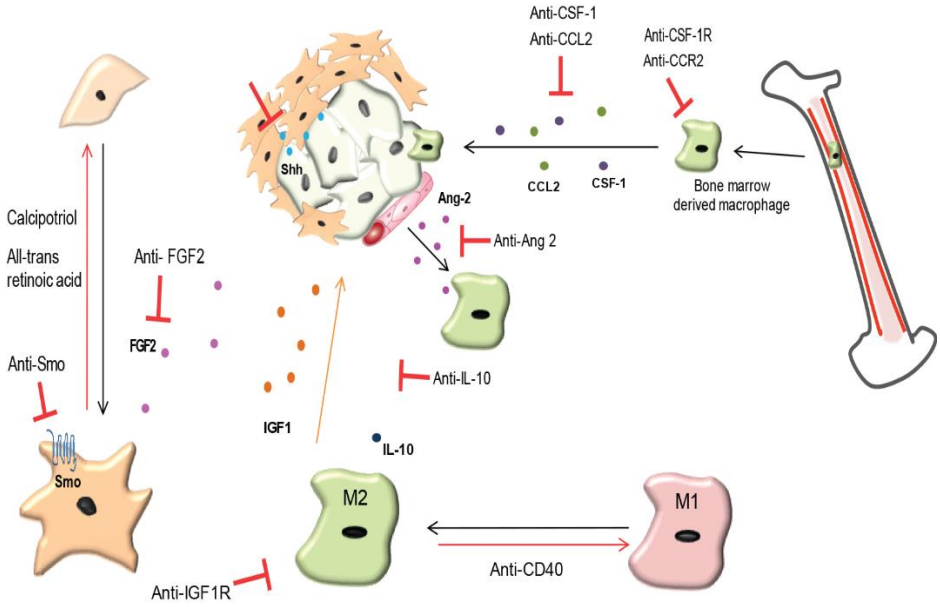

Figure 1.5 Therapeutic strategies to overcome chemoresistance mediated by TAMs and CAFs

CAFs: Reprogramming activated CAFs back towards a quiescent phenotype by anti-smoothened (Smo), anti-sonic hedgehog (Shh), all-trans retinoic acid and calcipotriol (vitamin D analogue) while fibroblast growth factor 2 (FGF2) targeting agents prevents resistance of tumour cells to anti-estrogens in breast cancer. TAMs: Repolarizing M2 macrophages back to an M1-like phenotype can be mediated by a CD40 agonist. Prevention of macrophage recruitment to tumour sites is currently being achieved by targeting the colony-stimulating factor 1 (CSF-1) and C-C motif chemokine 2 (CCL2) signalling axis. Anti-angiopoietin-2 (Ang-2) antibodies prevent TAM interaction with blood vessels. IL-10 produced by TAMs promotes chemoresistance which can be abrogated by treatment with anti-IL-10 antibodies. TAMs secrete insulin-like growth factor 1 (IGF-1) promoted survival in glioblastoma, blockade with IGF-1R inhibitor decreased tumour growth.

1.9 Pancreatic cancer

1.9.1 Pancreas anatomy and physiology

The pancreas is situated within the abdominal cavity and is located behind the stomach. It is a glandular organ functioning as part of the digestive system, regulating and aiding the digestion of proteins and carbohydrates, as well as mediating glucose homeostasis (Standring et al., 2005).

Anatomically the pancreas is separated into three sections: head, body and tail. The head of the pancreas is situated adjacent to the duodenum and the body, which is the largest part of the pancreas, is situated beneath the stomach (Fig 1.6). Finally, the tail of the pancreas extends to the left, neighbouring the hilum of the spleen (Fig 1.6). The head of the pancreas receives its blood supply through both the superior mesenteric and coeliac arteries. The splenic artery runs along the top of the pancreas and supplies the whole organ through its branching network. Due to its size, the different pancreas sections drain into specific veins; the body and neck sections drain into the splenic vein, and the pancreas head drains into the superior mesenteric and portal veins (Standring et al., 2005).

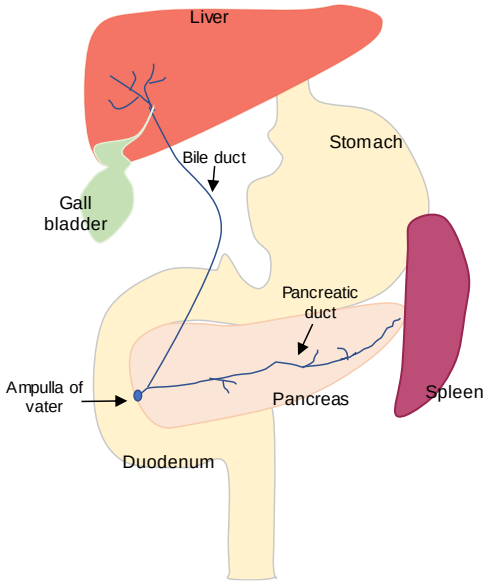

Figure 1.6 Anatomy of pancreas within the abdomen

The pancreas is located below the liver and the stomach in the abdomen. The head of the pancreas is abutted in the duodenum and the tail extends out towards the spleen. The bile duct from the liver and the pancreatic duct converge at the duodenum creating the ampulla of Vater to deliver digestive enzymes.

The pancreas performs both endocrine and exocrine functions. Endocrine units called the Islets of Langerhans produce of insulin and glucagon hormones which regulate blood sugar levels (Hezel et al., 2006). The other 80 % of the pancreas performs the

exocrine function, producing and delivering zymogen digestive enzymes to the duodenum and intestinal tract (Hezel et al., 2006). A branching network of acinar and ductal cells is present throughout the pancreas which culminate at the pancreatic duct. Zymogens released by acinar cells are channelled into the duodenum, along with bile, through the ampulla of Vater to aid digestion (Standring et al., 2005) (Fig 1.6).

1.9.2 Non-invasive precursor lesions

Malignancy in the pancreas begins as a non-invasive precursor lesions, most commonly pancreatic intraepithelial neoplasia (PanIN) and less commonly intraductal papillary mucinous neoplasm (IPMN) or mucinous cystic neoplasm (MCN) (Cooper et al., 2013). As genomic instability increases, and further oncogenic mutations are acquired, these precursor lesions progress into pancreatic ductal adenocarcinoma (PDAC) (Hezel et al., 2006, Hruban et al., 2007).

PanINs have three defined histological stages which mark the development of malignancy and the accumulation of genetic alterations. PanIN development begins with the reprogramming of acini and ductal cells causing them to lose their cellular identity (Fig 1.7) (Morris et al., 2010). At PanIN stage 1, it is estimated that 15-40 % of lesions acquire oncogenic Kirsten rat sarcoma viral oncogene homolog^{G12D} (Kras^{G12D}) mutation, triggering its constitutive activation resulting in enhanced cell proliferation (Aguirre et al., 2003) (Fig 1.7). Another common mutation seen at PanIN stage 1 is the inactivation of INK4a tumour suppressor gene which usually functions as a cyclin-dependent kinase inhibitor, therefore, at this stage control of the cell cycle is lost (Morris et al., 2010, Aguirre et al., 2003) (Fig 1.7). PanIN stage 3 is most likely to possess inactivating P53 mutations promoting evasion of apoptosis and preventing growth arrest in PanIN cells (Bailey et al., 2016, Morton et al., 2010). Around 53 % of PanINs possess Mothers against decapentaplegic homolog 4 (SMAD4) aberrations by stage 3 (Hansel et al., 2003, Maitra et al., 2003) (Fig 1.7). The loss of SMAD4

results in aberrant TGFß signalling leading to increased growth stimulation and reduced apoptosis cues (Furukawa et al., 2006, Duda et al., 2003)

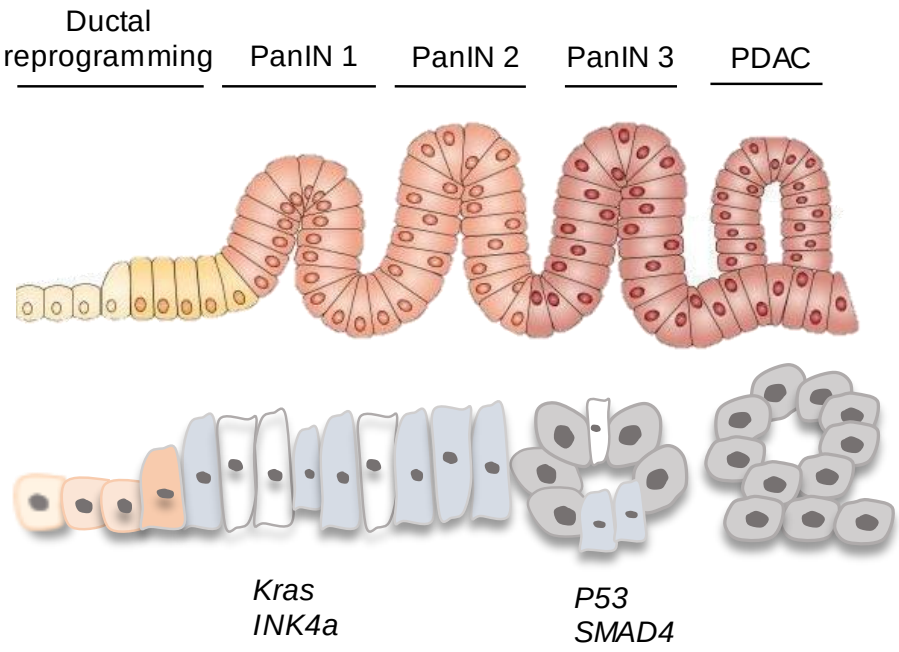

Figure 1.7 PDAC initiation and progression

The onset of PanIN development begins with reprogramming of acini and ductal cells through ductal reprogramming. PanIN stage 1 starts to form as the cells acquire KRas and INK4a mutations and cell morphology begins to alter. PanIN stage 2 shows cells with a loss of polarity and enlarged nuclei. PanIN stage 3 acquires P53 and SMAD4 mutations with the cell clustered to form lumens. Stage 3 leads to the development of pancreatic ductal adenocarcinoma (PDAC) with atypical neoplastic cells creating a lumen. Adapted from Morris et al., 2010.

1.9.3 Pancreatic ductal adenocarcinoma (PDAC)

PDAC is the 11th most prevalent form of cancer in the UK, with a 5 year survival rate of <7 % (Siegel et al., 2017). Establishment of PDAC in the pancreas can take up to ten years from non-invasive precursor lesions to a fully developed malignancy with established metastatic outgrowth (Yachida et al., 2010). Despite this long latency period, PDAC accounts for >85 % of pancreatic cancers detected (Li et al., 2004). Its nomenclature is based on histology studies which revealed PDAC grows with a ductal

morphology despite arising in acini or ductal cells (Humphris et al., 2014). PDAC occurs in the head of the pancreas in around 60-70 % of patients, a 20 % incidence in the pancreas body and 10-20 % of cases are spread diffusely throughout the pancreas (Humphris et al., 2014). The PDAC TME consists of a rich desmoplastic reaction comprised of myofibroblasts which can account for up to 80 % of the tumour mass along with infiltrating immune cells especially macrophages (Gunderson et al., 2016).

PDAC is often described as asymptomatic for the majority of the disease, however, this view is now changing with the discovery of type 3c diabetes mellitus caused by chronic pancreatitis and pancreatic cancer (Hart et al., 2016). Tumour growth often results in the obstruction of the common bile duct and pancreatic duct leading to jaundice and steatorrhoea respectively, usually resulting in tumour detection (Porta et al., 2005). A tumour mass arising in the head of the pancreas will require less time to create an obstruction than those lesions developed in the body and tail. This implies tumours in the body and tail of the pancreas may be more advanced when detected (Porta et al., 2005).

1.9.4 Risk factors

PDAC is known to carry a familial risk. It has been reported that PDAC sufferers in families with ≥ 2 affected first degree relatives represent 10% of all PDAC cases (Shi et al., 2009). Other risk factors for the development of PDAC include smoking, high alcohol usage, obesity with a BMI >35, chronic pancreatitis, diabetes mellitus and being of the male gender (Vincent et al., 2011, Kleeff et al., 2016).

1.9.5 PDAC metastasis

Due to the late detection of PDAC, it is characterised by a high rate of metastasis. Disseminated tumour cells from the primary mass travel through the lymphatic and

vascular systems to the liver and lungs. As the primary tumour grows, it penetrates the peritoneal cavity and spreads into the spleen (Humphris et al., 2014, Pandol et al., 2009). Detection and diagnosis are typically a consequence of symptoms of metastasis. Once the tumour has metastasised to the lungs patients will often experience breathing difficulties and metastatic outgrowth in the liver can lead to jaundice which usually results more invasive investigation and often will lead to a PDAC diagnosis (Claire et al., 2016).

Molecular aberrations acquired during PanIN progression and PDAC development have been shown to play key functions in metastasis. Mutated $KRas^{G12D}$ promotes migration of tumour cells whilst permitting survival in low-nutrient conditions which are often encountered during initial movement and seeding of metastatic cells (Qiu et al., 2011). Cells possessing Kras and INK4a mutations can promote NF-κB signalling promoting metastasis to liver and lungs in genetic PDAC mouse models (Aguirre et al., 2003). SMAD4 mutations specifically correlate with a higher metastatic burden (Iacobuzio-Donahue et al., 2009).

1.9.6 PDAC treatment

Treatment options for PDAC sufferers are limited due to the advanced nature of the disease at the time of diagnosis and the lack of effective chemotherapeutic agents. Approximately 20 % of patients are deemed viable for tumour resection, which along with adjuvant chemotherapy is the only potentially curative treatment available at this time. Despite this, it has been reported that many patients experience recurrence of the disease within a year of surgery, largely due to undetected micro-metastasis present in the body and/or the development of drug resistance during treatment (Labori et al., 2016). Resectable patients undergo a procedure to remove the primary lesion and a portion of the surrounding tissue. Borderline resectable patients are treated with neoadjuvant chemotherapy to shrink the tumour and are restaged before

proceeding. The majority of PDAC patients possess unresectable disease and are offered chemotherapy treatment which has shown low rates of prolonged survival (Spanheimer et al., 2014).

Gemcitabine chemotherapy administration is utilised for metastatic and locally advanced PDAC patients. Despite being the standard agent of care, gemcitabine has only a very modest effect, increasing survival of patients to 5.65 months compared to 4.41 months of untreated patients (Burris et al., 1997). Limited improvement is seen as initially gemcitabine-susceptible tumours become resistant within mere weeks of treatment (Kim and Gallick, 2008). Exactly how this occurs, and the role of the TME in chemoresistance is still under investigation.

A new regimen combining leucovorin, fluorouracil, irinotecan and oxaliplatin anti-neoplastic agents (FOLFIRINOX) has been studied in phase III trials in comparison to single agent gemcitabine. Median overall survival of FOLFIRINOX treated patients was increased to 11.1 months compared to 6.8 months of the gemcitabine group ($p < 0.001$). Despite this, median progression free survival with FOLFIRINOX was only 3.1 months longer than gemcitabine (Conroy et al., 2011). Although FOLFIRINOX provided a slightly increased survival time, its administration resulted in a significant number of frequent substantial toxicities compared to gemcitabine, thus limiting its administration (Conroy et al., 2011).

Albumin-bound paclitaxel (nab-paclitaxel) has shown promise as part of a multi-drug regimen in combination with FOLFIRINOX , shown in one study to convert > 20 % of locally advanced PDAC patients to resectable status (Faris et al., 2013). Nab-paclitaxel has also been trialled in combination with gemcitabine versus gemcitabine single agent. Nab-paclitaxel treatment increased median overall survival by 1.8 months (Von Hoff et al., 2011). Adverse events such as myelosuppression and

peripheral neuropathy were increased with nab-paclitaxel administration, restricting its use in the clinic (Von Hoff et al., 2011).

1.9.7 PDAC mouse models

The first model to faithfully reproduce human PDAC disease progression was the KC model, using a knock-in KRasG12D mutated oncogene in pancreatic lineages during embryonic development. KC mice were created by conditional KRasG12D mutation flanked by floxed STOP transcriptional cassette (LSL-KRasG12D) crossed with mice expressing Cre recombinase under control of Pdx1 promoter creating Pdx1-Cre;LSL-KRasG12D (Hingorani et al., 2003). These KC mice have been extensively characterised and exhibit the full extent of PDAC development including the complete spectrum of PanIN lesions which occur in human patients (Hingorani et al., 2003). Further development of this model to fully recapitulate the invasive and metastatic nature of PDAC was achieved in the KPC mouse model (LSL-KrasG12D/+; LSL-Trp53R172H/+; Pdx-1-Cre) (Hingorani et al., 2005). The KPC mouse model incorporated the conditionally expressed point mutation in $P53^{R175H}$ a mutant allele of the Li-Fraumeni human ortholog and routinely show full penetrance of PDAC metastasis (Olive et al., 2004).

1.10 Breast cancer

1.10.1 Breast anatomy and physiology

The breast is located above the ribcage and is situated on top of the pectoralis major muscle (Fig 1.8). The female breast is largely comprised of adipose and fibrous tissue which is penetrated by epithelial lobules. These lobules create to ductal networks leading to the nipple (Fig 1.8). This ductal structure is determined by the breasts function in milk production during lactation. When stimulated, epithelial cells secrete milk which travels through the network to the nipple. It is in these lobules and terminal

ducts in which cancer commonly arises (Fig 1.8). The male breast is also comprised of adipose and fibrous tissue but lacks lobules due to a lack of physiological need (Pandya and Moore, 2011). The internal mammary artery runs underneath the breast and serves as the blood supply for the breast tissue. Lymphatic vessels drain the tissue and flow either to internal mammary lymph nodes or towards the axillary lymph nodes (Pandya and Moore, 2011).

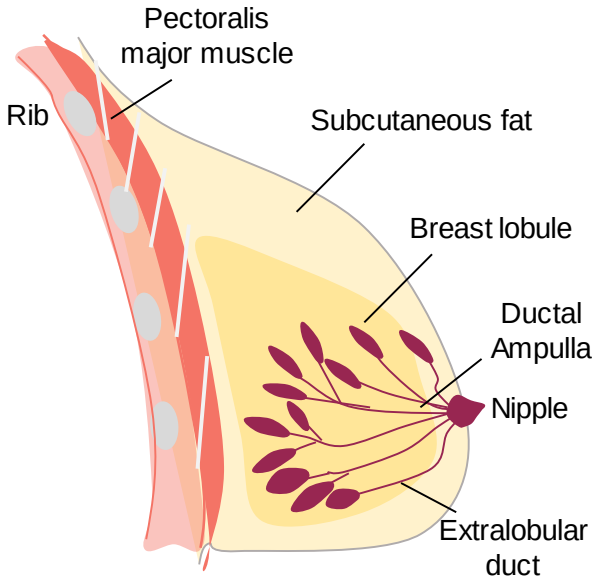

Figure 1.8 Breast anatomy

The breast is located on top of the rib cage and pectoralis major muscle. The majority of the breast tissue is comprised of adipose and fibrous tissue. Lobules running throughout the breast are comprised of milk-producing alveoli connected to extralobular ducts which ultimately culminate at the nipple delivery milk secretion.

1.10.2 Breast cancer subtypes

Breast cancer is the leading cause of cancer death in females worldwide, predicted to create 268,670 new cases and cause 41,400 deaths in the United States in 2018 (Siegel et al., 2017). Subtype nomenclature relays to the invasive nature of the breast

cancer and presence of receptors on the tumour cells. Non-invasive breast cancer is usually located within the ducts of the breast and lacks the ability to spread further. Invasive breast cancer is the most common type of breast cancer identified and has the potential to disseminate out from the breast tissue (Dai et al., 2015). A further three subtypes are defined based on molecular markers present on the tumour cells; hormone receptor positive (HR+) tumours which express estrogen (ER) and progesterone receptors (PR), HER2+ tumours (also HR-) and TNBC which is ER-, PR- and HER2- (Dai et al., 2015).

TNBC is a highly metastatic subtype that accounts for approximately 20 % of all breast cancer cases (Wahba and El-Hadaad, 2015). Overall TNBC has the poorest prognosis compared to other subtypes with a shorter progression free survival, higher risk of relapse and a lack of specific targeted treatment options (Chacon and Costanzo, 2010). TNBC is associated with younger women and a higher grade of tumour however this does not seem to impact the rate of women which elect to have their tumours surgically removed (Freedman et al., 2009).

Breast cancer begins with the development of atypical breast hyperplasia as a collection of abnormal yet benign cells, usually in a terminal duct. Accumulation of genetic aberrations in genes such as BRCA1 and BRCA2 tumour suppressor genes prompts the development of ductal carcinoma *in situ* (DCIS) contained within the ducts in 60-80 % of women. DCIS is described as a non-obligate precursor to invasive cancer, which occurs in 40% of patients (Sanders et al., 2005). The symptoms of breast cancer can vary and are not specific to subtype (Rivenbark et al., 2013). They generally include an area of thickened tissue in the breast, pain in armpit or breast, pitting or redness of the skin and a change in size or shape of the breast (McPherson et al., 2000).

1.10.3 Risk factors

Risk factors for developing breast cancer including aging, with most patients diagnosed over 50 years of age. A family history of breast cancer is associated with an increased risk, especially when linked to genes such as BRCA1 and BRCA2. ER+ breast cancer is promoted by estrogen therefore an early age of menstruation, pregnancy late in life or no pregnancy at all or starting menopause after the age of 55 can all influence tumour development. In the same vein, use of oral contraceptives or the use of combination hormone treatment for menopause has also been linked to an increased risk of breast cancer. Other risk factors are common to most types of cancer and include excessive alcohol consumption, obesity and lack of physical activity (McPherson et al., 2000, Garcia-Closas et al., 2006, Howell et al., 2014).

1.10.4 Breast cancer metastasis

Breast cancer has a propensity to give rise to metastasis in lungs, bones and brain, which can present up to ten years after treatment (Weigelt et al., 2005). However, 10-15 % of breast cancer patients develop metastasis within 3 years of primary tumour detection (Weigelt et al., 2005). Migrating tumour cells are often detected in axillary lymph nodes due to lymphatic drainage (Blackburn et al., 2017).

1.10.5 Breast cancer treatment

Breast cancer screenings are now performed for women aged 50-70 years. Mammograms image the breast tissue to identify cancerous lesions even before symptoms appear visible. If a mass is detected, patients receive adjuvant chemotherapy, however this treatment only produces a 3 % increase of 15-year survival rate in women aged >50 years (Abe et al., 2005).

For HR+ breast cancers (ER+ and PR+), hormone therapy is used to prevent the stimulation of estrogen signalling on cancer cells. Tamoxifen administration blocks

estrogen receptor binding and is used for the first line treatment of HR+ tumours. However, when patients become resistant to tamoxifen administration and a second treatment option of Fulvestrant is used to block the estrogen receptor. Administration studies of tamoxifen responders have shown receiving tamoxifen for 10 years post-initial treatment, reduced both breast cancer recurrence and mortality (Davies et al., 2013a).

HER2+ breast cancers are usually treated with trastuzumab, a monoclonal antibody specific to the HER2 receptor, to block downstream signalling. Trastuzumab also binds and flags the tumour cell for destruction by the immune system. Studies of trastuzumab administration have shown improved survival for HER2+ metastatic patients when treated with trastuzumab in combination with chemotherapy, such as docetaxel (Inoue et al., 2011).

Treatment of TNBC is problematic as it completely lacks the receptors for which many drugs have been developed such as trastuzumab or hormonal-based therapies (Bauer et al., 2007). Therefore, the treatment of metastatic TNBC includes radiotherapy and chemotherapy such as paclitaxel, as the standard of care, or docetaxel (Rakha et al., 2007, Schneider et al., 2008). Metastatic TNBC patients often become resistant to current chemotherapy treatments and as a result account for >90 % of breast cancer deaths (Marquette and Nabell, 2012). This highlights the need for new therapeutic targets to treat metastatic burden more effectively, especially that of TNBC.

1.10.6 Mouse models of TNBC

Invasive TNBC mouse models have been developed to recapitulate the human disease for use in scientific research. One such model uses mouse mammary tumour virus (MMTV) long terminal repeat (LTR) to drive the expression of mammary gland

specific polyomavirus middle T-antigen (PyMT). Expression of the middle T antigen results in the appearance of multifocal tumours in the mammary gland epithelium. Along with primary site tumours, the MMTV-PyMT mice also exhibit pulmonary metastasis. Py230 tumour cells isolated from this model have been identified as HR negative and HER2 low expression (Guy et al., 1992, Davie et al., 2007).

Orthotopic implantation of mammary cancer cells into syngeneic mice has also been shown to recapitulate the human disease. 4T1 mammary tumour cells were originally isolated from subpopulation 410.4 derived from a spontaneously arising mammary tumour in BALB/cfC3H mice (Dexter et al., 1978). Implantation of 4T1 cells into the mammary fatpad of BALB/c mice has been shown to create a primary tumour similar to the human disease along with metastasis the lung (Pulaski and Ostrand-Rosenberg, 1998).

1.11 Insulin and Insulin-like Growth Factor (IGF) signalling

The IGF and insulin signalling axis is comprised of three ligands: insulin, IGF-1 and IGF-2. These ligands bind to members of the receptor tyrosine kinase (RTK) family: IGF-1 receptor (IGF-1R), IGF-2 receptor (IGF-2R) and the insulin receptor (InsR) with varying degrees of affinity (Fig 1.9). IGF-1 and IGF-2 ligands bind primarily to IGF-1R which is expressed in almost every tissue (Bailyes et al., 1997, Federici et al., 1997). IGF-2R is generally regarded as a decoy receptor with no downstream signalling which binds and sequesters IGF-2 (Pollak, 2008). The InsR exists in two forms: InsR-A and InsR-B. InsR-B splice variant includes exon 11 and mediates glucose metabolism through the exclusive binding of insulin. InsR-A lacks exon 11 and can bind to all three ligands (Haeusler et al., 2018). To add further complexity, 40-90 % of IGF-1R exist as a hemi-receptor combined with either InsR-A or InsR-B. These hemi-receptors are bound by IGF-1 and IGF-2 with higher affinity than InsR-A (Fig 1.9) (Bailyes et al., 1997, Federici et al., 1997).

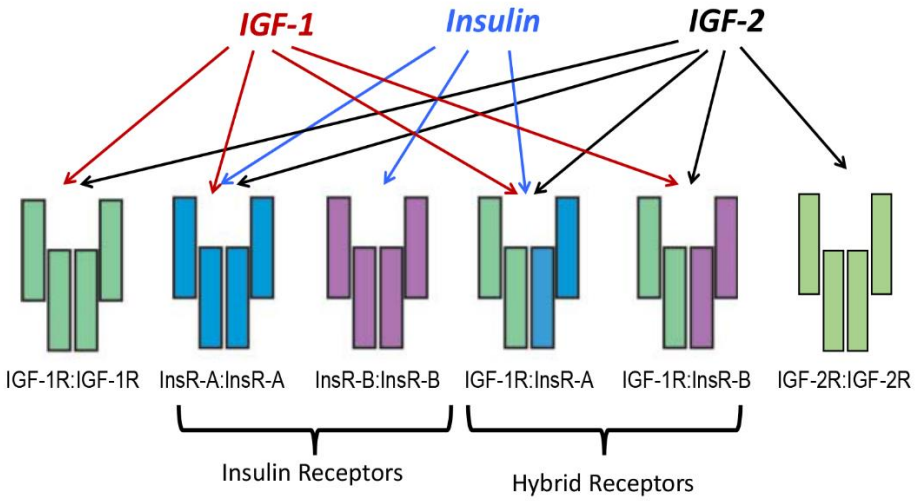

Figure 1.9 IGF and insulin ligands and receptors
IGF-1 and IGF-2 can bind to IGF-1R, InsR-A, IGF-1R: InsR-A hemi-receptor and IGF-1R: Ins-B hemi-receptor with varying affinity. Insulin ligand can bind InsR-A, InsR-B and IGF-1R: InsR-A hemi-receptor. IGF-2R can only bind IGF-2.

1.11.1 Downstream signalling

InsR-A, IGF-1R and IGF:InsR hemi-receptors mediate a variety of downstream signalling pathways. Upon ligand binding, IGF-1R and InsR undergo autophosphorylation and subsequently phosphorylate and activate downstream insulin receptor substrate 1 or insulin receptor substrate 2 (IRS1, IRS2). IRS1 and IRS2 function to increase and activate downstream PI3K and protein kinase B (AKT) (Zha and Lackner, 2010). Through AKT activation IGF signalling mediates a variety of pathways to prevent cell death, including resisting apoptosis via the release of B-cell lymphoma 2 (Bcl-2), promotion of glucose metabolism through the inhibition of Glycogen synthase kinase-3 (GSK-3) and the activation of protein synthesis by mechanistic target of rapamycin (mTOR) activation (Baserga, 1999).

Another activated pathway signals through SHC-transforming protein (Shc) and growth factor receptor associated protein 2 (Grb2) which in turn activate the Ras/Raf/MAPK signalling axis stimulating cellular proliferation (Pollak, 2008, Greer and Brunet, 2005). Downstream signalling specific to the insulin receptor mediates

glucose metabolism through PI3K associated mechanisms and the upregulation of glucose transporter Glut4 (Chang et al., 2004).

1.11.2 IGF/insulin function in normal tissues

As previously outlined, IGF signalling can regulate cell survival and has been shown to play a critical role in embryogenesis and tissue changes during puberty (Agrogiannis et al., 2014). IGF mediated promotion of cell survival can also interrupt programmed cell death mechanisms (Vincent and Feldman, 2002). Expression levels of IGF-1R correlate with induction of apoptosis; lower expression is detected in cells more susceptible to programmed cell death (Resnicoff et al., 1995). In normal tissues, InsR signalling functions to regulate glucose homeostasis by reducing the release and production of glucose therefore regulating blood glucose levels as well as mediating cell growth and differentiation (Chang et al., 2004).

1.11.3 IGF in PDAC

IGF signalling has been implicated in the progression of many cancers but also in mediating chemoresistance (Denduluri et al., 2015). The pancreas has a sufficient supply of ligands due to insulin production by ß cells in the islets of Langerhans in the pancreas and the production of IGF-1 and IGF-2 in the liver in response to growth hormone stimulation (Pollak, 2012). Based on this knowledge, it is unsurprising that IGF-1R has been reported as highly expressed in PDAC and IGF signalling could affect the basal growth of tumour cells (Bergmann et al., 1995, Ohmura et al., 1990). In fact, IGF-1R co-expression with epidermal growth factor receptor (EGFR) significantly correlates with poorer survival in PDAC patients (Valsecchi et al., 2012). Research into the role of IGF in the TME is now beginning to emerge, recently it was discovered fibroblasts exposed to pancreatic cancer cells secrete IGF, leading to pancreatic cancer cell survival and proliferation *in vitro* (Tape et al., 2016). However,

research into the effect of stromal IGF signalling and chemoresistance has been lacking in PDAC and requires further elucidation.

1.11.4 IGF in breast cancer

The IGF signalling axis has also been implicated in the promotion of breast cancer (Zhang et al., 2011, Denduluri et al., 2015, Pollak, 2012). Interestingly, IGF signalling has also been implicated in acquisition of resistance to ER and HER2 inhibition (Lu et al., 2001, Massarweh et al., 2008, Farabaugh et al., 2015). Of particular interest, it has been shown that tamoxifen ER+ cells possess a reduced number of IGF-1R, despite this InsR and AKT activation is unaltered with insulin and IGF-2 stimulation (Fagan et al., 2012). This report indicates both IGF-1 and IGF-2 signalling may support resistance of breast cancer cells to therapies (Fagan et al., 2012). Despite these insights, the role of IGF signalling in tumour progression and resistance to chemotherapy in breast cancer is not yet completely understood. IGF signalling has been shown to play a role in TNBC cancer. A panel of TNBC cell lines were shown to express IGF receptors and that stimulation with IGF-1 increases proliferation and promotes cell survival (Davison et al., 2011). However, the role of IGF signalling in chemoresistance seen in TNBC has yet to be investigated.

1.12 Aims of thesis

The aims of this thesis are:

1) to investigate the mechanisms of chemoresistance in PDAC and breast cancer mediated by the TME;

2) to identify specific molecules for targeting in preclinical models for use in combination with standard chemotherapeutic agents;

3) to identify factors that promote pancreatic cancer metastasis in preclinical models.

Chapter Two:

Materials and Methods

CONTENTS

2.1 Primary cells

2.1.1 Generation of primary KPC-derived pancreatic cancer cells

The murine pancreatic cancer cells KPC 3.5, FC1199, FC1242 and FC1245 were generated in the Tuveson lab (Cold Spring Harbor Laboratory, New York, USA). The cells were isolated from PDAC tumour tissues from LSL-KRas^{G12D}; LSL-Trp53^{R172H}; Pdx1-Cre (KPC) mice of a pure C57BL/6J background. Pancreatic tumours were harvested from KPC mice; a 3 mm^3 fragment of PDAC was excised, washed in 10 mL phosphate buffered saline (PBS), and finely diced with sterile razors. Tissues were incubated in 10 mL collagenase type V solution (2 mg/mL in Dulbecco's modified eagle medium (DMEM, Sigma Aldrich)) at 37 °C for 45 min with mixing to digest. Cells were centrifuged (300 *x g*) and resuspended in DMEM supplemented with 10 % foetal bovine serum (FBS, Sigma Aldrich) and 1 % penicillin/streptomycin (Sigma Aldrich) and plated in tissue culture treated plates. Cells were initially split at high dilutions (1:20 to 1:100) to dilute out contaminating stromal cells which do not tolerate aggressive splitting, whilst the cancer cells formed ductal-like colonies (Olive et al., 2009).

2.1.2 Generation of primary PyMT-derived breast cancer cells

Py230 cells (HR^- and HER2 low) were generated in the Ellies lab (University of California San Diego, USA) and obtained from spontaneously arising tumours in MMTV-PyMT C57BL/6J female mice by serial trypsinization and limiting dilution (Gibby et al., 2012).

2.2 Cell lines

All cells were authenticated, and periodically tested for mycoplasma contamination.

2.2.1 Pancreatic ductal adenocarcinoma (PDAC)

SUIT-2 and MIA-PaCa-2 human pancreatic cancer cell lines (both ATCC) were cultured in DMEM supplemented with 10 % FBS, 1 % penicillin/streptomycin, at 37 ^{o}C, 5 % CO_2 incubator.

Murine KPC 3.5, FC1199, FC1242 and FC1245 cells were cultured in DMEM supplemented with 10 % FBS, 1 % penicillin/streptomycin, at 37 ^{o}C, 5 % CO_2 incubator.

2.2.2 Breast cancer

Murine 4T1 cells (ATCC) were cultured in Roswell Park Memorial Institute (RPMI-1640) culture media (Life Technologies) supplemented with 10 % FBS, 1 % penicillin/streptomycin at 37 °C, in a 5 % CO_2 incubator. 4T1 cells are characterised as ER^{-}, PR^{-}, $HER2^{-}$ (Kau et al., 2012).

Murine Py230 cells were cultured in DMEM/F-12 culture media (Life Technologies) supplemented with 10 % FBS and 500 µL MITO serum extender (Corning), 1 % penicillin/ streptomycin at 37 °C, in a 5 % CO_2 incubator.

2.3 Generation of primary macrophages and primary pancreatic stellate cells

2.3.1 Primary human macrophages

Blood samples were taken from healthy human volunteers by a licensed phlebotomist. The blood was diluted 1:1 with MAC buffer (PBS (Ca^{2+}, Mg^{2+} free, Life Technologies) + 2 mM ethylenediaminetetraacetic acid (EDTA, Sigma Aldrich) + 0.5 % bovine serum albumin (BSA, Sigma Aldrich)). The blood/MAC buffer mix was layered on top of 12.5 mL histopaque-1077 (Sigma Aldrich) in a 50 mL falcon tube and subjected to density

gradient centrifugation 270 *x g* for 25 min, 1 acceleration and 0 brake at room temperature (RT). The middle serum layer was removed to facilitate the harvesting of the buffy coat layer. The collected monolayer was subsequently washed with MAC buffer and centrifuged at 270 *x g* for 10 min at 4 ^{o}C. CD14b^{+} monocytes were purified from the samples using magnetic bead affinity chromatography according to manufacturer's directions (Miltenyi Biotec). The monocytes were incubated with RPMI-1640 containing 10 % FBS and 50 ng/mL recombinant human macrophage colony stimulating factor (mCSF) (PeproTech) for 5 days to mature the monocytes into macrophages.

2.3.2 Primary murine macrophages

Murine macrophages were generated by flushing bone marrow from the femur and tibia of C57BL/6J or mixed 129/SvJae/C57BL/6 (PC) mice and flow through collected into MAC buffer. The bone marrow isolated cells were pelleted by centrifugation at 368 *x g* for 10 min at RT and the supernatant discarded. Red blood cells (RBC) were removed by a 5 min incubation with 5 mL RBC lysis buffer (Biolegend) and the reaction stopped with the addition of 10 mL of PBS. Leukocytes were pelleted by centrifugation at 368 *x g* for 10 min and the supernatant discarded. Monocytes were isolated through density gradient centrifugation by layering 5 mL leukocyte suspension on top of 4.5 mL histopaque-1083 (Sigma Aldrich) and centrifuged at 368 *x g* for 25 min, 1 acceleration and 0 brake at RT. The monocytes were harvested from the buffy coat layer and subsequently washed in MAC buffer, counted and plated for 5 days in DMEM containing 10 % FBS and 10 ng/mL murine mCSF (PeproTech) to promote macrophage differentiation.

2.3.3 Primary pancreatic stellate cells (PaSCs)

C57BL/6J mice were sacrificed via a schedule one method and pancreas extracted and placed in 0.9 % NaCl (Fisher Scientific) solution. Pancreas tissue was injected

with 1 mL enzyme mix (1.3 mg/mL collagenase D (Sigma Aldrich), 1 mg/mL protease from Streptomyces griseus (Sigma Aldrich) and 0.01 mg/mL DNase (Roche diagnostics)). The pancreas was then incubated in 10 mL enzyme mix in a 50 mL falcon tube at 37 ^{o}C and agitated at 240 rpm for 10 min and reduced to 120 rpm for 4 min using in a shaking incubator (Incu-shaker mini, Benchmark). The tissue was finely minced using scalpels until it resembled a fine paste and then further incubated at 37 ^{o}C for 7 min at 120 rpm agitation. The cells were pelleted at 500 *x g* for 10 min and subsequently washed in Gey's balanced salt solution (GBSS, recipe in table 3.1). The cell solution was passed through a 500 µm mesh (Spectrum Labs) and washed again with 20 mL GBSS. The PaSCs were isolated from the cell mixture using density gradient centrifugation. The cells were resuspended in a mixture of 9.5 mL of GBSS and 8 mL 28.7 % nycodenz (Progen) and split evenly into two 15 mL falcon tubes and 3 mL GBSS layered on top. Tubes were centrifuged at 1400 *x g* for 2 min at 4 ^{o}C with 1 acceleration and 0 brake and PaSCs were harvested from the fuzzy layer. PaSCs were activated by culturing on uncoated plastic dishes with in Iscove's Modified Dulbecco's Medium (IMDM) (Sigma Aldrich) supplemented with 10 % FBS.

Table 3.1 Gey's Balanced Salt Solution (GBSS) recipe

Reagent	**Weight(g/L)**
NaCl	7
KCl	0.37
$MgCl_2 \cdot 6H_2O$	0.210
$MgSO_4$ (anhydrous)	0.0342
Na_2HPO_4 (anhydrous)	0.1196
KH_2PO_4 (anhydrous)	0.030
Glucose	1
$NaHCO_3$	2.27
$CaCl_2 \cdot 2H_2O$	0.2252

2.4 Generation of conditioned media (CM)

2.4.1 Macrophage (MCM) and myofibroblast (MyoCM) conditioned media

To generate macrophage (MCM) and myofibroblasts conditioned media (MyoCM), murine macrophages or activated PaSCs were plated to 70 % confluency in 10 cm

dishes, were washed twice with PBS and cultured in serum-free DMEM for 24 to 36 hr. Supernatant was harvested and filtered to remove debris and dead cells using a 0.22 µm syringe filter (Fisher Scientific) and stored at 4 ^{o}C until use.

2.4.2 Tumour conditioned media (TCM)

To generate KPC 3.5, FC1199, FC1242 and FC1245 conditioned media, 500,000 cells were plated into 10 cm dishes and were cultured in serum-free DMEM for 24 to 36 hr. Conditioned media was then processed as described in section 2.4.1.

2.5 Treatment with chemotherapy, MCM, blocking antibodies, and recombinant IGF

SUIT-2, MIA-PaCa-2, and KPC-derived cells were cultured in DMEM with 2 % FBS for 24 hr, pre-treated for 3 hr with MCM, or MyoCM, recombinant IGF (PeproTech 100-11) at 100 ng/mL, or IGF-blocking antibody (Abcam 9572) at 10 mg/mL followed by gemcitabine (Sigma Aldrich G2463) at 200 nmol/L, nab-paclitaxel 10, 100, or 1,000 nmol/L, paclitaxel (Sigma Aldrich T7402) at 200 nmol/L or 5-FU (Sigma Aldrich F6627) at 100 mmol/L. Cells were harvested after 24 to 36 hr and analyzed for cell death by annexin-V / propidium iodide staining kit (Affymetrix) and flow cytometry analysis.

2.6 Cell cycle analysis

KPC-derived pancreatic cancer cells were treated with isogenic mouse MCM, IGF blocking antibody (Abcam 9572) at 10 µg/mL or recombinant IGF (PeproTech 100-11) at 100 ng/mL. Cells were harvested via trypsinisation and subsequently fixed with 100 % ice-cold methanol (Sigma Aldrich) for 10-15 min. The cells were centrifuged at 956 *x g* for 5 min. To remove RNA contamination, cells were treated with 10 µg/mL of RNase A (Sigma Aldrich) for 45 min at RT whilst being passed through an insulin syringe to ensure a single cell suspension. Cells were mixed with PBS containing 10 µg/mL of propidium iodide (Invitrogen) and subjected to flow cytometry analysis.

2.7 RTK array

Performed by Dr. Ainhoa Mielgo

Cells were either serum starved for 24 hr and treated with MCM for 2 hr, harvested, and lysed in radioimmunoprecipitation assay buffer (RIPA) (150 mmol/L NaCl, 10 mmol/L Tris-HCl pH 7.2 (Sigma Aldrich), 0.1 % SDS (Fisher Scientific), 1 % Triton X-100 (Sigma Aldrich), 5 mmol/L EDTA) supplemented with complete protease inhibitor mixture (Sigma Aldrich), Halt phosphatase inhibitor cocktail (Invitrogen), 1 mmol/L phenylmethylsufonylfluoride (Sigma Aldrich) and 0.2 mmol/L sodium orthovanadate (Sigma Aldrich). Cell lysates were analyzed with the Phospho-RTK Array Kit (R&D Systems) according to manufacturer's instructions.

2.8 Syngeneic mouse models

2.8.1 PDAC preclinical mouse models

2.8.1.1 Pancreatic cancer orthotopic model 1

1 x 10^6 primary FC1242 KPC-derived luciferase/zsGreen cells (luc/zsGreen) isolated from a pure C57BL/6J background, as previously described in section 2.1.1, were resuspended in 30 µL Corning growth factor reduced Matrigel Basement Membrane Matrix (VWR). The cells were injected into the tail of the pancreas of immunocompetent syngeneic C57BL/6J 6-8 week-old female mice. Tumours were established for one week before beginning treatment. Mice were dosed by intraperitoneal injection (i.p.) with gemcitabine (100 mg/kg) (Selleckchem), IGF-1/2 blocking antibody xentuzumab (100 mg/kg) kindly provided by Boehringer Ingelheim, or IgG1 isotype control antibody (Abcam), every 2–3 days for 10–15 days before harvest.

2.8.1.2 Pancreatic cancer orthotopic model 2

Orthotopic pancreatic tumours were initiated by implanting 1 x 10^6 primary KPC-derived cells in 30 µL Corning growth factor reduced Matrigel Basement Membrane

Matrix into the pancreas of immunocompetent syngeneic female 6-8 week-old mice on a mixed background 129/SvJae/C57BL/6J. As tumours in this model grow slower, tumours were established for three weeks before beginning treatment.

2.8.1.3 Pancreatic cancer orthotopic model 3

1 x 10^6 FC1199 luc/zsGreen, FC1242 luc/zsGreen or FC1245 luc/zsGreen cells from a pure C57BL/6J background, were injected in 30 µL Corning growth factor reduced Matrigel Basement Membrane Matrix into the tail of the pancreas in immunocompetent syngeneic C57BL/6J 6-8 week-old female mice. Tumours were left to grow until meeting humane endpoint point as dictated by project license restrictions, requiring culling by a schedule one method. Humane endpoint for the moderate study plan dictated as: 20 % weight loss, restrictions in movement, loss of appetite and dehydration.

2.8.2 Invasive breast cancer preclinical model

2.8.2.1 Syngeneic orthotopic breast cancer model 1

2 x 10^6 Py230 luc/zsGreen labelled cells in 60 µL Corning growth factor reduced Matrigel Basement Membrane Matrix were injected into the fatpad of the third mammary gland of immunocompetent syngeneic C57BL/6J 6–8 week-old female mice.

2.8.2.2 Syngeneic orthotopic breast cancer model 2

5 x 10^5 4T1 luc/zsGreen labelled cells in 60 µL of Corning growth factor reduced Matrigel Basement Membrane Matrix were injected into the fatpad of the third mammary gland of syngeneic BALB/c 6–8 week-old female mice.

Breast tumours were measured with calipers twice a week and treatment started when tumours measured between 5-8 mm^2 mean diameter. Mice were administered i.p. with IgG isotype control antibody (Abcam), paclitaxel (100 mg/kg) (Sigma Aldrich),

IGF-1/2 blocking antibody xentuzumab (100 mg/kg) or paclitaxel with xentuzumab, twice a week for 15 days. At humane endpoint, primary tumours and lungs were harvested, imaged using IVIS spectrum technology (Perkin Elmer) and tissues were digested for FACS sorting and analysis or formalin-fixed and paraffin-embedded by Liverpool Tissue Bank. Humane endpoint for the moderate study plan dictated as tumour maximum of mean diameter of 1.5 cm for therapeutic studies (according to Workman et al., 2010), 20% emaciation, limited movement and ulceration.

2.9 IVIS spectral imaging

IVIS spectral imaging of bioluminescence was used for orthotopically implanted tumour cells expressing firefly luciferase using IVIS spectrum system (Caliper Life Sciences). *In vivo* imaging of tumours required i.p. injection of 200 µL D-luciferin dissolved in PBS (150 mg/kg, PerkinElmer) with an incubation time of 10 min. Animals were anaesthetised and imaged using automated optimal exposure for 1 min. Organs were resected for *ex vivo* imaging coated in 100 µL D-luciferin for 1 min and imaged for 1 min at automated optimal exposure.

The luciferase-generated light emitted from organs was measured by Living Image software (PerkinElmer). A region of interest (ROI) was drawn around the entire organ to calculate photons and area size. Normalisation of photon values was performed to abrogate differences in fields of view and times of acquisition. Relative bioluminescence signal was calculated using photon per second mode in the living image software normalising to imaging area (total flux) as recommended by the manufacturer.

2.10 Hematoxylin and Eosin (H&E) staining

Formalin fixed and paraffin embedded (FFPE) tissues generated by Liverpool Tissue Bank were sectioned at 4 µm thickness and processed through hydration, H&E staining and dehydration steps (Table 3.2).

Table 3.2 H&E staining steps and incubation times

Hydration		
Step	**Solution**	**Time**
1	Xylene	5 mins
2	100% ethanol x 3	20 secs
3	95% ethanol	20 secs
4	80% ethanol	20 secs
5	70% ethanol	20 secs
6	Tap water	2 mins
H&E		
1	Haematoxylin	10 mins
2	Tap water	20 secs
3	1% Acid alcohol	5 secs
4	Scott's Tap Water	2 mins
5	Eosin	2 mins pancreas 3 min liver/lung
6	Tap water	Till water runs clear
Dehydration		
1	70% ethanol	1min
2	80% ethanol	1min
3	95% ethanol	1min
4	Absolute ethanol	1min X 3
5	Xylene	3 mins X 2

All reagents listed above from Sigma Aldrich
Acid alcohol: 1 mL Hydrochloric acid (Thermo Fisher), 50 mL 70 % Ethanol
Eosin: 1 g Eosin Y (Sigma Aldrich), 20 mL distilled water (dH_2O), 80 mL 100% Ethanol

2.11 Identification and quantification metastatic burden

FFPE lungs were serially sectioned through the entire lung using microtome at 4-5 µm thickness. Sections were stained with H&E and images were taken using a Zeiss Observer Z1 Microscope (Zeiss) to identify foci. The number of foci were counted, and total area of metastatic foci were measured using Zen imaging software. Metastatic burden was calculated by the following equations:

No. of foci per 100 mm^2: *(Average no. foci per section/ average tissue area per section (mm^2)) *100*

Average metastatic lesion size (mm^2): *Average total area of metastasis (mm^2)/ average number of foci per section*

Total metastatic burden: *Sum of area of each foci of each section*

2.12 Immunoblotting of protein lysates

Cells were harvested and lysed in RIPA buffer supplemented with a complete protease inhibitor mixture, a phosphatase inhibitor cocktail, 1 mmol/L phenylmethylsufonylfluoride and 0.2 mmol/L sodium orthovanadate. Protein lysate concentrations were quantified using a bicinchoninic acid (BCA) assay (Pierce). Samples were made to 1 µg/µL with 3x loading buffer (187.5 mM Tris base, 9 % SDS, 30 % glycerol, 0.05 % bromophenol blue and 10 % β-mercaptoethanol (all Sigma Aldrich)), heated to 95 ^oC for 10 min and run on SDS-PAGE gels. Proteins were transferred onto polyvinylidene fluoride (PVDF) membranes (Bio-Rad) using a transblot turbo (Bio-Rad) and blocked 1 hr with either 5 % non-fat dry milk (NFDM) or BSA depending on antibody requirements. Membranes were incubated with primary antibodies overnight rocking at 4 ^oC. Membranes were washed three times for 10 min

in tris-buffered saline with Tween 20 (TBS-T) and incubated with their corresponding secondary antibodies for 1 hr rocking at RT. Membranes were imaged in a dark room using X-ray film or using ChemiDoc imaging system (Bio-Rad). Antibodies used in these experiments are listed in appendix (i).

2.12.1 Immunoblotting of secreted proteins

Proteins from CM were concentrated using StrataClean Resin (Agilent Technologies). 10 µL of strataclean resin was used per sample and 1 mL of CM incubated at a time and vortexed for 1 min to allow protein binding. Samples were centrifuged for 2 min at 2000 *x g* and steps repeated for total 5 mL CM binding. Strataclean resin was mixed with 2x loading buffer and heated to 95 ^{o}C for 10 min. Samples were run and membranes treated as described in section 2.12.

2.13 Gene expression by quantitative PCR (qPCR)

Total RNA was isolated from purified cells using Qiagen RNeasy kit (Qiagen) following manufacturer's instructions. cDNA was prepared from 1 µg RNA per sample using QuantiTect reverse transcription kit (Qiagen) according to manufacturer's instructions, and qPCR was performed using gene-specific QuantiTect Primer Assay primers (Qiagen) using 5x HOT FIREPol® EvaGreen® qPCR Mix Plus (Solis Biodyne). The qPCR reaction was run on Stratagene Mx3005P (Thermo Fisher) under the following cycling conditions: 1 cycle: 95 ^{o}C for 15 min. 45 cycles: 95 ^{o}C for 15 sec, 60 ^{o}C for 20 sec, 72 ^{o}C for 30 sec, 78 ^{o}C for 11 sec. 1 cycle: 95 ^{o}C for 1 min, 55 ^{o}C for 30 sec and 97 ^{o}C continuously. Relative expression levels were normalized to *gapdh* expression according to the formula: $2^{-(\Delta CT\text{gene of interest } \Delta Ct\text{gapdh})}$ (Schmittgen and Livak, 2008). Primers used in these experiments are listed in appendix (iv).

2.14 Immunohistochemistry

FFPE tissues were sectioned at 4-5 µm width using a microtome and mounted onto glass slides (VWR). The mounted sections were deparaffinised and primed by antigen retrieval using an automated DAKO PT-link system (Agilent), using either high pH (9 pH) or low pH (6 pH) retrieval buffers (DAKO) depending on antibody specifications. Tissues were blocked for 20 min with peroxidase (DAKO) to prevent non-specific staining and washed three times for 10 min in TBS-T. Tissues were immunostained using the DAKO envision+ system-HRP (DAKO). Tissues were incubated with primary antibodies for 2 hr at RT and were subsequently washed three times with TBS-T for 10 min. Subsequently, samples were incubated with secondary HRP-conjugated antibody (from DAKO envision kit) for 1 hr at RT. Tissue staining was developed using diamino-benzidine (DAB) (DAKO) and counterstained with haematoxylin and fixed in xylene. Coverslips were mounted using DPX mountant (Sigma Aldrich). All antibodies were prepared in antibody diluent from DAKO envision kit and are listed in appendix (ii).

2.15 Immunofluorescence

PDAC tissue was frozen in Tissue-tek Optimal cutting temperature compound (OCT) (Sakura Finetek UK Ltd) and stored at -80 ^{o}C. Tissue sections were cut at 4-5 µm thickness using a Cryostat (Leica) and mounted on a glass slide. The sections were fixed for 2 min in ice-cold acetone (Sigma Aldrich) and washed three times for 5 min in PBS. Tissues were subsequently permeabilized using 0.1 % Triton X-100 in PBS for 2 min and again washed three times for 5 min in PBS. Non-specific binding was reduced by blocking with 8 % goat serum (Abcam) in PBS for 1 hr at RT in a humid chamber. Tissues were incubated with primary antibodies overnight at RT in a humid chamber. The slides were washed three times in PBS for 5 min and incubated with their corresponding secondary antibody (1:500 dilution) and DAPI nuclear stain (1:600) for 2 hr at room temperature. The slides were washed three times for 5 min

with a final wash in dH_20 and mounted with fluorescent mounting media (DAKO). Antibodies used in these experiments are listed in appendix (iii).

2.16 FACS sorting of cell populations from murine tumours

Single cell suspensions from murine pancreatic and breast tumours were prepared by mechanical and enzymatic disruption in Hanks Balanced Salt Solution (HBSS) (Sigma Aldrich) with 1 mg/mL Collagenase P (Roche). Cell suspensions were centrifuged for 5 min at 423 *x g*, resuspended in HBSS and filtered through a 500 µm polypropylene mesh (Spectrum Laboratories). Cells were resuspended in 1 mL 0.05 % Trypsin (Life Technologies) and incubated at 37 ^oC for 5 min. Cells were filtered through a 70 µm cell strainer (VWR) and resuspended in PBS + 1 % BSA. Cells were blocked for 10 min on ice with Fc Block (BD Pharmingen, Clone 2.4G2) and then stained with FACS antibodies listed in appendix (iv). Samples were sorted on the FACS ARIA (BD Biosciences) for tumour cells (Sytox-/ CD45-/ zsGreen+), non-immune stromal cells ($Sytox^-/CD45^-/zsGreen^-$), macrophages ($Sytox^-/CD45^+/F4/80^+$) /M1-like TAMs ($Sytox^-/CD45^+/F4/80^+/CD206^-$) /M2-like TAMs ($Sytox^-/CD45^+/F4/80^+/CD206^+$).

2.17 SILAC mass spectrometry secretome sample preparation

FC1199, FC1242 and FC1245 cells were incubated with non-phenol red serum-free R6K6, R10K8 and R0K0 SILAC media respectively, for 24 hr. CM was collected into 15 mL falcon tubes and centrifuged 423 *x g* for 5 mins. The supernatant was collected and filtered using a 0.22 µm syringe filter and kept at 4 ^oC until prepared for mass spectrometry.

Samples were prepared by Deborah Simpson, Centre for Proteome Research

SILAC CM was dispensed into four replicate tubes with 2 mL of each individual label in each (6 mL of 1:1:1 mix). 1 mL of CM mix from each replicate was bound to 10 µL

of strataclean resin beads, the samples were vortexed for 1 min, centrifuged at 2000 *x g* for 2 min and the depleted supernatant transferred to a fresh tube and retained. 1 mL of CM was consecutively bound to the beads four times. The beads were washed three times with 1 mL of 25 mM ammonium bicarbonate and re-suspended in 80 µL of 25 mM ammonium bicarbonate and 5 µl of 1 % (w/v) Rapigest (Waters). 25 mM ammonium bicarbonate was added and the samples were heated at 80 ^{o}C for 10 min with shaking. Samples were reduced by the addition of 5 µL of 60 mM Dithiothreitol (DTT) in 25 mM ammonium bicarbonate and heated at 60 ^{o}C for 10 min. Samples were cooled and 5 µL of 180 mM iodoacetamide in 25 mM ammonium bicarbonate added and samples incubated at RT for 30 min in the dark. Trypsin (Porcine trypsin sequencing grade, Promega) (1 µg) was added and the samples incubated at 37 ^{o}C overnight on a rotary mixer.

The following day, the digests were acidified to remove Rapigest surfactant by the addition of 1 %(v/v) Trifluoroacetic acid (TFA) (acidity checked using pH paper) and incubated at 37 ^{o}C for 45 min. Samples were then centrifuged at 17,000 *x g* for 30 min and the clarified supernatants transferred to 0.5 mL low-bind tubes. Samples were centrifuged for a further 30 min and 10 µL transferred to total recovery vials for Liquid chromatography- high resolution mass spectrometry (LC-HRMS) analysis.

2.17.1 SILAC mass spectrometry

Samples were run by Deborah Simpson, Centre for Proteome Research

Liquid chromatography- tandem mass spectrometry (LC-MSMS) analyses were conducted on a QExactive HF quadrupole-Orbitrap mass spectrometer coupled to a Dionex Ultimate 3000 RSLC nano-liquid chromatograph (Thermo Fisher). The column was maintained at 40 ^{o}C, and the effluent introduced directly into the integrated nano-electrospray ionisation source operating in positive ion mode.

2.17.2 SILAC mass spectrometry analysis

2.17.2.1 Maxquant SILAC analysis

Mass spectrometry raw files from QExactive Orbitrap were analysed using Maxquant software (version 1.5.3.17) to perform peak picking, quantitative measuring and protein identification using incorporated Andromeda peptide search engine and UniprotKB database of Mus musculus (mouse) FASTA protein sequences. Group specific parameters selected for a multiplicity of 3 and trypsin digestion. Maxquant output ratios were filtered by the removal of identified contaminants and proteins not present in every replicate (NaN) or only identified by 1 peptide.

2.17.2.2 LIMMA in R

Statistical analysis was performed on sorted Maxquant output ratios using R studio (version 3.4.1) and LIMMA stats package (version 3.7), performing ANOVA statistical analysis with empirical Bayes distribution (Ritchie et al., 2015).

2.17.2.3 Perseus principal component analysis (PCA) and Multiscatter plot

Perseus software (version 1.5.8.5) was used to perform principal component analysis evaluating statistical significance of protein expression with a q-value of 0.05 for Benjamini-Hochberg false discovery rate (FDR) for each protein robustly identified in each replicate mass spectrometry run (Tyanova et al., 2016). A multiscatter plot was created based on gene ontology of biological processes with Pearson correlation coefficient calculated per comparison.

2.17.2.4 SecretomeP, SignalP, TMHMM and Uniprot database analysis

SecretomeP: FASTA sequences of identified proteins were analysed by SecretomeP 2.0 server. Proteins with an NN_score score ≥0.6 without a SignalP positive identification was deemed to be non-classically secreted.

SignalP: FASTA sequences of identified proteins were analysed by SignalP 4.1 server. Proteins with a positive D-score predicting the presence of a signal peptide associated with classical secretion.

TMHMM: FASTA sequences of identified proteins were analysed by TMHMM v2.0 server. Proteins predicted to contain transmembrane helices based in the amino acid sequence were deemed as spanning the cellular membrane.

Uniprot: Used to identify gene ontology of associated cellular component

2.18 Statistical Methods

Statistical significance for *in vitro* assays and animal studies was assessed using unpaired two-tailed Student t test or one-way ANOVA coupled with Tukey's post hoc tests or Bonferroni post hoc tests, and the GraphPad Prism 5 program. Proteomic data was assessed by one-way ANOVA, Multiscatter plots analysed with Pearson correlation and PCA analysis by Benjamini-Hochberg cut off (0.05 FDR) using R statistical package.

2.19 Institutional approvals

Experimental animals: Mice were maintained under specific pathogen-free conditions and experiments were performed under an approved project licence (reference number: 403725) as according to current UK legislation, at the Biomedical Science Unit at the University of Liverpool. All mice used were immunocompetent C57BL/6J 6-8 week-old female mice.

Human material: All studies involving blood collection were approved by the National Research Ethics (Research Integrity and Governance Ethics committee- Reference: RETH000807). All individuals provided informed consent for blood donation on approved institutional protocols.

Chapter Three:

Chemoresistance in pancreatic cancer is driven by stromal-derived insulin-like growth factors

CONTENTS

3.1 INTRODUCTION

3.1.1 Chemoresistance

Drug resistance is one of the biggest challenges in cancer treatment and has been identified as the major cause of recurrence in the majority of cancer patients (Holohan et al., 2013, McMillin et al., 2013). Multiple factors can contribute to the development of therapy resistance thus allowing tumour progression. In solid tumours, extrinsic means of mediating chemoresistance is largely dominated by a rich pro-tumoural microenvironment (Noy and Pollard, 2014, Mantovani and Allavena, 2015, De Palma and Lewis, 2013, Junttila and de Sauvage, 2013). Although macrophages have the potential to remove cancer cells, it has been shown that polarised M2-like TAMs actually promote tumour initiation, progression and metastasis whilst also protecting tumours from cytotoxic agents (Lin et al., 2001, Qian et al., 2011, Qian et al., 2015, Schmid et al., 2011, Schmid et al., 2013, Shree et al., 2011, Bruchard et al., 2013, Weizman et al., 2014, DeNardo et al., 2011, Mitchem et al., 2013, Nielsen et al., 2016). CAFs present in the TME have also been reported to protect against chemotherapeutic agents and promote further tumour growth (Zhang et al., 2017, Qiao et al., 2018). However, the precise molecular mechanisms utilised by TAMs and CAFs to support tumour progression are not completely understood, and the use of combination therapies which simultaneously target both pro-tumoural stromal cells and cancer cells are only beginning to emerge.

3.1.2 PDAC

Pancreatic cancer is a devastating disease with <7 % of patients surviving for 5 years after diagnosis (Siegel et al., 2017). This is largely due to the high occurrence of chemoresistance, especially to gemcitabine, the current standard of care (Kim and Gallick, 2008). The stromal compartment of PDAC is extremely rich with non-malignant TAMs and CAFs abundantly present. Bi-directional interactions between stromal and PDAC cells are known to influence tumour cell behaviour including growth

and motility (Hanahan and Coussens, 2012, Quail and Joyce, 2013). This is largely mediated by secreted factors as TAMs and CAFs are not always in direct contact with tumour cells. However, the stromal signalling promoting chemoresistance in PDAC is only partially understood and requires further investigation.

3.1.3 PDAC mouse models

The use of immunocompetent preclinical mouse models which faithfully recapitulate the human disease is essential to elucidate stromal interactions as the majority of the stroma is comprised of infiltrating immune cells. Interestingly, orthotopic implantation of KPC-derived PDAC tumour cells into the tail of the pancreas of syngeneic recipient mice has been shown to develop PDAC with full penetrance (Jiang et al., 2014). The use of KPC-derived tumour cells orthotopically implanted into immunocompetent mice can therefore be used as a preclinical to investigate chemoresistance *in vivo*.

3.1.4 Insulin and IGF signalling

The IGF signalling axis uses three secreted ligands: insulin, IGF-1 and IGF-2. These bind to IGF-1R, IGF-2R and InsR with varying degrees of affinity (Bailyes et al., 1997). Upon ligand binding, the IGF-1R and InsR undergo autophosphorylation and subsequently phosphorylate and activate downstream insulin receptor substrate 1 or 2 (IRS1, IRS2). IRS1 or IRS2 functions to increase and activate downstream phosphoinositide 3- kinase (PI3K) and subsequently protein kinase B (AKT) (Zha and Lackner, 2010). AKT activation prevents cell death, promotes glucose metabolism and activates protein synthesis (Baserga, 1999). The role of IGF signalling in PDAC is still limited and requires attention.

3.1.5 Hypothesis

TAMs and CAFs present in the PDAC tumour microenvironment contribute to chemoresistance therefore tumour progression in preclinical mouse models.

3.1.6 Aims

- To identify TAMs and CAFs in the tumour microenvironment
- To identify secreted factors which promote chemoresistance
- Identify pro-survival signalling pathways in the tumour cells
- Trial blocking antibodies in PDAC preclinical mouse model

3.2 RESULTS

3.2.1 Macrophages can be differentiated from bone marrow monocytes in culture

To cultivate primary murine macrophages *in vitro*, the hind legs of C57BL/6J mice were harvested post-mortem and bone marrow flushed from the femur and tibia to collect bone marrow monocytes. To promote differentiation into macrophages, the bone marrow monocytes were incubated with cell culture media supplemented with mCSF-1 for 5 days, which has been shown to differentiate macrophages towards an M2-like phenotype (Lawrence and Natoli, 2011) (Fig 3.1). To collect macrophage-secreted factors, the cells were incubated with serum free culture medium for use in further studies.

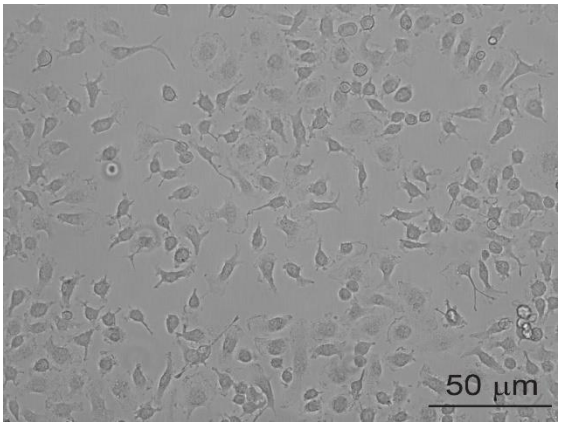

Figure 3.1 Murine Bone marrow derived macrophages in culture

Primary macrophages created by harvesting bone marrow from femur and tibia of C57BL/6J mice. Mononuclear cells isolated via density centrifugation and matured for 5 days *in vitro* using mCSF-1 (10 ng/mL) to create adherent M2-like macrophages. Scale bar, 50 μm.

3.2.2 Macrophage conditioned media (MCM) induces chemoresistance towards gemcitabine in PDAC cells *in vitro*.

Chemoresistance is a major obstacle which arises during PDAC treatment. Macrophages are one of the most abundant cell types in the PDAC TME which may be implicated in the induction of chemoresistance. To investigate whether macrophage-secreted factors reduced cell death, mouse KPC-derived pancreatic cancer cells called KPC 3.5 were cultured *in vitro* and incubated with or without macrophage conditioned media (MCM) and in the presence or absence of the standard PDAC chemotherapeutic agent gemcitabine (200 nmol/L). FACS analysis of apoptosis/necrosis, by annexin V/propidium iodide (PI) staining, showed the addition of MCM reduced the levels of cell death in gemcitabine treated cells, whilst no effect was seen in untreated cells (Fig 3.2).

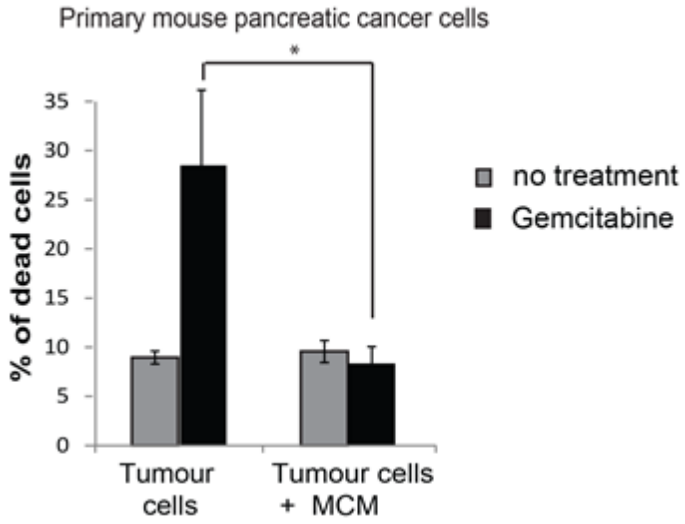

Figure 3.2 MCM induces chemoresistance in PDAC cells treated with gemcitabine

Mouse primary KPC-derived pancreatic cancer cells, KPC 3.5, were cultured in the presence or absence of conditioned media from mouse primary macrophages and treated with 200 nmol/L gemcitabine for 24 hr or left untreated. Percentage of cell death was quantified by flow cytometry annexin V/ PI staining. (Error bars, SD (n = 3 biological replicates); two-tailed unpaired t test; *, P ≤ 0.05.)

3.2.3 MCM activates the insulin receptor and insulin-like growth factor receptor on pancreatic cancer cells

To determine which receptors were stimulated by MCM incubation and could therefore cause chemoresistance, human SUIT-2 pancreatic cancer cells were incubated with or without human MCM. The lysates from these cells were then analysed using a phospho-receptor tyrosine kinase (pRTK) array, identifying three activated RTKs: insulin receptor (InsR), AXL receptor and ephrin receptor (Fig 3.3). Of these receptors, insulin/IGF-1 receptor signalling has previously been reported to be involved in drug resistance in other cancer types (Denduluri et al., 2015). However, a direct role of macrophage-derived IGF mediated chemoresistance in PDAC has yet to be elucidated.

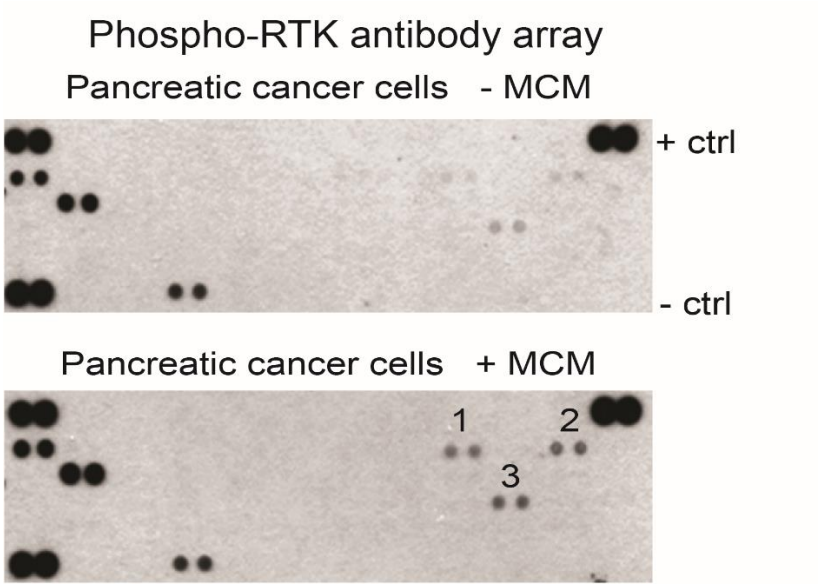

Figure 3.3 MCM causes phosphorylation of three RTKS on PDAC cells
Human pancreatic cancer SUIT-2 cells were serum starved for 24 hr and exposed for 2 hr to human MCM or left unexposed. Protein lysates were subjected to a phospho-receptor tyrosine kinase (pRTK) array. RTK's identified as activated: 1, phospho-insulin receptor; 2, phospho-AXL receptor; 3, phospho-Ephrin receptor. Performed by *Dr. Mielgo*.

3.2.4 Primary macrophages express and secrete IGF-1 and IGF-2

The insulin receptor can be ligated and activated by three ligands: insulin, IGF-1, and IGF-2 (Pollak, 2012). Therefore, it was necessary to determine which of these ligands were expressed by macrophages and therefore activating the InsR on PDAC cells. qPCR analysis to elucidate expression levels of the three ligands in primary murine macrophages revealed the major ligands expressed as *Igf-1* and *Igf-2* but not *Insulin* (Fig 3.4).

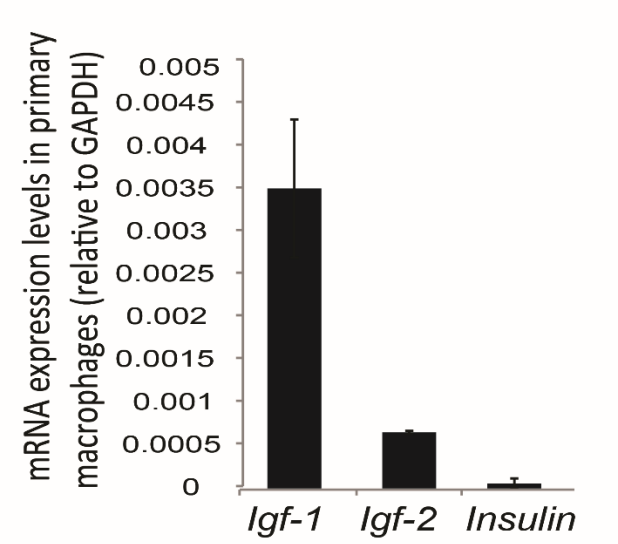

Figure 3.4 *Igf-1* and *Igf-2* genes are expressed by murine macrophages
Primary isolated bone-marrow derived murine macrophages analysed by qPCR for quantification of *Igf-1*, *Igf-2*, and *Insulin* mRNA expression levels relative to *GAPDH* housekeeping gene levels. (Error bars, SEM, n=3 biological replicates).

To confirm this result at the protein level, CM and cell lysates were collected from primary macrophages. Cell lysates and proteins concentrated from the CM were immunoblotted for IGF-1 and IGF-2, revealing both to be expressed and secreted by primary murine macrophages (Fig 3.5).

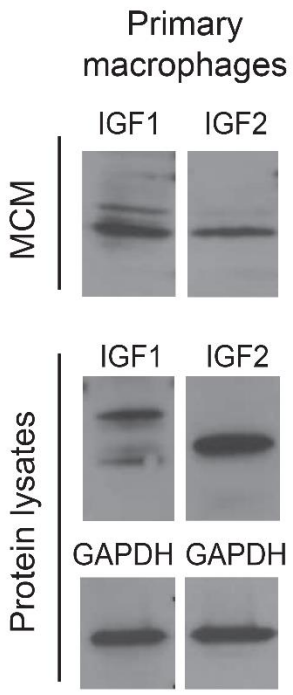

Figure 3.5 IGF-1 and IGF-2 proteins are both expressed intracellularly and secreted by primary macrophages

Immunoblotting analysis of IGF-1 and IGF-2 ligand expression in primary isolated bone marrow-derived macrophage protein lysates and macrophage conditioned media (MCM) (2ml of CM bound to 10 µL strataclean beads to concentrate) with GAPDH loading control.

These results show that MCM contained IGF-1 and IGF-2 which resulted in insulin receptor activation on PDAC tumour cells. However, it is also possibility that tumour cells themselves could produce and secrete IGF ligands which could act in an autocrine manner. To determine whether this was the case, mRNA expression levels of *Igf-1, Igf-2* and *Insulin* were analysed in the KPC 3.5 pancreatic cancer cells. qPCR analysis showed tumour cells expressed *Igf-1* but to a much lesser degree than macrophages (Fig 3.6)

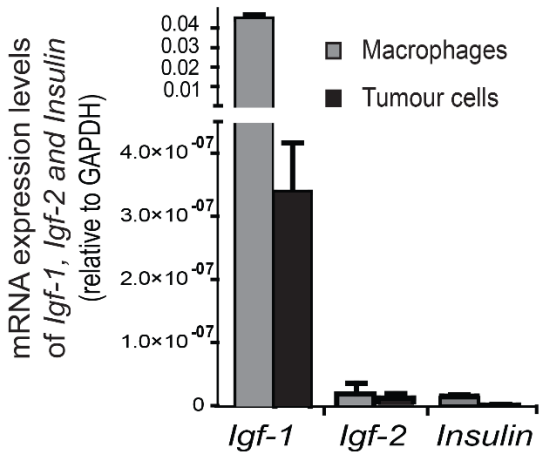

Figure 3.6 Macrophages produce higher levels of *Igf-1* and *Igf-2* than tumour cells

Comparison of primary isolated bone marrow-derived macrophages and KPC 3.5 tumour cells expression levels of *Igf-1*, *Igf-2* and *Insulin* mRNA determine by qPCR gene expression quantification, relative to *GAPDH* (Error bars, SEM, n=3 biological replicates, 3 technical replicates per sample).

Thus, these findings suggest that activation of the insulin receptor on pancreatic cancer cells is triggered through paracrine macrophage-derived IGF-1/IGF-2 signalling. To confirm this finding, KPC 3.5 PDAC cells were stimulated with MCM or recombinant IGF (rec IGF). The lysates were then subject to immunoblotting for phosphorylated InsR (pInsR) detecting phosphorylation at Y1162/Y1163 but also for phosphorylated IGF-1 receptor (pIGF-1R) detecting phosphorylation at Y1135/Y1136 as this can also be activated by IGF-1 and IGF-2 ligands. This revealed MCM and recIGF both caused activation of InsR and IGF-1R in PDAC cells (Fig 3.7 A). Densitometry analysis of the immunoblotting revealed KPC 3.5 cells increased pIns/IGF-1R levels when treated with MCM or rec IGF when compared to total insulin receptor or IGF-1 receptor expression (Fig 3.7 B).

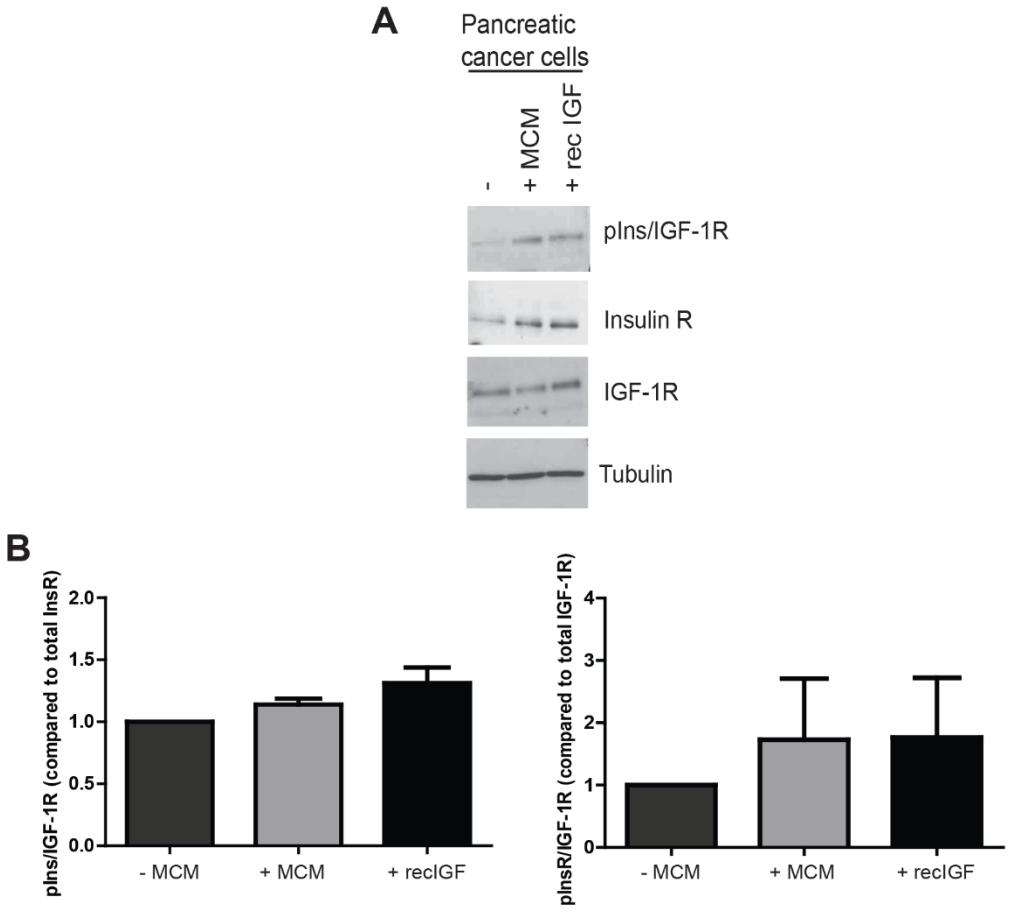

Figure 3.7 MCM and rec IGF activates Ins/IGF-1R signalling on PDAC cells
A) Immunoblotting analysis of murine primary KPC 3.5 pancreatic cancer cells either serum starved, exposed to MCM, or exposed to recombinant IGF for 3 hr. Probed for phospho insulin/IGF-1 receptors, total insulin receptor, total IGF-1R receptor and tubulin loading control. **B)** Increase in pInsR/IGF-1R compared to total InsR (left) and total IGF-1R (right) relative to tubulin loading control quantified from 2 independent experiments by densitometry.

3.2.5 Blockade of macrophage-derived IGFs prevents Ins/IGF-1R activation

Incubation of PDAC tumour cells with MCM has shown chemotherapy-induced cell death can be prevented *in vitro* (Fig 3.2) and it was also identified that InsR and IGF-1R were activated in response MCM incubation (Fig 3.7). It was therefore important to determine whether IGF-1 and IGF-2 were responsible for the induction of chemoresistance.

To address this question, we acquired an IGF-neutralizing antibody (ab9572) which specifically bound and inhibited IGF-1 activity, thus preventing ligation with either the InsR or IGF-1R. Firstly, human SUIT-2 PDAC cells were incubated with or without MCM or with IGF blocking antibody (Ab). Interestingly, MCM stimulation alone significantly increased levels of pInsR/pIGF-1R and caused activation of downstream signalling components IRS1, IRS2, AKT and MEK (Fig 3.8 A and B). This activation was abrogated with the addition of the IGF blocking Ab (Fig 3.8 A and B).

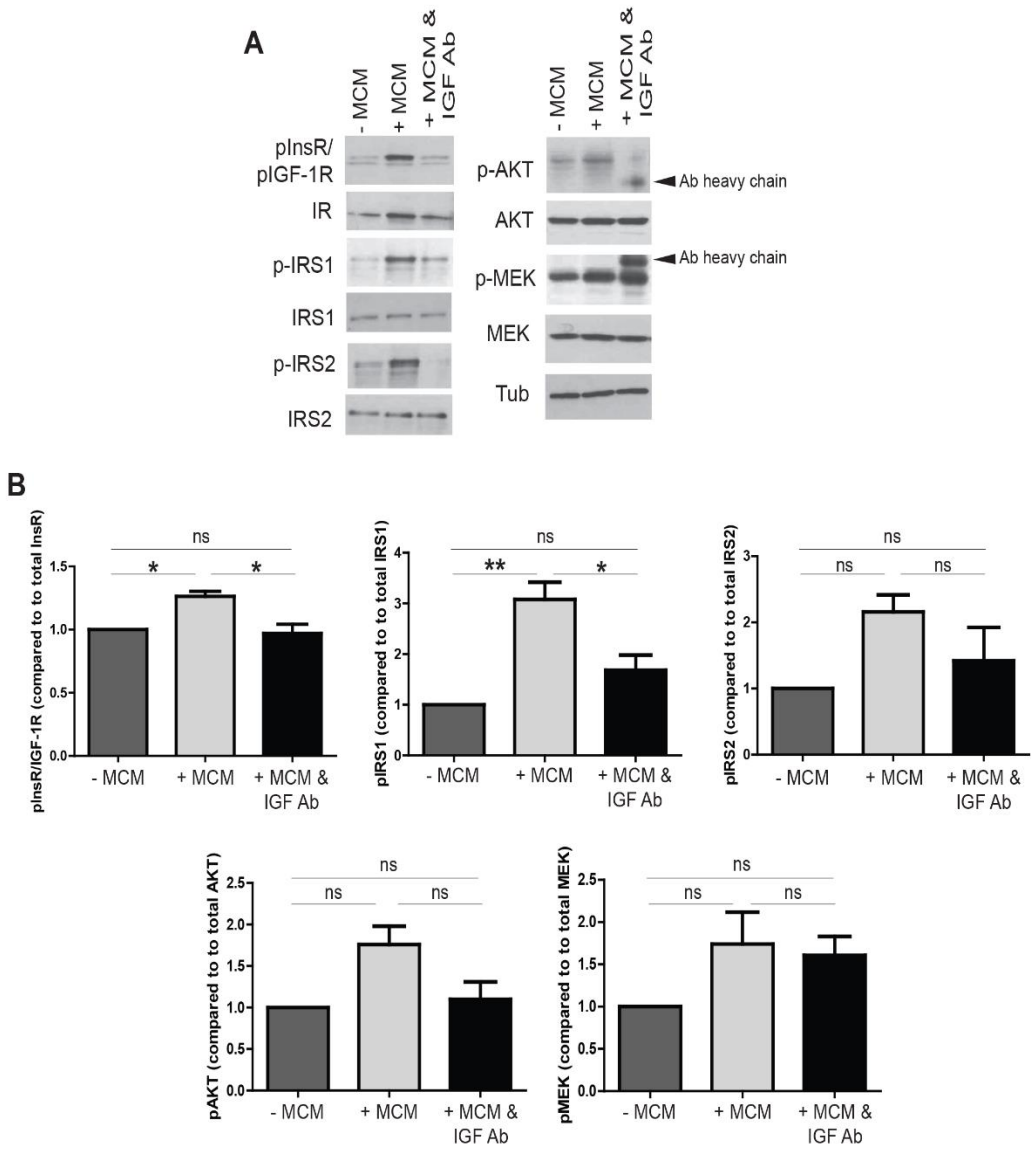

Figure 3.8 Incubation of PDAC cells with IGF blocking Ab prevents Ins/IGF-1R activation and downstream signalling

A) Immunoblotting analysis of SUIT-2 cells untreated or treated with MCM or MCM with IGF-blocking antibody (ab9572) for 3 hr. Probed for phospho insulin/IGF-1 receptors, total insulin receptor, phospho IRS1, total IRS1, phospho IRS2, total IRS2, phospho AKT, total AKT, phospho MEK, total MEK and tubulin loading control. Antibody heavy chains indicated. **B)** Quantification of western blot showing levels of p-insulin/IGF-1R compared to total Insulin receptor, p-IRS1 compared to total IRS1, p-IRS2 compared to total IRS2, p-AKT compared to AKT and p-MEK compared to total MEK, all relative to tubulin loading control. Error bars, SEM (n = 3 biological replicates); **, $p \leq 0.001$, *, $p \leq 0.01$, ns, non=significant using one-way ANOVA and Bonferroni post hoc test.

To investigate whether IGF signalling was directly responsible for induced chemoresistance in PDAC cells, KPC 3.5 cells were incubated with or without gemcitabine, MCM, IGF blocking Ab or rec IGF and cell death was measured using annexin V/PI staining. This confirmed the previous results that gemcitabine treatment alone induced significant cell death which was reduced with the addition of MCM (Fig 3.9). However, the addition of an IGF blocking Ab prevented MCM-mediated chemoresistance, suggesting IGF ligands are responsible for promoting cell survival towards gemcitabine challenge (Fig 3.9). This is supported by the fact rec IGF alone was sufficient to mediate chemoresistance towards gemcitabine in PDAC cancer cells (Fig 3.9).

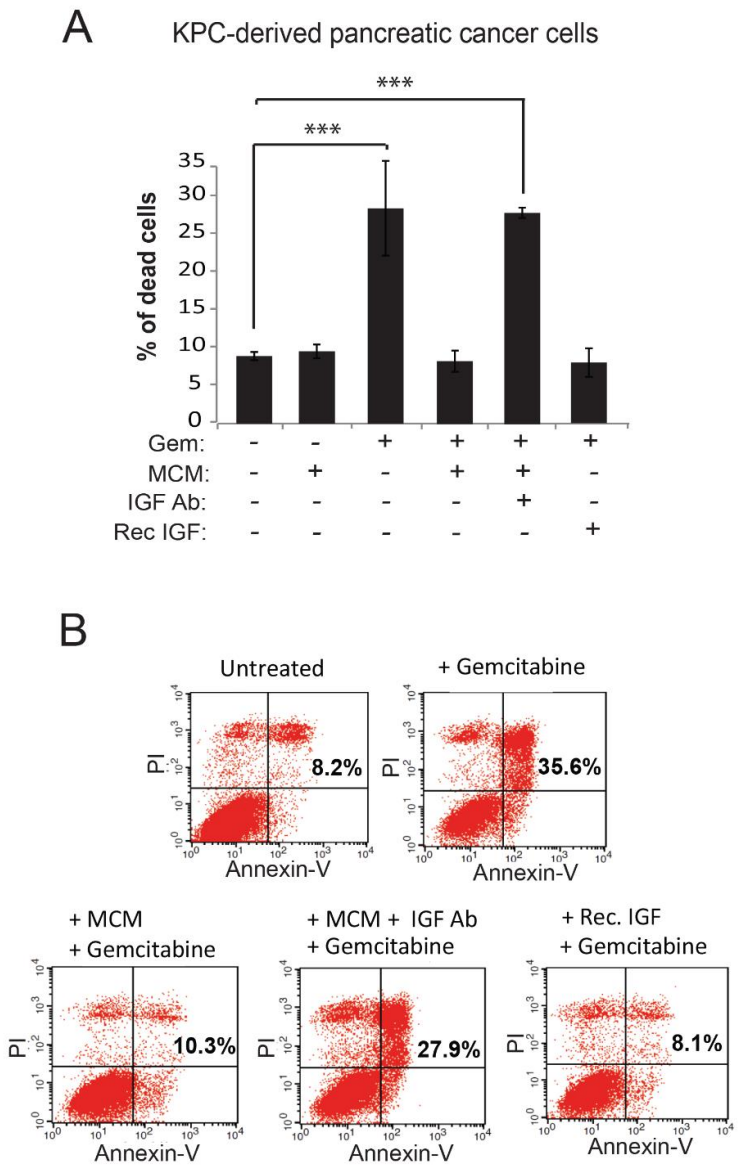

Figure 3.9 MCM and rec IGF promote chemoresistance in PDAC cells

A) Quantification of annexin V/PI detected cell death by FACS in primary mouse KPC-derived pancreatic cancer cells untreated or treated with gemcitabine (200 nmol/L), MCM, IGF blocking antibody (10 mg/mL), or recombinant IGF (100 ng/mL) for 24 hr. Error bars, SD. (n = 3 biological replicates); ***, $p \leq 0.005$ using one-way ANOVA and Tukey post hoc test. **B)** Representative flow cytometry dot blots of KPC-derived cells exposed to gemcitabine, MCM, IGF-blocking antibody, and recombinant IGF.

To confirm the results seen by flow cytometry, levels of cell death were analysed by immunoblotting for cleaved caspase-3 in KPC 3.5 cells treated with gemcitabine alone, or combination with MCM or recIGF (Fig 3.10 A). The significant levels of cell death were induced by gemcitabine alone, however in accordance with annexin V/PI staining, cell death was reduced with addition of either MCM or rec IGF (Fig 3.10 A and B).

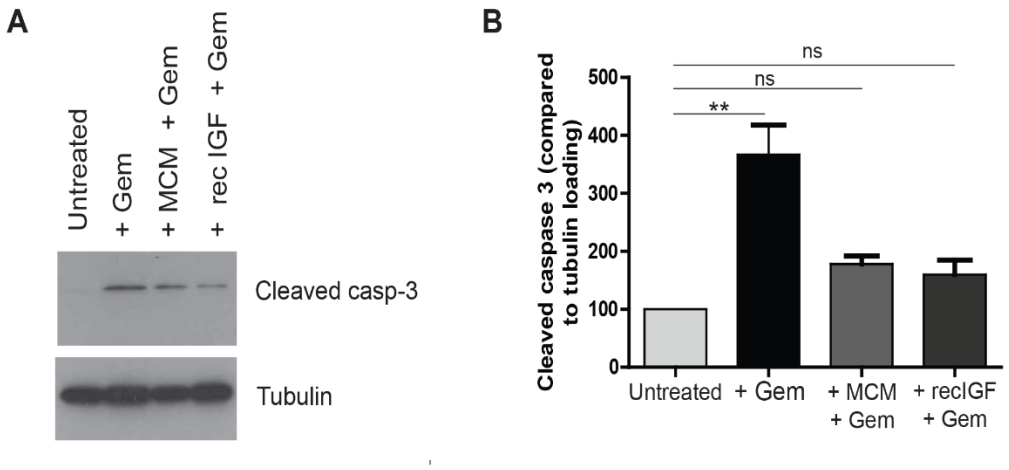

Figure 3.10 MCM and rec IGF decrease levels of cleaved caspase 3 in PDAC cells

A) Immunoblotting analysis for cell death of KPC 3.5 pancreatic cancer cells either untreated, treated with gemcitabine (200 nmol/L), MCM (2mL) with gemcitabine (200 nmol/L), or recombinant IGF (100 ng/mL) with gemcitabine (200 nmol/L) for 24 hr. Probed for cleaved caspase-3 expression as a cell death marker and tubulin as loading control. **B)** Quantification of cleaved caspase-3 expression levels detected by western blotting in treated KPC 3.5 cells, compared to tubulin loading control. Error bars, SEM (n = 3 biological replicates); **, $p \leq 0.001$, ns, non-significant, using one-way ANOVA and Bonferroni post hoc test.

To further investigate this phenomenon, to determine whether IGF signalling promoted resistance to other chemotherapeutic agents used to treat PDAC patients. Therefore, KPC 3.5 cells were treated with nab-paclitaxel alone at 10 nM, 100 nM, 1000 nM, or in combination with MCM or rec IGF and analysed by annexin V/PI staining. The addition of MCM or rec IGF significantly reduced cell death caused by nab-paclitaxel at all concentrations tested, although MCM reduced death to a slightly lesser extent than rec IGF (Fig 3.11)

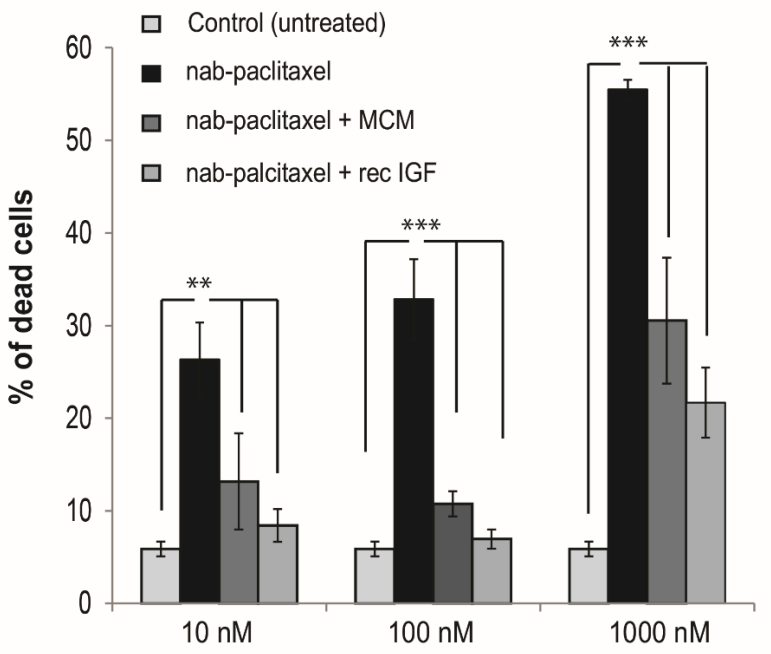

Figure 3.11 MCM and rec IGF promote chemoresistance towards Nab-paclitaxel

Quantification of cell death in KPC 3.5 cultured in the presence or absence of MCM or recombinant IGF and treated with 10, 100, or 1000 nmol/L nab-paclitaxel for 36 hr and indicated by annexin V/PI staining and flow cytometry analysis. Error bars, SD (n = 3); ***, $p \leq 0.005$; **, $p \leq 0.01$ using one-way ANOVA and Tukey post hoc test.

As IGF ligand activation of InsR and IGF-1R had been seen to promote resistance to gemcitabine and nab-paclitaxel in KPC 3.5 pancreatic cancer cells *in vitro*, it was important to investigate this phenomenon further using other PDAC cell lines. Human SUIT-2, human MIA-PaCa-2 and murine KPC 3.5 PDAC cells were grown *in vitro* and incubated with either gemcitabine, paclitaxel or 5-FU in combination MCM or MCM with IGF blocking Ab. Quantification of annexin V/PI staining showed MCM reduced cell death incidence in all three cell lines, treated with any of the three chemotherapeutic agents (Fig 3.12 A, B and C). This protective effect provided by MCM was reversed in all cells and treatments with the addition of IGF blocking Ab, thereby confirming IGF ligands as responsible for the induction of chemoresistance in this model (Fig 3.12 A, B and C).

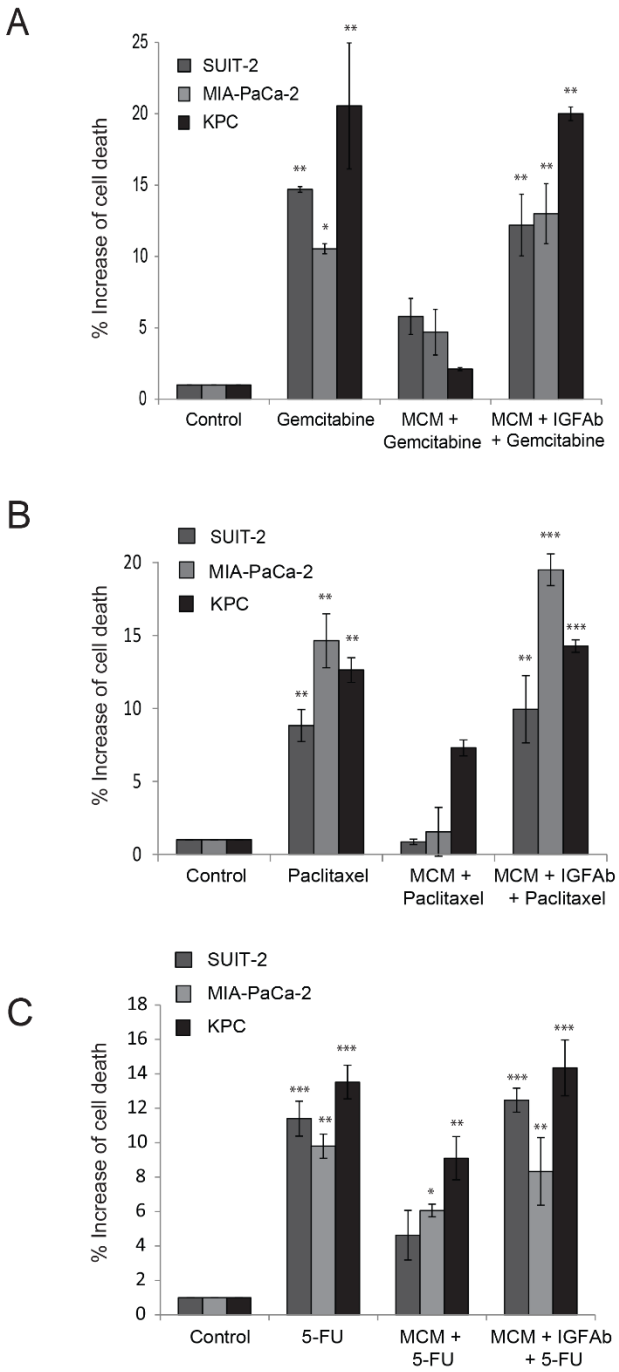

Figure 3.12 MCM enhances resistance of pancreatic cancer cells to gemcitabine, 5-FU and paclitaxel in an IGF-dependent manner.

Quantification of annexin V/PI stain detected cell death in human SUIT-2, MIA-PaCa-2 and murine KPC-derived pancreatic cancer cells. **A)** Treated with gemcitabine (200nmol/L), MCM and IGF blocking antibody (10 mg/mL) for 24 hr. **B)** Treated with paclitaxel (200nmol/L), MCM and IGF blocking antibody (10 mg/mL) for 24 hr. **C)** Treated with 5-FU (100nmol/L), MCM and IGF blocking antibody (10 mg/mL) for 24 hr. Error bars represent SEM (n=3 biological replicates), *** $p \leq 0.005$, ** $p \leq 0.01$, * $p \leq 0.05$ compared to control using one-way ANOVA and Tukey's post-hoc test.

The previous findings suggest an important role for macrophage-derived IGFs in the activation of the Ins/IGF-1R survival signalling in pancreatic cancer cells, thus enhancing resistance to chemotherapy. However, resistance was seen to be reduced with the addition of an IGF blocking antibody. Based on this data, IGF appears to be an attractive target in PDAC, deeming it necessary to determine whether the targeting of IGF ligands could have negative effects on cellular growth and survival in the absence of chemotherapy. To answer this question, KPC 3.5 cells were incubated with MCM, IGF-blocking Ab, or rec IGF alone to analyse perturbations in their cell cycle. This analysis showed incubation with either MCM, or rec IGF did not alter the survival or proliferation of cancer cells in the absence of chemotherapy (Fig 3.13). Importantly, incubation with an IGF blocking Ab did not have adverse effects of cell survival or proliferation suggesting it could be well tolerated *in vivo* (Fig 3.13).

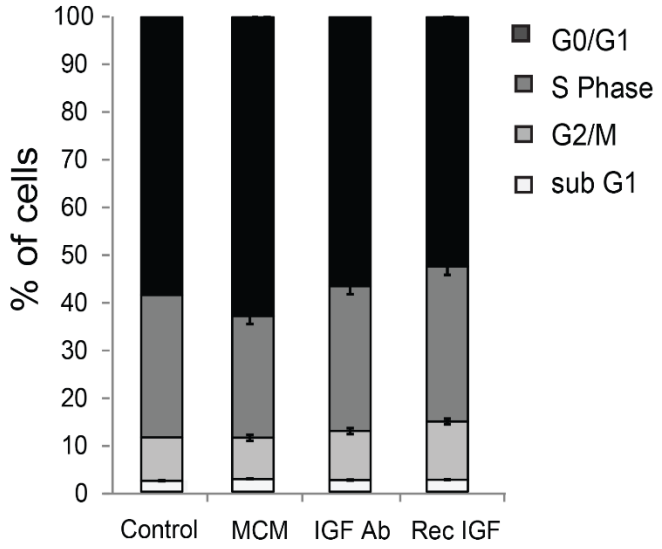

Figure 3.13 In the absence of chemotherapy, addition of MCM, IGF blockade or rec IGF does not affect proliferation or survival of pancreatic cancer cells. Cell cycle analysis of primary mouse KPC 3.5 cancer cells exposed to MCM, IGF blocking antibody (10 µg/mL) or recombinant IGF (100 ng/mL) for 3 hr. Quantification of propidium iodide incorporation into DNA detected by flow cytometry.

3.2.6 TAMS are a source of IGF ligands in the PDAC TME *in vivo*

Macrophage-derived IGF ligands have been shown to induce resistance to chemotherapy *in vitro.* However, *in vitro* cell culture can induce abnormalities in cell signalling, consequently it was necessary to confirm activation of Ins/IGF-1R on tumour cells and TAMs as IGF sources in the pancreatic TME *in vivo*.

To analyse IGF function *in vivo* an orthotopic PDAC mouse model was utilised using primary murine cancer cells derived from the KPC genetically engineered PDAC mouse model (Hingorani et al., 2005), These cells were surgically orthotopically implanted into the pancreas in syngeneic recipient mice and tumours grown for 29 days and subsequently harvested (Fig 3.14 A).

Hematoxylin and eosin (H&E) staining of the collected PDAC tissue revealed the orthotopic PDAC tumours had a distinctly altered ductal morphology compared to a naïve mouse pancreas, indicating the majority of tissue was PDAC (Fig 3.14 B). Immunohistochemical staining of the tumour tissue revealed infiltration by $CD206^{+}$ M2-like macrophages and increased activation of Ins/IGF-1R on tumour cells compared to naïve pancreas (Fig 3.14 B).

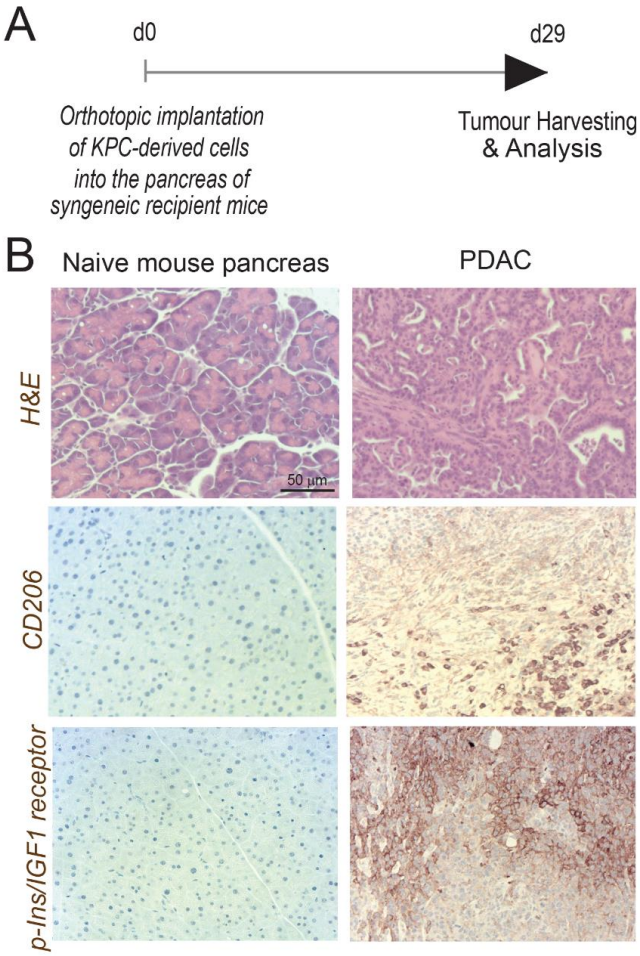

Figure 3.14 Orthotopic PDAC tumours are infiltrated by macrophages and have active phosphorylated Ins/IGF-1R

KPC-derived tumour cells were orthotopically implanted into the pancreas tail of syngeneic recipient mice. Pancreas from naïve mice and pancreatic tumours from implanted mice were harvested day 29 after implantation. Images show H&E, CD206, and phospho-insulin/IGF-1 receptor staining of naïve mouse pancreas and murine PDAC tissue samples, scale bar 50 µm.

Further characterisation of the tumours revealed an increased infiltration by $CD68^+$ macrophages and the increased presence of cancer-associated fibrosis comprised of αSMA^+ myofibroblasts (Fig 3.15 A and B). Immunofluorescent staining of the same tumour tissue for $EpCAM^+$ tumour cells and αSMA^+ CAFs confirmed the myofibroblast rich stromal surrounds the PDAC tumour cells (Fig 3.15 C), a phenomenon which is also seen in human PDAC as fibrosis can account for up to 80 % of the tumour mass (Gunderson et al., 2016, Zhu et al., 2014, Pylayeva-Gupta et al., 2016, Torres et al., 2013). These results suggest the human PDAC disease phenotype was recapitulated in multiple orthotopically implanted mice.

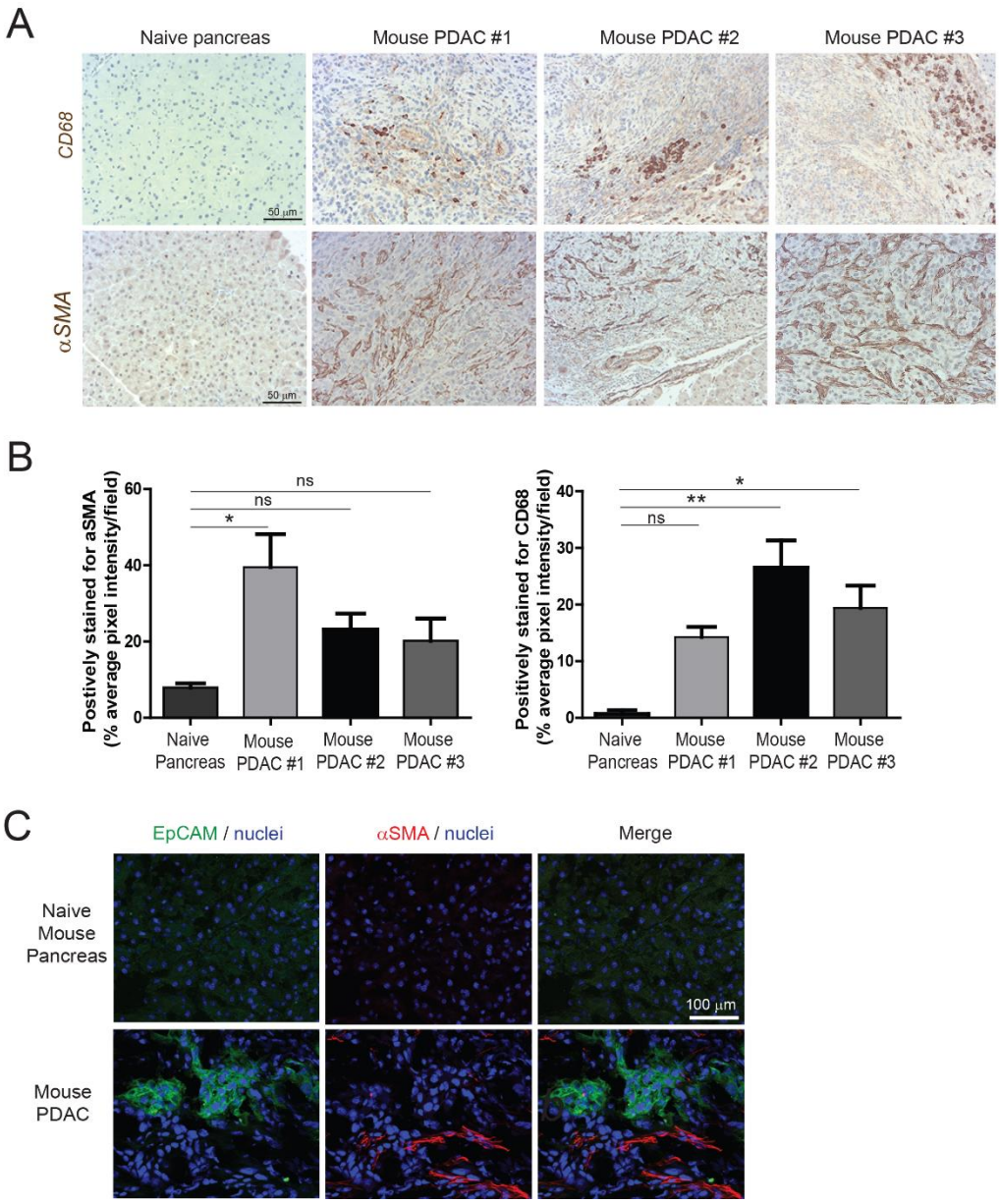

Figure 3.15 Macrophages and CAFs infiltrate orthotopic PDAC tumours

A) Immunohistochemical staining of αSMA and CD68 in paraffin embedded tissues from naïve mouse pancreas and orthotopic mouse pancreatic tumours. Scale bar, 50 μm. **B)** Quantification of immunohistochemical staining of αSMA+ myofibroblasts and CD68+ macrophages in naïve pancreas and PDAC tumour-bearing mice. Error bars, SEM (n=3 images per mouse). **C)** Immunofluorescent staining of EpCAM (green), αSMA (red) and nuclei (blue) in frozen tissues from naïve mouse pancreas and orthotopic mouse pancreatic tumours. Scale bar, 100 μm.

Therefore, to determine whether the *in vitro* findings of macrophage-derived IGF induced chemoresistance was also recapitulated *in vivo*, F4/80$^+$ TAMs and F4/80$^-$ cells were FACS sorted from the tumour tissue. qPCR analysis revealed F4/80$^+$ TAMs expressed higher levels of both *Igf-1* and *Igf-2* compared to F4/80$^-$ cells, suggesting macrophages are still sources of IGF ligands *in vivo* (Fig 3.16).

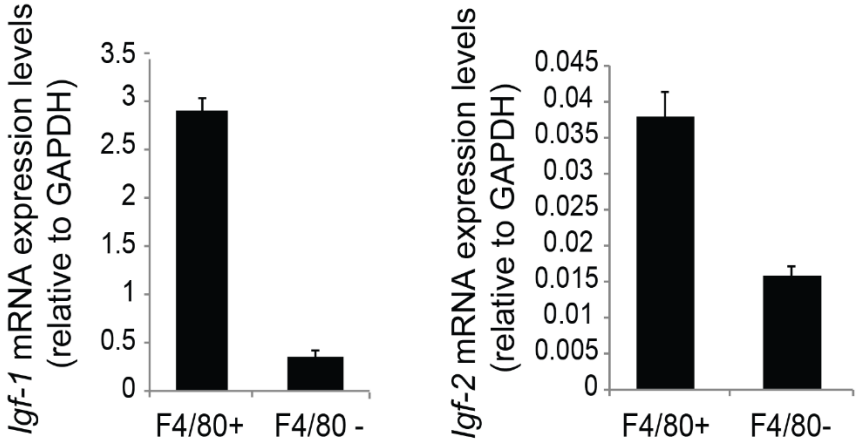

Figure 3.16 F4/80$^+$ TAMs express high levels of *Igf*-1 and *Igf-2*
Quantification of *Igf-1* (left) and *Igf-2* (right) mRNA expression levels in F4/80$^+$ macrophages and F4/80$^-$ mixed cell population, FACS sorted from digested murine orthotopic pancreatic tumours. Error bars, SD (n = 3 technical replicates).

To confirm this result, a second KPC-derived cell line stably transfected with zsGreen reporter gene, FC1242 luc/zsGreen, were orthotopically implanted into the pancreas of syngeneic recipient C57BL/6J mice and tumours were harvested 23 days after implantation (Fig 3.17 A). The harvested tumours were stained and FACS sorted for tumour cells (Sytox$^-$, CD45$^-$, zsGreen$^+$), non-immune stromal cells (Sytox$^-$, CD45$^-$, zsGreen$^-$), M1-like macrophages (Sytox$^-$, CD45$^+$, F4/80$^+$, CD206$^-$) and M2-like macrophages (Sytox$^-$, CD45$^+$, F4/80$^+$, CD206$^+$) (Fig 3.17 B). Knowing that myofibroblasts can account for up to 80 % of the tumour mass, the sorted non-immune stromal cells were analysed by qPCR which revealed high levels of αSMA expression typical of activated fibroblasts (Fig 3.17 C).

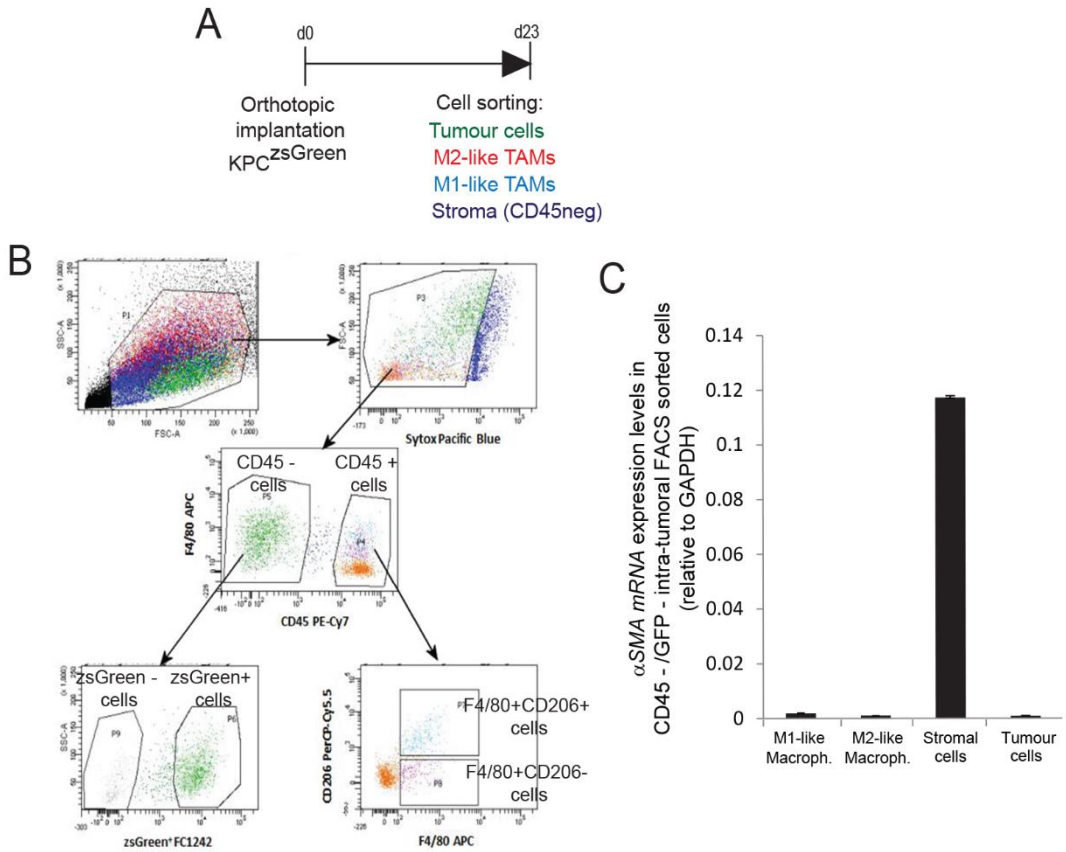

Figure 3.17 FACS sorted non-immune stromal cells express high levels of αSMA myofibroblast marker

A) KPC-derived tumour cells, FC1242 luc/zsGreen, were orthotopically implanted into the pancreas of syngeneic recipient (C57BL/6J) mice. Tumours were harvested and digested at day 23 after implantation and tumour cells, non-immune stromal cells, M1-like and M2-like macrophages were sorted by flow cytometry. **B**) Gating strategy used to sort $CD45^-/zsGreen^+$ KPC-derived tumour cells, $CD45^-/zsGreen^-$ non-immune stromal cells, $CD45^+/F4/80^+/CD206^-$ M1-like macrophages and $CD45^+/F4/80^+/CD206^+$ M2-like macrophages from mouse pancreatic tumours. **C**) Quantification of *αSMA* mRNA expression levels in the FACS sorted populations isolated from pancreatic tumours (n=3 technical replicates).

To confirm macrophages as a source of IGF ligands in the new orthotopic mouse model TME, the FACS sorted populations were analysed by qPCR. M2-like macrophages and αSMA$^+$ myofibroblasts were shown to be sources of *Igf-1* and *Igf-2* expression in the orthotopic model (Fig 3.18).

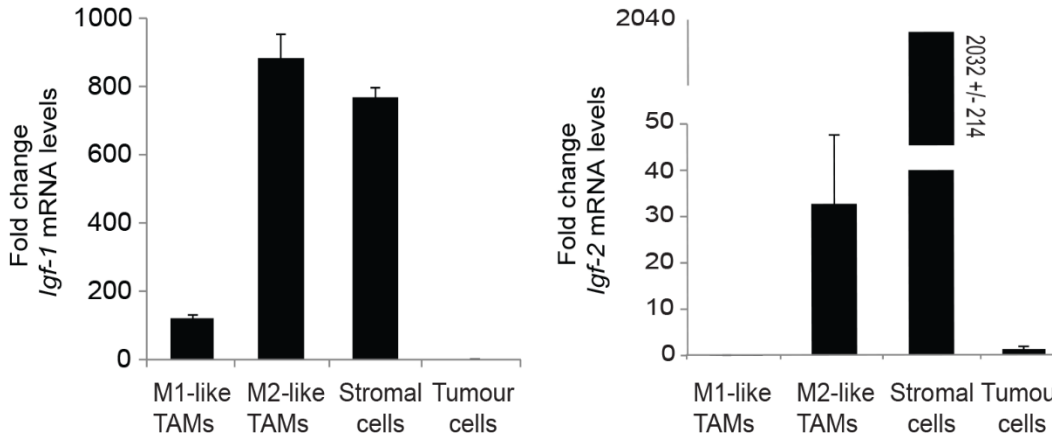

Figure 3.18 M2-like TAMs and αSMA$^+$ stromal cells express the high levels of *Igf*-1 and *Igf-2*

Quantification of *Igf-1* (left) and *Igf-2* (right) mRNA expression levels in CD45$^+$/F4/80$^+$/CD206$^-$ M1-like macrophages, CD45$^+$/F4/80$^+$/CD206$^+$ M2-like macrophages, CD45$^+$/zsGreen$^+$ non-immune stromal cells, and CD45$^+$/zsGreen$^+$ tumour cells isolated from murine pancreatic tumours. Error bars, SD (n = 3 technical replicates).

3.2.7 αSMA$^+$ myofibroblasts are also stromal producers of IGF-1 and IGF-2

It was interesting to find αSMA$^+$ non-immune stromal cells also expressed a high level of *Igf-1* and *Igf-2.* Both myofibroblasts and macrophages are abundant in the PDAC TME and CAFs may also be responsible for activation of the InsR and IGF-1R on PDAC tumour cells. To confirm this, pancreatic stellate cells (PaSCs) were isolated from naïve mouse pancreas and cultured on plastic to induce activation confirmed by αSMA expression (Fig 3.19).

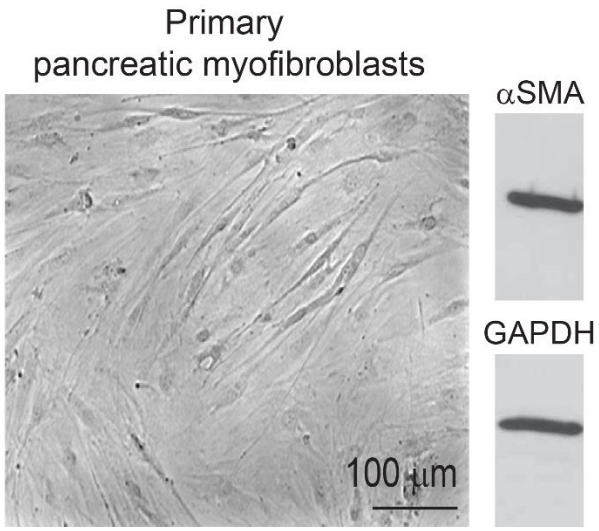

Figure 3.19 PaSCs express αSMA when activated

Left, Light microscopy image of primary isolated, activated murine PaSCs in culture. Scale bar 100 μm. Right, immunoblotting of αSMA and GAPDH as loading control of primary mouse activated PaSCs.

To create CAFs, freshly isolated and activated PaSCs were incubated with tumour conditioned media (TCM). qPCR analysis showed myofibroblasts expressed both *Igf-1* and *Igf-2* under basal conditions (Fig 3.20 A). However, the addition of TCM to the culture enhanced expression levels of both *Igf-1* and *Igf-2* (Fig 3.20 A). Myofibroblast conditioned media (MyoCM) and cell lysates confirmed the qPCR results, detecting IGF-1 and IGF-2 as both expressed and secreted (Fig 3.20 B).

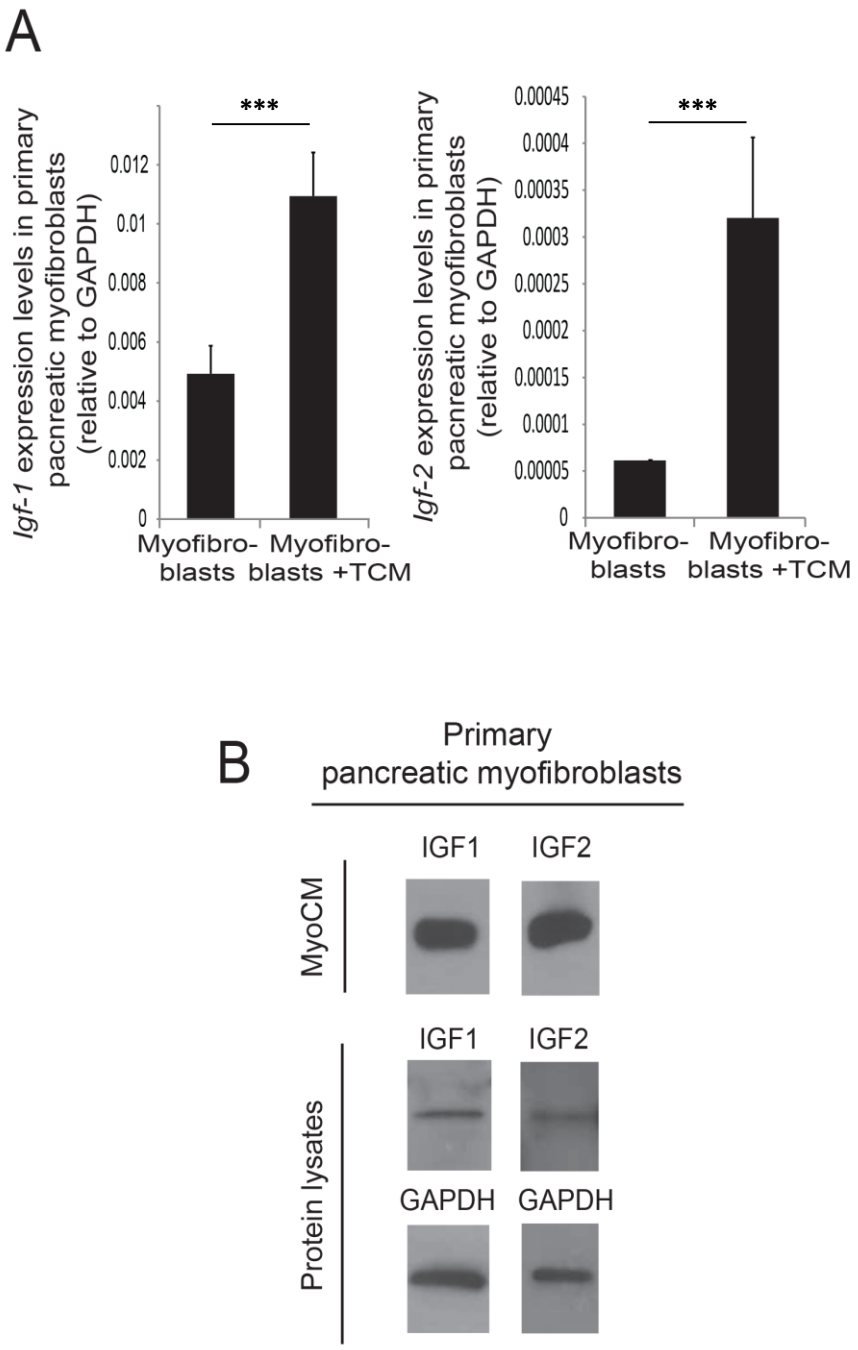

Figure 3.20 Myofibroblasts express IGF-1 and IGF-2

A) Quantification of *Igf-1* (left) and *Igf-2* (right) mRNA expression levels in pancreatic myofibroblasts exposed or unexposed to KPC-derived tumour conditioned media (TCM). Error bars, SEM (n = 3 biological replicates each with 3 technical replicates) *** p-value ≤ 0.0001 using unpaired t test. **B)** Immunoblotting analysis of IGF-1 and IGF-2 ligands in pancreatic myofibroblast conditioned media (MyoCM) and myofibroblast lysates. GAPDH loading control.

Previously, MCM was used to promote chemoresistance in tumour cells when challenged with gemcitabine, paclitaxel or 5-FU *in vitro* (Fig 3.12). After discovering myofibroblasts as another stromal source of IGFs, it was necessary to investigate whether IGFs in MyoCM could reproduce this phenomenon. Therefore, PDAC tumour cells were incubated with either gemcitabine, paclitaxel or 5-FU alone or with MyoCM and/or IGF blocking Ab to assess changes in cell survival. Quantification of annexin V/PI staining revealed all the chemotherapeutic agents significantly induced tumour cell death (Fig 3.21). Yet, the addition of MyoCM reduced levels cell death levels in all treatments which was reversed with the addition of IGF blocking antibody (Fig 3.21).

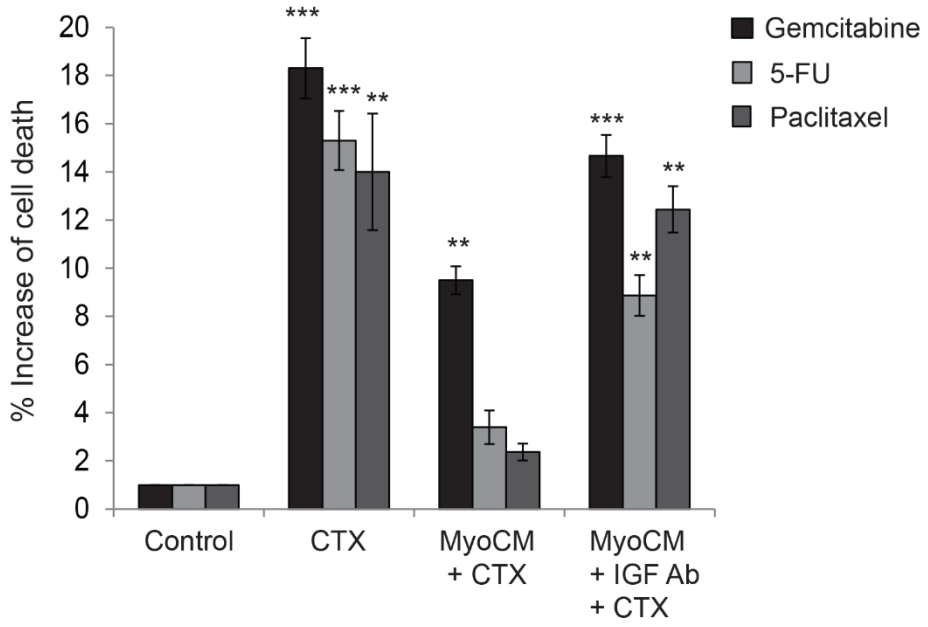

Figure 3.21 MyoCM confers resistance to neoplastic agents which is alleviated by addition of IGF blocking Ab

Quantification of annexin V/PI detected cell death in KPC-derived pancreatic cancer cells treated with gemcitabine, paclitaxel or 5-FU, myofibroblast conditioned media (MyoCM) or IGF blocking antibody for 24 hr. Error bars represent SEM (n=3 biological replicates), *** $p \leq 0.005$, ** $p \leq 0.01$, * $p \leq 0.05$ compared to control using one-way ANOVA and Tukey's post-hoc test.

3.2.8 Blockade of IGFs improves response to gemcitabine in a preclinical model of PDAC

Macrophages and myofibroblasts are the most abundant non-malignant stromal cells within the TME in PDAC (Feig et al., 2012). The previous results had shown TAMs and CAFs from the orthotopic PDAC TME expressed and secreted IGF-1 and IGF-2. These ligands induced resistance to chemotherapy in PDAC cells treated *in vitro*, which was reversed with the addition of an IGF blocking Ab.

To test whether this phenomenon was seen in the *in vivo* preclinical model, mice were orthotopically implanted with FC1242 luc/zsGreen KPC-derived tumour cells and treated with isotope control IgG antibody (n=6), gemcitabine alone (n=6), xentuzumab IGF-1/2 blocking Ab alone (n=6) or gemcitabine in combination with xentuzumab (n=6) (Fig 3.22 A).

Size and weight of the harvested tumours revealed gemcitabine treatment alone had little effect on primary tumour growth in this model (Fig 3.22 B). Xentuzumab IGF-blocking Ab (Boehringer Ingelheim) treatment alone showed only a modest effect on restricting tumour growth, however when used in combination with gemcitabine, tumour size was significantly reduced compared to gemcitabine alone (Fig 3.22 B)

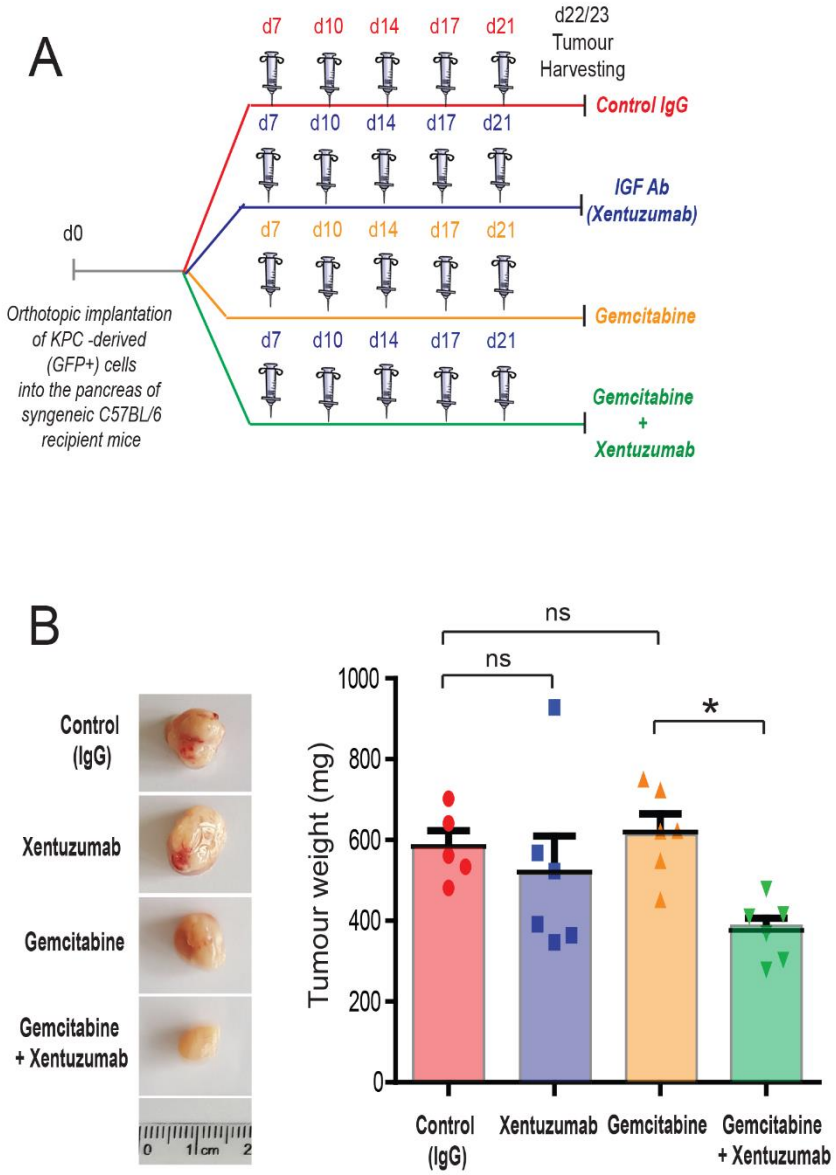

Figure 3.22 Combination Tx of xentuzumab with gemcitabine reduces tumour size

A) FC1242 luc/zsGreen-derived pancreatic tumour cells were orthotopically implanted into the pancreas of syngeneic C57BL/6J recipient mice. Starting at day 7 after implantation, mice were treated bi-weekly by intraperitoneal injection with either control IgG antibody, gemcitabine (100 mg/kg), IGF-blocking antibody xentuzumab (100 mg/kg), or a combination of gemcitabine with xentuzumab. **B)** Representative images of tumours at harvest and tumour weights (n = 6 mice per group); *, $p \leq 0.05$ using one-way ANOVA and Tukey post hoc test.

Immunohistochemical staining of the harvested tumour tissue confirmed xentuzumab treatment alone and in combination with gemcitabine reduced activation of Ins/IGF-1R on PDAC cells by preventing stimulation by IGF ligands (Fig 3.23 A).

To interpret how combination xentuzumab with gemcitabine treatment reduced tumour size, the tissues were also stained for cleaved caspase-3 as a marker of cell death (Fig 3.23 A). Quantification of cleaved caspase-3 revealed significantly higher levels of cell death in combination gemcitabine and xentuzumab treated tumours compared to control IgG, gemcitabine alone, or xentuzumab alone (Fig 3.23 B).

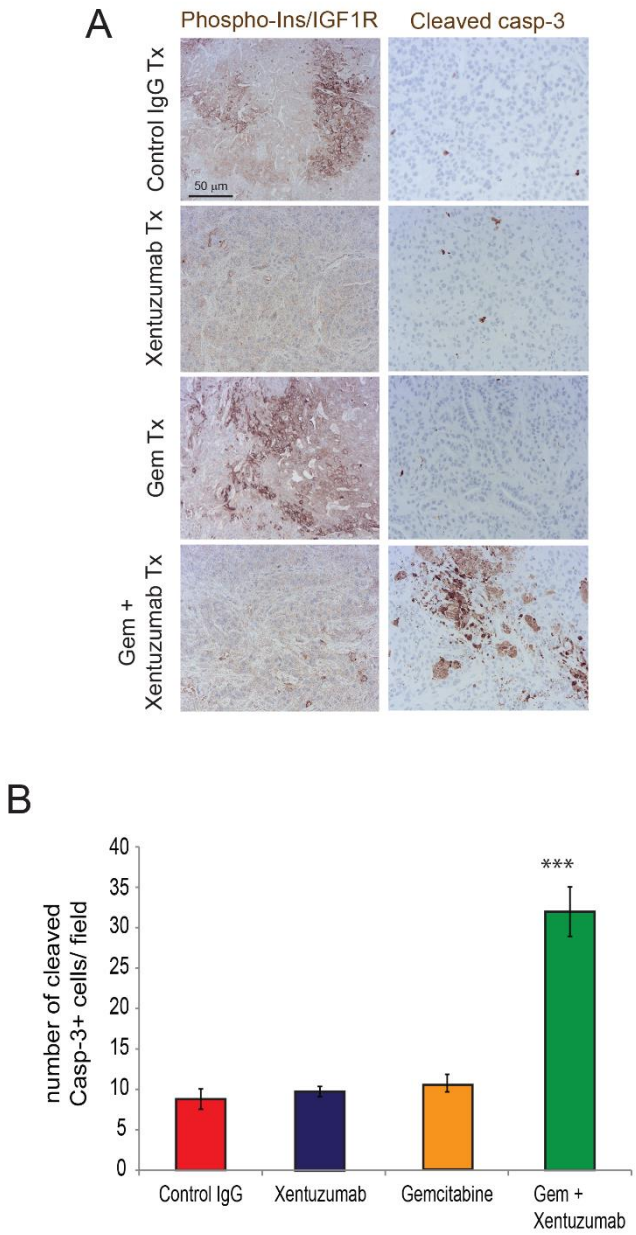

Figure 3.23 Xentuzumab with gemcitabine treatment increases levels of tumour cell death

A) Immunohistochemical staining of phospho-Ins/IGF-1R and cleaved caspase-3 in pancreatic tumours treated with IgG (control), gemcitabine, xentuzumab IGF-blocking antibody, or gemcitabine with xentuzumab. **B)** Quantification of cleaved caspase-3 positive dead cells in tumours treated with IgG (control), gemcitabine, xentuzumab IGF-blocking antibody, or gemcitabine with xentuzumab (8–11 fields counted/ mouse tumour); ***, $p \leq 0.005$ compared with other treatment groups, using one-way ANOVA and Tukey post hoc test.

To confirm the results of the *in vivo* experiment, it was repeated but instead using a commercially available IGF blocking Ab (ab9572, Abcam) which was previously used *in vitro*. Tumours were grown for 21 days and treated three times with either control IgG, gemcitabine alone or gemcitabine in combination with ab9572 IGF blocking Ab by intraperitoneal injection (Fig 3.24 A). Tumours harvested 30 days after implantation again revealed a significant decrease in size in the combination gemcitabine with ab9572 IGF blocking Ab treated mice compared to control IgG and gemcitabine alone treatments (Fig 3.24 B).

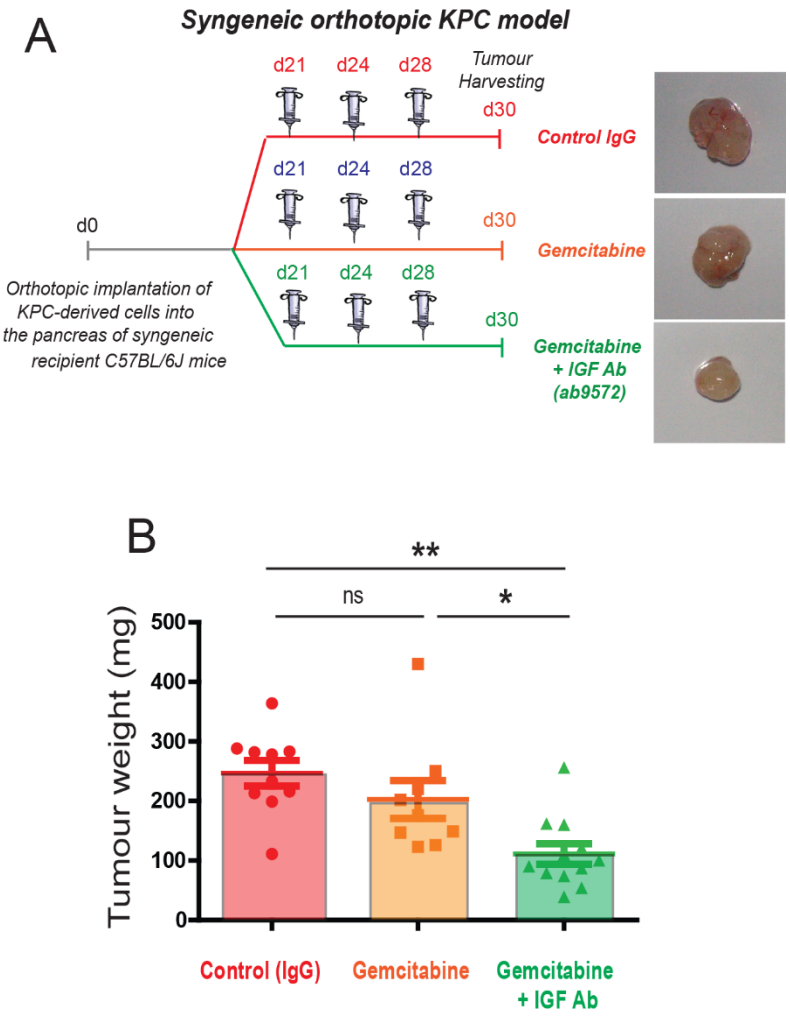

Figure 3.24 Gemcitabine treatment in combination with IGF-blocking Ab decreases tumour growth

A) FC1242 luc/zsGreen pancreatic cancer cells were orthotopically implanted in the pancreas of syngeneic recipient mice. Mice were treated by intraperitoneal injection twice a week with IgG antibody, gemcitabine alone, or gemcitabine with an IGF-blocking antibody (ab9572). Tumours were harvested at day 30 and representative images are shown. **B)** Tumour weights are shown (n = 9–12 mice per group). **, $p \leq 0.01$; *, $p \leq 0.05$ using one-way ANOVA and Tukey post hoc test.

Immunohistochemical staining for pInsR and pIGF-1R revealed the ab9572 IGF-blocking antibody reduced activation of InsR and IGF-1R to a similar extent as xentuzumab (Fig 3.25).

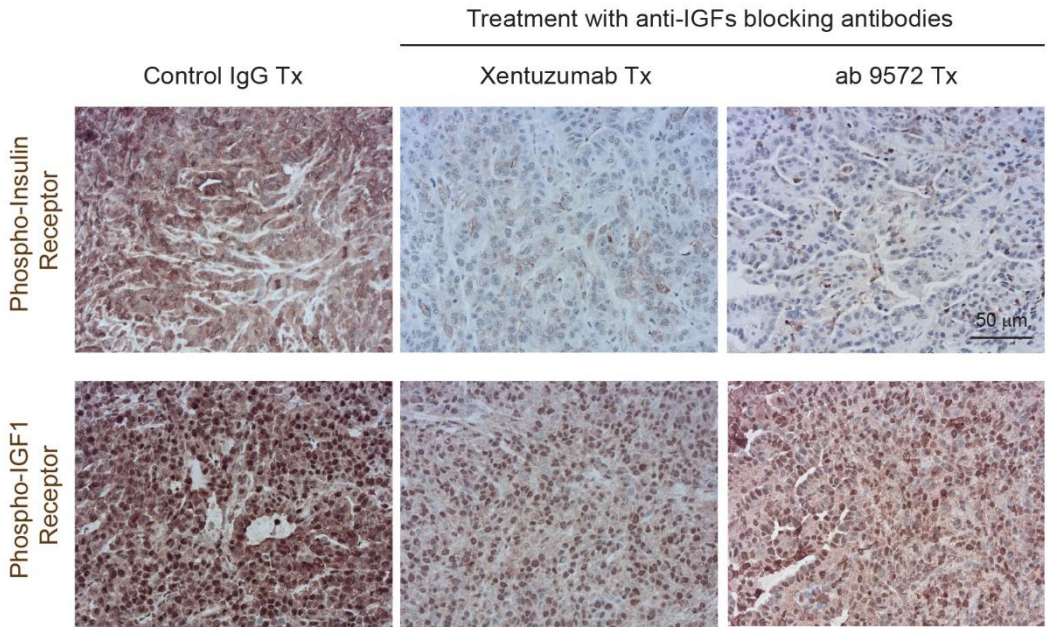

Figure 3.25 IGF blockade decreases activation of InsR and IGF-1R in murine pancreatic tumours

Comparison of insulin and IGF-1 receptor activation in control treated, xentuzumab IGF blocking Ab treated or ab9572 IGF blocking Ab treated mice. Immunohistochemical staining of phospho-Insulin receptor (top) and phospho-IGF-1 receptor (bottom) in control (IgG) treated mouse pancreatic tumours, and tumours treated with IGF blocking antibodies xentuzumab and ab9572 (n=1 mouse per stain). Scale bar, 50 µm.

Staining of pIns/IGF-1R confirmed receptor activation in IgG and gemcitabine treated tissues (Fig 3.26 A).To confirm a reduction in tumour size was due to increase gemcitabine efficacy and therefore increased cell death, tissues were stained for cleaved caspase-3 (Fig 3.26 A). Cleaved caspase-3 levels were confirmed as significantly higher in mice treated with gemcitabine and ab9572 IGF-blocking Ab (Fig 3.26 B).

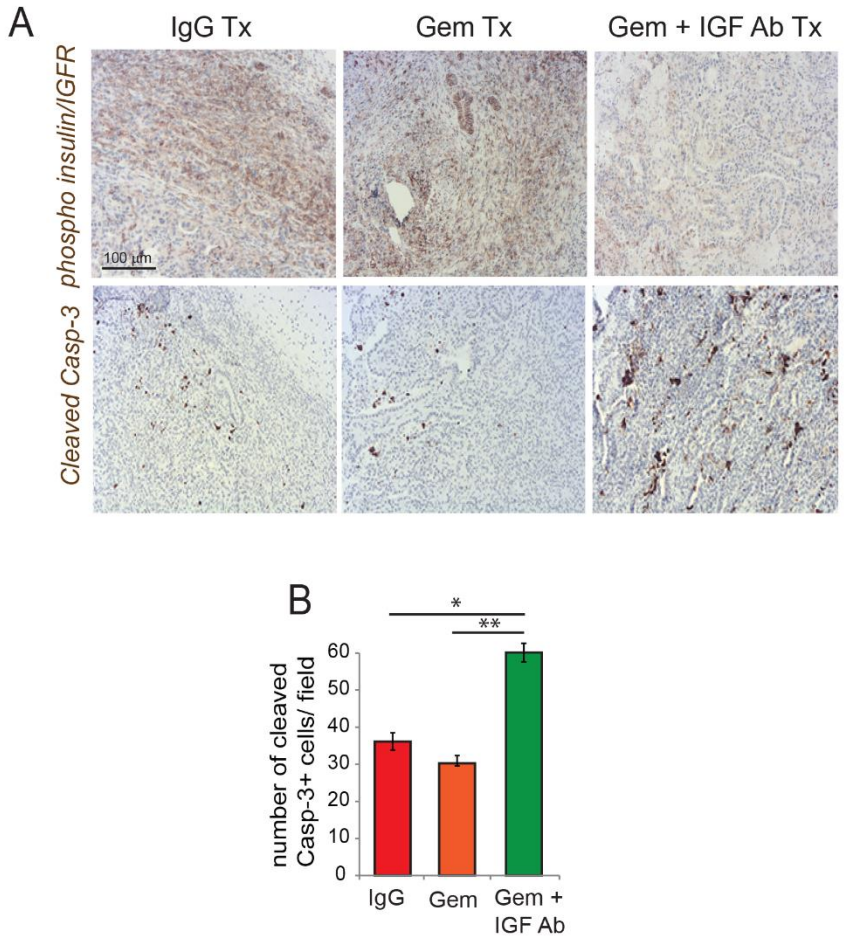

Figure 3.26 Combination treatment gemcitabine with ab9572 IGF-blocking Ab increases cell death

A) Immunohistochemical staining of phospho-insulin/IGF-1R, and cleaved caspase-3 in pancreatic tumours treated with IgG, gemcitabine, or gemcitabine with IGF-blocking antibody ab9572. **B)** Quantification of cleaved caspase-3 positive dead cells in pancreatic tumours from mice treated with IgG control antibody, gemcitabine, or gemcitabine with ab9572 IGF-blocking antibody (6–8 fields counted/mouse tumour), **, $p \leq 0.01$ using one-way ANOVA and Tukey post hoc test.

3.2.9 Paclitaxel or 5-FU in combination with xentuzumab increases levels of cell death

Although gemcitabine is the current standard of care for PDAC patients, it is not the only chemotherapy used for patient treatment. As previously shown *in vitro,* MCM and MyoCM confer resistance to tumour cells when challenged with gemcitabine, 5-FU or paclitaxel (Fig 3.12 and Fig 3.21). This trait was confirmed in PDAC *in vivo* models treated with gemcitabine. Therefore, it was also important to investigate whether IGF signalling promoted chemoresistance against 5-FU and paclitaxel *in vivo*.

To determine whether 5-FU or paclitaxel would have a similar synergy with xentuzumab treatment, FC1242 luc/zsGreen cells were implanted into C57BL/6J mice and divided into the treatment groups; control IgG (n=6), 5-FU (n=6), 5-FU with xentuzumab (n=6), paclitaxel (n=6) and paclitaxel with xentuzumab (n=6) for a total of 5 treatments (Fig 3.27 A). The weights of the harvested tumours revealed the combination treatments of 5-FU with xentuzumab and paclitaxel with xentuzumab both caused a slight decrease in tumour growth in this model (Fig 3.27 B).

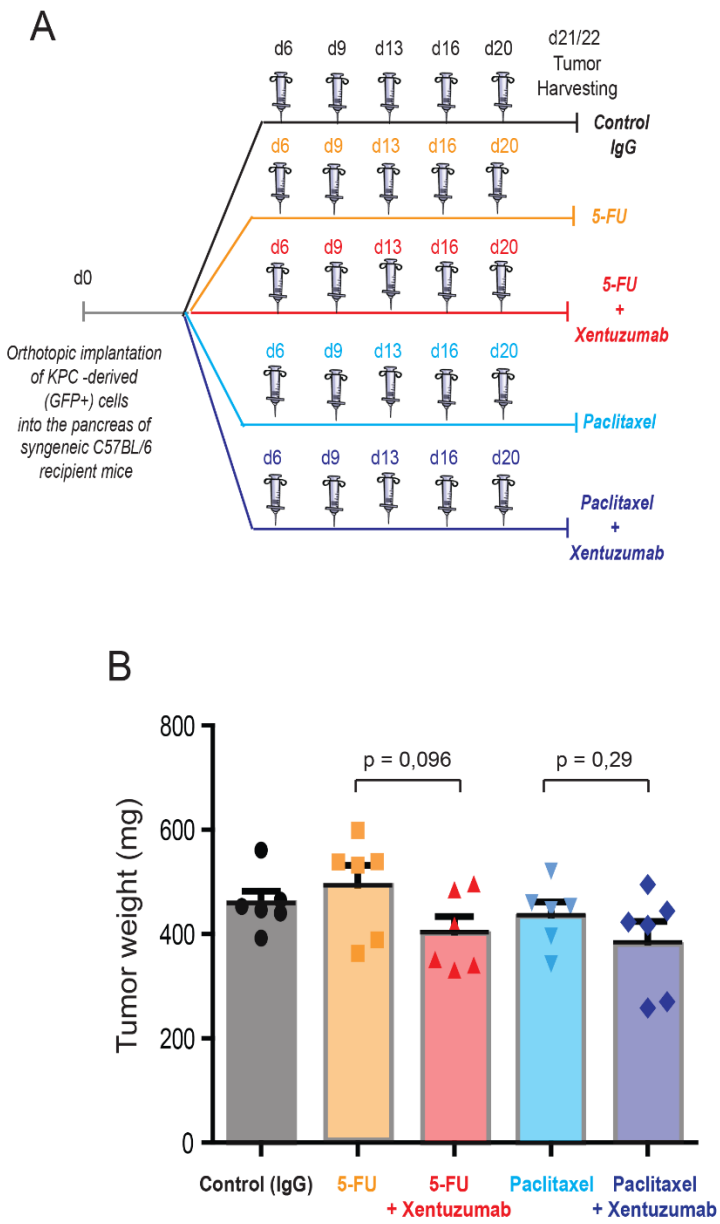

Figure 3.27 5-FU and paclitaxel with xentuzumab modestly reduces tumour size

A) FC1242 luc/zsGreen derived pancreatic tumour cells were orthotopically implanted into the pancreas of syngeneic C57BL/6J recipient mice, and mice were treated, starting at day 6 after tumour implantation, bi-weekly i.p., with either control IgG antibody, 5-FU (50 mg/kg), paclitaxel (10 mg/kg), a combination of 5-FU with xentuzumab (100 mg/kg) or a combination of paclitaxel with xentuzumab. **B)** Tumour weights (n=6 mice per group); p values obtained using unpaired two tailed T-test.

Levels of cleaved caspase-3 showed an increase in cell death in both combination treatment groups, however not by a large margin (Fig 3.28). Taken together, these findings indicate that functional blockade of IGFs significantly increases the response of pancreatic tumours to mainly gemcitabine *in vivo*.

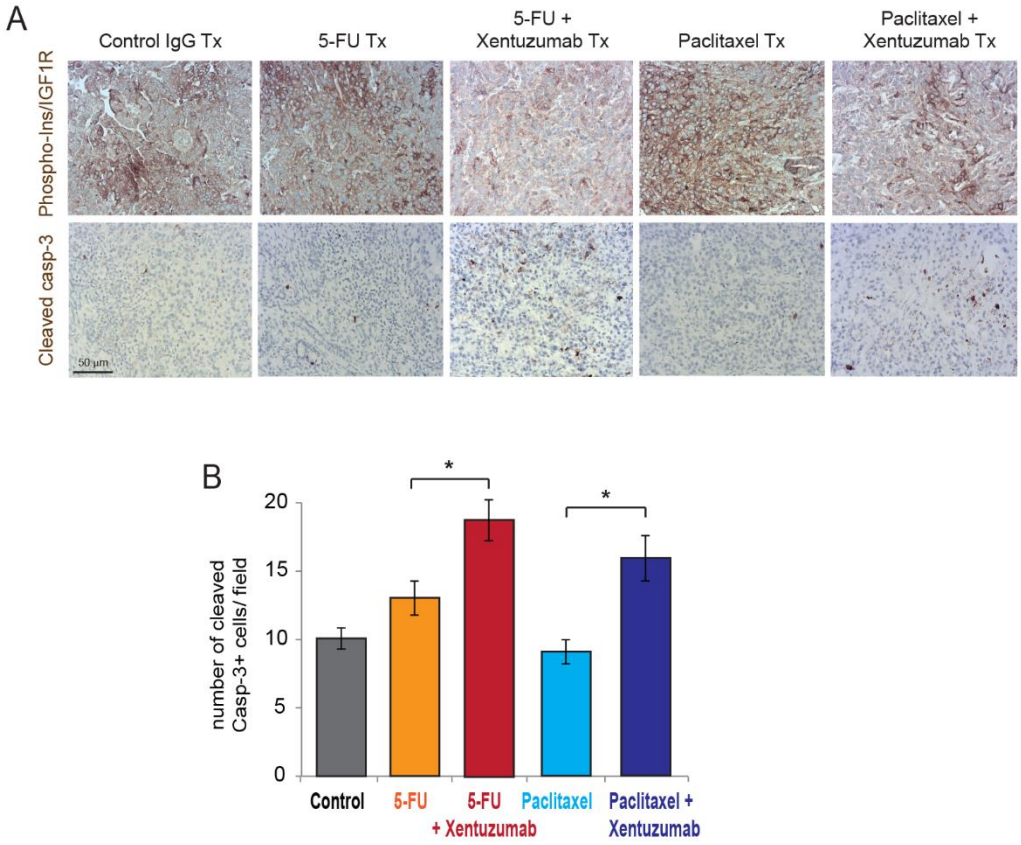

Figure 3.28 Combination of 5-FU and paclitaxel with xentuzumab significantly increased levels of cell death

A) Immunohistochemical staining of phospho-Ins/IGF-1R and cleaved caspase-3 in pancreatic tumours treated with IgG (control), 5-FU, 5-FU with xentuzumab, paclitaxel, and paclitaxel with xentuzumab. Scale bar, 50 µm. **B)** Quantification of cleaved caspase-3 positive dead cells in tumours treated with IgG (control), 5-FU, 5-FU with xentuzumab, paclitaxel, and paclitaxel with xentuzumab (3-5 fields counted/ tumour tissues from 5-6 mice per treatment group), * $p \leq 0.05$ using unpaired two tailed T-test.

3.3 DISCUSSION

The findings described in this chapter indicate that stromal-derived IGF-1 and IGF-2 from TAMs and CAFs are inducers of chemoresistance in KPC-derived PDAC cells *in vitro* and *in vivo* against gemcitabine administration. The results obtained using an orthotopic preclinical PDAC model suggest the use of IGF-blocking antibodies in combination with chemotherapy, specifically gemcitabine, may increase effectiveness of gemcitabine treatment of pancreatic cancer patients.

The role of the TME in response to chemotherapy has been subject to speculation due to the TME's bi-directional signalling with tumour cells which can influence many aspects of tumour progression. Based on the findings in this chapter, TAMs and CAFs, the most abundant cells in the PDAC TME, appear to play a direct role in the induction of chemoresistance in pancreatic cancer cells against gemcitabine. TAM and CAF-secreted IGFs participate in a paracrine signalling loop which bind and activate the InsR and IGF-1R on tumour cells activating survival pathways thereby reducing the response of pancreatic cancer cells to chemotherapy, specifically gemcitabine.

In agreement with the findings described here, a recent study using a proteomic approach has reported fibroblasts secrete IGF after exposure to KPC-pancreatic tumour cells, promoting cancer cell survival and increased proliferation *in vitro* (Tape et al., 2016). In this chapter, it has further been confirmed that IGF production by both fibroblasts and macrophages in the TME occurs in PDAC tumours *in vivo* and contributes towards tumour cell survival.

Chemoresistance is a large obstacle in effective PDAC treatment, it has routinely been shown that gemcitabine administration has little effect in PDAC patients (Mitchem et al., 2013, Gunderson et al., 2016, Zhu et al., 2014). Our preclinical PDAC

model mimicked this modest response and has further shown that IGF signalling induced resistance towards gemcitabine in this model. Thus revealing the therapeutic opportunity of combining IGF inhibition, with gemcitabine, the current standard chemotherapeutic for PDAC. In orthotopic preclinical models of PDAC used here, inhibition of IGFs increased PDAC sensitivity to gemcitabine shown by a reduction in tumour size and increased levels of cell death within the primary tumour mass. However, further studies should be undertaken to elucidate the exact mechanism behind IGF's effect on gemcitabine efficacy. Such as whether increased amounts of gemcitabine are taken up in response to IGF blockade or whether downstream effectors of gemcitabine metabolism are affected.

So far IGF-1R inhibitors have been unsuccessful in PDAC in the clinic, often due to aberrations in metabolism (Zha et al., 2010, Guha, 2013, King et al., 2014, Gradishar et al., 2016). However, IGF blocking Ab's, such as xentuzumab used here, are being developed to bind IGF ligands and prevent proliferative but not metabolic signalling. Two IGF-blocking antibodies, MEDI-573 and xentuzumab, are currently being evaluated in phase II clinical trials for metastatic breast cancer (MEDI-573), and metastatic breast cancer and castration-resistant prostate cancer (xentuzumab; Clinicaltrials.gov identifiers: NCT02204072, NCT01446159, NCT02123823). However, clinical trials are currently lacking for PDAC, and our pre-clinical model work would support future investigations.

The stromal compartment of PDAC is comprised of a variety of non-malignant cells and extra-cellular matrix proteins which function to support tumour initiation, progression and drug resistance. This could explain the limited effectiveness of the recent therapies developed for PDAC, which only exert a modest effect as they specifically target tumour cells. Current therapies have not significantly improved patient outcome and thus, therapies which target both the neoplastic cells and the

pro-tumourigenic functions of the stromal compartment will likely achieve a better therapeutic response.

Overall the studies in this chapter suggest that in PDAC, stromal-derived IGFs can reduce response to chemotherapy via an IGF ligand - Ins/IGF-1R paracrine signalling axis and provide the rationale for further investigation into the combination of gemcitabine with IGF signalling blockade in pancreatic cancer treatment (Ireland et al. 2016).

Chapter Four:

Blockade of insulin-like growth factors increases efficacy of paclitaxel in metastatic breast cancer

CONTENTS

4.1 INTRODUCTION

4.1.1 Triple negative breast cancer (TNBC)

Breast cancer is a solid tumour which is currently the leading cause of cancer death in females worldwide (Siegel et al., 2017). TNBC is a highly metastatic subtype of breast cancer that accounts for ~ 20 % of all breast cancer cases, but has limited efficacious treatment options (Wahba and El-Hadaad, 2015). The current standard of care for metastatic TNBC includes radiotherapy and chemotherapy such as paclitaxel the standard agent, however, these treatments lack specificity due to the deficiency of targets such as hormone or HER2 receptors which are found in other breast cancer subtypes (Rakha et al., 2007, Schneider et al., 2008). Based on this, the TNBC subtype has the poorest survival rate, due to the absence of specific targeted therapy and its biology being comparatively less understood compared to other subtypes (Bauer et al., 2007).

Breast cancer has a propensity to give rise to metastasis at distant sites such as lungs, bone and brain which can present up to 10 years after treatment (Weigelt et al., 2005). Patients with metastatic breast cancer ultimately become resistant to chemotherapy treatment and as a result account for >90 % of breast cancer deaths (Marquette and Nabell, 2012), highlighting the need for new therapeutic targets to treat metastatic burden more effectively.

4.1.2 TNBC TME and chemoresistance

A tumours response to therapy can be influenced by its surrounding TME (Klemm and Joyce, 2015, Fantozzi and Christofori, 2006). Macrophages are the most abundant leukocytes in the breast TME (Williams et al., 2016) and an increased TAM presence has been shown to correlate with a poorer prognosis (Bingle et al., 2002, Campbell et al., 2011, Leek et al., 1996). TNBC also possesses a rich desmoplastic reaction

surrounding the tumour which comprises of several subtypes of activated CAF, which perform subtype-dependent functions (Costa et al., 2018).

Chapter 3 of this thesis describes the role of IGF signalling in PDAC chemotherapy resistance. The tumour stroma of PDAC and breast cancer share similar characteristics in that they both exhibit infiltrating macrophages and the presence of dense fibrosis. The IGF signalling axis has been implicated in promoting cancer progression in several tumour types including breast cancer (Zhang et al., 2011, Denduluri et al., 2015, Pollak, 2008). IGF signalling has also been implicated in breast cancer resistance to estrogen and HER2 receptor inhibition (Zhang et al., 2011, Lu et al., 2001, Massarweh et al., 2008, Farabaugh et al., 2015). However, the role of IGF signalling in chemoresistance in TNBC breast cancer is not yet completely understood (Farabaugh et al., 2015).

4.1.3 TNBC mouse models

To fully investigate the role of IGF signalling in TNBC chemoresistance it was necessary to utilise immunogenic preclinical models which recapitulate the human disease. MMTV-PyMT mice have been shown to develop breast cancer which is recapitulative of human TNBC, with tumour cells lacking expression of hormone receptors and low expression of HER2 (Guy et al., 1992, Davie et al., 2007). Py230 cells isolated from this model can be orthotopically implanted into recipient mice to create TNBC-like tumours (Maglione et al., 2001). 4T1 cells isolated from a spontaneously arising tumour in BALB/cfC3H mice (Dexter et al., 1978) also create a breast tumour along with pulmonary metastasis when orthotopically implanted into BALB/c mice (Pulaski and Ostrand-Rosenberg, 1998)

4.1.4 Hypothesis

Stromal TAMs and CAFs play an active role in IGF signalling in TNBC tumours and influence chemoresistance in this setting.

4.1.5 Aims

- Creation of preclinical TNBC mouse model
- Identify TAMs and CAFs as sources of IGF in primary tumour
- Investigate pulmonary metastasis in mouse model
- Analyse the stroma at the metastatic site and presence of IGF
- Block IGF signalling *in vivo* to assess effect on tumour progression in combination with chemotherapy treatment

4.2 RESULTS

4.2.1 TAMs and CAFs are the main sources of IGF-1 and IGF-2 in primary tumours in Py230 invasive breast cancer mouse model

Due to the previous findings in the PDAC mouse model described in chapter 3 and the similarities between PDAC and breast cancer TME, we investigated the effect of Ins/IGF-1R activation in the promotion of chemoresistance in TNBC.

To analyse this, Py230 luc/zsGreen (HR^-, Her2 low) murine breast cancer cells from MMTV-PyMT genetically engineered spontaneous breast cancer model were orthotopically implanted into the mammary fat pad of isogenic immunocompetent recipient C57BL/6J mice. Tumours were harvested 42 days after implantation and processed for FACS sorting of TAMs, CAFs and tumours cells (Fig 4.1 A).

TAM infiltration into the tumour tissue was characterised by immunofluorescent staining which showed high levels of $F4/80^+$ macrophage infiltration surrounding actively proliferating $Ki67^+$ tumour cells (Fig 4.1 B). Immunohistochemical staining of the same tissue showed the tumour mass had active InsR and IGF-1R signalling and these tumour cells were surrounded by M2-like ($CD68^+$, $CD206^+$) macrophages (Fig 4.1 C).

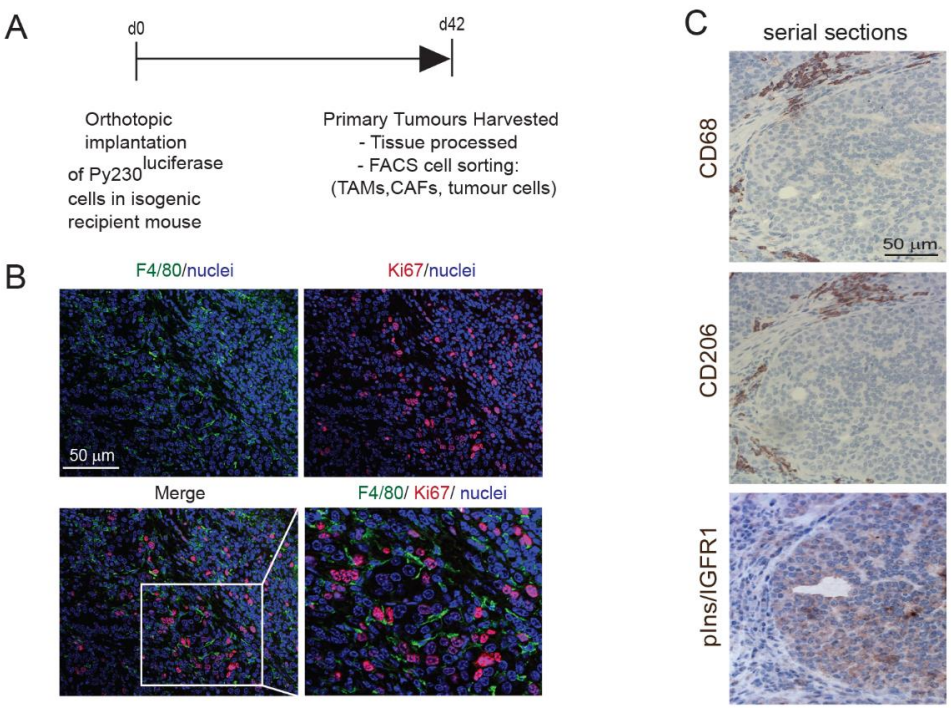

Figure 4.1 Murine TNBC tumours have activated Ins/IGF-1 receptors and are infiltrated by macrophages

A) Py230 tumour cells were subcutaneously implanted into the third mammary gland of syngeneic recipient mice. **B)** Images show immunofluorescent staining for F4/80 (green), Ki67 (red), and nuclei (blue) in murine breast cancer tissue harvested at day 42 after tumour implantation, scale bar 50 µm. **C**) Serial sections of immunohistochemical staining for CD68, CD206 and phospho-Ins/IGF-1 receptor in murine breast tumours. Scale bar 50 µm.

As the murine TNBC tissue showed activated Ins/IGF-1R it was important to identify the stromal source(s) of the IGF-1 and IGF-2 ligands in the TME. Tumour cells ($CD45^-$, $zsGreen^+$), non-immune stromal cells ($CD45^-$, $zsGreen^-$) and TAMs ($CD45^+$, $F4/80^+$) were FACS sorted from the Py230 tissue (Fig 4.2 A) and analysed by qPCR. Non-immune stromal cells were shown to highly express *αSMA,* indicating the majority of cell population were αSMA^+ CAFs (Fig 4.2 B).

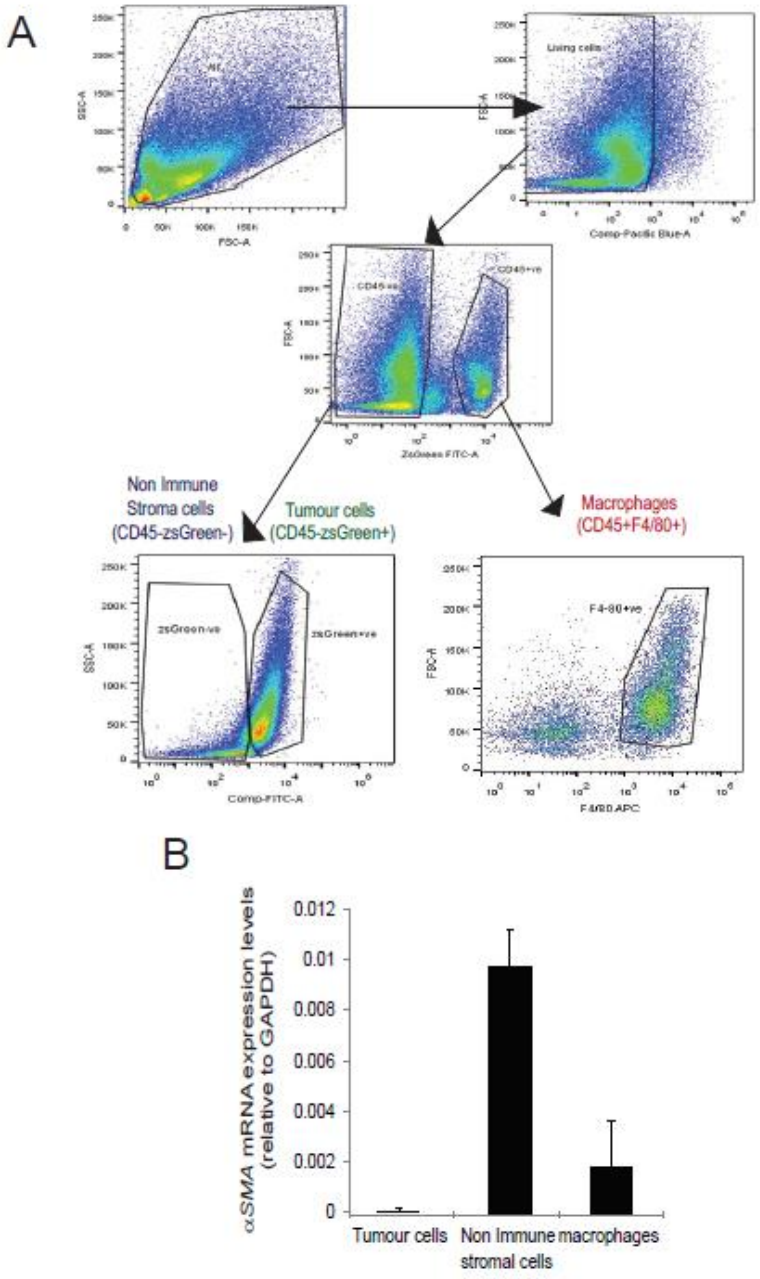

Figure 4.2 Gating strategy for FACS-sorting tumour cells, macrophages and non-immune stromal cells.

A) Gating strategy used to FACS sort alive (Sytox-), CD45^{-} (APC-Cy7) /zsGreen^{+} Py230 breast cancer cells, CD45^{-}(APC-Cy7)/zsGreen^{-} non-immune stromal cells, CD45^{+}(APC-Cy7)/F4/80^{+}(APC) macrophages from day 42 harvested mouse Py230 primary orthotopic breast tumours. **B)** qPCR quantification of *αSMA* mRNA expression levels indicative of activated myofibroblasts in tumour cells, non-immune stromal cells and macrophages FACS sorted from primary breast tumours (n=3 technical replicates).

To determine which of the sorted cell populations expressed IGF ligands and were therefore responsible for activating Ins/IGF-1 receptors on tumour cells, qPCR analysis was performed for *Igf-1* and *Igf-2* ligand expression. Macrophages expressed the highest levels of *Igf-1* (Fig 4.3 A), whereas both TAMs and CAFs were both shown to be the major sources of *Igf-2* expression in the primary site TME (Fig 4.3 B).

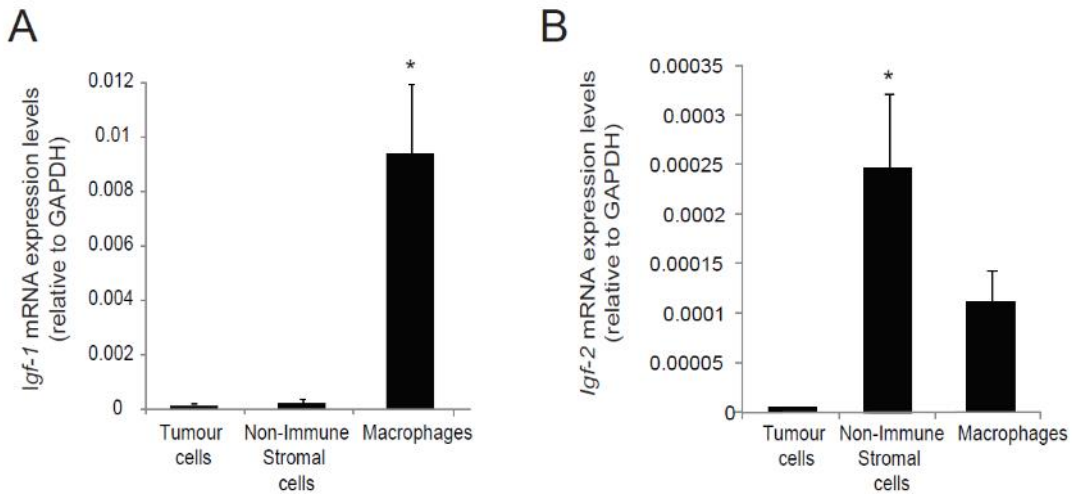

Figure 4.3 Macrophages and non-immune stromal cells express *Igf-1* and *Igf-2* in the primary TME

Quantified mRNA expression levels in tumour cells, non-immune stromal cells and tumour-associated macrophages FACS sorted from murine breast cancer tumours. **A)** *Igf-1* expression, **B)** *Igf-2* expression. Error bars represent SEM (n = 3 technical replicates), * p value ≤ 0.05 using one-way ANOVA and Bonferroni post hoc test.

To determine the location of the CAF stromal cells in relation to the tumour cells, tissues were immunofluorescently stained revealing αSMA$^+$ CAFs surrounded actively dividing Ki67$^+$ tumour cells in the primary breast cancer tissue (Fig 4.4).

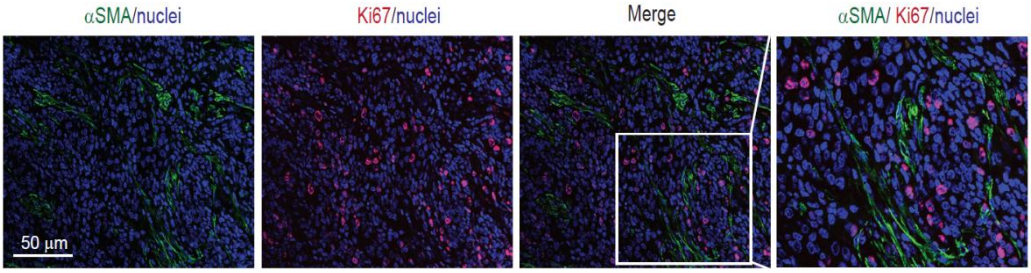

Figure 4.4 αSMA$^+$ CAFs cells surround actively dividing breast tumour cells Immunofluorescently stained primary orthotopic PY230 breast tumour tissue harvested day 42 after implantation. αSMA+ (green) cancer-associated fibroblast are seen surrounding actively dividing tumour cells (Ki67+, red), and nuclei (blue) in primary breast tumours. Scale bar 50 µm.

4.2.2 Metastasis-associated macrophages and fibroblasts remain sources of IGF-1 and IGF-2 in pulmonary metastatic lesions

Human TNBC breast cancer is a highly invasive disease which usually metastasizes to the lung. To analyse if this was also seen the Py230 TNBC-like orthotopic syngeneic model, metastatic foci in lungs were confirmed by bioluminescence *ex vivo* imaging using IVIS technology to detect Py230 luc/zsGreen cells, and foci were subsequently detected in sectioned lung tissue via hematoxylin and eosin (H&E) staining (Fig. 4.5).

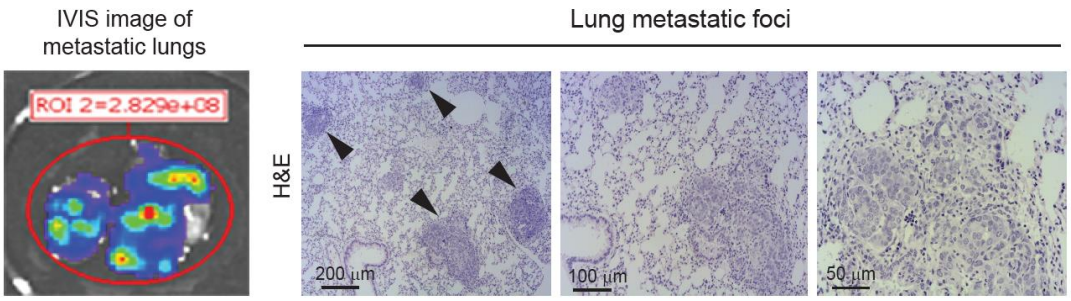

Figure 4.5 Lung metastatic foci are formed in Py230 orthotopically implanted mice

Left, identification of metastatic tumour lesions in the lung by bioluminescent imaging technique to detect Py230 luc/zsGreen breast cancer cells. Right, images show H&E staining of metastatic foci in the lungs. Arrows indicate metastatic foci, scale bars 200 µm, 100µm, and 50 µm.

Lung sections which were identified as having metastatic foci by serial sectioning and H&E staining, were immunofluorescently stained for macrophages ($F4/80^+$), myofibroblasts (αSMA^+) and proliferating tumour cells ($Ki67^+$). This staining showed, similar to the primary tumour, metastatic lesions had actively proliferating tumour cells surrounded by macrophages and myofibroblasts in the stroma (Fig 4.6).

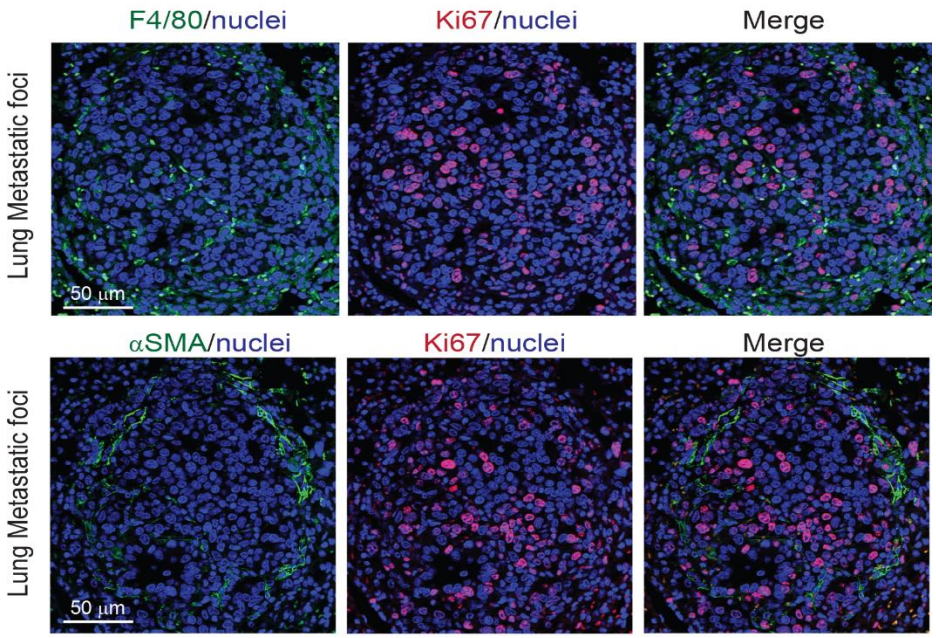

Figure 4.6 Macrophages and myofibroblasts surround dividing tumour cells in pulmonary metastatic foci.

Immunofluorescent staining of Py230 metastatic foci in lungs harvested 42 days after primary site implantation. Confirmed presence of F4/80+ (green) metastasis associated macrophages (top), αSMA+ (green) metastasis associated fibroblasts (bottom) surrounding actively dividing Ki67+ (red) cells, and nuclei (blue). Scale bar 50 μm.

As TAMs and CAFs in the primary TME were stromal sources of IGF-1 and IGF-2 ligands it was logical to investigate whether this phenomenon was also seen the pulmonary metastatic foci. To address this question, metastatic tumour cells ($CD45^-$, $zsGreen^+$), non-immune stromal cells ($CD45^-$, $zsGreen^-$) and metastasis associated-macrophages (MAMs) ($CD45^+$, $F4/80^+$) were FACS sorted from the collected lungs (Fig 4.7 A). Again, to confirm the presence of myofibroblasts, qPCR analysis showed the non-immune stromal cells from metastatic foci expressed the highest levels of *αSMA* indicating the majority of the cells were CAFs (Fig 4.7 B)

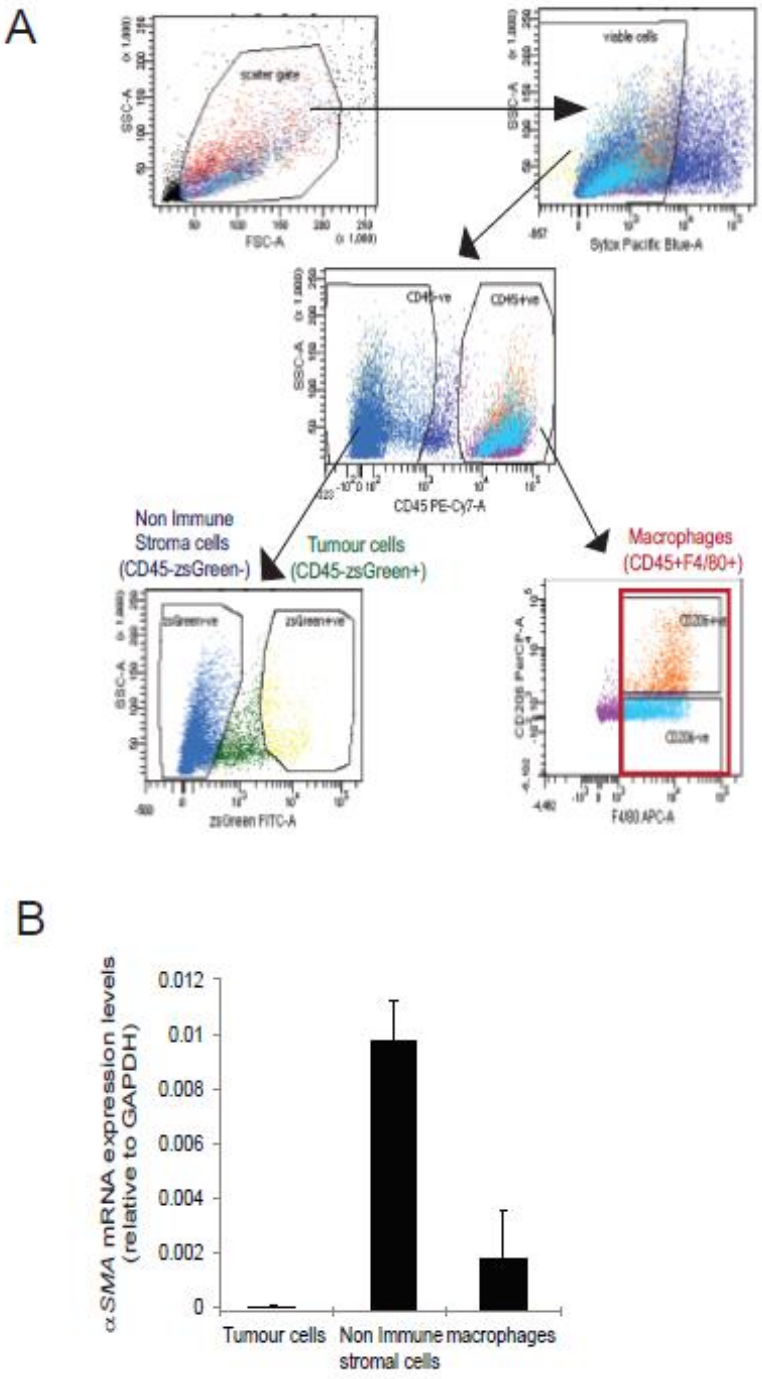

Figure 4.7 FACS gating strategy to sort for tumour cells, myofibroblasts and macrophages

A) Gating strategy used to FACS sort $CD45^{-}$/$zsGreen^{+}$ metastatic Py230 breast cancer cells, CD45-/zsGreen- non-immune stromal cells, $CD45^{+}F4/80^{+}$ macrophages from mouse lung metastatic foci harvested 43 days after primary site implantation **B)** Quantification of *αSMA* mRNA expression levels in the different cell populations isolated from lung metastatic foci using flow cytometry (n=3 technical replicates).

The FACS sorted populations were analysed by qPCR for *Igf-1* and *Igf-2* expression. Similar to the observation at the primary site, MAMs and metastasis-associated fibroblasts (MAFs) expressed high levels of *Igf-1* and *Igf-2*, whereas disseminated breast cancer cells do not express these ligands (Fig. 4.8 A and B). Together, these findings provide evidence that macrophages and fibroblasts are the sources of IGF-1 and IGF-2 both at the primary and the metastatic site in the Py230 invasive breast cancer model.

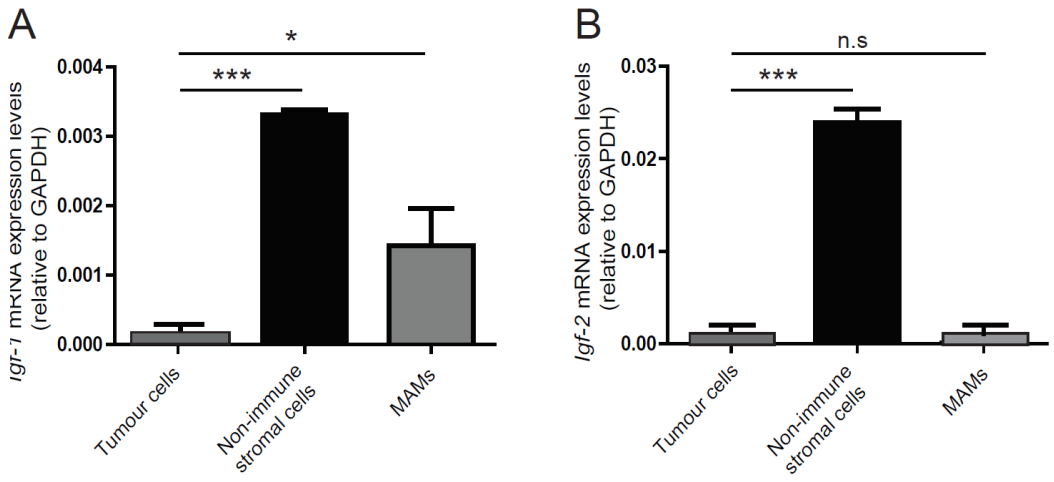

Figure 4.8 Expression of *Igf-1* and *Igf-2* in tumour cells, non-immune stromal cells and macrophages from lung metastasis.

Quantification of mRNA expression levels in metastatic tumour cells, metastasis-associated non-immune stromal cells and metastasis-associated macrophages isolated from pulmonary metastasis by FACS sorting. **A)** *Igf-1* expression, **B)** *Igf-2* expression. Error bars represent SEM (n = 3 technical replicates), * p-value ≤ 0.05, *** p-value ≤ 0.0001, using one-way ANOVA and Bonferroni post hoc test.

4.2.3 Combination treatment with paclitaxel and IGF blocking antibody reduces tumour cell proliferation and metastasis in an orthotopic Py230 model

Based on the findings in chapter 3 of this thesis, IGF signalling may also affect breast cancer progression and metastasis when challenged with paclitaxel, a standard agent used in the treatment of breast cancer. To test this, mice were orthotopically implanted with Py230 luc/zsGreen TNBC-like cells and treated with isotype control IgG antibody (n=8), xentuzumab IGF-1/2 blocking antibody (n=8), paclitaxel (n=8), or a combination of xentuzumab with paclitaxel (n=8) (Fig. 4.9 A).

To determine the effectiveness of xentuzumab IGF blocking Ab in the Py230 breast cancer model, tumours were harvested and stained by immunohistochemistry for pIns/IGF-1R. Control IgG and paclitaxel treated mice showed high levels of Ins/IGF-1R activation in the primary tumours (Fig 4.9 B and C). Xentuzumab treatment as a single agent and in combination with paclitaxel markedly reduced activation levels of Ins/IGF-1R, confirming that xentuzumab had reached the tumour and blocked IGF signalling (Fig 4.9 B and C).

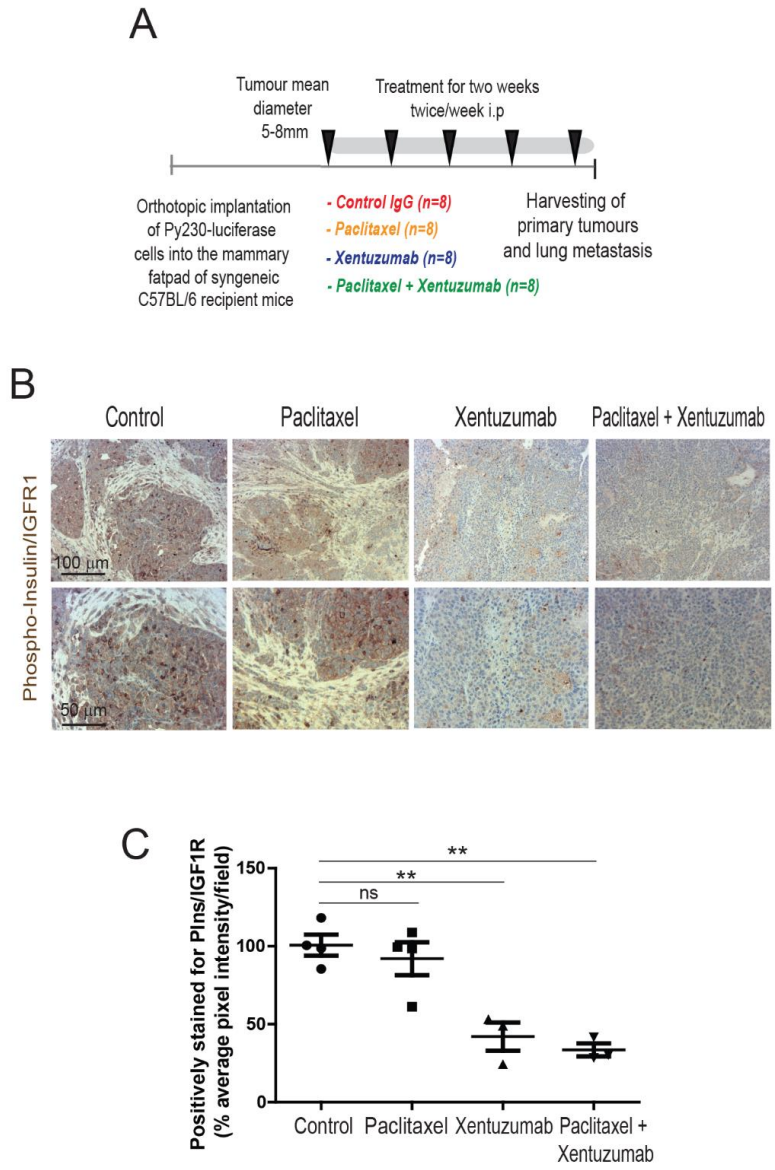

Figure 4.9 Py230 orthotopic breast cancer model treated with xentuzumab shows a reduction in Ins/IGF-1R activation

A) Py230 luc/zsGreen cells were orthotopically implanted into the third mammary fatpad of syngeneic C57BL/6J recipient mice. Treatment was started when tumours reached between 5–8mm^2, twice a week i.p., with control IgG antibody, IGF blocking antibody xentuzumab (100 mg/kg), paclitaxel (100 mg/kg), or a combination of xentuzumab with paclitaxel (n = 8 mice per group). **B)** Immunohistochemical staining of phospho-insulin/IGF-1R in breast tumours treated with IgG (control), paclitaxel, xentuzumab or paclitaxel with xentuzumab. Scale bars 100 µm and 50 µm. **C)** Quantification of immunohistochemical staining of pInsR/IGF-1R. Error bars represent SEM (4 fields counted/mouse tumour, n =4 mice per treatment group). Ns non-significant, ** p-value ≤ 0.001, using one-way ANOVA and Bonferroni post hoc test.

To determine when to begin treatment of the mice and to monitor tumour progress throughout the experiment, the growth of the primary tumours was measured bi-weekly using calipers. These measurements revealed no differences in primary tumour growth throughout the course of treatment (Fig 4.10 A). Despite this, treatment could still have an effect on tumour composition, therefore, the tissues were immunofluorescently stained for Ki67 to determine the levels of proliferating tumour cells. These levels were shown to be modestly reduced by both paclitaxel and xentuzumab single treatments and significantly reduced by the combination treatment of xentuzumab with paclitaxel compared to control IgG (Fig 4.10 B and C).

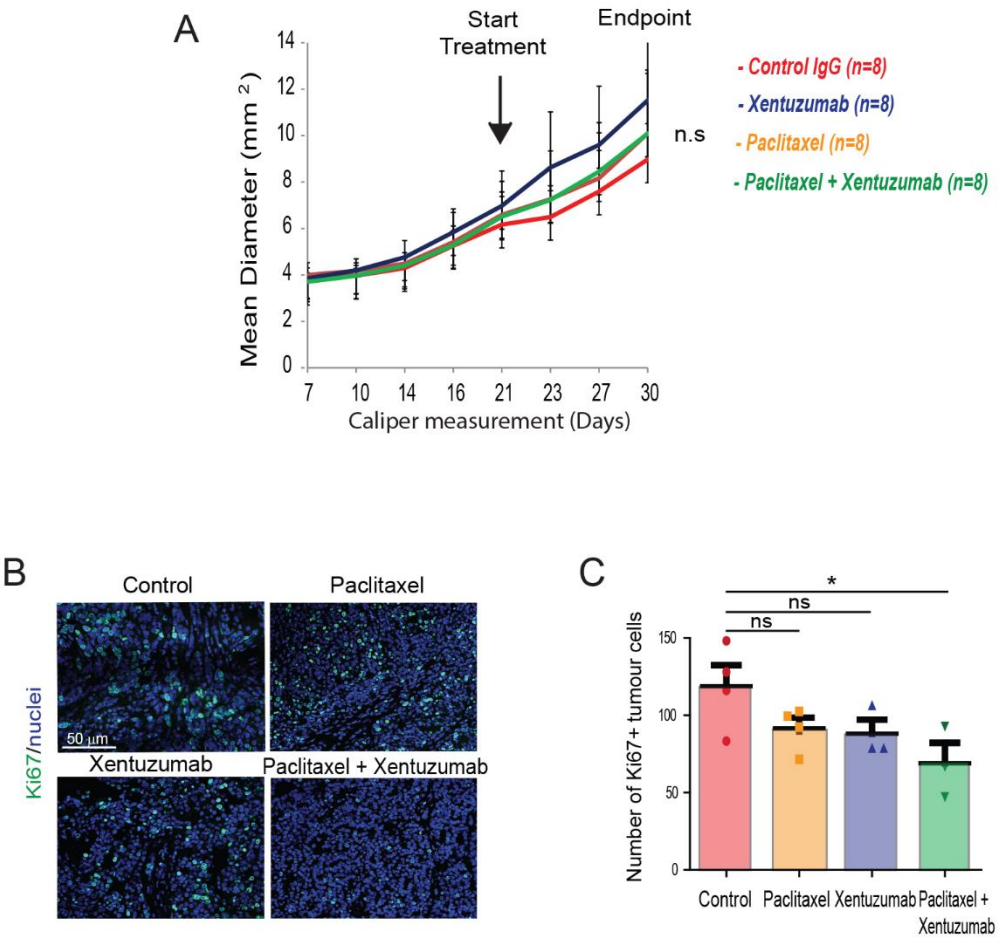

Figure 4.10 Tumour cell proliferation is significantly decreased with paclitaxel and xentuzumab combination treatment

A) Tumour mean diameter (mm^2) measured by calipers before and during treatment with IgG control, xentuzumab, paclitaxel and paclitaxel with xentuzumab. **B)** Immunofluorescent staining of Ki67 in primary tumours treated with IgG (control), paclitaxel, xentuzumab, or paclitaxel with xentuzumab, scale bar 50 µm. **C)** Quantification of Ki67 staining. Error bars represent SEM (3–5 fields counted/mouse tumour, n = 3–4 mice per treatment group), * $p \leq 0.05$ using one-way ANOVA and Bonferroni post hoc test.

TAM infiltration into the primary tumour was analysed by flow cytometry analysis of the $CD45^+/F4/80^+$ macrophage population (Fig 4.11 A). Quantification of the $F4/80^+$ macrophage population among $CD45^+$ cells revealed no significant difference between the percentage of macrophages found infiltrating the primary tumour mass in any treatment groups (Fig 4.11 B).

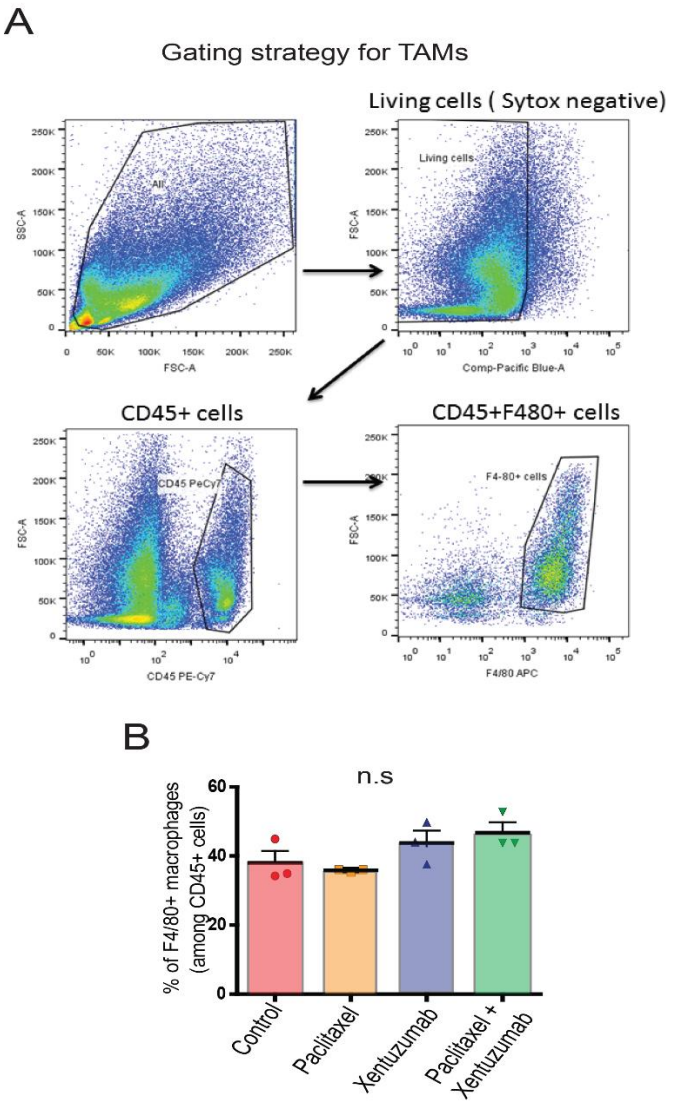

Figure 4.11 No significant differences are seen in TAM infiltration in any treatment groups

A) Flow cytometry gating strategy to analyse $Sytox^-/CD45^+/F4/80^+$ macrophages in the digested tumour. **B)** Quantification of $F4/80^+$ macrophages among $CD45^+$ immune cells in control IgG, paclitaxel, xentuzumab and paclitaxel with xentuzumab treated tumours (n=3 technical replicates). Error bars represent SEM, (n= 3 biological replicates), ns, non-significant.

The Py230 orthotopic mouse model recapitulates metastasis to the lung, therefore we were also able to investigate whether treatment effected pulmonary metastatic burden. Firstly, mice with metastatic foci were identified by IVIS imaging and H&E staining of the lung foci. This revealed 7/8 mice in each of the control IgG, paclitaxel and xentuzumab treatment groups mice with metastatic foci (Fig 4.12 A). However, the combination treatment of xentuzumab with paclitaxel showed a reduction of lung metastasis incidence, with only 5/8 mice possessing detectable lesions (Fig 4.12 A). However, statistical analysis revealed the incidence of metastatic lesions was not significantly associated with their treatment received (Fig 4.12 B).

A

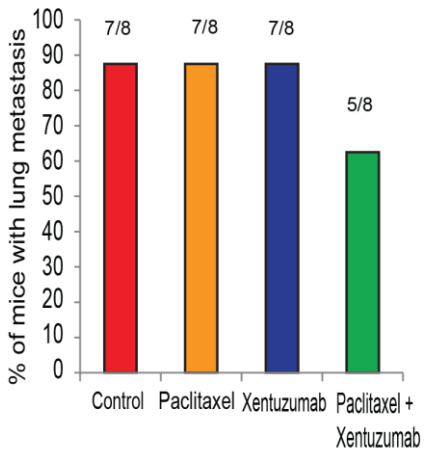

B

	Positive for metastasis	Negative for metastasis	Total
Control	7	1	8
Paclitaxel	7	1	8
Xentuzumab	7	1	8
Paclitaxel + Xentuzumab	5	3	8
Total	26	6	**32**

Chi-square: 2.46, p= 0.48

Figure 4.12 Quantification of mice with pulmonary metastatic foci

A) Percentage of mice presenting with lung metastatic foci per treatment group detected by IVIS imaging and H&E staining. (n = 8 mice/group). **B)** Contingency table and results from statistical analysis showing no significant correlation between treatment and presence of lung metastasis. Chi-square = 2.46; p = 0.48.

The reduction of metastatic incidence could be due to an overall decrease in disseminated tumour cells seeding in the lung. To investigate this, the average number of foci per 100 mm^2 was quantified through H&E staining of the entire lung and identification by light microscopy. This analysis did not reveal significant changes in the average number of lesions in any treatment group (Fig 4.13). Interestingly, paclitaxel treated mice showed a slight increase in the number of foci compared to the other treatment groups (Fig 4.13).

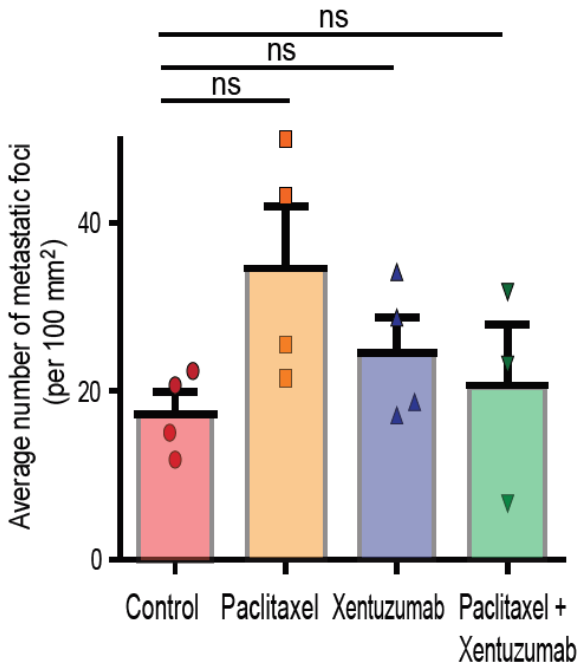

Figure 4.13 Paclitaxel treated mice show a slight increase in average number of foci per 100 mm^2

Quantification of number of lung metastatic foci per 100 mm^2 in whole lung H&E stained sections of mice treated with control IgG, paclitaxel, xentuzumab, or paclitaxel with xentuzumab, (n=4 lungs per group) ns, non-significant differences using one-way ANOVA and Bonferroni post hoc test.

As significant differences were not seen in the seeding of disseminated tumour cells, it was possible the outgrowth of foci was affected by treatment, ultimately reducing metastatic burden. The average metastatic lesion size was calculated for each treatment group by measuring foci sizes throughout the entire lung. Paclitaxel treatment alone and xentuzumab alone modestly reduced the average lesion size compared to control IgG treated mice, but not by a significant margin (Fig 4.14 A and B). Interestingly, mice which received the combination treatment of paclitaxel with xentuzumab showed a bigger yet still modest reduction in foci lesion size compared to control IgG treated mice (Fig 4.14 A and B).

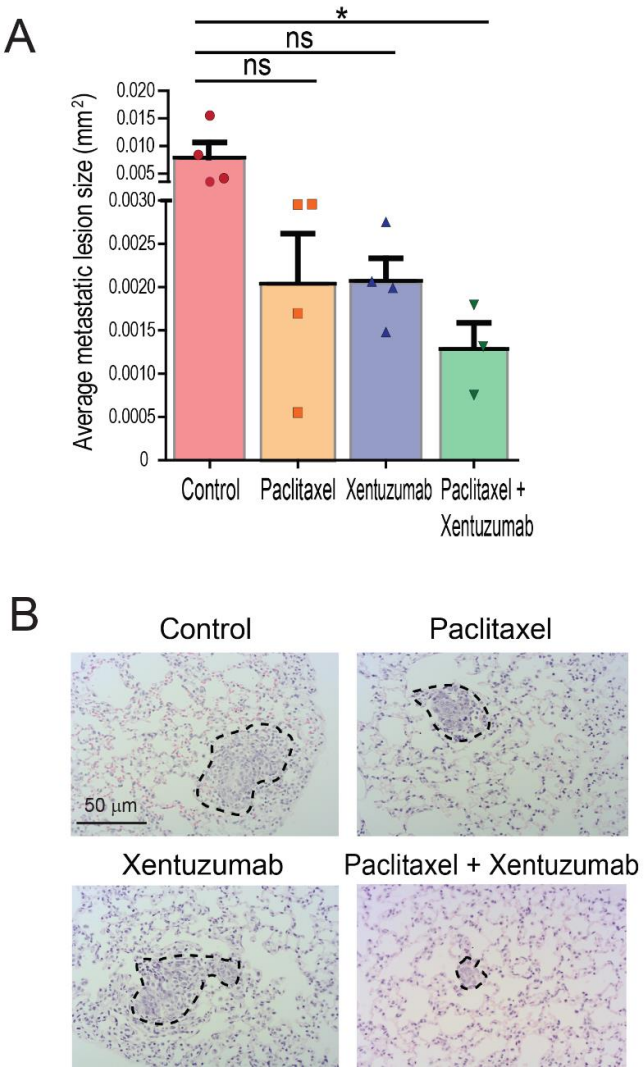

Figure 4.14 Combination treatment of paclitaxel with xentuzumab significantly reduced average metastatic lesion size

A) Average size of pulmonary metastatic lesions (mm^2) in whole sectioned lungs stained by H&E mice treated with control IgG, paclitaxel, xentuzumab, or paclitaxel with xentuzumab, (n=4 per group) * $p \leq 0.05$, using one-way ANOVA and Bonferroni post hoc test. **B)** Representative H&E staining of lung metastatic foci (outlined by dashed line) in mice treated with control IgG, paclitaxel, xentuzumab, or paclitaxel with xentuzumab. Scale bar 50 µm.

The combination of foci size and frequency provided a measure of total metastatic burden, which was calculated for each treatment group. Paclitaxel treatment and xentuzumab treatment alone reduced metastatic burden in the Py230 orthotopic TNBC-like mouse model, which was further modestly reduced by combination treatment of paclitaxel and xentuzumab (Fig 4.15). These data suggest that treatment with either paclitaxel or xentuzumab or in combination likely impairs outgrowth of disseminated breast cancer cells in metastatic foci.

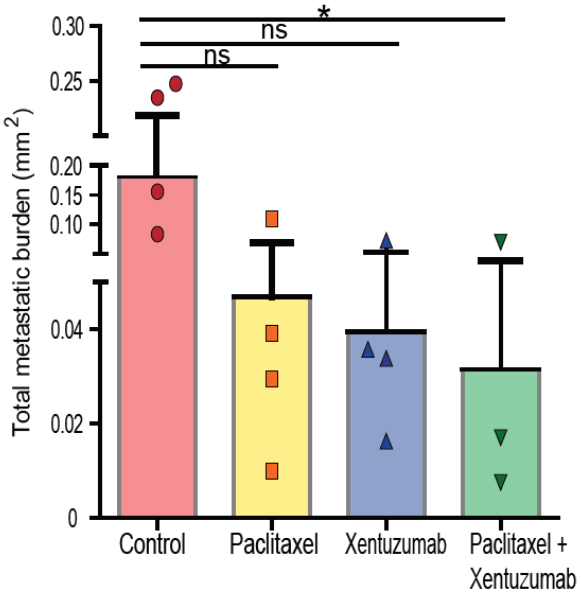

Figure 4.15 Combination paclitaxel with xentuzumab treatment significantly reduces total metastatic burden

Total metastatic burden (mm^2) in whole lungs stained by H&E of mice treated with control isotype IgG antibody, paclitaxel, xentuzumab, and paclitaxel with xentuzumab, (n=4 per group) * $p \leq 0.05$, using one-way ANOVA and Bonferroni post hoc test

4.2.4 Paclitaxel and IGF blocking antibody combination treatment reduces tumour cell proliferation and metastasis in a syngeneic orthotopic 4T1 model

To confirm the results seen in the Py230 model, 4T1 (HR^-, $HER2^-$) luc/zsGreen cells were implanted into the mammary fatpad of syngeneic BALB/c mice and treated with IgG control antibody (n=8), paclitaxel (n=9), xentuzumab (n=8), or paclitaxel with xentuzumab (n=9) (Fig. 4.16 A). To determine whether xentuzumab treatment was also effective in this model, tumours were immunohistochemically stained for pIns/IGF-1R. In accordance with the previous model, Ins/IGF-1R activation was significantly reduced in mice treated with xentuzumab alone and paclitaxel with xentuzumab combination (Fig. 4.16 B and C).

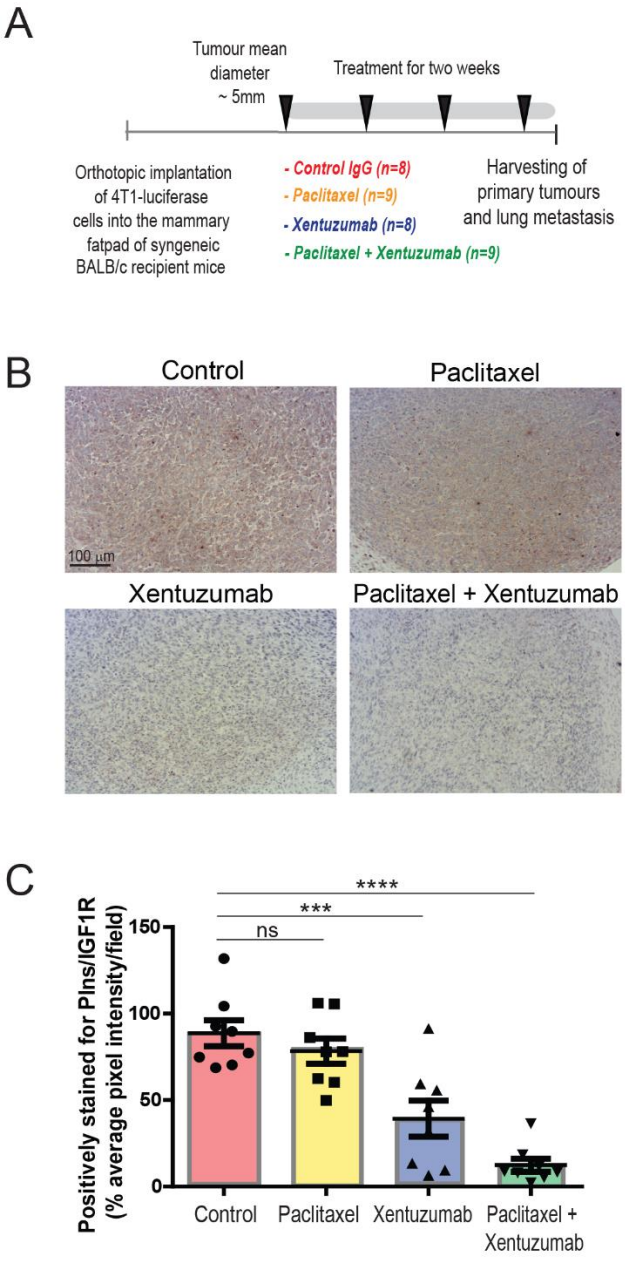

Figure 4.16 4T1 breast cancer cells possess active insulin and IGF-1 receptor signalling. A) 4T1 luc/zsGreen cells were orthotopically implanted into the third mammary fatpad of syngeneic Balb/c recipient mice and were treated when tumours reached ~ 5 mm^2 mean diameter, over 2 weeks the mice received four treatments by i.p. with control human IgG antibody (10 mg/kg) (n = 8 mice), xentuzumab IGF blocking antibody (100 mg/kg) (n = 8 mice), paclitaxel (100 mg/kg) (n = 9 mice) or combination of xentuzumab with paclitaxel (n = 9 mice). **B)** Immunohistochemical staining of phospho-Ins/IGF-1R in 4T1 breast tumours. Scale bar 100 µm. **C)** Quantification of immunohistochemical staining of pInsR/IGF-1R. Error bars represent SEM (3 fields counted/mouse tumour, n =8 mice per treatment group). Ns non-significant, *** p-value ≤ 0.001, **** p-value ≤ 0.0001 using one-way ANOVA and Bonferroni post hoc test.

As with the previous model, tumour growth was measured bi-weekly using calipers to determine when to begin treatment and to continuously monitor the effect of treatment on primary tumour growth. Interestingly in this breast cancer model, primary tumour growth was significantly reduced by paclitaxel treatment and further significantly reduced by the combination treatment of paclitaxel with xentuzumab (Fig. 4.17).

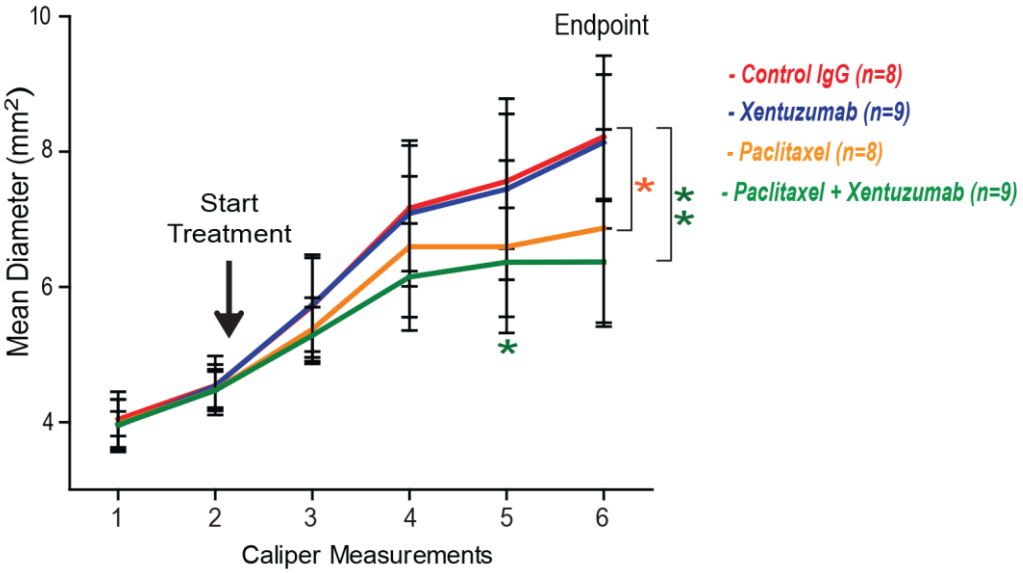

Figure 4.17 Primary tumour growth is retarded by paclitaxel and combination paclitaxel with xentuzumab treatment

Graph showing tumour mean diameter (mm^2) measured by calipers before and during treatment with isotype IgG control, xentuzumab, paclitaxel, and paclitaxel with xentuzumab. Error bars represent SEM (IgG antibody and xentuzumab n = 8, paclitaxel and paclitaxel with xentuzumab n = 9), * p-value ≤ 0.05, ** p-value ≤ 0.01 using two-way ANOVA and Bonferroni post hoc test.

Again intrinsic changes were seen in tumour composition, paclitaxel treated mice exhibited a significant reduction in Ki67^{+} cells compared to control IgG treated mice (Fig 4.18 A and B). However a more significant decrease was caused by combination paclitaxel with xentuzumab treatment (Fig 4.18 A and B).

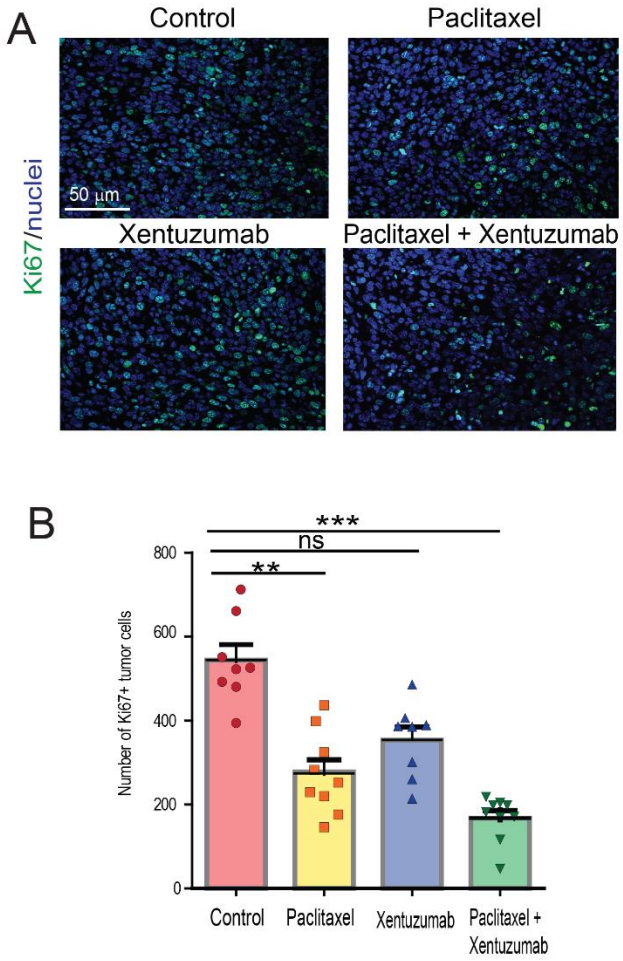

Figure 4.18 Paclitaxel alone and combination treatment significantly reduces Ki67^{+} cells in the primary tumour

A) Immunofluorescent staining of Ki67 in primary tumours treated with IgG (control), paclitaxel, xentuzumab, or paclitaxel with xentuzumab. Scale bar 50 µm. **B)** Quantification of Ki67 staining. A total of 3–5 fields counted/mouse tumour, n = 8–9 mice per treatment group, ns, non-significant differences, ** $p \leq 0.01$, *** ≤ 0.0001 p using one-way ANOVA and Bonferroni post hoc test.

The presence of pulmonary metastasis was analysed in the 4T1 breast cancer model, revealing xentuzumab alone or in combination with paclitaxel treatment reduced the number of mice presenting with pulmonary metastasis (Fig 4.19 A). To analyse changes in tumour cell seeding, the average number of metastatic foci per 100 mm^2 was calculated. Paclitaxel alone and in combination with xentuzumab treatment both significantly reduced the average number of metastatic foci per 100 mm^2 compared to control IgG treated mice (Fig 4.19 B).

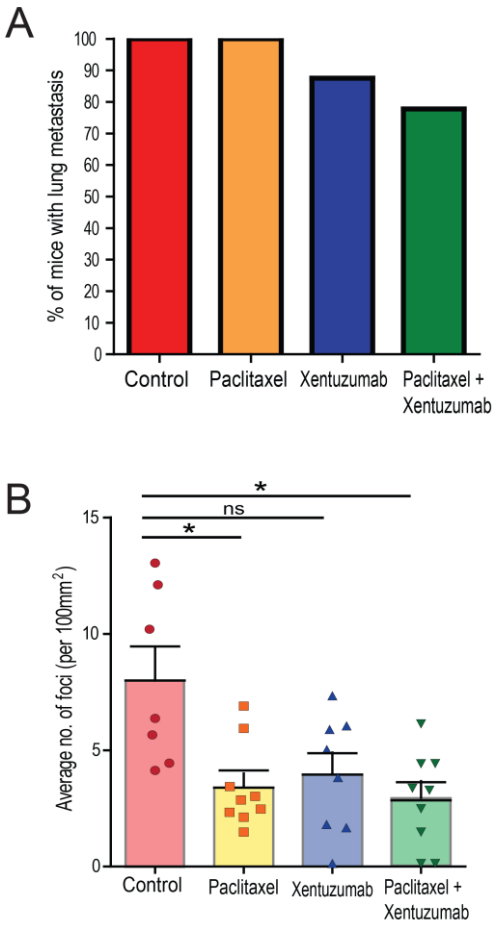

Figure 4.19 Paclitaxel and paclitaxel with xentuzumab treatment reduced metastatic incidence and reduced average number of foci

A) Percentage of mice presenting with lung metastasis per treatment group. **B)** Quantification of number of lung metastatic foci per 100mm^2 in mice treated with control IgG (n=7), paclitaxel (n=9), xentuzumab (n=8), or paclitaxel with xentuzumab (n=9). Error bars represent SEM, ns, non-significant differences, * p value ≤ 0.05, using one-way ANOVA and Bonferroni post hoc test.

Average metastatic foci size was calculated to indicate changes in metastatic outgrowth. This analysis revealed the combination treatment of paclitaxel with xentuzumab significantly reduced the average metastatic lesion size compared to control IgG treated mice (Fig 4.20 A and B).

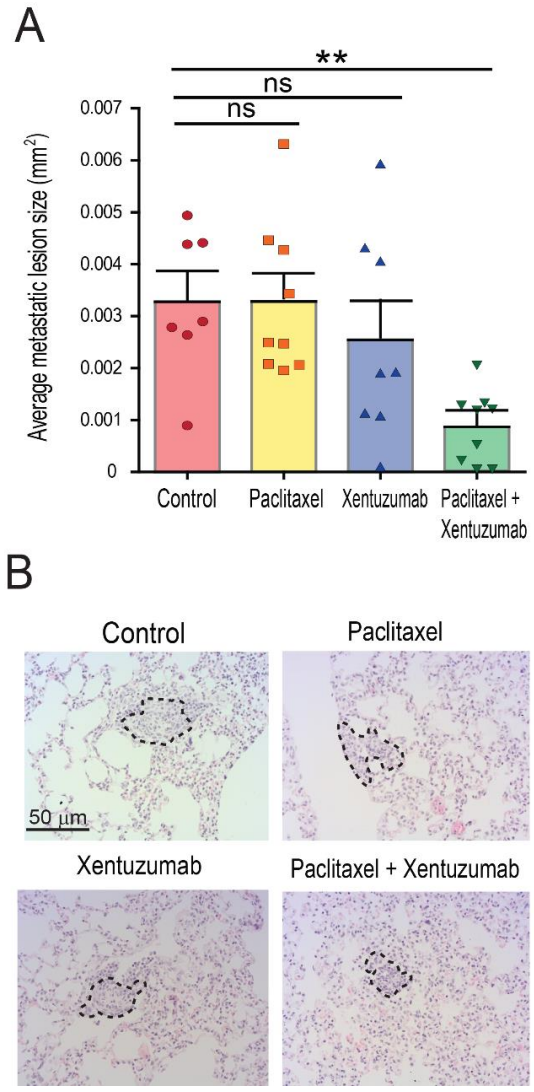

Figure 4.20 Combination treatment paclitaxel with xentuzumab significantly reduces metastatic lesion size

A) Average size of pulmonary metastatic lesions (mm^2) in whole lungs of mice treated with control IgG, paclitaxel, xentuzumab, or paclitaxel with xentuzumab. Error bars represent SEM. (n=7-9 lungs per treatment group), ns, non-significant differences, ** $p \leq 0.01$, using one-way ANOVA and Bonferroni post hoc test. **B)** Representative H&E staining of lung metastatic foci in treatment group, indicated by dashed line. Scale bar 50 µm

Foci size and frequency were combined in order to calculate total metastatic burden; which revealed the combination treatment of paclitaxel with xentuzumab significantly reduced overall metastatic burden of 4T1 implanted mice compare to IgG treated control, although paclitaxel alone and xentuzumab alone both reduced burden, suggesting an additive effect (Fig 4.21).

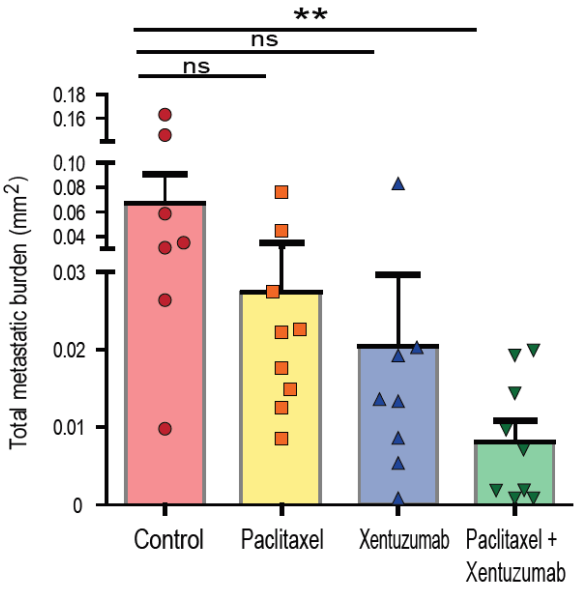

Figure 4.21 Combination treatment paclitaxel with xentuzumab significantly reduced total metastatic burden

Total metastatic burden (mm^2) in whole lungs of mice treated with control IgG, paclitaxel, xentuzumab, and paclitaxel with xentuzumab (n=7–9 lungs per treatment group). Error bars represent SEM., ns, non-significant differences, ** $p \leq 0.01$, using one-way ANOVA and Bonferroni post hoc test.

4.3 DISCUSSION

Breast cancer, and in particular TNBC, are highly metastatic and potentially lethal diseases which require identification of specific molecular targets and development of more effective therapies (Schneider et al., 2008, Bauer et al., 2007). IGF signalling been reported to support the progression of HR+ and HER2+ breast cancer along with conferring resistance to established therapies (Zhang et al., 2011, Lu et al., 2001, Massarweh et al., 2008, Farabaugh et al., 2015). However, the precise role of IGF in TNBC had remained elusive (Farabaugh et al., 2015).

In the invasive TNBC models used here, it was found that TAMs and CAFs secrete IGF-1 and IGF-2 at both the primary tumour site and pulmonary metastatic site. Zhang et al., previously reported CAF-derived IGF-1 primes breast cancer cells for bone metastasis (Zhang et al., 2013). This study in combination with the data shown here suggest stromal-derived IGF from TAMs and CAFs may play an important role in the metastatic process of breast cancer and in this particular case may promote dissemination to the lungs or at least support outgrowth in the lungs.

To investigate the therapeutic potential of blocking IGF signalling in invasive breast cancer xentuzumab, an IGF-1/2 blocking antibody developed by Boehringer Ingelheim, was tested in two preclinical mouse models of invasive TNBC breast cancer, which metastasized to the lungs. In both models, however more significantly in the 4T1 model, combination treatment of xentuzumab with paclitaxel reduced incidence of metastasis, as well as a reduction of tumour cell proliferation compared to monotherapy of either agent. In agreement with these findings, Gooch et al., previously showed that IGF-1 promotes proliferation of paclitaxel treated cells *in vitro* (Gooch et al., 1999). Interestingly, in this study administration of xentuzumab was shown to increase the efficacy of paclitaxel the commonly used chemotherapeutic agent for the treatment of invasive breast cancer; decreasing pulmonary metastatic

lesion size however not the number of foci suggesting that the combination treatment likely affects outgrowth of metastatic tumour cells rather than metastatic seeding.

IGF-1R inhibitors have been assessed in clinical trials for metastatic HR+ breast cancer, as well as TNBC, but have shown limited success (Robertson et al., 2013, Ma et al., 2013, Jones et al., 2015, Gradishar et al., 2016, Guha, 2013, Lodhia et al., 2015). Two IGF ligand blocking antibodies, xentuzumab and MEDI-573, are currently being evaluated in clinical trials in HR+ metastatic breast cancer patients in combination with everolimus and exemestane (NCT02123823) and in hormone sensitive metastatic breast cancer in combination with letrozole (NCT01446159), respectively. In contrast to IGF-1R antibodies, IGF blocking antibodies neutralize both ligands IGF-1 and IGF-2 and thereby inhibit proliferative signalling through both insulin and IGF-1 receptors without affecting insulin metabolic signalling (Friedbichler et al., 2014).

Breast cancer cells survive poorly in isolation and participate in a complex relationship with surrounding stromal and immune cells in the TME, which can support tumour cell survival, proliferation and dissemination to other organs (Qian et al., 2015, Shree et al., 2011, DeNardo et al., 2011, Lin et al., 2001, Zhang et al., 2013). CAFs and TAMs are the most abundant stromal cells in solid cancers, including breast cancer. However, different populations of CAFs and TAMs with both pro- and anti-tumourigenic functions co-exist (Ohlund et al., 2017, Mills et al., 2016, Augsten, 2014). Therefore, therapies aiming to specifically inhibit tumour supporting functions of stromal cells, without affecting their anti-tumourigenic functions, may be more effective than ablation therapies in restraining tumour progression (Quail and Joyce, 2013, Aslakson and Miller, 1992). The findings in this chapter suggest IGF blockade in combination with paclitaxel, reduces tumour cell proliferation levels, also reducing pulmonary metastasis without affecting macrophage infiltration. In conclusion, this

study suggests that stromal-derived IGFs may support breast cancer pulmonary metastasis outgrowth and may modulate tumour cell response to paclitaxel (Ireland et al. 2018).

Chapter Five:

PDAC tumours with varying metastatic potential express differing secretome profiles

CONTENTS

5.1 INTRODUCTION

5.1.1 PDAC

Pancreatic cancer is a highly metastatic disease which infiltrates into the peritoneum and uses the lymphatic and vascular system to spread into the liver and lungs (Humphris et al., 2014, Pandol et al., 2009). Patients are usually described as being asymptomatic until metastasis impedes bodily function resulting in jaundice or breathing difficulty due to blockage of the common bile duct or growth in the lung respectively (Claire et al., 2016).

Although most cancer patients succumb due to cachexia, a high metastatic burden significantly effects the quality of a patient's life. Tumours grow as a tissue, with cells possessing varying genetic mutations performing different functions. This genetic heterogeneity can create tumours with varying propensity for metastatic outgrowth (Meacham and Morrison, 2013). This means PDAC is not uniform among patients and some will experience a more aggressive disease than others.

Chapter 3 of this thesis utilised an orthotopic mouse model of PDAC. PDAC tumour cells from the KPC GEMM were implanted into the tail of the pancreas creating a PDAC tumour mass with ductal structures, but also developed the associated rich TME with infiltrating macrophages and desmoplasia of activated fibroblasts. However, metastasis was not investigated in this orthotopic model and cells isolated from the KPC GEMM may also have varying metastatic potential. Metastatic potential and disease progression can be mediated by many factors but in particular, by secreted proteins which interact with surrounding cells to promote movement and invasion.

5.1.2 Mesothelin

In healthy tissues, mesothelin expression is limited to mesothelial cells which line the pleura, peritoneum and pericardium (Hassan et al., 2004). Mesothelin exists as a 71

kDa precursor protein which is proteolytically cleaved by the endoprotease furin to create two protein products: N-terminus megakaryocyte potentiating factor (MPF) and C-terminus mature mesothelin (mMSLN) (Chang and Pastan, 1996). MPF is a 31 kDa protein secreted from cells and functions as a cytokine to stimulate colony formation of bone marrow megakaryocytes through IL-3 stimulation in the bone marrow (Yamaguchi et al., 1994). mMSLN is a 40 kDa glycoprotein which can remain membrane bound through a glycophosphatidylinositol (GPI) anchor or shed from the cell via cleavage by TNF-α converting enzyme (Chang and Pastan, 1996, Zhang et al., 2011, Dangaj et al., 2011). The exact function of mMSLN is not known but it may function as a cell surface adhesion protein (Kojima et al., 1995, Chang and Pastan, 1996).

5.1.3 Mesothelin in cancer

Mesothelin has been identified as a tumour antigen in neoplasia arising in mesothelial cells. However, it has also been confirmed as aberrantly expressed in other cancers including pancreatic, ovarian, lung, stomach cholangiocarcinoma and TNBC (Hassan et al., 2004, Ho et al., 2007, Tchou et al., 2012, Argani et al., 2001). It has been shown in tumours that mMSLN can bind to mucin 16 (Muc16) which has been associated with progression of mesothelioma and ovarian cancer into the peritoneum (Rump et al., 2004). Due to the secreted nature of mesothelin, it has been found at elevated levels in the serum of breast and lung cancer patients compared to healthy volunteers (Robinson et al., 2003). Although mesothelin as a blood biomarker for PDAC patients has currently been unsuccessful (Sharon et al., 2012). One important finding in ovarian cancer has shown that mMSLN cleaved from the cell can engage with the mannose receptor of TAMs, promoting an immunosuppressive phenotype and therefore tumour progression (Dangaj et al., 2011).

5.1.4 Hypothesis

Tumour cells can influence their own progression through the secretion of specific factors. These secreted factors differ between tumour cells of differential metastatic potential.

5.1.5 Aims

- To identify tumour cells with differing metastatic potential using a preclinical orthotopic mouse model
- To SILAC label tumour cells and analyse secreted factors by mass spectrometry
- Bioinformatic analysis of SILAC mass spectrometry data
- Identification of differing factors secreted by KPC-derived PDAC cell lines

5.2 RESULTS

5.2.1 Orthotopically implanted FC1242, FC1245 and FC1199 cells create tumours with varied aggressiveness

Human PDAC disease and the KPC genetic PDAC mouse model are known to metastasise to the liver and lungs (Humphris et al., 2014, Pandol et al., 2009, Hingorani et al., 2003). As shown in chapter 3 of this thesis, orthotopic implantation of KPC-derived PDAC tumour cells into the tail of the pancreas creates a tumour mass recapitulative of the human disease. This posed the question as to whether the orthotopic implantation model also recapitulated metastasis to the liver and lungs after an extended period of tumour growth (Fig 5.1 A).

To investigate this in our model, three KPC-derived cell lines, FC1199 luc/zsGreen, FC1242 luc/zsGreen and FC1245 luc/zsGreen were each implanted into the pancreas of syngeneic C57BL/6J recipient mice (n=3 per cell line) to determine which cell line created the largest metastatic burden (Fig 5.1 B). To maximise the potential of metastasis occurring, the mice were maintained until they met humane endpoint as dictated by project license restrictions. To monitor welfare, the mice were checked three times a week to supervise weight loss, restrictions in movement, dehydration and loss of appetite.

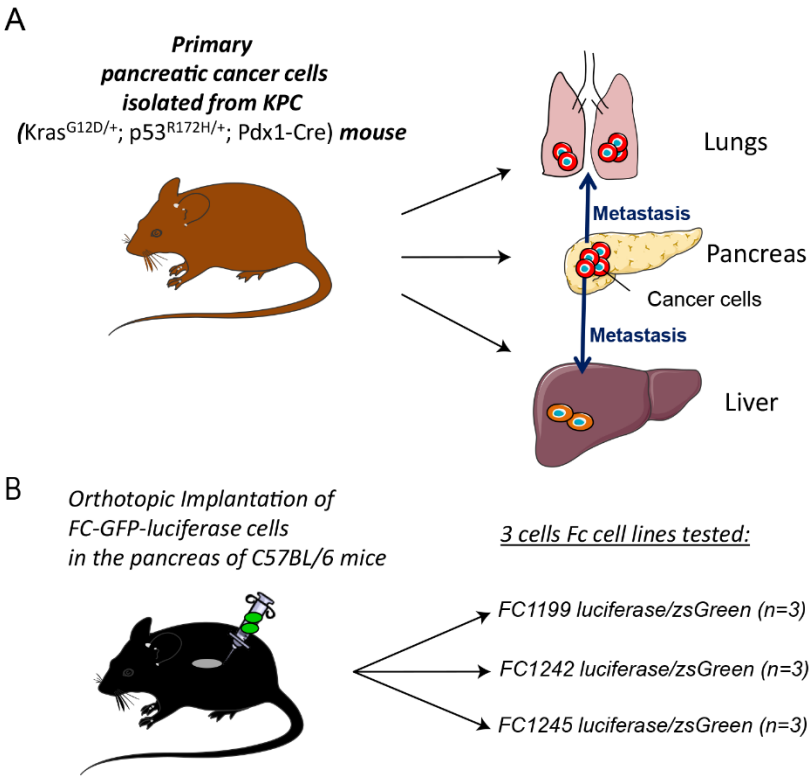

Figure 5.1 Schematic of orthotopic implantation into pancreas and metastasis to liver and lungs

A) Cells isolated from the Kras$^{G12D/+;}$ p53$^{R172H/+}$; Pdx1-Cre genetic PDAC mouse model were orthotopically implanted into the tail of the pancreas of syngeneic recipient C57BL/6J mice. PDAC cells penetrate the peritoneum and colonise the liver and lungs creating metastatic foci. **B)** KPC-derived cell lines FC1199 luc/zsGreen, FC1242 luc/zsGreen and FC1245 luc/zsGreen were implanted into the pancreas of C57BL/6J mice (n=3 mice per cell line).

Unexpectedly, the three FC1245 tumour-bearing mice met humane endpoint at 19, 22 and 25 days after implantation due to 20 % weight loss and restriction of movement and were culled via a schedule one method in accordance with project license restrictions (Fig 5.2 A). One FC1242 tumour bearing mouse was culled at 51 days after implantation meeting endpoint description due to 20 % weight loss, however, the remaining FC1242 (n=2) and FC1199 (n=3) tumour bearing mice were culled on day 56 after implantation due to deterioration of their general condition (Fig 5.2 A).

At the time of harvesting, primary PDAC tumour, liver and lungs were resected. Interestingly, FC1245 tumours showed no significant differences in size compared to FC1242 or FC1199 tumours despite being harvested around 30 days earlier (Fig 5.2 B).

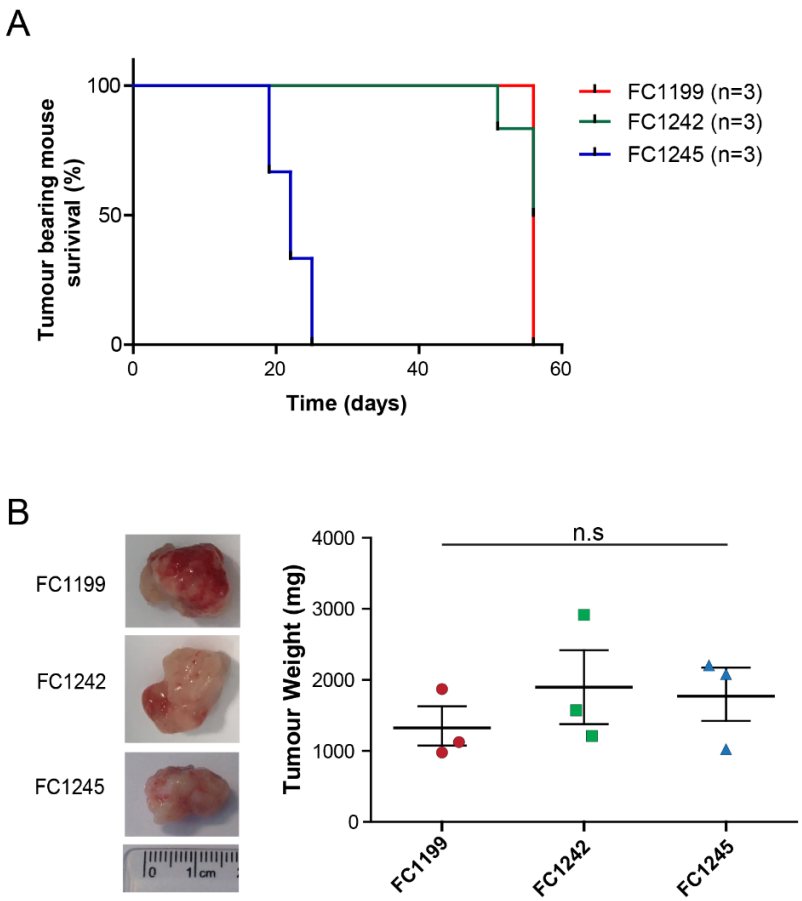

Figure 5.2 FC1245-tumour bearing mice exhibit reduced survival but no significant change in tumour size

A) Survival percentage of FC1199, FC1242 and FC1245 tumour bearing mice over the course of the experiment (n=3 mice per cell line). **B)** Representative images of harvested tumours and tumour weights at time of harvesting for FC1199, FC1242 and FC1245 tumours (n=3 tumours per cell line). n.s = non-significant p = 0.5995 using one-way ANOVA and Tukey post hoc test

Before sacrifice, two mice from each cell implantation group (FC1199 mice Cage (Cg) 1.1 and Cg1.3, FC1242 mice Cg2.2 and Cg2.3 and FC1245 mice Cg3.1 and Cg4.2) were imaged using IVIS technology to detect *in vivo* signal from luc/zsGreen tumour cells. A high signal was detected in the abdomen, approximately in the location of the pancreas, in all mice imaged (representative images Fig 5.3). Post mortem *ex vivo* IVIS imaging of resected primary tumour, liver and lungs confirmed solid PDAC tumours were formed and liver and lung metastasis was established by all cell lines (Fig 5.3).

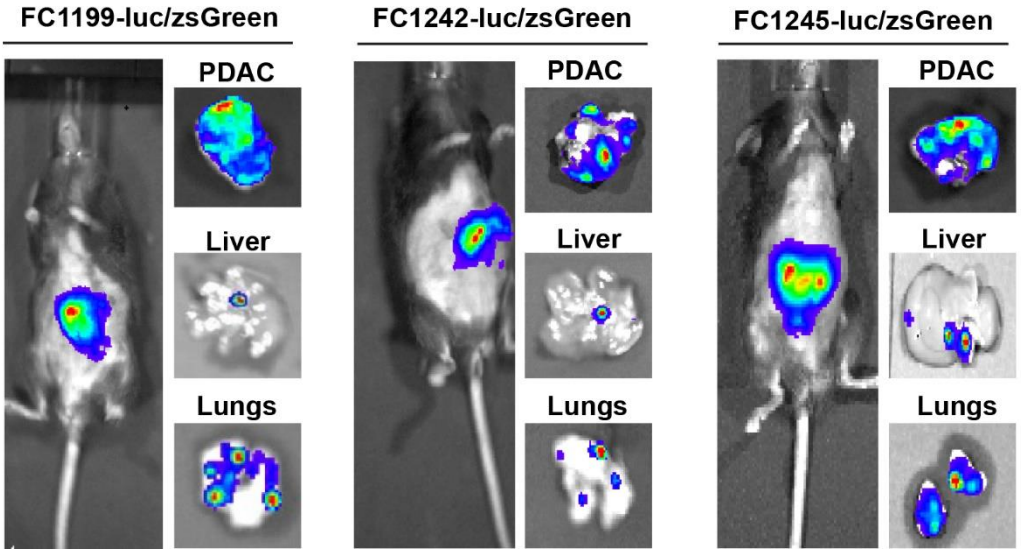

Figure 5.3 *In vivo* and *ex vivo* IVIS imaging confirms the presence of liver and lung metastasis

IVIS imaging of *in vivo* FC1199 luc/zsGreen, FC1242 luc/zsGreen and FC1245 luc/zsGreen tumour bearing mice, 1 minute exposure. *Ex vivo* IVIS imaging of primary PDAC tumour, liver and lungs to detect zsGreen+ tumour cells, 1 minute exposure.

IVIS analysis of the *ex vivo* PDAC tumours revealed, aside from the Cg1.1 FC1199 tumour, all tumours collected on day 56 had very similar levels of luciferase activity indicating the tumours have grown to a similar extent (Fig 5.4 A). Interestingly, the FC1245 tumours had comparatively higher luciferase activity at days 19 and 22 after implantation than the majority of tumours harvested at day 56, despite the non-significant changes in tumour mass (Fig 5.4 A).

Liver metastasis was confirmed by analysis of *ex vivo* IVIS readings. FC1245 livers exhibited high levels of luciferase activity (total flux per second) indicative of higher numbers of luc/zsGreen tumour cells at days 19 and 22 after implantation (Fig 5.4 B). FC1199 Cg1.1 mouse liver exhibited the highest luciferase activity (total flux per second) (Fig 5.4 B). FC1242 livers harvested at day 56 exhibited the lowest levels of liver metastasis among the three cell lines. (Fig 5.4 B).

Ex vivo lung metastasis imaging revealed FC1199 lungs again showed mouse Cg1.1 had the highest levels of total flux indicating more tumour cells (Fig 5.4 C). FC1245 lungs possessed metastasis, although mouse Cg3.1 harvested at day 22 had signal similar to or higher than day 56 lungs, excluding FC1199 Cg1.1 (Fig 5.4 C). Overall, the levels of total flux detected in FC1245 livers and lungs were higher than the majority of livers and lungs harvested at day 56, indicating metastasis had occurred sooner or more successfully with this cell line compared to FC1199 and FC1242 cell lines (Fig 5.4 B and C).

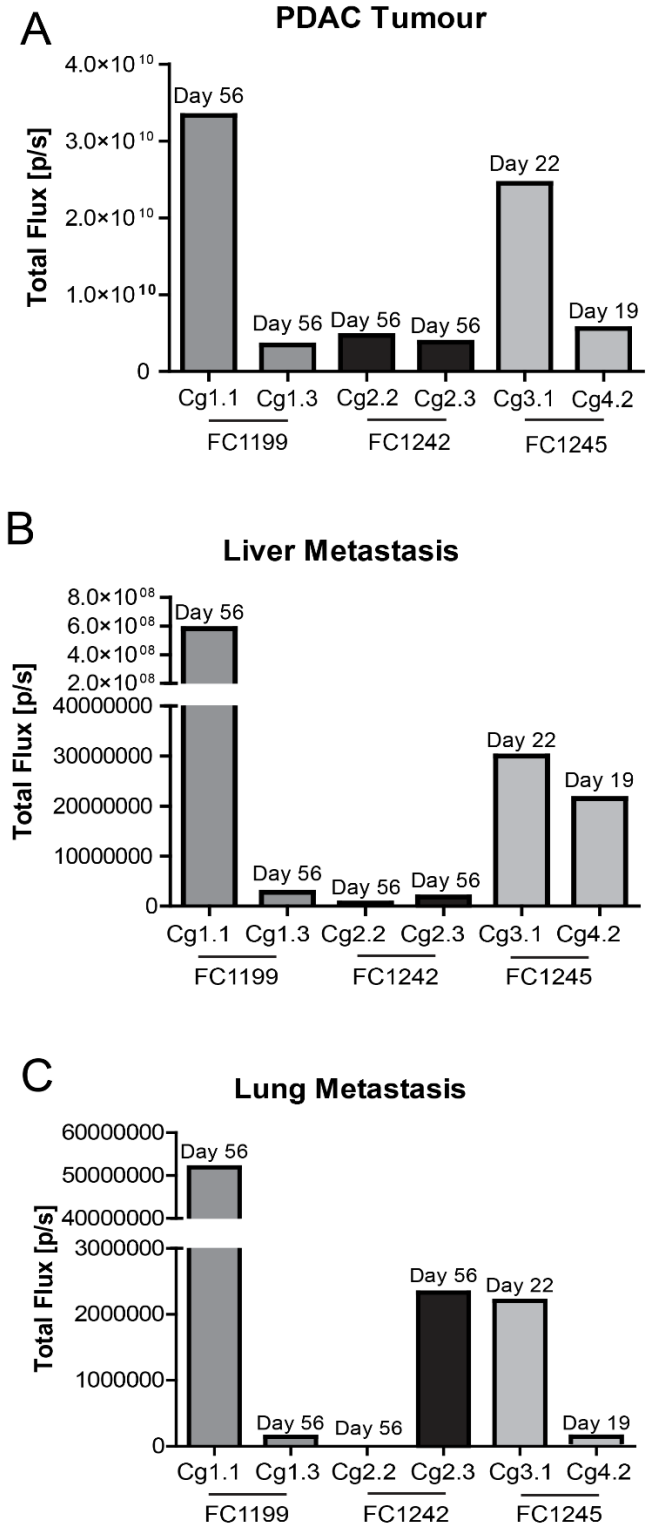

Figure 5.4 FC1245 tumours exhibit metastasis to liver and lungs by day 19
Quantification of *ex vivo* IVIS imaging detecting luciferase activity (total flux per second) of FC1199 mice Cg1.1 and Cg1.3, FC1242 mice Cg2.2 and Cg2.3 and FC1245 mice Cg3.1 and Cg4.2. **A)** Primary PDAC tumours, **B)** Liver metastasis, **C)** Lung metastasis. Day of harvesting indicated for each tumour.

5.2.2 FC1245 tumours show a slight decrease in vasculature and collagen deposition compared to FC1199 and FC1242 tumours.

Due to the differences seen in metastatic potential and the severe decrease in life expectancy with FC1245 implanted mice, it was important to investigate whether any major differences were obvious within the primary tumour itself. Therefore, the primary PDAC tumours were serially sectioned and immunohistochemically stained for CD31 vasculature marker, CD3 T cell marker, αSMA myofibroblast marker and picrosirius red staining for collagen deposition (Fig 5.5 A). Quantification of CD31 staining for endothelial cells revealed a tendency of FC1245 tumours to possess reduced vasculature, although this was not significantly decreased (Fig 5.5 B). Presence of CD3 T cells showed no significant differences between the tumours, although FC1199 showed a slight decrease in T cell infiltration (Fig 5.5 B). As previously mentioned, CAFs are an abundant cell type in the TME which has been reported to both restrain and support tumour growth. Identification of αSMA^{+} CAFs in the tumours showed variable results across all tumours of FC1199, FC1242 and FC1245 origin and ultimately showed no significant difference among the tumour types (Fig 5.5 B). Perturbations in collagen deposition can affect the migration of tumour cells and therefore influence metastasis. Quantification of picrosirius red staining revealed no significant differences, however, FC1245 tumours showed a slight decrease compared to FC1199 and FC1242 primary tumours (Fig 5.5 B).

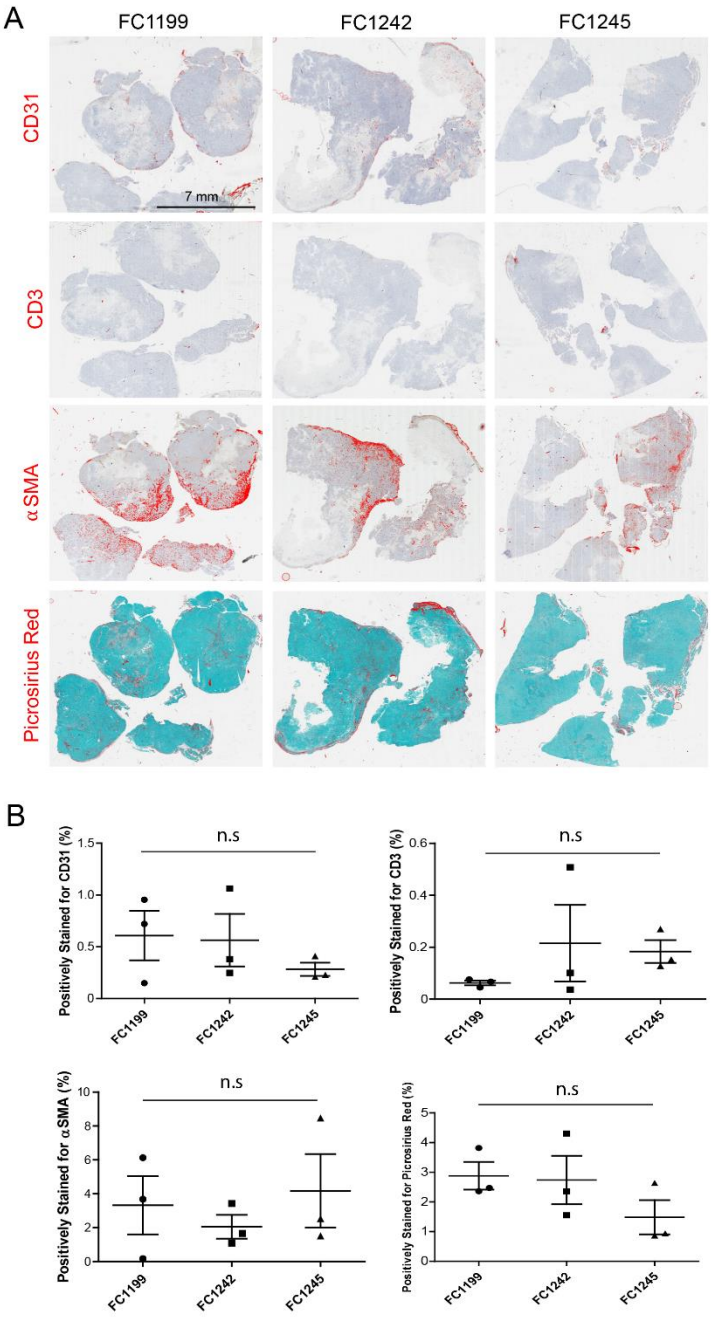

Figure 5.5 FC1199, FC1242 and FC1245 tumours show no significant differences in primary tumour composition

A) Immunohistochemical staining of serial sections of FC1199, FC1242 and FC1245 tumours for CD31 vascular marker, CD3 T cell marker, αSMA CAF marker and picrosirius red collagen deposition, scale bar 7 mm. **B)** Quantification of CD31 positive staining n.s. = non-significant p=0.5147, CD3- positive cells p=0.4844, αSMA-positive stain p=0.6771 and picrosirius red stain p=0.3040, using one-way ANOVA and Tukey post hoc test in FC1199, FC1242 and FC1245 tumours (n=3 tissues stained per marker).

5.2.3 Rationale for a proteomic approach to determine secretome differences between FC1199, FC1242 and FC1245 cells

It is known that the tumour and the TME partake in a bi-directional cross-talk which can influence tumour progression (Hanahan and Coussens, 2012). Therefore, FC1245 tumour cells may produce an altered secretome profile to support their increased metastatic potential. Although not significant, the tissue stainings revealed a slight decrease in vasculature and collagen deposition which could also be mediated by secreted factors. These reasons provided the rationale to investigate the secretome profiles of the FC1199, FC1242 and FC1245 tumour cells to determine any altered secreted factors which could influence tumour progression and metastasis (Fig 5.6).

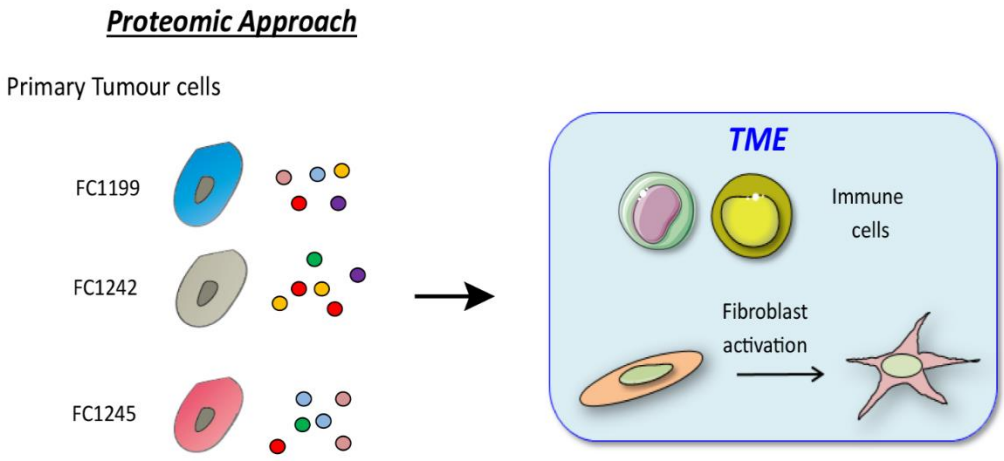

Figure 5.6 Proteomic experimental rationale to investigate FC1199, FC1242 and FC1245 cells

A schematic to depict the rationale behind a proteomic approach to determine secretome profile of FC1199, FC1242 and FC1245 primary murine PDAC tumour cells generated from the KPC GEMM of PDAC. To investigate differences in tumour secretome profile which may identify factors which signal to immune cells and mediate fibroblast activation in the tumour microenvironment altering the tumour progression.

5.2.4 SILAC mass spectrometry approach for secreted factors

Stable isotope labelling with amino acids in cells culture (SILAC) mass spectrometry is an attractive proteomic approach in this case as it enables quantitative analysis of proteins rather than qualitative identification. FC1199, FC1242 and FC1245 tumour cells may secrete the same factors but their expression levels of the proteins may be altered influencing TME interactions.

The FC1245, FC11199 and FC1242 tumour cells were incubated with light, medium and heavy SILAC media respectively, to allow incorporation of carbon 13 and nitrogen 15 labelled amino acids into proteins. The CM was collected and subjected to a triplex liquid chromatography tandem mass spectrometry (LC-MS/MS) to identify quantitative changes in secreted proteins (Fig 5.7).

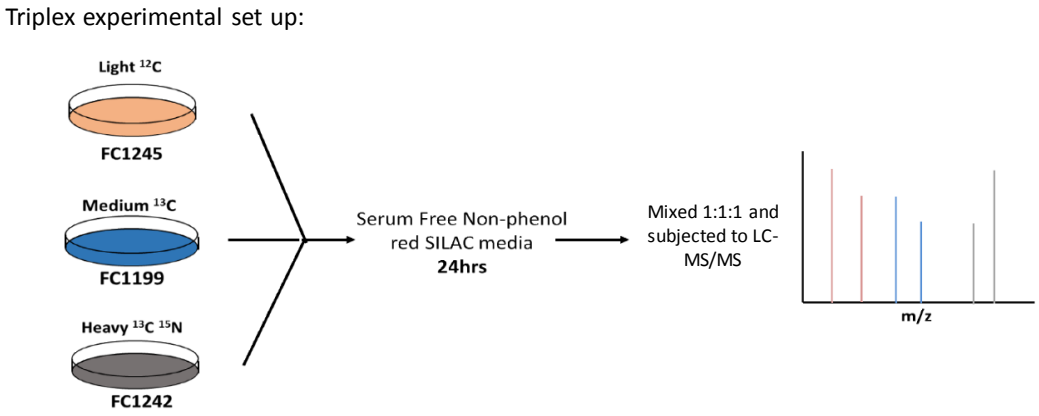

Figure 5.7 SILAC mass spectrometry experimental design

PDAC tumour cells incubated with serum free non-phenol red SILAC media: FC1245 cells with light R0K0 ^{12}C SILAC media, FC1199 cells with medium R6K6 ^{13}C media and FC1242 cells with heavy R10K8 ^{13}C and ^{15}N media *in vitro*. Media was collected after 24 hr incubation and mixed 1:1:1 and analysed by liquid chromatography tandem mass spectrometry (LC-MS/MS) (n=4 biological replicates).

5.2.5 Reliability of SILAC mass spectrometry data

The raw files from LC-MS/MS were run through Maxquant software to perform peak picking and create ratios for the quantitative measure of secreted proteins. Due to the nature of Maxquant SILAC sample analysis, the output created ratios of Heavy/Light (FC1242/FC1245), Medium/Light (FC1199/FC1245) and Heavy/Medium (FC1242/FC1199) labelled samples for each replicate (n=4). Principal component analysis (PCA) was performed by means of quality control on the four triplex replicates. FC1242/FC1245, FC1199/FC1245 and FC1242/FC1199 ratios perfectly separated, with the replicates each building a segregated cluster confirming reproducibility (Fig 5.8).

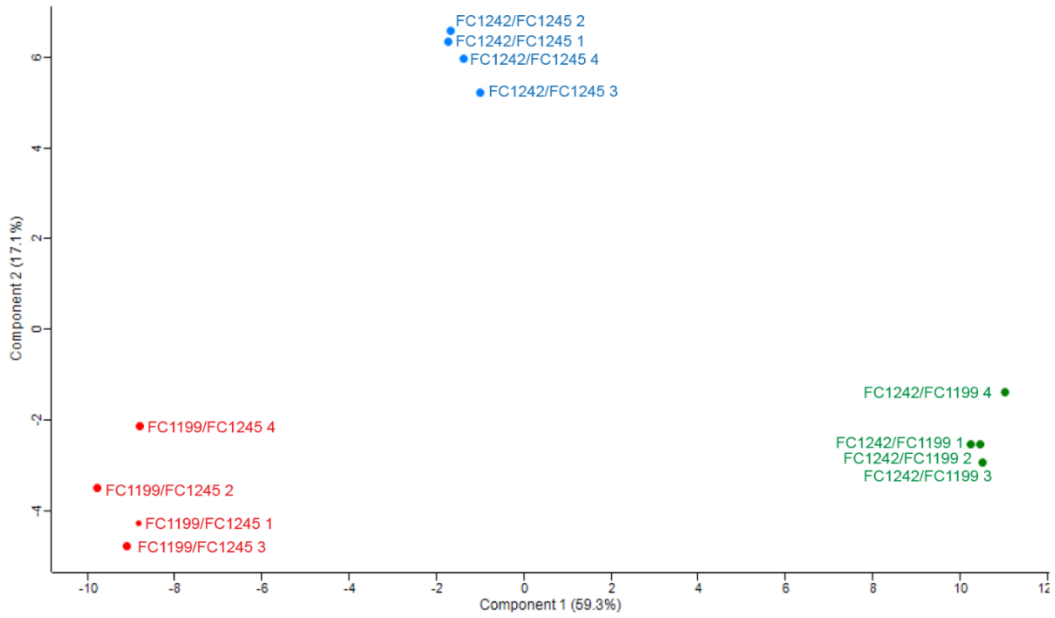

Figure 5.8 Principal component analysis of SILAC replicates shows a high degree of similarity

Principal component analysis (PCA) of triplex secretome SILAC mass spectrometry replicates analysed by Perseus software. PCA based on gene ontology of biological processes annotation using Benjamini-Hochberg cut off (FDR=0.05). Replicates of triplex samples were processed into FC1199/FC1245, FC1242/FC1245 and FC1242/FC1199 ratios which cluster independently.

To further investigate the relationship between individual replicates, the linear correlation between individual samples was calculated to identify any replicates which should be regarded as outliers. Direct comparisons of replicates all resulted in a Pearson correlation coefficient of ≥0.9 indicating a high similarity between replicates (Fig 5.9)

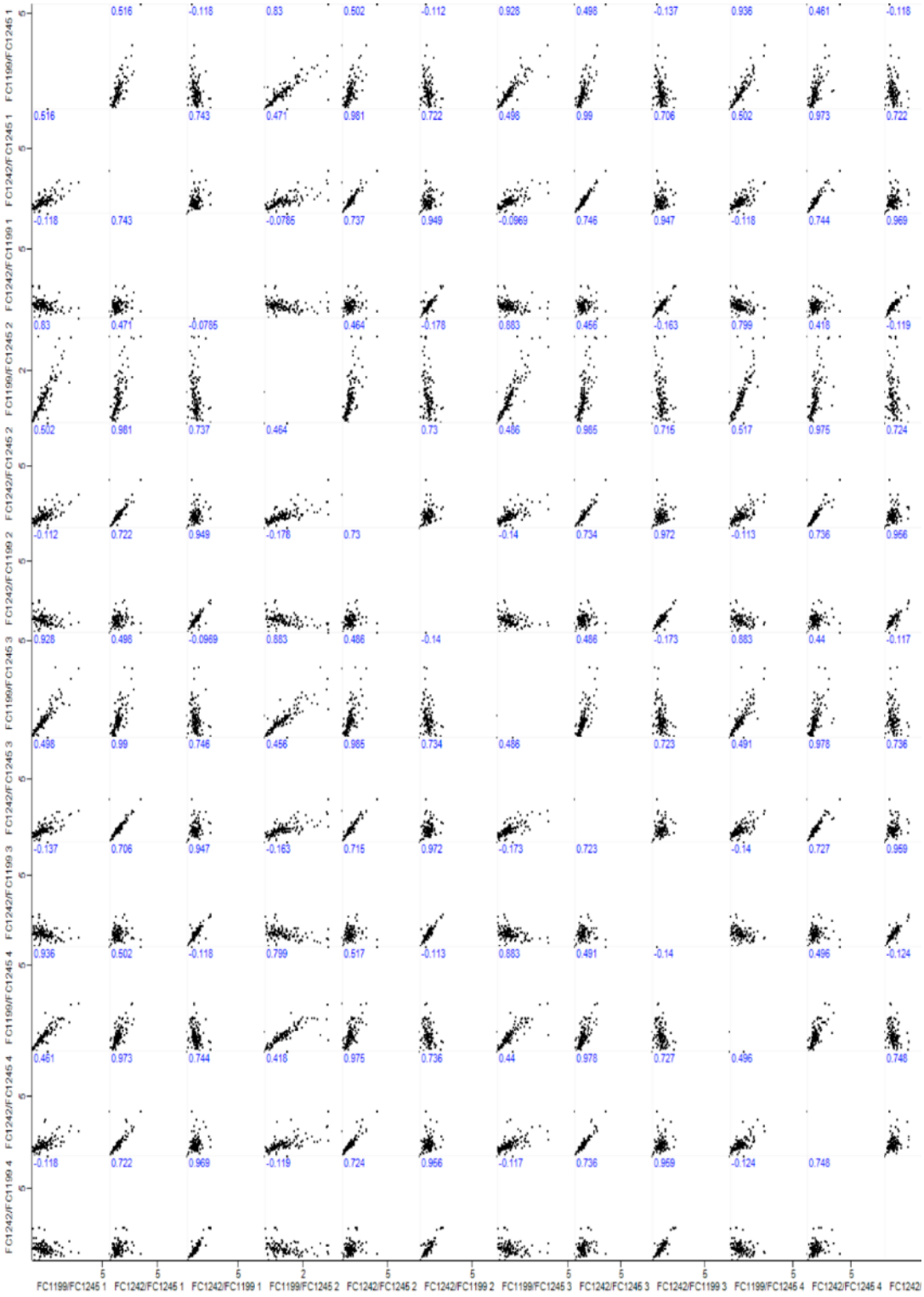

Figure 5.9 Pearson correlation shows sample replicates are highly comparable Comparison of SILAC samples by multiscatter plot showing linear correlation of proteins detected in each replicate FC1199/FC1245, FC1242/FC1245 and FC1242/FC1245 created by Perseus software. Pearson correlation coefficient calculated for every sample comparison and shown in blue at top left of each graph.

5.2.6 Identification of significantly differentially abundant proteins in FC1245 samples

To identify proteins with differing abundance between FC1199, FC1242 and FC1245 cell lines, analysis of variance (ANOVA) statistical analysis was performed using the LIMMA statistical package in R. The results were visualised by volcano plots in which p value (-log10) was plotted against fold change (log2) allowing significantly abundant proteins to be identified ($p \leq 0.01$). A comparison of FC1245 and FC1199 samples revealed 32 significantly enriched proteins secreted by FC1245 cells compared to 44 significantly enriched proteins secreted by FC1199 cells (Fig 5.10 A, Sup. Table 1A). Comparison of FC1245 and FC1242 samples revealed 47 significantly enriched proteins secreted by FC1245 cells compared to 33 significantly enriched proteins secreted by FC1242 cells (Fig 5.10 B, Sup. Table 1B).

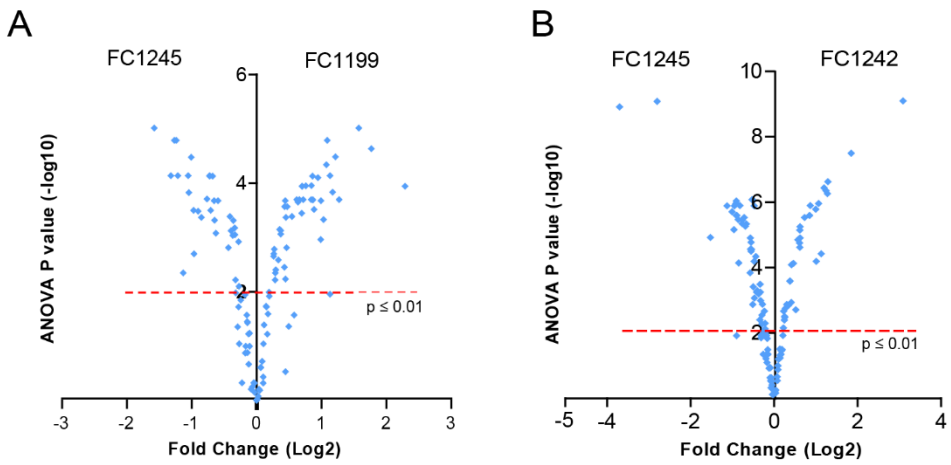

Figure 5.10 Volcano plots reveal significantly differentially regulated proteins in each sample

Volcano plots depicting ANOVA statistical analysis of protein abundance (-log10) against protein fold change (log2) identifying significantly enriched proteins in each sample above $p \leq 0.01$ using ANOVA (indicated by dashed red line)**. A)** FC1245 vs FC1199 **B)** FC1245 vs FC1242.

FC1245 tumours grew more aggressively *in vivo* compared to both FC1199 and FC1242 tumours, resulting in reduced life expectancy (Fig 5.2). Potential candidate proteins which influence FC1245's increased progression are likely to be present at increased abundance compared to both FC1199 and FC1242 secretion levels. Comparison of FC1245, FC1242 and FC1199 samples allowed the identification of consistently significantly enriched proteins secreted by FC1245 samples compared to FC1199 (Fig 5.11 A) and FC1242 (Fig 5.11 B).

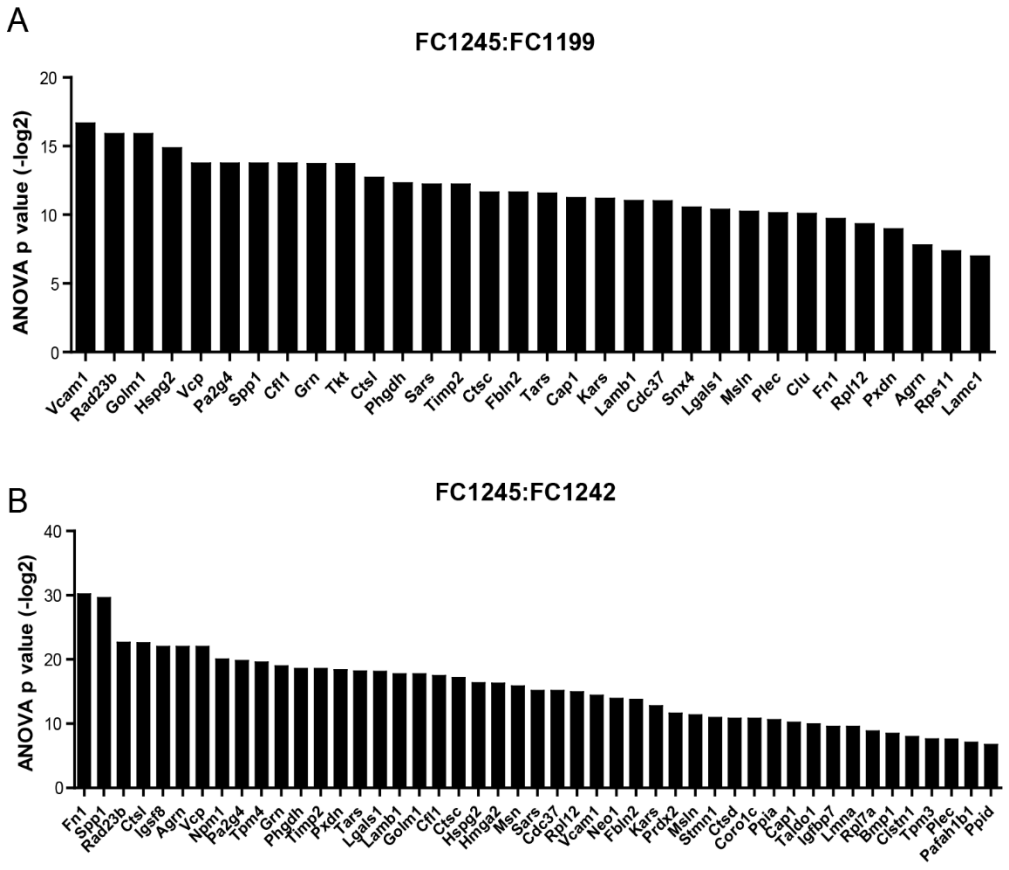

Figure 5.11 Significantly upregulated proteins secreted by FC1245 tumour cells

Identification of proteins secreted at significantly increased abundance by FC1245 tumour cells, $p \leq 0.01$ using ANOVA. Gene names indicated, shown against ANOVA p value (-log2). **A)** FC1245 tumour cells compared to FC1199 tumour cells (32 proteins present at significantly increased abundance). **B)** FC1245 tumour cells compared to FC1242 tumour cells (47 proteins present at significantly increased abundance).

A two-way comparison of the significantly differentially secreted proteins in each sample revealed 19 proteins were consistently present at significant abundance in FC1245 cells compared to both FC1199 and FC1242 cells (Fig 5.12, Sup. Table 1 A-C).

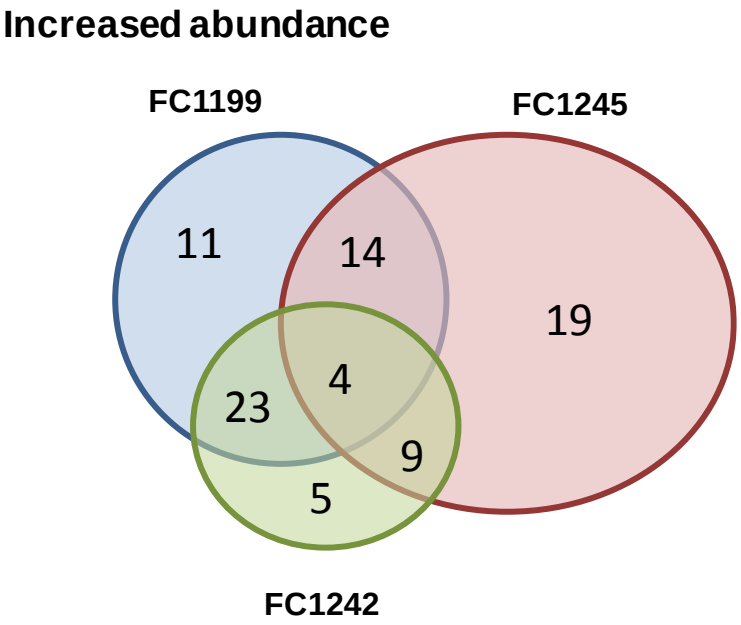

Figure 5.12 Nineteen proteins are consistently significantly secreted by FC1245

Venn diagram identifying 19 proteins consistently enriched in FC1245 samples compared to both FC1199 and FC1242. 5 proteins were consistently enriched in FC1242 samples compared to both FC1245 and FC1199. 11 proteins were identified as consistently enriched in FC1199 samples compared to both FC1245 and FC1242 samples. 14 proteins were identified as consistently increased in both FC1199 and FC1245 samples, 9 proteins were expressed by both FC1245 and FC1242 and 23 proteins both expressed by FC1199 and FC1242. 4 proteins were significantly expressed by all cell lines.

It was important to confirm that the nineteen proteins of increased abundance from FC1245 cells were truly secreted. Each protein identified by Maxquant was searched in SecretomeP, SignalP and TMHMM databases along with Uniprot gene ontology (GO) to identify secretion characteristics (Table 5.1). From this analysis, eleven proteins were identified as either classically or non-classically secreted (Table 5.1, shown in red). Of these eleven enriched secreted proteins, mesothelin was identified as a protein of interest due to its identification in 60 samples of resected primary human PDAC and its ability to regulate growth and apoptosis in PDAC (Argani et al., 2001).

	Protein Name	Genes	Secretome P	Signal P	TMHMM	Uniprot	Reported in PDAC or other cancers?	References
1	UV excision repair protein RAD23 homolog B	Rad23b	0.236	N	0	Nucleus	Upregulated in IPMN	(Sato et al., 2004)
2	Cathepsin L1	Ctsl	0.686	Y	0	Lysosome	Levels in plasma may be used as a potential prognostic marker for the disease	(Singh et al., 2014)
3	Agrin	Agrn	0.44	N	1	Cell membrane	Low levels present in PDAC liver metastasis	(Somoracz et al., 2010)
4	Transitional endoplasmic reticulum ATPase	Vcp	0.163	N	0	Cytosol	Identified as differentially regulated in PDAC	(Yamamoto et al., 2004)
5	Proliferation-associated protein 2G4	Pa2g4	0.261	N	0	Cytoplasm	No	
6	Granulins	Grn	0.651	Y	0	Secreted	Present in PDAC liver metastasis	(Nielsen et al., 2016)
7	D-3-phosphoglycerate dehydrogenase	Phgdh	0.54	N	0	Secreted	Decreased in PDAC by mass spectrometry	(Pan et al., 2011)
8	Metalloproteinase inhibitor 2	Timp2	0.866	Y	0	Secreted	Direct target of miR-221/222 (overexpression promotes PDAC)	(Xu et al., 2015)
9	Threonine--tRNA ligase	Tars	0.275	N	0	Cytoplasm	Reportedly decreased in PDAC	(Pan et al., 2011)
10	Galectin-1	Lgals1	0.402	N	0	ECM	Increase progression and reduce survival of PDA	(Liu and Rabinovich, 2005)
11	Laminin subunit beta-1	Lamb1	0.391	Y	0	Secreted	Upregulated in metastasis of adenocarcinomas	(Segara et al., 2005)
12	Dipeptidyl peptidase 1	Ctsc	0.76	Y	0	Lysosome	Tissue-specific regulator of squamous carcinogenesis	(Yu et al., 2009)
13	60S ribosomal protein L12	Rpl12	0.865	N	0	Cytoplasm	Increased in PanINs	(Prasad et al., 2005)
14	Fibulin-2	Fbln2	0.477	Y	0	ECM	Driver of malignant progression in lung adenocarcinoma	(Baird et al., 2013)
15	Serine--tRNA ligase, cytoplasmic	Sars	0.203	N	0	Nucleus	Not reported	
16	Hsp90 co-chaperone Cdc37	Cdc37	0.259	N	0	Cytoplasm	Increased in PDAC	(Buchholz et al., 2005)
17	Lysine--tRNA ligase	Kars	0.278	N	0	ECM	RNA levels are increased 2 fold in PanIN 1a,1b and 2	(Prasad et al., 2005)
18	Mesothelin	Msln	0.609	Y	0	Secreted	Regulate growth and decrease apoptosis in PDAC cell lines. Identified in 60 resected PDAC lesions.	(Argani et al., 2001)
19	Adenylyl cyclase-associated protein 1	Cap1	0.347	N	0	PM	Overexpressed in pancreatic cancers	(Yamazaki et al., 2009)

Table 5.1 Significantly secreted FC1245 proteins compared to both FC1199 and FC1242

19 proteins consistently enriched by FC1245 cells compared to FC1199 and FC1242 secretome profiles. Protein names, gene names, secretomeP NN_score, signalP D-score, TMHMM score, Uniprot gene ontology (GO), literature search of previous reports in PDAC or other cancers. Classically and non-classically secreted proteins are shown in red.

5.2.7 Mesothelin expression in FC1245 cells

SILAC mass spectrometry was performed on *in vitro* samples, therefore it was important to confirm the findings using *in vivo* tissue. Mass spectrometry identified mesothelin as abundant in FC1245 cells, however this detected sequence encompasses both MPF and mMSLN (Fig 5.13 A). We decided to focus these studies on mMSLN due to its implications in interacting with TAMs in ovarian cancer (Dangaj et al., 2011). To confirm whether mMSLN was differentially expressed in FC1245, FC1242 and FC1199 cells, it was necessary to use an antibody which bound specifically to the 40 kDa C-terminus portion of mesothelin. The mesothelin antibody Orb14370 (Biorbyt) binds specifically to the C-terminus region of precursor mesothelin (sequence: GLGLQGGIPNGYLVL) and therefore to cleaved 40 kDa mMSLN (Fig 5.13 B).

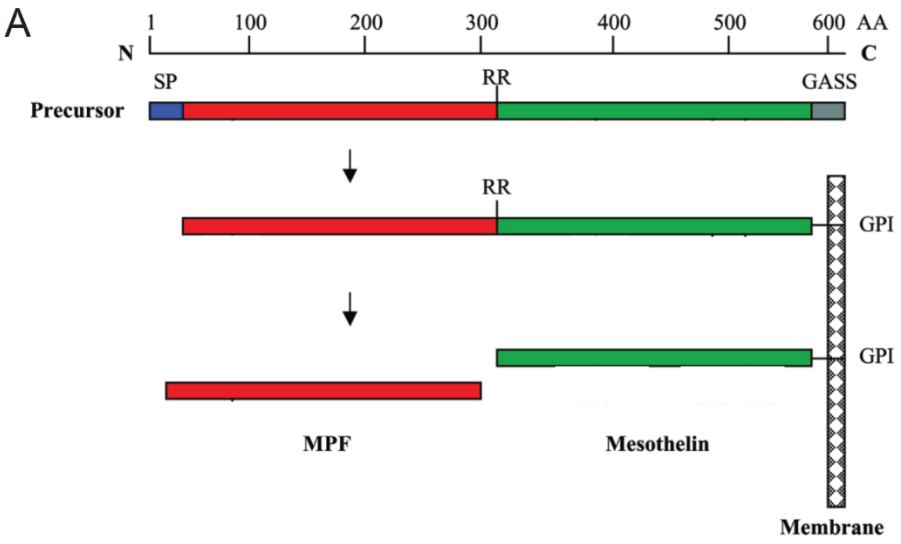

B

Mesothelin Ab Biorbyt # Orb14370 binding sequence: GLGLQGGIPNGYLVL

>sp|Q61468|MSLN_MOUSE Mesothelin OS=Mus musculus OX=10090 GN=Msln PE=1 SV=1
N-terminus: MALPTARPLLGSCGSPICSRSFLLLLLSLGWIPRLQTQTTKTSQEATLLHAVNGAADFAS
LPTGLFLGLTCEEVSDLSMEQAKGLAMAVRQKNITLRGHQLRCLARRLPRHLTDEELNAL
PLDLLLFLNPAMFPGQQACAHFFSLISKANVDVLPRRSLERQRLLMEALKCQGVYGFQVS
EADVRALGGLACDLPGKFVARSSEVLLPWLAGCQGPLDQSQEKAVREVLRSGRTQYGPPS
KWSVSTLDALQSLVAVLDESIVQSIPKDVKAEWLQHISRDPSRLGSKLTVIHPRFRRDAE
QKACPPGKEPYKVDEDLIFYQNWELEACVDGTMLARQMDLVNEIPFTYEQLSIFKHKLDK
TYPQGYPESLIQQLGHFFRYVSPEDIHQWNVTSPDTVKTLLKVSKGQKMNAQAIALVACY
LRGGGQLDEDMVKALGDIPLSYLCDFSPQDLHSVPSSVMWLVGPQDLDKCSQRHLGLLYQ
KACSAFQNVSGLEYFEKIKTFLGGASVKDLRALSQHNVSMDIATFKRLQVDSLVGLSVAE
VQKLLGPNIVDLKTEEDKSPVRDWLFRQHQKDLDRLGLGLQGGIPNGYLVLDFNVREAFS
SRASLLGPGFVLIWIPALLPALRLS - C-terminus

Figure 5.13 Mesothelin Ab Orb14370 binds to the C-terminus portion of mesothelin

A) Schematic showing the maturation of mesothelin protein. Precursor 71 kDa protein mesothelin is synthesized with a potential signal peptide (SP) and the glycosylphosphatidyl inositol anchor signal sequence (GASS) are predicted at the NH2 terminus and the COOH terminus, respectively. The precursor protein has a furin cleavage site (RR). Cleavage at the furin site generates membrane-bound mature mesothelin (green) and the secretory protein megakaryocyte-potentiating factor (red). (Hassan et al., 2004). **B)** Identification of mesothelin antibody Orb14370 binding site on full length mesothelin, highlighted in yellow. From UniprotKB mesothelin FASTA amino acid sequence (ref: Q61468 MSLN_MOUSE).

To confirm the presence of mesothelin in the *in vivo* setting, FC1245 tumours and naïve murine pancreas were immunohistochemically stained revealing a lack of mesothelin in healthy tissue but high expression in FC1245 tumour tissue (Fig 5.14 A and B).

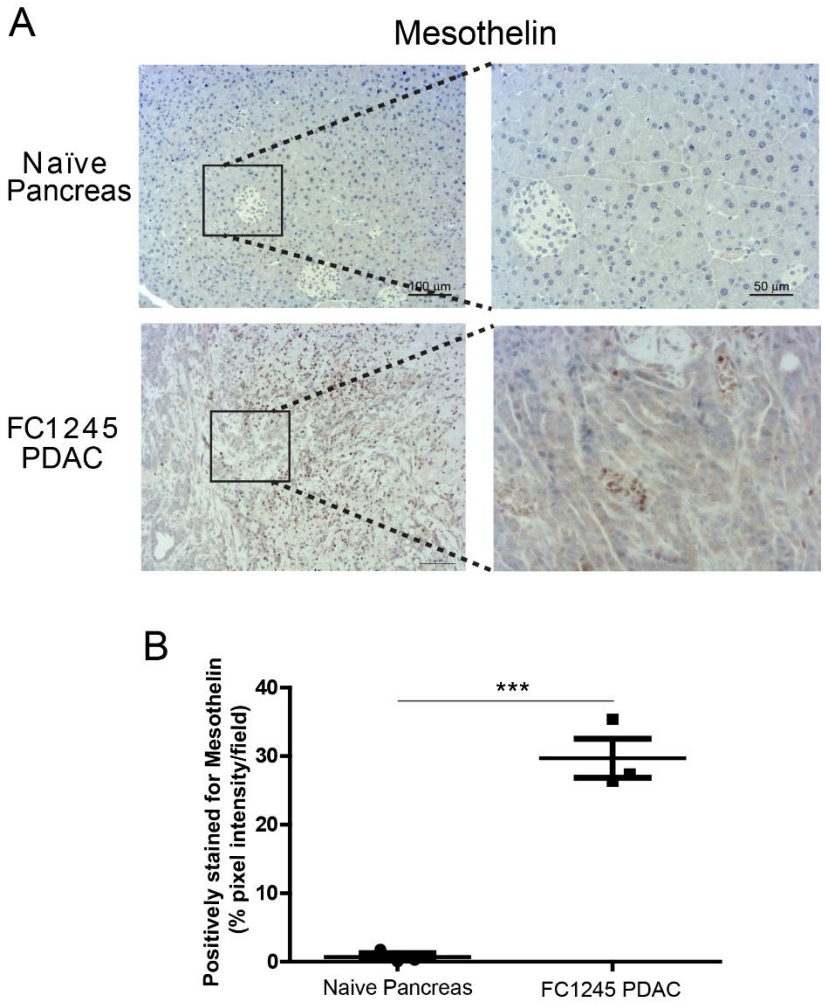

Figure 5.14 Mesothelin is detected in FC1245 tumour tissues and not in healthy pancreas

A) Immunohistochemical staining of mesothelin in healthy mouse pancreas and FC1245 murine tumour. Scale bars 100 µm and 50 µm. **B)** Quantification of immunohistochemical staining of mesothelin in naïve murine pancreas and FC1245 PDAC tumour. Error bars represent SEM (3 fields counted/mouse, n =3 mice per group). *** p-value ≤ 0.001, using one-way ANOVA and Bonferroni post hoc test.

To confirm the secretion of mMSLN by the FC1245 tumour cells, CM was concentrated and analysed by immunoblotting. FC1245 protein lysate showed a full length precursor mesothelin, whereas CM highly expressed mMSLN and distinctly lacks the full length precursor protein (Fig 5.15).

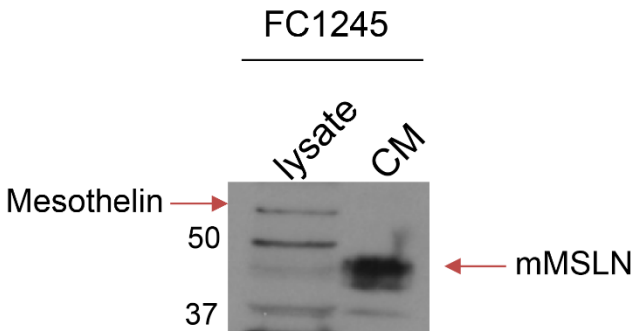

Figure 5.15 FC1245 tumour cells secrete 40 kDa mMSLN

Immunoblotting of FC1245 cell lysate and FC1245 concentrated conditioned media for the presence of mesothelin. Arrows indicate 71 kDa precursor mesothelin protein and cleaved 40 kDa mMSLN protein detected.

5.2.8 Mesothelin expression in FC1245, FC1242 and FC1199 cells

As the presence of precursor mesothelin was detected in FC1245 lysates and mMSLN was secreted by FC1245 tumour cells, it was important to confirm the results of the SILAC mass spectrometry analysis comparing expression against FC1199 and FC1242 cells. Firstly, all three cell lines expressed *Msln*, although surprisingly FC1199 cells expressed significantly more than FC1242 cells (Fig 5.16).

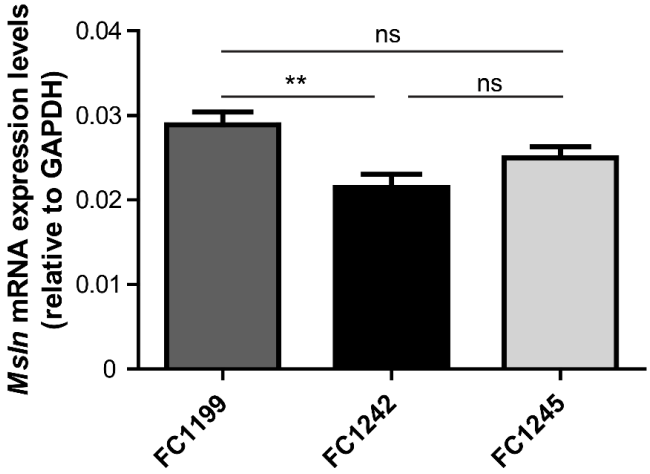

Figure 5.16 FC1199, FC1242 and FC1245 cell lines express *Msln*

Msln mRNA expression levels quantified in murine PDAC FC1199, FC1242 and FC145 tumour cells relative to GAPDH housekeeping gene. Error bars represent SEM (n = 3 technical replicates), ** $p \leq 0.01$ using one-way ANOVA and Tukey post hoc test.

However, mRNA expression levels do not always correlate with protein expression levels. Therefore, immunohistochemical staining of all FC1245, FC1242 and FC1199 tumours and naïve pancreas was performed for mesothelin. This again showed no positive staining in the healthy pancreas (Fig 5.17 A). All tumours showed positive staining for mesothelin however, FC1199 tumours possessed much weaker staining and FC1245 tissues expressed significantly higher levels of mesothelin (Fig 5.17A and B).

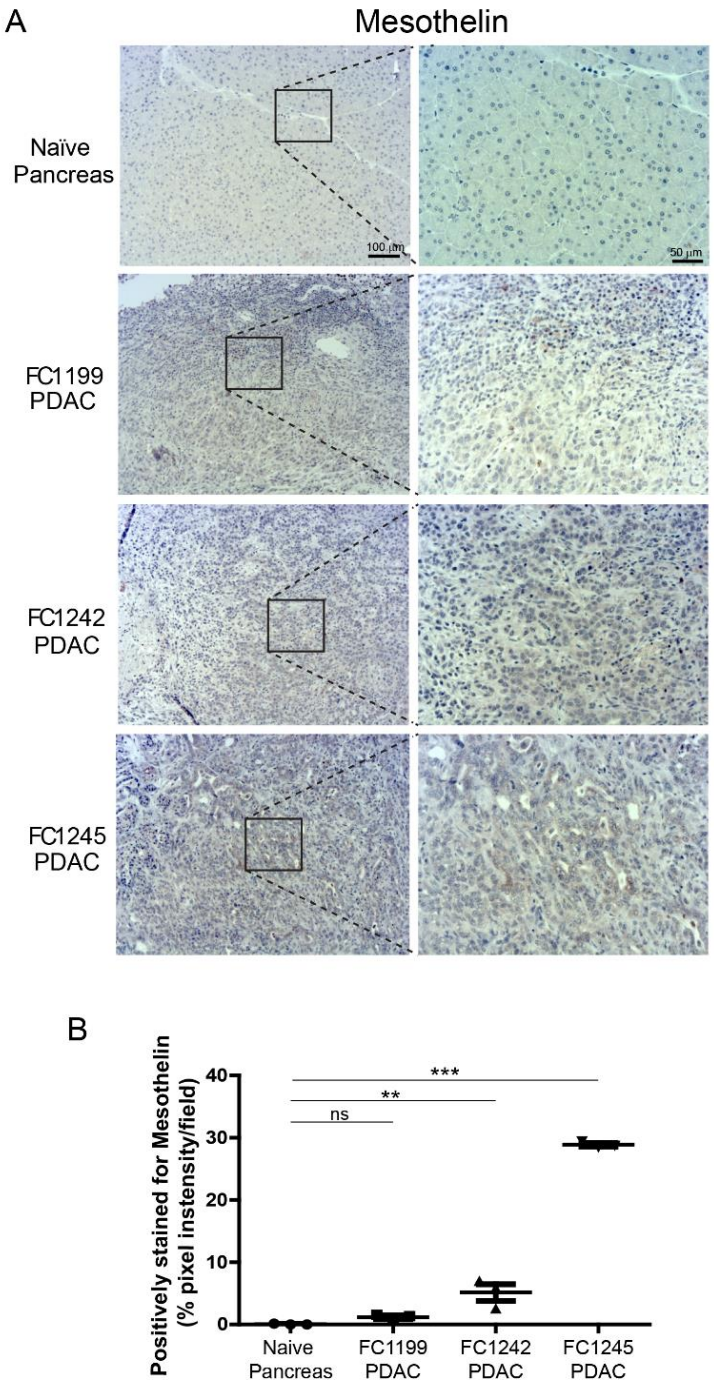

Figure 5.17 Mesothelin expression is limited to tumour tissue but at varying extents

A) Immunohistochemical staining of mesothelin in healthy pancreas, FC1199 PDAC, FC1242 PDAC and FC1245 PDAC. Scale bars 100 µm and 50 µm. **B)** Quantification of immunohistochemical staining of mesothelin in naïve murine pancreas, FC1199 PDAC, FC1242 PDAC and FC1245 PDAC tumour tissue. Error bars represent SEM (3 fields counted/mouse, n =3 mice per group). ** p-value ≤ 0.01, *** p-value ≤ 0.001, using one-way ANOVA and Bonferroni post hoc test.

To confirm that the FC1245 tumour cells secrete mesothelin at higher levels than FC1199 and FC1242 cells, CM was collected from all three cell lines and analysed by immunoblotting. This confirmed the results of the IHC and SILAC mass spectrometry that FC1245 cells secrete mMSLN at higher levels than FC1199 and FC1242 cells (Fig 5.18).

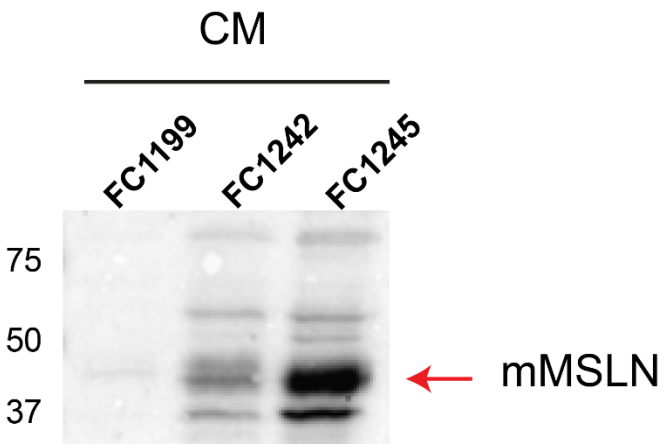

Figure 5.18 FC1245 cells secrete the highest levels of mMSLN

Immunoblotting of concentrated conditioned media collected from murine PDAC cells: FC1199, FC1242 and FC1245 for secreted mesothelin. Arrow indicates presence cleaved 40kDa mMSLN.

5.3 DISCUSSION

The work in this chapter has revealed cells from the KPC PDAC genetic mouse model can create tumours with varying aggressiveness when orthotopically implanted into syngeneic mice. Orthotopic implantation of FC1245 cells resulted in mice with reduced life expectancy and an increased propensity for liver and lung metastasis compared to FC1242 and FC1199 implanted cells.

Staining of the different tumour tissues revealed no significant changes in desmoplasia, T cell infiltration or αSMA+ myofibroblasts. Instead, only slight decreases in collagen deposition and CD31 vascular cells were seen in the FC1245 tumours compared to the FC1199 and FC1242 tumours. As major differences in tumour composition were not apparent, these results suggested differences governing tumour cell dissemination may be due to secreted factors.

Human PDAC patients possess genetic heterogeneity and varying levels of disease aggressiveness (Claire et al., 2016). Tumours are known to secrete factors which interact with the surrounding tumour stroma and neighbouring tumour cells to support outgrowth (Hanahan and Coussens, 2012). The use of SILAC mass spectrometry to quantitatively analyse the differences in tumour secretome between the three cell lines revealed nineteen consistently significantly enriched proteins secreted by the FC1245 cells compared to both FC1199 and FC1242 cell lines.

Mesothelin was identified as a protein of interest as it was enriched in FC1245 cells in the SILAC proteomic approach and has previously been reported in PDAC. Investigation into the function of mesothelin in PDAC proliferation and migration has so far shown conflicting results (Zheng et al., 2012, Zervos et al., 2016, Bharadwaj et al., 2011). *In vitro* analysis using qPCR, immunoblotting and IHC confirmed the

FC1245 cell line released higher levels of mMSLN expression compared to FC1199 and FC1242 cells.

Research into mesothelin as a blood biomarker to aid tumour diagnosis has been unsuccessful in PDAC patients despite tumour cells highly expressing mesothelin on their surface (Sharon et al., 2012). This is interesting as it has been detected in the serum of lung and breast cancer patients (Robinson et al., 2003). These results could be explained by the involvement of the rich PDAC TME restricting its release into the circulatory system, although these studies are currently lacking. In ovarian cancer, it has been shown that cleaved mMSLN can engage with CD206 receptors on TAMs and induce an immune suppressive phenotype (Dangaj et al., 2011). However, interactions of mMSLN with other stromal components and in different tumours has not been explored (Fig 5.19).

Mesothelin has been identified as a tumour antigen and has received attention as a suitable target in cancer therapy. Amatuximab (MORAb-009) is a high-affinity chimeric (mouse/human) monoclonal IgG1/k antibody with high affinity and specificity for mesothelin and has been developed and recently trialled for efficacy in PDAC patients in combination with gemcitabine treatment. The phase 2 trial of Amatuximab with gemcitabine (NCT00570713) failed to show any advantage over gemcitabine as a single agent. Amatuximab has been reported to bind specifically to the N-terminal fragment of mesothelin which binds to Muc16 receptor and therefore reduces metastasis (Ma et al., 2012). However, C-terminal cleaved mMSLN would still be free to function and this may explain the lack of success seen in the clinical trial, interestingly this is the proportion identified as upregulated in PDAC in this work. Overall, mMSLN warrants further exploration in PDAC due its detection in the more aggressive FC1245 tumours.

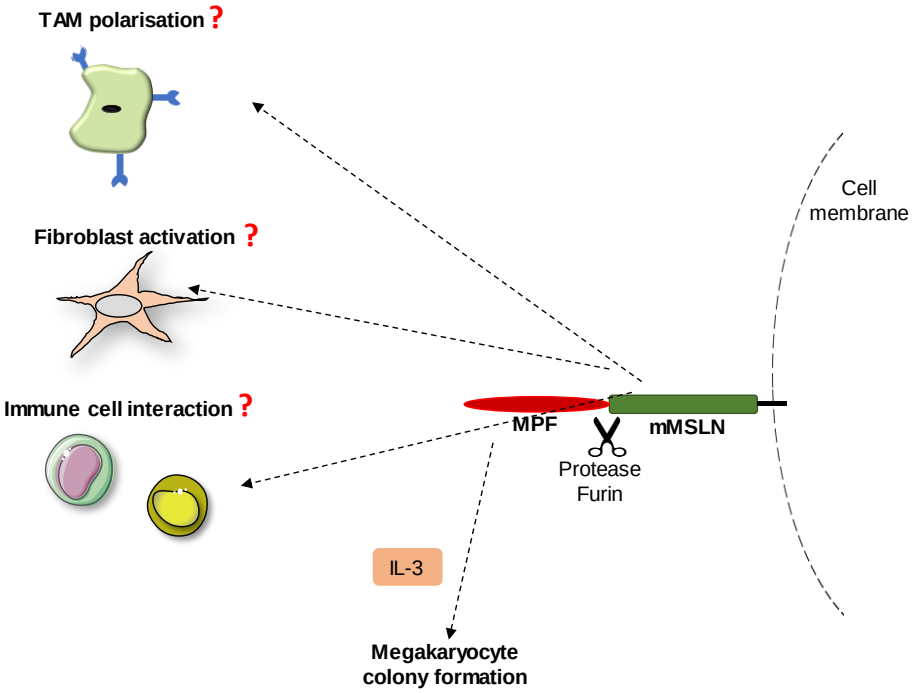

Figure 5.19 Functions of mesothelin in PDAC

Mesothelin is cleaved into N-terminal megakaryocyte potentiating factor (MPF) and C-terminal mature mesothelin (mMSLN). MPF interacts with IL-6 and potentiates megakaryocyte colony formation. mMSLN may bind to CD206 receptor on TAMs promoting M2 polarisation or mediate fibroblast activation or other immune cell actions.

Chapter Six:

Concluding Discussion

CONTENTS

6.1 INTRODUCTION

Chemoresistance and metastatic spread and are the major causes of mortality in cancer patients. PDAC and TNBC are two solid cancers which exhibit high levels of metastatic spread and resistance against their respective standard agents of care (Humphris et al., 2014, Pandol et al., 2009, Kim and Gallick, 2008, Weigelt et al., 2005, Marquette and Nabell, 2012). The TME of both invasive breast cancer and PDAC are rich with non-malignant stromal cells recruited to the tumour, the most abundant of which being macrophages and myofibroblasts. These TAMs and CAFs have been implicated in the promotion of tumour progression and survival (Paulus et al., 2006, Wyckoff et al., 2007, Bergers et al., 2000, Bonde et al., 2012, Costa et al., 2018). The current treatments available for both types of cancer exclusively target neoplastic cells which ultimately leads to patients acquiring resistance to the drug. Investigation into the role of the TME in chemoresistance and identification of new therapeutic targets which mediate resistance are therefore required. High levels of metastasis and advanced stage of disease reduce quality of life for cancer patients. Identification of tumour-released factors which mediate progression and aggressiveness may also provide future therapeutic targets.

6.2 SUMMARY OF THE WORK IN THIS THESIS

This thesis set out to elucidate how the TME in solid tumours, PDAC and TNBC, influences response to chemotherapeutic intervention, along with identifying factors that mediate tumour progression. Specifically, studies within this thesis were designed to explore secreted factors from macrophages and myofibroblasts, to identify ligands responsible for enhancing tumour cell survival when challenged with chemotherapy and testing signalling blockade in preclinical mouse models of neoplasia. Moreover, this thesis set out to determine variations in PDAC tumour progression *in vivo* using KPC-derived cell lines and to identify variable factors produced by the tumour cells. The objectives of this thesis have been met as IGF

signalling has been identified to enhance chemoresistance in both PDAC and invasive breast cancer (Fig 6.1 and 6.2) and the identification of increased abundance of mesothelin in advanced PDAC tumours.

The first experimental chapter of this thesis investigated PDAC resistance to gemcitabine treatment. Human and murine PDAC cell lines tested *in vitro* showed MCM and MyoCM increased tumour cell survival after gemcitabine chemotherapy administration. Investigation into stromal-derived factors identified IGF-1 and IGF-2 as some factors responsible for promoting survival of tumour cells. Further to these findings, preclinical PDAC mouse models treated with IGF blocking antibody in combination with gemcitabine exhibited higher levels of cell death within the primary tumour (Fig 6.1). These results suggest that IGF blockade is well tolerated in mice and may have future therapeutic potential in the clinic.

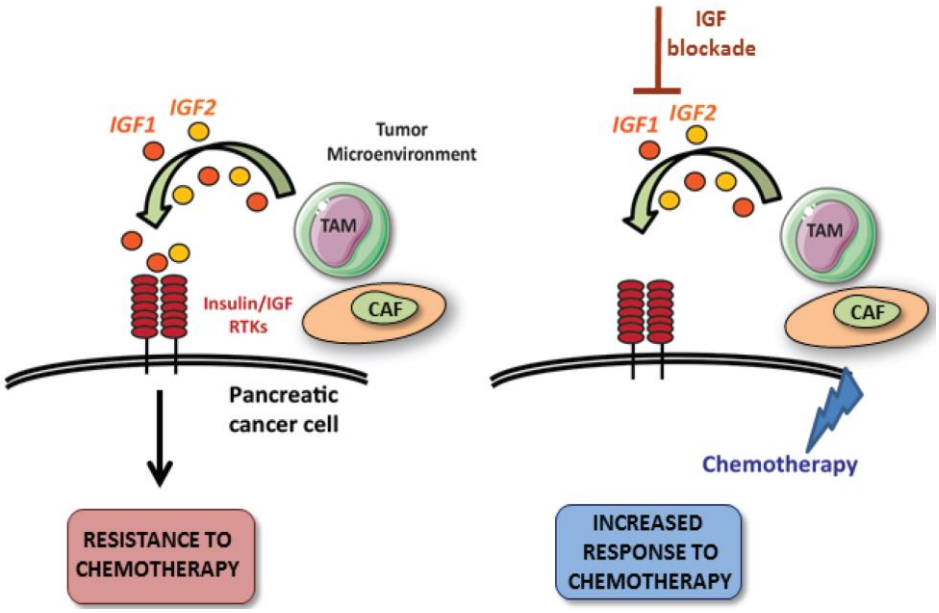

Figure 6.1 IGF signalling promotes chemoresistance in PDAC

The role of stroma-derived IGF in activation of the insulin/IGF-1R signalling survival pathway and in mediating chemoresistance of pancreatic cancer cells. TAMs and CAFs in the TME secreted IGF-1/2 which activate Insulin/IGF-1 receptors on tumour cells promoting resistance. IGF blockade in combination with gemcitabine resulted in increased levels of cell death.

The second experimental chapter in this thesis investigated the phenomenon of IGF-mediated chemoresistance in TNBC-like invasive breast cancer. Preclinical models of implanted breast cancer cells were shown to recapitulate the human TNBC primary disease, including development of pulmonary metastasis. TAMs and CAFs were identified as stromal sources of IGF-1 and IGF-2 in both the primary tumour site and metastatic foci. The administration of IGF blocking antibody in combination with paclitaxel, the standard agent of care, reduced primary tumour growth in the 4T1-mouse model and reduced overall metastatic burden in both preclinical models (Fig 6.2).

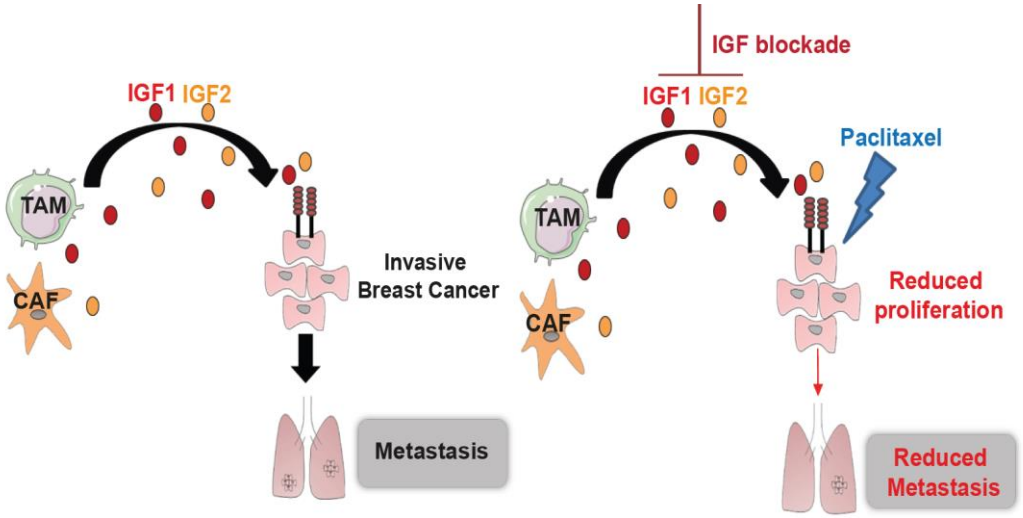

Figure 6.2 IGF signalling promotes chemoresistance in TNBC-like breast cancer

The role of stroma-derived IGF-1 and IGF-2 in regulating the response of metastatic breast cancer to paclitaxel. TAMs and CAFs in the breast TME secreted IGF-1/2 which activate Insulin/IGF-1 receptors on breast tumour cells promoting resistance. IGF blockade in combination with paclitaxel resulted reduced tumour cell proliferation at the primary site and reduced pulmonary metastatic burden.

The third experimental chapter of this thesis set out to analyse spontaneous metastasis in the preclinical orthotopic PDAC model. Implantation of three KPC-derived cell lines, FC1199, FC1242 and FC1245, revealed variance in their aggressive nature and metastatic potential. The FC1245 tumour bearing mice experienced a severely reduced life expectancy and early onset of metastasis compared to both FC1199 and FC1242 tumour bearing mice. SILAC proteomic analysis identified secreted proteins from the three cell lines. Nineteen proteins were identified as consistently enriched from FC1245 cells compared to FC1199 and FC1242 cells. Of these proteins, mesothelin was identified as a protein of interest due to the action of C-terminus mMSLN in TAM polarisation in ovarian cancer but unexplored functions in PDAC progression and interaction with the TME. *In vitro* validation of the SILAC mass spectrometry confirmed FC1245 cells secreted higher levels of mMSLN.

6.3 Limitations of experimental studies

6.3.1 Limitations of animal studies

As with any scientific study, the data presented herein must be interpreted within the context and limitations of the experimental framework. The preclinical orthotopic PDAC mouse model used is subject to project licence restrictions which limit the size of tumours grown and animal welfare deterioration. This is limiting as PDAC patients are often at an advanced disease stage when diagnosed and their treatment initiated. Comparatively, tumours are implanted in the mouse model and treated soon afterwards. Another caveat to consider is the administration of chemotherapy. Patients are given gemcitabine in a specific weekly dosing schedule comprising of eight weeks, which is not feasible in this preclinical model due to the previously outlined restrictions.

The orthotopic preclinical breast cancer model was also subject to limitations. According to project licence restrictions, primary tumours were limited to 1.5 cm^2 and visible ulceration defined as an endpoint. Breast cancer patients may develop lesions at larger sizes which could influence the effectiveness of treatment. Although the mice developed pulmonary metastasis which occurred within the time frame of the experiment, breast cancer patients can experience metastasis up to 10 years after treatment, which cannot be mimicked in this model. Again, chemotherapy administration was adapted for the mouse model and was therefore given in a shorter space of time, whereas TNBC patients are administered paclitaxel every 3 weeks.

6.3.2 Limitations of proteomic analysis

Although SILAC mass spectrometry is a sensitive detection system, analysis of the data required a triage approach to recognise robustly identified proteins present in each replicate and those that are truly secreted. Therefore, any proteins which were not detected in every replicate (represented by NaN) or were only identified by 1 peptide by Andromeda peptide search engine were removed from analysis. This decision was taken to maintain robust analysis and minimise mis-identified proteins. Confirmation of secreted protein characteristics were identified by SignalP, SecretomeP, TMHMM, Uniprot database searching for classical and non-classical secretion. Proteins deemed as non-secreted by these databases may still be released from cells packaged in exosomes, vesicles, or by other means not currently known. Exclusion of any of these proteins may have resulted in particular proteins or expression changes being overlooked. Identification of mesothelin as a protein of interest was based on statistical analysis and literature searching. The other upregulated proteins identified may still be implicated in conferring to tumour progression and may be the focus of future studies.

6.4 Future directions

6.4.1 IGF blockade in cancer

The work in this thesis has shown that IGF blockade promotes efficacy of gemcitabine and paclitaxel chemotherapeutic agents in our preclinical mouse models of PDAC and TNBC-like breast cancer respectively. Future directions for these studies would require testing of other commonly used chemotherapeutic agents *in vivo* along with the completion of clinical trials using both xentuzumab and Medi-573 IGF-1/2 blocking antibodies to reveal whether the combination has efficacy in patients.

IGF blocking antibodies are not currently in clinical trials for PDAC. However, IGF-1R antagonists have been assessed in PDAC trials in combination with chemotherapy but all studies were prematurely terminated due to a lack of improved survival (Kindler et al., 2012, Fuchs et al., 2015, Tabernero et al., 2015). In contrast to IGF-1R inhibition, IGF blocking antibodies neutralize both IGF-1 and IGF-2 ligands and thereby inhibit proliferative signalling through both insulin and IGF-1 receptors without affecting metabolic insulin signalling (Friedbichler et al., 2014). This may provide a more beneficial outcome and should be investigated in PDAC.

In breast cancer, Medi-573 is currently being assessed in hormone sensitive HER2- metastatic breast cancer in combination with letrozole (NCT01446159). Xentuzumab is being trialled in HR+ metastatic breast cancer patients in combination with everolimus and exemestane (NCT02123823). These trials are still currently active but have not published any interim results to date. TNBC trials have not been established but may show promising results.

Future directions should also encompass investigating the effect of IGF blockade in patients with obesity. Obesity is associated with an increased risk of the cancer development including pancreatic and post-menopausal breast cancer (Vainio et al.,

2002). Importantly, it is hypothesised hyperinsulinemia can promote cancer development through the reduction of IGF binding protein 1, thus increasing levels of active IGF-1 (Giovannucci, 2003, Calle and Kaaks, 2004). This hypothesis would fit the data presented in this thesis and therefore warrants further investigation into the role of macrophage and myofibroblast-derived IGFs during tumour initiation. As the development of diabetes mellitus often precedes a PDAC diagnosis, investigation into the administration of IGF blocking antibodies to newly diagnosed diabetic patients may prevent PDAC tumour development.

6.4.2 Investigation into mesothelin in PDAC

Chapter 5 of this thesis identified mMSLN as a protein of interest in PDAC progression due its previous implications as a tumour antigen and its polarising activity on TAMs previously seen in ovarian cancer (Argani et al., 2001, Dangaj et al., 2011). Interestingly, mesothelin has been detected in the serum of lung and breast cancer patients but not in PDAC patients despite its high expression at the cellular level (Robinson et al., 2003, Sharon et al., 2012). This phenomenon may be due to the dense stromal compartment surrounding PDAC, in which stromal cells may be interacting with mesothelin preventing it from entering the circulation. Therefore, future work should investigate the interactions of mMSLN with stromal components such as macrophages and fibroblast. mMSLN can bind to Mucin16 in the peritoneum (Rump et al., 2004), however the presence of this receptor on fibroblasts and macrophages is not yet known. Reciprocally, mMSLN still bound to tumour cells by their GPI anchor may still interact with surrounding stromal cells or other tumour cells and therefore elucidation of activated downstream signalling of mMSLN should also be included. This thesis has shown cleaved mMSLN is upregulated in murine PDAC tissue, however further investigation of mesothelin in PDAC progression should also encompass cleaved MPF by investigating its secretion by *in vitro* techniques.

6.5 CONCLUDING REMARKS

In summary, the key findings presented in this thesis are:

- TAM and CAF-derived IGF-1 and IGF-2 in the orthotopic PDAC TME enhance chemoresistance to gemcitabine.
- Combination treatment of IGF blocking antibody and gemcitabine increased cell death in our preclinical mouse models of PDAC.
- TAM and CAF-derived IGF-1 and IGF-2 enhanced chemoresistance to paclitaxel in TNBC at both the primary site and pulmonary metastatic site in our orthotopic model.
- Combination treatment of IGF blocking antibody and paclitaxel reduced metastatic burden and primary tumour size in 4T1 preclinical mouse model.
- KPC GEMM- derived PDAC cell lines vary in aggressiveness when orthotopically implanted into syngeneic recipient mice.
- mMSLN is highly expressed by FC1245 KPC cells which may correlate with increased metastatic potential.

Supplementary Data

SUPPLEMENTARY DATA

Supplementary Table 1A, *LIMMA output from FC1245 R0K0 compared to FC1199 R6K6 mass spectrometry Maxquant data*. ANOVA analysis of FC1245:FC1199 mass spectrometry using expression ratios and Medium and Light intensities quantified by Maxquant software. Significant proteins shown in red ($p \leq 0.01$).

Cell line	Majority Protein IDs	Protein names	Gene names	logFC	adj.P.Val
FC1245	Q3UPN1;P29533	Vascular cell adhesion protein 1	Vcam1	-1.57705	9.6E-06
FC1245	Q3TJ52;P54728	UV excision repair protein RAD23 homolog B	Rad23b	-1.26901	1.62E-05
FC1245	Q91XA2;G3X8U4	Golgi membrane protein 1	Golm1	-1.23814	1.62E-05
FC1245	E9PZ16;B1B0C7	Basement membrane-specific heparan sulfate proteoglycan core protein	Hspg2	-1.00994	3.33E-05
FC1245	Q01853	Transitional endoplasmic reticulum ATPase	Vcp	-1.32117	7.24E-05
FC1245	P50580;D3YVH7	Proliferation-associated protein 2G4	Pa2g4	-1.21518	7.24E-05
FC1245	P10923;F8WIP8	Osteopontin	Spp1	-1.0556	7.24E-05
FC1245	P18760;F8WGL3;E9Q1T2	Cofilin-1	Cfl1	-0.72634	7.24E-05
FC1245	Q3U9N4;P28798	Granulins;Acrogranin;Granulin-1;Granulin-2;Granulin-3;Granulin-4;Granulin-5;Granulin-6;Granulin-7	Grn	-0.72359	7.42E-05
FC1245	P40142	Transketolase	Tkt	-0.67822	7.42E-05
FC1245	P06797	Cathepsin L1;Cathepsin L1 heavy chain;Cathepsin L1 light chain	Ctsl	-1.04641	0.000149
FC1245	Q61753	D-3-phosphoglycerate dehydrogenase	Phgdh	-0.76386	0.000195
FC1245	Q8C483;P26638;A2AFS0	Serine--tRNA ligase, cytoplasmic	Sars	-0.59395	0.000209
FC1245	Q6PI17;P25785;B1AQJ3	Metalloproteinase inhibitor 2	Timp2	-0.65571	0.00021
FC1245	E9Q2Q0;P97821	Dipeptidyl peptidase 1	Ctsc	-0.97258	0.000315
FC1245	Q3TGL4;G5E8B3;P37889-2;P37889	Fibulin-2	Fbln2	-0.70687	0.000315
FC1245	Q9D0R2	Threonine--tRNA ligase, cytoplasmic	Tars	-0.90048	0.000329

FC1245	P40124	Adenylyl cyclase-associated protein 1	Cap1	-0.41298	0.000411
FC1245	Q99MN1;Q8R2P8	Lysine--tRNA ligase	Kars	-0.85075	0.000426
FC1245	E9QN70;P02469	Laminin subunit beta-1	Lamb1	-0.64716	0.000481
FC1245	Q61081	Hsp90 co-chaperone Cdc37	Cdc37	-0.35924	0.000485
FC1245	Q91YJ2	Sorting nexin-4	Snx4	-0.33938	0.000662
FC1245	P16045	Galectin-1	Lgals1	-0.3965	0.000747
FC1245	Q61468	Mesothelin;Megakaryocyte-potentiating factor;Mesothelin, cleaved form	Msln	-0.62716	0.000829
FC1245	E9QMZ5	Plectin	Plec	-0.33665	0.000889
FC1245	Q06890	Clusterin	Clu	-0.36837	0.000915
FC1245	G5E8M2;G5E8B8;P11276	Fibronectin;Anastellin	Fn1	-0.27675	0.001188
FC1245	P35979	60S ribosomal protein L12	Rpl12	-0.43427	0.001532
FC1245	Q3UQ28	Peroxidasin homolog	Pxdn	-0.96555	0.001994
FC1245	A2ASQ1-3;A2ASQ1-2;A2ASQ1	Agrin	Agrn	-1.13266	0.004468
FC1245	E9PXE7;P62281;D3Z3M6	40S ribosomal protein S11	Rps11	-0.32376	0.006046
FC1245	F8VQJ3;P02468	Laminin subunit gamma-1	Lamc1	-0.2721	0.00787
FC1245	Q93092	Transaldolase	Taldo1	-0.32117	0.010453
FC1245	P21107-2;D3Z2H9;Q8K0Z5;E9Q5J9	Tropomyosin alpha-3 chain	Tpm3;Tpm3-rs7	-0.1779	0.011359
FC1245	Q9WUM4	Coronin-1C	Coro1c	-0.2439	0.014121
FC1245	Q8C243;P18242;F6Y6L6	Cathepsin D	Ctsd	-0.27769	0.018997
FC1245	P26041	Moesin	Msn	-0.15141	0.026739
FC1245	G3UYZ1;Q8R366	Immunoglobulin superfamily member 8	Igsf8	-0.14463	0.035178
FC1245	Q6IRU2	Tropomyosin alpha-4 chain	Tpm4	-0.14239	0.037014
FC1245	Q80X90	Filamin-B	Flnb	-0.2923	0.044019
FC1245	Q61171;D3Z4A4	Peroxiredoxin-2	Prdx2	-0.10946	0.05802
FC1245	P35700;B1AXW5;B1AXW6;G3UW54;B1AXW4	Peroxiredoxin-1	Prdx1	-0.12486	0.059668
FC1245	P62908;D3YV43	40S ribosomal protein S3	Rps3	-0.26898	0.090546
FC1245	Q61937;Q9DAY9;Q5SQB0;Q5SQB5;E9Q5T3	Nucleophosmin	Npm1;Gm5611	-0.16736	0.099656

FC1245	O88342	WD repeat-containing protein 1	Wdr1	-0.10977	0.099656
FC1245	P28352	DNA-(apurinic or apyrimidinic site) lyase	Apex1	-0.14166	0.131287
FC1245	Q61001	Laminin subunit alpha-5	Lama5	-0.17471	0.133063
FC1245	Q02053	Ubiquitin-like modifier-activating enzyme 1	Uba1	-0.12232	0.214518
FC1245	P13020-2;P13020	Gelsolin	Gsn	-0.22338	0.473448
FC1245	F8WH23;Q61581;E9Q5D9;F8WII5	Insulin-like growth factor-binding protein 7	Igfbp7	-0.0441	0.473448
FC1245	P58252	Elongation factor 2	Eef2	-0.03224	0.478386
FC1245	Q6NZM2;E9QQ01;P98063	Bone morphogenetic protein 1	Bmp1	-0.06357	0.561655
FC1245	E9QLA4;E9QLA3;E9QK04;P97798-5;P97798-2;P97798-3;P97798-4;P97798	Neogenin	Neo1	-0.0858	0.617598
FC1245	P48678;P48678-2;P48678-3	Prelamin-A/C;Lamin-A/C	Lmna	-0.03121	0.704455
FC1245	P52480	Pyruvate kinase PKM	Pkm	-0.00096	0.985531
FC1199	P62806	Histone H4	Hist1h4a	1.575865	9.6E-06
FC1199	P30681	High mobility group protein B2	Hmgb2	1.088066	1.62E-05
FC1199	Q8CBB6	Histone H2B	Hist1h2br	1.769042	2.31E-05
FC1199	P27773	Protein disulfide-isomerase A3	Pdia3	1.215077	3.27E-05
FC1199	E9Q0A1;Q3UL54;Q8BVY0	Ribosomal L1 domain-containing protein 1	Rsl1d1	1.074888	4.57E-05
FC1199	P07356;B0V2N7;B0V2N8	Annexin A2;Annexin	Anxa2	1.132839	7.24E-05
FC1199	E9Q616;F7BRM2	Ahnak	Ahnak	0.862002	7.42E-05
FC1199	Q60817;	Nascent polypeptide-associated complex subunit alpha	Naca	0.945263	7.87E-05
FC1199	P52927;Q6NSP9	High mobility group protein HMGI-C	Hmga2	0.844229	0.00011
FC1199	A2AGN7;B7ZCF1;O88685;F6Q2E3	26S protease regulatory subunit 6A	Psmc3	0.757826	0.000111
FC1199	P63158;D3Z351;D3YZ18;D3YVC6	High mobility group protein B1	Hmgb1	0.700392	0.000113
FC1199	P17918;E9Q7Z3	Proliferating cell nuclear antigen	Pcna	0.70027	0.000114
FC1199	B8JJN0;F6VQX8;B8JJM5	Complement factor B;Complement factor	Gm20547;Cfb	2.28959	0.000114

	;P04186;B8JJM6	B Ba fragment;Complement factor B Bb fragment			
FC1199	O89093-2;O89093;F8WHA7	C-C motif chemokine 20;C-C motif chemokine	Ccl20	1.171771	0.000146
FC1199	P11499;E9Q3D6	Heat shock protein HSP 90-beta	Hsp90ab1	0.618305	0.000199
FC1199	G3XA10;Q8VEK3	Heterogeneous nuclear ribonucleoprotein U	Gm28062;Hnrnpu	0.659748	0.000201
FC1199	E9PZV5;P20152	Vimentin	Vim	0.719226	0.000201
FC1199	D3Z3R0;D3YXT4;D3YVE6;F6TJZ4;P12970;D3YU93;F6YI27;F6U2H0;F6ZVW4	60S ribosomal protein L7a	Rpl7a	0.840763	0.000201
FC1199	Q91UZ6	DNA segment, Chr 17, human D6S56E 5, isoform CRA_c	D17H6S56E-5	1.272456	0.000201
FC1199	P17095	High mobility group protein HMG-I/HMG-Y	Hmga1	0.868685	0.000202
FC1199	Q9R0P5	Destrin	Dstn	0.993266	0.000209
FC1199	P51859;E0CXA0;E0CYW7	Hepatoma-derived growth factor	Hdgf	0.442787	0.00021
FC1199	G5E839;P80315	T-complex protein 1 subunit delta	Cct4	0.638982	0.000221
FC1199	Q8K3I3;P50228	C-X-C motif chemokine 5;GCP-2(1-78);GCP-2(9-78)	Cxcl5	0.432256	0.00027
FC1199	E9Q2Z4;A3KGL9;B7ZCQ3;F6W687;P09602;Q5XK38	Non-histone chromosomal protein HMG-17	Gm16494;Hmgn2	0.470609	0.00027
FC1199	P62960	Nuclease-sensitive element-binding protein 1	Ybx1	0.884219	0.000304
FC1199	P26040	Ezrin	Ezr	0.694497	0.000355
FC1199	P54227;D3Z1Z8;D3Z5N2	Stathmin	Stmn1	0.54579	0.000411
FC1199	Q8BMJ3;Q60872;Q3UTA4;Q3TQZ4;E9Q5G6	Eukaryotic translation initiation factor 1A, X-chromosomal;Eukaryotic translation initiation factor 1A	Eif1ax;Eif1a;Gm8300;Gm2016	0.451531	0.000426
FC1199	P14148;D3Z6N4;F6XI62	60S ribosomal protein L7	Rpl7	1.032597	0.000467
FC1199	P63242;Q8BGY2	Eukaryotic translation initiation factor 5A-1;Eukaryotic translation initiation factor 5A-2	Eif5a;Eif5a2	0.353793	0.000706
FC1199	P60710;F8WI82;E9Q1F2;E9Q5F4	Actin, cytoplasmic 1;Actin, cytoplasmic 1, N-terminally processed	Actb	0.370697	0.000743

FC1199	P97467;E9Q704	Peptidyl-glycine alpha-amidating monooxygenase	Pam	0.370419	0.000861
FC1199	P10126;D3YZ68;D3Z3I8;B7ZBW3;P62631	Elongation factor 1-alpha 1;Elongation factor 1-alpha 2	Eef1a1;Eef1a2	0.989749	0.001087
FC1199	Q62266	Cornifin-A	Sprr1a	0.462172	0.001532
FC1199	Q6PDM2;Q6PDM2-3;Q6PDM2-2	Serine/arginine-rich splicing factor 1	Srsf1	0.270404	0.001636
FC1199	P17742	Peptidyl-prolyl cis-trans isomerase A	Ppia	0.264907	0.001994
FC1199	B7FAV1;B7FAU9;Q8BTM8	Filamin-A	Flna	0.26162	0.002204
FC1199	Q8BJW6	Eukaryotic translation initiation factor 2A	Eif2a	0.336042	0.002572
FC1199	Q9CY58-3;Q9CY58-2;Q9CY58;Q9CY58-4	Plasminogen activator inhibitor 1 RNA-binding protein	Serbp1	0.427715	0.00351
FC1199	Q9Z2U0	Proteasome subunit alpha type-7	Psma7	0.29337	0.003942
FC1199	P09405	Nucleolin	Ncl	0.28685	0.004468
FC1199	P08249	Malate dehydrogenase, mitochondrial	Mdh2	0.446215	0.005828
FC1199	Q78PY7;Q3TJ56	Staphylococcal nuclease domain-containing protein 1	Snd1	0.283516	0.006046
FC1199	P09411	Phosphoglycerate kinase 1	Pgk1	0.192588	0.010095
FC1199	O08553	Dihydropyrimidinase-related protein 2	Dpysl2	1.130453	0.01103
FC1199	P20029	78 kDa glucose-regulated protein	Hspa5	0.195957	0.012043
FC1199	Q02819;D3Z7D7	Nucleobindin-1	Nucb1	0.143749	0.018468
FC1199	Q3U111;P26043;Q7TSG6	Radixin	Rdx	0.152075	0.018997
FC1199	Q9EPL2-2;Q9EPL2	Calsyntenin-1;Soluble Alc-alpha;CTF1-alpha	Clstn1	0.176588	0.025368
FC1199	E9PX72	Glyceraldehyde-3-phosphate dehydrogenase	Gapdh;Gm7293	0.578934	0.026739
FC1199	Q9CR16	Peptidyl-prolyl cis-trans isomerase D	Ppid	0.11569	0.040451
FC1199	O70475;D3Z3F7	UDP-glucose 6-dehydrogenase	Ugdh	0.494024	0.043138
FC1199	P17182;Q6PHC1	Alpha-enolase	Eno1	0.163742	0.060053
FC1199	P30416;F7CAT1;	Peptidyl-prolyl cis-trans isomerase FKBP4	Fkbp4	0.106386	0.090013
FC1199	Q9D8N0	Elongation factor 1-gamma	Eef1g	0.084608	0.189551

FC1199	Q60864	Stress-induced-phosphoprotein 1	Stip1	0.0617	0.247624
FC1199	P24369	Peptidyl-prolyl cis-trans isomerase B	Ppib	0.066101	0.247624
FC1199	E9PYL7;F2Z4A3	FAT atypical cadherin 1	Fat1	0.443347	0.294436
FC1199	Q60709;Q61482;Q06335-2;Q06335	Amyloid-like protein 2	Aplp2	0.101062	0.367465
FC1199	Q8CGC7	Bifunctional glutamate/proline--tRNA ligase;Glutamate--tRNA ligase;Proline--tRNA ligase	Eprs	0.100679	0.475322
FC1199	P63017;Q504P4	Heat shock cognate 71 kDa protein	Hspa8	0.037336	0.617598
FC1199	P62983;E9Q9J0	Ubiquitin-40S ribosomal protein S27a	Rps27a	0.048031	0.65055
FC1199	P63005;P63005-2	Platelet-activating factor acetylhydrolase IB subunit alpha	Pafah1b1	0.023912	0.83535
FC1199	Q8VDD5	Myosin-9	Myh9	0.012274	0.941623
FC1199	O70251	Elongation factor 1-beta	Eef1b	0.001377	0.985531

Supplementary Table 1B *LIMMA output from FC1245 R0K0 compared to FC1242 R10K8 mass spectrometry Maxquant data*. ANOVA analysis of FC1245:FC1242 mass spectrometry using expression ratios and Heavy and Light intensities quantified by Maxquant software. Significant proteins shown in red ($p \leq 0.01$).

Cell line	Majority protein IDs	Protein names	Gene names	logFC	adj.P.Val
FC1245	G5E8M2;G5E8B8;P11276	Fibronectin;Anastellin	Fn1	-2.80087	8.25E-10
FC1245	P10923;F8WIP8	Osteopontin	Spp1	-3.70079	1.22E-09
FC1245	Q3TJ52;P54728	UV excision repair protein RAD23 homolog B	Rad23b	-1.26126	1.52E-07
FC1245	P06797	Cathepsin L1	Ctsl	-1.23366	1.60E-07
FC1245	G3UYZ1;Q8R366	Immunoglobulin superfamily member 8	Igsf8	-1.86141	2.37E-07
FC1245	A2ASQ1-3;A2ASQ1-2	Agrin;Agrin N-terminal 110 kDa subunit	Agrn	-1.68244	2.37E-07
FC1245	Q01853	Transitional endoplasmic reticulum ATPase	Vcp	-1.2109	2.37E-07
FC1245	Q61937;Q9DAY9;Q5SQB0	Nucleophosmin	Npm1	-0.90464	9.21E-07
FC1245	P50580;D3YVH7	Proliferation-associated protein 2G4	Pa2g4	-0.91267	1.09E-06
FC1245	Q6IRU2	Tropomyosin alpha-4 chain	Tpm4	-0.81534	1.26E-06
FC1245	Q3U9N4;P28798	Granulins;Acrogranin;Granulin-1;Granulin-2;Granulin-3;Granulin-4;Granulin-5;Granulin-6;Granulin-7	Grn	-1.0038	1.95E-06
FC1245	Q61753	D-3-phosphoglycerate dehydrogenase	Phgdh	-0.90583	2.52E-06
FC1245	Q6PI17;P25785;B1AQJ3	Metalloproteinase inhibitor 2	Timp2	-0.89034	2.52E-06
FC1245	Q3UQ28	Peroxidasin homolog	Pxdn	-0.71549	2.91E-06
FC1245	Q9D0R2	Threonine--tRNA ligase, cytoplasmic	Tars	-0.85869	3.37E-06
FC1245	P16045	Galectin-1	Lgals1	-0.76099	3.49E-06
FC1245	E9QN70;P02469	Laminin subunit beta-1	Lamb1	-0.75978	4.56E-06

FC1245	Q91XA2;G3X8U4	Golgi membrane protein 1	Golm1	-0.66451	4.57E-06
FC1245	P18760;F8WGL3;E9Q1T2	Cofilin-1	Cfl1	-0.68713	5.42E-06
FC1245	E9Q2Q0;P97821	Dipeptidyl peptidase 1;	Ctsc	-0.96287	6.87E-06
FC1245	E9PZ16;B1B0C7	Basement membrane-specific heparan sulfate proteoglycan core protein	Hspg2	-1.52466	1.20E-05
FC1245	P52927;Q6NSP9	High mobility group protein HMGI-C	Hmga2	-0.56555	1.24E-05
FC1245	P26041	Moesin	Msn	-0.54871	1.68E-05
FC1245	Q8C483;P26638;A2AFS0	Serine--tRNA ligase, cytoplasmic	Sars	-0.56404	2.72E-05
FC1245	Q61081	Hsp90 co-chaperone Cdc37	Cdc37	-0.53819	2.75E-05
FC1245	P35979	60S ribosomal protein L12	Rpl12	-0.54703	3.16E-05
FC1245	Q3UPN1;P29533	Vascular cell adhesion protein 1	Vcam1	-0.43866	4.58E-05
FC1245	E9QLA4;E9QLA3	Neogenin	Neo1	-0.47729	6.43E-05
FC1245	Q3TGL4;G5E8B3;P37889-2;P37889	Fibulin-2	Fbln2	-0.84742	7.22E-05
FC1245	Q99MN1;Q8R2P8	Lysine--tRNA ligase	Kars	-0.57258	0.000143
FC1245	Q61171;D3Z4A4	Peroxiredoxin-2	Prdx2	-0.33466	0.00032
FC1245	Q61468	Mesothelin;Megakaryocyte-potentiating factor;Mesothelin, cleaved form	Msln	-0.4962	0.000384
FC1245	P54227;D3Z1Z8;D3Z5N2	Stathmin	Stmn1	-0.40234	0.000509
FC1245	Q8C243;P18242;F6Y6L6	Cathepsin D	Ctsd	-0.41798	0.000561
FC1245	Q9WUM4	Coronin-1C	Coro1c	-0.32693	0.000561
FC1245	P17742;E9Q1E3	Peptidyl-prolyl cis-trans isomerase A	Ppia	-0.36615	0.000632
FC1245	P40124	Adenylyl cyclase-associated protein 1	Cap1	-0.47172	0.000844
FC1245	Q93092	Transaldolase	Taldo1	-0.32449	0.00102
FC1245	F8WH23;Q61581;E9Q5D9;F8WII5	Insulin-like growth factor-binding protein 7	Igfbp7	-0.27566	0.001321
FC1245	P48678;P48678-2;P48678-3	Prelamin-A/C;Lamin-A/C	Lmna	-0.50724	0.001344

FC1245	D3Z3R0;D3YXT4;D3YVE6;F6TJZ4	60S ribosomal protein L7a	Rpl7a	-0.23181	0.002151
FC1245	Q6NZM2;E9QQ01;P98063	Bone morphogenetic protein 1	Bmp1	-0.28504	0.002809
FC1245	Q9EPL2-2;Q9EPL2	Calsyntenin-1;Soluble Alc-alpha;CTF1-alpha	Clstn1	-0.33716	0.003977
FC1245	P21107-2;D3Z2H9;Q8K0Z5;E9Q5J9	Tropomyosin alpha-3 chain	Tpm3;Tpm3-rs7	-0.21228	0.005037
FC1245	E9QMZ5;Q9QXS1-3;E9Q3W4	Plectin	Plec	-0.28867	0.005267
FC1245	P63005;P63005-2	Platelet-activating factor acetylhydrolase IB subunit alpha	Pafah1b1	-0.2143	0.007441
FC1245	Q9CR16	Peptidyl-prolyl cis-trans isomerase D	Ppid	-0.25327	0.009311
FC1245	Q8BJW6;Q8BJW6-2	Eukaryotic translation initiation factor 2A	Eif2a	-0.20897	0.010103
FC1245	Q8VDD5	Myosin-9	Myh9	-0.31319	0.011777
FC1245	P17182;Q6PHC1	Alpha-enolase	Eno1	-0.2169	0.011829
FC1245	P13020-2;P13020	Gelsolin	Gsn	-0.89472	0.012067
FC1245	Q61001	Laminin subunit alpha-5	Lama5	-0.18148	0.012067
FC1245	P20029	78 kDa glucose-regulated protein	Hspa5	-0.3097	0.013955
FC1245	P35700;B1AXW5;B1AXW6;G3UW54;B1AXW4	Peroxiredoxin-1	Prdx1	-0.16195	0.014675
FC1245	P62908;D3YV43	40S ribosomal protein S3	Rps3	-0.15	0.032336
FC1245	Q9CY58-3;Q9CY58-2;Q9CY58;Q9CY58-4	Plasminogen activator inhibitor 1 RNA-binding protein	Serbp1	-0.26031	0.044811
FC1245	P17095	High mobility group protein HMG-I/HMG-Y	Hmga1	-0.14337	0.044811
FC1245	P62983;E9Q9J0;E9Q0Z8;E9Q4P0;E9Q5F6	Ubiquitin-40S ribosomal protein S27a	Rps27a;Uba52;Kxd1;Ubc;Ubb	-0.18922	0.04608
FC1245	E9PXE7;P62281;D3Z3M6	40S ribosomal protein S11	Rps11	-0.18984	0.060841
FC1245	O88342	WD repeat-containing protein 1	Wdr1	-0.16954	0.08002
FC1245	F8VQJ3;P02468	Laminin subunit gamma-1	Lamc1	-0.10146	0.113711
FC1245	P40142	Transketolase	Tkt	-0.08705	0.115524

FC1245	Q02053	Ubiquitin-like modifier-activating enzyme 1	Uba1	-0.11483	0.120128
FC1245	P51859;E0CXA0;E0CYW7	Hepatoma-derived growth factor	Hdgf	-0.0935	0.232554
FC1245	Q9Z2U0	Proteasome subunit alpha type-7	Psma7	-0.06746	0.232554
FC1245	O70251	Elongation factor 1-beta	Eef1b	-0.07579	0.287538
FC1245	A3KGL9;B7ZCQ3;F6W687;P09602;Q5XK38	Non-histone chromosomal protein HMG-17	Hmgn2	-0.06705	0.304888
FC1245	P63017;Q504P4	Heat shock cognate 71 kDa protein	Hspa8	-0.04689	0.387982
FC1245	P09405	Nucleolin	Ncl	-0.06925	0.46963
FC1245	P24369	Peptidyl-prolyl cis-trans isomerase B	Ppib	-0.03444	0.520284
FC1245	Q8CGC7	Bifunctional glutamate/proline--tRNA ligase	Eprs	-0.03614	0.752289
FC1245	Q60864	Stress-induced-phosphoprotein 1	Stip1	-0.01595	0.752289
FC1242	Q8K3I3;P50228	C-X-C motif chemokine 5;GCP-2(1-78);GCP-2(9-78)	Cxcl5	3.088823	7.92E-10
FC1242	B8JJN0;F6VQX8;B8JJM5	Complement factor B	Cfb	1.847933	3.20E-08
FC1242	E9Q616;F7BRM2	Ahnak	Ahnak	1.292232	2.37E-07
FC1242	P62806	Histone H4	Hist1h4a	1.198726	3.65E-07
FC1242	Q91UZ6	DNA segment, Chr 17, human D6S56E 5, isoform CRA_c	D17H6S56E-5	1.243566	4.45E-07
FC1242	Q8CBB6;Q921L4;Q8CGP2;Q8CGP1;Q6ZWY9	Histone H2B	Hist1h2br	1.278259	5.45E-07
FC1242	Q9R0P5	Destrin	Dstn	1.067895	1.09E-06
FC1242	P26040	Ezrin	Ezr	0.867968	1.26E-06
FC1242	P10126;D3YZ68	Elongation factor 1-alpha 1	Eef1a1;Eef1a2	0.997776	1.64E-06
FC1242	P07356;B0V2N7;B0V2N8	Annexin A2;Annexin	Anxa2	0.852984	2.52E-06
FC1242	Q60817;P70670	Nascent polypeptide-associated complex subunit alpha	Naca	0.733319	2.91E-06
FC1242	P97467;E9Q704	Peptidyl-glycine alpha-amidating monooxygenase	Pam	0.621469	5.55E-06

FC1242	A2AGN7;B7ZCF1;O88685;F6Q2E3	26S protease regulatory subunit 6A	Psmc3	0.61582	7.07E-06
FC1242	Q91YJ2	Sorting nexin-4	Snx4	0.62148	1.24E-05
FC1242	P30681	High mobility group protein B2	Hmgb2	0.571297	1.40E-05
FC1242	Q06890;E9PUU2;E9PXG5;E9Q8Y5;E9Q9B8	Clusterin;Clusterin beta chain;Clusterin alpha chain	Clu	0.614143	1.75E-05
FC1242	O08553	Dihydropyrimidinase-related protein 2	Dpysl2	0.617449	2.41E-05
FC1242	E9PX72;E9PX42;P16858;E9PZH9;E9QAC7;E9Q9E5	Glyceraldehyde-3-phosphate dehydrogenase	Gapdh	1.130828	3.76E-05
FC1242	Q60709;Q61482;Q06335-2;Q06335	Amyloid-like protein 2	Aplp2	1.010859	6.43E-05
FC1242	P63158;D3Z351;D3YZ18;D3YVC6	High mobility group protein B1	Hmgb1	0.465768	7.42E-05
FC1242	P30416;F7CAT1;D6RDE2	Peptidyl-prolyl cis-trans isomerase FKBP4	Fkbp4	0.416924	8.15E-05
FC1242	Q9D8N0	Elongation factor 1-gamma	Eef1g	0.376768	0.000258
FC1242	O89093-2;O89093;F8WHA7	C-C motif chemokine 20;C-C motif chemokine	Ccl20	0.382655	0.000258
FC1242	G5E839;P80315	T-complex protein 1 subunit delta	Cct4	0.413234	0.001159
FC1242	E9Q0A1;Q3UL54;Q8BVY0	Ribosomal L1 domain-containing protein 1	Rsl1d1	0.302226	0.001333
FC1242	O70475;D3Z3F7	UDP-glucose 6-dehydrogenase	Ugdh	0.344839	0.001421
FC1242	P27773	Protein disulfide-isomerase A3	Pdia3	0.27173	0.001773
FC1242	P11499;E9Q3D6	Heat shock protein HSP 90-beta	Hsp90ab1	0.519432	0.001929
FC1242	Q02819;D3Z7D7	Nucleobindin-1	Nucb1	0.231744	0.002151
FC1242	P52480	Pyruvate kinase PKM	Pkm	0.253271	0.003118
FC1242	P60710;F8WI82;E9Q1F2	Actin, cytoplasmic 1	Actb	0.259922	0.003298
FC1242	Q78PY7;Q3TJ56	Staphylococcal nuclease domain-containing protein 1	Snd1	0.250211	0.004043
FC1242	E9PZV5;P20152	Vimentin	Vim	0.225792	0.006919

FC1242	E9PYL7;F2Z4A3	FAT atypical cadherin 1	Fat1	0.212877	0.011777
FC1242	P58252	Elongation factor 2	Eef2	0.138426	0.030846
FC1242	P62960	Nuclease-sensitive element-binding protein 1	Ybx1	0.182924	0.032336
FC1242	P28352;F6QA74;	DNA-(apurinic or apyrimidinic site) lyase	Apex1	0.198437	0.032336
FC1242	P17918;E9Q7Z3	Proliferating cell nuclear antigen	Pcna	0.171484	0.035194
FC1242	G3XA10;Q8VEK3	Heterogeneous nuclear ribonucleoprotein U	Hnrnpu	0.166215	0.044811
FC1242	Q8BMJ3;Q60872;Q3UTA4;Q3TQZ4;E9Q5G6	Eukaryotic translation initiation factor 1A,	Eif1ax;Eif1a;Gm8300;Gm2016	0.146768	0.047767
FC1242	P09411	Phosphoglycerate kinase 1	Pgk1	0.143672	0.057394
FC1242	P08249	Malate dehydrogenase, mitochondrial	Mdh2	0.120376	0.060354
FC1242	Q80X90	Filamin-B	Flnb	0.106402	0.062385
FC1242	B7FAV1;B7FAU9;Q8BTM8	Filamin-A	Flna	0.094025	0.099433
FC1242	P63242;Q8BGY2	Eukaryotic translation initiation factor 5A-1;Eukaryotic translation initiation factor 5A-2	Eif5a;Eif5a2	0.095452	0.131436
FC1242	Q6PDM2;Q6PDM2-3;Q6PDM2-2	Serine/arginine-rich splicing factor 1	Srsf1	0.07773	0.217206
FC1242	Q62266	Cornifin-A	Sprr1a	0.074576	0.287538
FC1242	Q3U111;P26043;Q7TSG6	Radixin	Rdx	0.042234	0.55012
FC1242	P14148;D3Z6N4;F6XI62	60S ribosomal protein L7	Rpl7	0.036295	0.688329

Supplementary Table 1C *LIMMA output from FC1242 vs FC1199 mass spectrometry Maxquant data*. ANOVA analysis of FC1242:FC1199 mass spectrometry using expression ratios and Heavy and Medium intensities quantified by Maxquant software. Significant proteins shown in red ($p \leq 0.01$).

Cell line	Majority protein IDs	Protein names	Gene names	logFC	adj.P.Val
FC1199	P10923;F8WIP8	Osteopontin	Spp1	-2.42602	1.45E-06
FC1199	G5E8M2;G5E8B8;P11276	Fibronectin;Anastellin	Fn1	-2.39562	1.45E-06
FC1199	P52927;Q6NSP9	High mobility group protein HMGI-C	Hmga2	-1.34208	4.25E-06
FC1199	G3UYZ1;Q8R366	Immunoglobulin superfamily member 8	Igsf8	-1.44674	5.93E-06
FC1199	O89093-2;O89093;F8WHA7	C-C motif chemokine 20;C-C motif chemokine	Ccl20	-1.05329	1.08E-05
FC1199	D3Z3R0;D3YXT4;D3YVE6;F6TJZ4	60S ribosomal protein L7a	Rpl7a	-0.85429	1.50E-05
FC1199	P27773	Protein disulfide-isomerase A3	Pdia3	-0.76807	3.53E-05
FC1199	P17095	High mobility group protein HMG-I/HMG-Y	Hmga1	-0.86322	3.94E-05
FC1199	P54227;D3Z1Z8;D3Z5N2	Stathmin	Stmn1	-0.71649	8.77E-05
FC1199	P14148;D3Z6N4;F6XI62	60S ribosomal protein L7	Rpl7	-0.83958	0.000137
FC1199	P17742;E9Q1E3	Peptidyl-prolyl cis-trans isomerase A	Ppia	-0.49525	0.000197
FC1199	Q9CY58-3;Q9CY58-2;Q9CY58;Q9CY58-4	Plasminogen activator inhibitor 1 RNA-binding protein	Serbp1	-0.61616	0.000285
FC1199	E9Q2Z4;A3KGL9;B7ZCQ3;F6W687;P09602;Q5XK38	Non-histone chromosomal protein HMG-17	Hmgn2	-0.45761	0.000412
FC1199	B8JJN0;F6VQX8;B8JJM5	Complement factor B	Cfb	-0.62541	0.000495
FC1199	Q61937;Q9DAY9;Q5SQB0;Q5SQB5;E9Q5T3	Nucleophosmin	Npm1	-0.88183	0.000731
FC1199	E9PZV5;P20152	Vimentin	Vim	-0.31713	0.001006
FC1199	Q6IRU2	Tropomyosin alpha-4 chain	Tpm4	-0.51413	0.001016
FC1199	G3XA10;Q8VEK3	Heterogeneous nuclear ribonucleoprotein U	Gm28062; Hnrnpu	-0.46637	0.001016

FC1199	Q8BJW6;Q8BJW6-2	Eukaryotic translation initiation factor 2A	Eif2a	-0.57362	0.001268
FC1199	Q62266	Cornifin-A	Sprr1a	-0.40019	0.001338
FC1199	P62960	Nuclease-sensitive element-binding protein 1	Ybx1	-0.48932	0.001518
FC1199	P48678;P48678-2;P48678-3	Prelamin-A/C;Lamin-A/C	Lmna	-0.38443	0.001518
FC1199	Q9Z2U0	Proteasome subunit alpha type-7	Psma7	-0.27819	0.001518
FC1199	P62806	Histone H4	Hist1h4a	-0.41523	0.002312
FC1199	Q8VDD5	Myosin-9	Myh9	-0.24081	0.002808
FC1199	E9PZ16;B1B0C7;E9QL02;Q05793;Q3UHH3	Basement membrane-specific heparan sulfate proteoglycan core protein	Hspg2	-0.62196	0.00315
FC1199	P17918;E9Q7Z3	Proliferating cell nuclear antigen	Pcna	-0.47466	0.00315
FC1199	P30681	High mobility group protein B2	Hmgb2	-0.42387	0.00315
FC1199	Q8CBB6	Histone H2B	Hist1h2br	-0.36339	0.003329
FC1199	P51859;E0CXA0;E0CYW7	Hepatoma-derived growth factor	Hdgf	-0.37508	0.00407
FC1199	P13020-2;P13020	Gelsolin	Gsn	-0.67147	0.004262
FC1199	Q61171;D3Z4A4	Peroxiredoxin-2	Prdx2	-0.2592	0.004682
FC1199	P17182;Q6PHC1	Alpha-enolase	Eno1	-0.255	0.004815
FC1199	Q9EPL2-2;Q9EPL2	Calsyntenin-1;Soluble Alc-alpha;CTF1-alpha	Clstn1	-0.48908	0.005425
FC1199	Q6NZM2;E9QQ01;P98063	Bone morphogenetic protein 1	Bmp1	-0.18966	0.005425
FC1199	E9Q0A1;Q3UL54;Q8BVY0	Ribosomal L1 domain-containing protein 1	Rsl1d1	-0.47449	0.007483
FC1199	Q3U9N4;P28798	Granulins;Acrogranin;Granulin-1;Granulin-2;Granulin-3;Granulin-4;Granulin-5;Granulin-6;Granulin-7	Grn	-0.34951	0.013024
FC1199	P20029	78 kDa glucose-regulated protein	Hspa5	-0.54535	0.014803
FC1199	P09405	Nucleolin	Ncl	-0.421	0.014803
FC1199	P63005;P63005-2	Platelet-activating factor acetylhydrolase IB subunit alpha	Pafah1b1	-0.26076	0.014803
FC1199	Q9CR16	Peptidyl-prolyl cis-trans isomerase D	Ppid	-0.19412	0.018073
FC1199	P35979	60S ribosomal protein L12	Rpl12	-0.25286	0.018324
FC1199	Q6PDM2;Q6PDM2-3;Q6PDM2-2	Serine/arginine-rich splicing factor 1	Srsf1	-0.21259	0.020134

FC1199	P11499;E9Q3D6	Heat shock protein HSP 90-beta	Hsp90ab1	-0.17572	0.024521
FC1199	F8WH23;Q61581;E9Q5D9;F8WII5	Insulin-like growth factor-binding protein 7	Igfbp7	-0.12006	0.036359
FC1199	P16045	Galectin-1	Lgals1	-0.12564	0.039333
FC1199	Q8BMJ3;Q60872;Q3UTA4	Eukaryotic translation initiation factor 1A,	Eif1ax;Eif1a;	-0.09496	0.052159
FC1199	E9PXE7;P62281;D3Z3M6	40S ribosomal protein S11	Rps11	-0.16785	0.060628
FC1199	Q60817;P70670	Nascent polypeptide-associated complex subunit alpha	Naca	-0.15119	0.065443
FC1199	P63242;Q8BGY2	Eukaryotic translation initiation factor 5A-1;Eukaryotic translation initiation factor 5A-2	Eif5a;Eif5a2	-0.10443	0.067892
FC1199	B7FAV1;B7FAU9;Q8BTM8	Filamin-A	Flna	-0.07195	0.118528
FC1199	E9QN70;P02469	Laminin subunit beta-1	Lamb1	-0.12968	0.201804
FC1199	P35700;B1AXW5;B1AXW6;G3UW54;B1AXW4	Peroxiredoxin-1	Prdx1	-0.10212	0.2326
FC1199	Q9WUM4	Coronin-1C	Coro1c	-0.04755	0.258745
FC1199	P26041	Moesin	Msn	-0.0884	0.283482
FC1199	P63158;D3Z351;D3YZ18;D3YVC6	High mobility group protein B1	Hmgb1	-0.05437	0.292983
FC1199	Q8CGC7	Bifunctional glutamate/proline--tRNA ligase	Eprs	-0.04271	0.294598
FC1199	P40124	Adenylyl cyclase-associated protein 1	Cap1	-0.10043	0.410992
FC1199	E9QLA4;E9QLA3	Neogenin	Neo1	-0.30266	0.433635
FC1199	O08553	Dihydropyrimidinase-related protein 2	Dpysl2	-0.30762	0.449134
FC1199	P62983;E9Q9J0;E9Q0Z8;E9Q4P0	Ubiquitin-40S ribosomal protein S27a	Rps27a;Uba52;Kxd1;Ubc;Ubb	-0.13696	0.459137
FC1199	Q6PI17;P25785;B1AQJ3	Metalloproteinase inhibitor 2	Timp2	-0.03388	0.460015
FC1199	P24369	Peptidyl-prolyl cis-trans isomerase B	Ppib	-0.01741	0.711622
FC1199	E9PYL7;F2Z4A3	FAT atypical cadherin 1	Fat1	-0.16301	0.73757
FC1199	Q93092	Transaldolase	Taldo1	-0.00811	0.879176
FC1199	P09411	Phosphoglycerate kinase 1	Pgk1	-0.00845	0.880232
FC1199	P06797	Cathepsin L1;Cathepsin L1 heavy chain;Cathepsin L1 light chain	Ctsl	-0.0083	0.891117

FC1199	A2ASQ1-3;A2ASQ1-2;A2ASQ1	Agrin;Agrin N-terminal 110 kDa subunit	Agrn	-0.03733	0.901895
FC1199	O70251	Elongation factor 1-beta	Eef1b	-0.00488	0.92655
FC1199	O70475;D3Z3F7	UDP-glucose 6-dehydrogenase	Ugdh	-0.00841	0.9698
FC1199	P63017;Q504P4	Heat shock cognate 71 kDa protein	Hspa8	-0.00068	0.985578
FC1242	Q8K3I3;P50228	C-X-C motif chemokine 5;GCP-2(1-78);	Cxcl5	2.87775	2.99E-07
FC1242	Q06890;E9PUU2;E9PXG5;E9Q8Y5;E9Q9B8	Clusterin;Clusterin beta chain;Clusterin alpha chain	Clu	1.223041	4.25E-06
FC1242	Q3UPN1;P29533	Vascular cell adhesion protein 1	Vcam1	1.172848	1.50E-05
FC1242	Q91YJ2	Sorting nexin-4	Snx4	1.152415	1.54E-05
FC1242	P40142	Transketolase	Tkt	0.669876	3.94E-05
FC1242	Q91XA2;G3X8U4	Golgi membrane protein 1	Golm1	0.700457	5.05E-05
FC1242	Q9D8N0	Elongation factor 1-gamma	Eef1g	0.456302	0.000187
FC1242	P26040	Ezrin	Ezr	0.420667	0.000282
FC1242	Q80X90	Filamin-B	Flnb	0.558398	0.000285
FC1242	Q60709;Q61482;Q06335-2;Q06335	Amyloid-like protein 2	Aplp2	0.903753	0.000322
FC1242	Q78PY7;Q3TJ56	Staphylococcal nuclease domain-containing protein 1	Snd1	0.360601	0.000602
FC1242	P52480	Pyruvate kinase PKM	Pkm	0.450165	0.000689
FC1242	E9Q616;F7BRM2	Ahnak	Ahnak	0.420107	0.001094
FC1242	P58252	Elongation factor 2	Eef2	0.398648	0.001268
FC1242	P97467;E9Q704;F8VQA4;E9Q8R9	Peptidyl-glycine alpha-amidating monooxygenase	Pam	0.27673	0.001361
FC1242	Q02053	Ubiquitin-like modifier-activating enzyme 1	Uba1	0.307965	0.001518
FC1242	P28352;F6QA74;D3Z124	DNA-(apurinic or apyrimidinic site) lyase;DNA-(apurinic or apyrimidinic site) lyase, mitochondrial	Apex1	0.448494	0.001518
FC1242	E9QMZ5;Q9QXS1-3	Plectin	Plec	0.313411	0.002249
FC1242	Q3UQ28	Peroxidasin homolog	Pxdn	0.611725	0.002316
FC1242	F8VQJ3;P02468	Laminin subunit gamma-1	Lamc1	0.328677	0.002576
FC1242	Q02819;D3Z7D7	Nucleobindin-1	Nucb1	0.411369	0.002846
FC1242	P60710;F8WI82	Actin, cytoplasmic 1	Actb	0.216162	0.003779
FC1242	Q61001	Laminin subunit alpha-5	Lama5	0.28965	0.003857

FC1242	P30416;F7CAT1;D6RDE2	Peptidyl-prolyl cis-trans isomerase FKBP4	Fkbp4	0.356235	0.00407
FC1242	P18760;F8WGL3;E9Q1T2	Cofilin-1	Cfl1	0.171168	0.00553
FC1242	Q60864	Stress-induced-phosphoprotein 1	Stip1	0.162863	0.009476
FC1242	P50580;D3YVH7	Proliferation-associated protein 2G4	Pa2g4	0.314549	0.011916
FC1242	E9PX72;E9PX42;P16858;E9PZH9;E9QAC7;E9Q9E5	Glyceraldehyde-3-phosphate dehydrogenase	Gapdh	0.233837	0.016735
FC1242	G5E839;P80315	T-complex protein 1 subunit delta	Cct4	0.146096	0.036359
FC1242	Q01853	Transitional endoplasmic reticulum ATPase	Vcp	0.177819	0.038687
FC1242	Q99MN1;Q8R2P8	Lysine--tRNA ligase	Kars	0.109758	0.0487
FC1242	O88342	WD repeat-containing protein 1	Wdr1	0.191226	0.064594
FC1242	Q3U111;P26043;Q7TSG6	Radixin	Rdx	0.27526	0.082635
FC1242	Q61468	Mesothelin;Megakaryocyte-potentiating factor;Mesothelin, cleaved form	Msln	0.220696	0.083461
FC1242	E9Q2Q0;P97821	Dipeptidyl peptidase 1	Ctsc	0.144256	0.144139
FC1242	P21107-2;D3Z2H9;Q8K0Z5;E9Q5J9	Tropomyosin alpha-3 chain	Tpm3;Tpm3-rs7	0.101366	0.15294
FC1242	Q9D0R2	Threonine--tRNA ligase, cytoplasmic	Tars	0.15914	0.159084
FC1242	Q8C483;P26638;A2AFS0	Serine--tRNA ligase, cytoplasmic	Sars	0.078665	0.201804
FC1242	Q3TGL4;G5E8B3;P37889-2;P37889	Fibulin-2	Fbln2	0.114903	0.232764
FC1242	Q61081	Hsp90 co-chaperone Cdc37	Cdc37	0.056799	0.383233
FC1242	Q9R0P5	Destrin	Dstn	0.086924	0.387918
FC1242	A2AGN7;B7ZCF1;O886855;F6Q2E3	26S protease regulatory subunit 6A	Psmc3	0.078311	0.417186
FC1242	Q8C243;P18242;F6Y6L6	Cathepsin D	Ctsd	0.123372	0.437337
FC1242	P62908;D3YV43	40S ribosomal protein S3	Rps3	0.043111	0.459701
FC1242	P10126;D3YZ68;D3Z3I8;B7ZBW3;P62631	Elongation factor 1-alpha 1;Elongation factor 1-alpha 2	Eef1a1;Eef1a2	0.197636	0.500115
FC1242	Q3TJ52;P54728	UV excision repair protein RAD23 homolog B	Rad23b	0.036676	0.531032

FC1242	P07356;B0V2N7;B0V2N8	Annexin A2;Annexin	Anxa2	0.021647	0.71453
FC1242	Q61753	D-3-phosphoglycerate dehydrogenase	Phgdh	0.010067	0.885344
FC1242	Q91UZ6	DNA segment, Chr 17, human D6S56E 5	D17H6S56E-5	0.058041	0.885344
FC1242	P08249	Malate dehydrogenase, mitochondrial	Mdh2	0.003222	0.957459

Appendix

i) Antibodies used for immunoblotting

Antibody	Company	Catalogue no.	Dilution	Blocking agent
IGF-1	Abcam	ab9572	1:500	2.5 % BSA
IGF-2	Abcam	ab9574	1:1000	5 % NFDM
Phospho-Insulin R (Y1162/Y1163)/ IGF-I R (Y1135/Y1136) Antibody	R&D	AF2507	1:400	5 % NFDM
Insulin	Abcam	ab137747	1:1000	2.5 % BSA
IGF-1R	R&D	AF305-NA	1:1000	5 % NFDM
cleaved caspase 3	Cell signalling	9661	1:1000	5 % NFDM
Alpha smooth muscle actin (αSMA)	Abcam	ab7817	1:1000	2.5 % BSA
Mesothelin	Biorbyt	Orb14370	1:500	5 % BSA
pIRS1	Millipore	09-432	1:1000	5 % BSA
IRS1	Cell Signalling	CST23825	1:1000	5% BSA
pIRS2	Biorbyt	Orb34833	1:500	5 % BSA
IRS2	Cell Signalling	CST4502s	1:1000	5 % BSA
pAKT	Cell signalling	CST4060	1:1000	5% BSA
AKT	Cell signalling	CST9272	1:1000	5% BSA
pMEK	Cell signalling	CST2338	1:1000	5% BSA
MEK	Cell signalling	CST9126s	1:1000	5% BSA
Tubulin	Sigma Aldrich	T6199	1:5000	2.5 % BSA
GAPDH	Sigma Aldrich	G9545	1:10,000	2.5 % BSA
Secondary antibodies	**Company**	**Catalogue no.**	**Dilution**	**Blocking agent**
Rabbit-IgG-HRP linked	Cell Signalling Technology	7074S	1:5000	
Mouse-IgG-HRP linked	Cell Signalling Technology	7076S	1:5000	
Donkey anti Goat HRP linked	Abcam	ab97120	1:10,000	

ii) Antibodies used for immunohistochemistry:

Antibody	Company	Catalogue no.	Dilution	Antigen retrieval pH
CD206	Abcam	ab8919	1:50	low
Phospho-Insulin R (Y1162/Y1163)/ IGF-I R (Y1135/Y1136)	R&D	AF2507	1:50	high
CD68	DAKO	M081401-2	1:2000	high
αSMA	Abcam	ab5694	1:100	low
Cleaved caspase 3	Cell Signalling Technology	9661	1:300	high
Phospho-insulinR	LS Biosciences	LS-C177981	1:100	low
Phospho-IGF-1R	Biorbyt	orb97626	1:100	high
CD31	Cell Signalling Technology	77699	1:100	low
CD3	Abcam	Ab5690	1:100	high
Mesothelin	Biorbyt	Orb14370	1:500	high

iii) Antibodies for immunofluorescence

Antibody	Company	Catalogue no.	Dilution
EpCAM	BD pharmingen	552370	1:100
αSMA	Abcam	Ab7817	1:100
F4/80	Biolegend	123102	1:200
Ki67	Abcam	Ab15580	1:1000
anti mouse 488	Abcam	Ab150105	1:500
anti rat 488	Abcam	Ab96887	1:500
anti rabbit 594	Abcam	Ab150080	1:500
anti mouse 594	Abcam	Ab98639	1:500
DAPI	Gibco	D21490	1:600

iv) Antibodies for flow cytometry

Antibody	Company	Cat no.	Clone	Fluorochrome	Dilution
Sytox viability marker	Life Technologies	S34857		Pacific blue	1:500
CD45	Biolegend	103113	30-F11	PE-Cy7	1:100
F4/80	Biolegend	123115	BM8	APC	1:100
CD206	Biolegend	141715	C068C2	PerCP-Cy5.5	1:100

v) Primers for qPCR

Protein Name	Gene Name	Primer description	Reference
Insulin-like growth factor 1	*Igf-1*	Mm_ IGF1_1_SG QuantiTect Primer Assay	QT00154469
Insulin-like growth factor 2	*Igf-2*	Mm_IGF2 _1_SG QuantiTect Primer Assay	QT00109879
Insulin	*Insulin*	Mm_INS _1_SG QuantiTect Primer Assay	QT01660855
Alpha smooth muscle actin	*αSMA*	Mm_Acta2_1_SG QuantiTect Primer Assay	QT00140119
Mesothelin	*Msln*	Mm_Msln_1_SG QuantiTect Primer Assay	QT00104573

BIBLIOGRAPHY

Abe, O., Abe, R., Enomoto, K., Kikuchi, K., Koyama, H., Masuda, H., et al. (2005) 'Effects of chemotherapy and hormonal therapy for early breast cancer on recurrence and 15-year survival: an overview of the randomised trials', *Lancet*, vol. 365, no. 9472, pp. 1687-1717.

Agrogiannis, G.D., Sifakis, S., Patsouris, E.S. & Konstantinidou, A.E. (2014) 'Insulin-like growth factors in embryonic and fetal growth and skeletal development (Review)', Molecular Medicine Reports, vol. 10, no. 2, pp. 579-584.

Aguirre, A.J., Bardeesy, N., Sinha, M., Lopez, L., Tuveson, D.A., Horner, J., et al. (2003) 'Activated Kras and Ink4a/Arf deficiency cooperate to produce metastatic pancreatic ductal adenocarcinoma', *Genes & Development*, vol. 17, no. 24, pp. 3112-3126.

Apte, M.V., Haber, P.S., Applegate, T.L., Norton, I.D., McCaughan, G.W., Korsten, M.A., et al. (1998) 'Periacinar stellate shaped cells in rat pancreas: identification, isolation, and culture', *Gut*, vol. 43, no. 1, pp. 128-133.

Apte, M.V., Haber, P.S., Darby, S.J., Rodgers, S.C., McCaughan, G.W., Korsten, M.A., et al. (1999) 'Pancreatic stellate cells are activated by proinflammatory cytokines: implications for pancreatic fibrogenesis', *Gut*, vol. 44, no. 4, pp. 534-541.

Argani, P., Iacobuzio-Donahue, C., Ryu, B., Rosty, C., Goggins, M., Wilentz, R.E., et al (2001) 'Mesothelin is overexpressed in the vast majority of ductal adenocarcinomas of the pancreas: Identification of a new pancreatic cancer marker by serial analysis of gene expression (SAGE)', *Clinical Cancer Research*, vol. 7, no. 12, pp. 3862-3868.

Arnold, T. & Betsholtz, C. (2013) *The importance of microglia in the development of the vasculature in the central nervous system*, *Vascular Cell,* vol. 5, no 4, 10.1186/2045-824x-5-4.

Asahina, K., Tsai, S.Y., Li, P., Ishii, M., Maxson, R.E., Sucov, H.M., et al. (2009) 'Mesenchymal Origin of Hepatic Stellate Cells, Submesothelial Cells, and Perivascular Mesenchymal Cells During Mouse Liver Development', *Hepatology*, vol. 49, no. 3, pp. 998-1011.

Asahina, K., Zhou, B., Pu, W.T. & Tsukamoto, H. (2011) 'Septum Transversum-Derived Mesothelium Gives Rise to Hepatic Stellate Cells and Perivascular Mesenchymal Cells in Developing Mouse Liver', *Hepatology*, vol. 53, no. 3, pp. 983-995.

Aslakson, C.J. & Miller, F.R. (1992) 'Selective events in the metastatic process defined by analysis of the sequential dissemination of subpopulations of a mouse mammary-tumor', *Cancer Research*, vol. 52, no. 6, pp. 1399-1405.

Augsten, M. (2014) 'Cancer-associated fibroblasts as another polarized cell type of the tumor microenvironment', *Front Oncol*, vol. 4, no. 27, p. 62.

Bachem, M.G., Schneider, E., Gross, H., Weidenbach, H., Schmid, R.M., Menke, A., et al. (1998) 'Identification, culture, and characterization of pancreatic stellate cells in rats and humans', *Gastroenterology*, vol. 115, no. 2, pp. 421-432.

Bailey, J.M., Hendley, A.M., Lafaro, K.J., Pruski, M.A., Jones, N.C., Alsina, J., et al. (2016) 'p53 mutations cooperate with oncogenic Kras to promote adenocarcinoma from pancreatic ductal cells', *Oncogene*, vol. 35, no. 32, pp. 4282-4288.

Bailey, J.M., Swanson, B.J., Hamada, T., Eggers, J.P., Singh, P.K., Caffery, T., et al. (2008) 'Sonic Hedgehog Promotes Desmoplasia in Pancreatic Cancer', *Clinical Cancer Research*, vol. 14, no. 19, pp. 5995-6004.

Bailyes, E.M., Nave, B.T., Soos, M.A., Orr, S.R., Hayward, A.C. & Siddle, K. (1997) 'Insulin receptor/IGF-1 receptor hybrids are widely distributed in mammalian tissues: quantification of individual receptor species by selective immunoprecipitation and immunoblotting', *Biochemical Journal*, vol. 327, pp. 209-215.

Baird, B.N., Schliekelman, M.J., Ahn, Y.-H., Chen, Y., Roybal, J.D., Gill, B.J., et al. (2013) 'Fibulin-2 Is a Driver of Malignant Progression in Lung Adenocarcinoma', Plos One, vol. 8, no. 6.

Baserga, R. (1999) 'The IGF-I receptor in cancer research', *Experimental Cell Research*, vol. 253, no. 1, pp. 1-6.

Bauer, K.R., Brown, M., Cress, R.D., Parise, C.A. & Caggiano, V. (2007) 'Descriptive analysis of estrogen receptor (ER)negative, progesterone receptor (PR)-negative, and HER2-negative invasive breast cancer, the so-called triple-negative phenotype - A population-based study from the California Cancer Registry', *Cancer*, vol. 109, no. 9, pp. 1721-1728.

Beatty, G.L., Chiorean, E.G., Fishman, M.P., Saboury, B., Teitelbaum, U.R., Sun, W.J., et al. (2011) 'CD40 Agonists Alter Tumor Stroma and Show Efficacy Against Pancreatic Carcinoma in Mice and Humans', *Science*, vol. 331, no. 6024, pp. 1612-1616.

Benedetti-Panici, P., Bermudez, A., Blake, P., Cardenas, J., Chang, T.C., Chiara, S., et al. (2003) 'Neoadjuvant chemotherapy for locally advanced cervical cancer: a systematic review and meta-analysis of individual patient data from 21 randomised trials', *European Journal of Cancer*, vol. 39, no. 17, pp. 2470-2486.

Bergers, G. & Benjamin, L.E. (2003) 'Tumorigenesis and the angiogenic switch', *Nature Reviews Cancer*, vol. 3, no. 6, pp. 401-410.

Bergers, G., Brekken, R., McMahon, G., Vu, T.H., Itoh, T., Tamaki, K., et al. (2000) 'Matrix metalloproteinase-9 triggers the angiogenic switch during carcinogenesis', *Nature Cell Biology*, vol. 2, no. 10, pp. 737-744.

Bergmann, U., Funatomi, H., Yokoyama, M., Berger, H.G. & Korc, M. (1995) 'Insulin-like growth-factor-I overexpression in human panceratic cancer - evidence for autocrine and paracrine roles', *Cancer Research*, vol. 55, no. 10, pp. 2007-2011.

Bharadwaj, U., Marin-Muller, C., Li, M., Chen, C.Y. & Yao, Q.Z. (2011) 'Mesothelin overexpression promotes autocrine IL-6/sIL-6R trans-signaling to stimulate pancreatic cancer cell proliferation', Carcinogenesis, vol. 32, no. 7, pp. 1013-1024.

Bingle, L., Brown, N.J. & Lewis, C.E. (2002) 'The role of tumour-associated macrophages in tumour progression: implications for new anticancer therapies', *Journal of Pathology*, vol. 196, no. 3, pp. 254-265.

Biswas, S.K., Allavena, P. & Mantovani, A. (2013) 'Tumor-associated macrophages: functional diversity, clinical significance, and open questions', *Seminars in Immunopathology*, vol. 35, no. 5, pp. 585-600.

Biswas, S.K. & Mantovani, A. (2010) 'Macrophage plasticity and interaction with lymphocyte subsets: cancer as a paradigm', *Nature Immunology*, vol. 11, no. 10, pp. 889-896.

Blackburn, H.L., Ellsworth, D.L., Shriver, C.D. & Ellsworth, R.E. (2017) 'Breast Cancer Metastasis to the Axillary Lymph Nodes: Are Changes to the Lymph Node "Soil" Localized or Systemic?', *Breast Cancer-Basic and Clinical Research*, vol. 11, pp. 1-5.

Blaner, W.S., O'Byrne, S.M., Wongsiriroj, N., Kluwe, J., D'Ambrosio, D.M., Jiang, H.F., et al. (2009) 'Hepatic stellate cell lipid droplets: A specialized lipid droplet for retinoid storage', *Biochimica Et Biophysica Acta-Molecular and Cell Biology of Lipids*, vol. 1791, no. 6, pp. 467-473.

Bonde, A.K., Tischler, V., Kumar, S., Soltermann, A. & Schwendener, R.A. (2012) 'Intratumoral macrophages contribute to epithelial-mesenchymal transition in solid tumors', *Bmc Cancer*, vol. 12, no. 35, p. 35.

Brechbuhl, H.M., Finlay-Schultz, J., Yamamoto, T.M., Gillen, A.E., Cittelly, D.M., Tan, A.C., et al. (2017) 'Fibroblast Subtypes Regulate Responsiveness of Luminal Breast Cancer to Estrogen', *Clinical Cancer Research*, vol. 23, no. 7, pp. 1710-1721.

Bruchard, M., Mignot, G., Derangere, V., Chalmin, F., Chevriaux, A., Vegran, F., et al. (2013) 'Chemotherapy-triggered cathepsin B release in myeloid-derived suppressor cells activates the Nlrp3 inflammasome and promotes tumor growth', *Nature Medicine*, vol. 19, no. 1, pp. 57-64.

Buchholz, M., Braun, M., Heidenblut, A., Kestler, H.A., Kloppel, G., Schmiegel, W., et al. (2005) 'Transcriptome analysis of microdissected pancreatic intraepithelial neoplastic lesions', Oncogene, vol. 24, no. 44, pp. 6626-6636.

Burris, H.A., Moore, M.J., Andersen, J., Green, M.R., Rothenberg, M.L., Madiano, M.R., et al. (1997) 'Improvements in survival and clinical benefit with gemcitabine as first-line therapy for patients with advanced pancreas cancer: A randomized trial', *Journal of Clinical Oncology*, vol. 15, no. 6, pp. 2403-2413.

Calle, E.E. & Kaaks, R. (2004) 'Overweight, obesity and cancer: Epidemiological evidence and proposed mechanisms', Nature Reviews Cancer, vol. 4, no. 8, pp. 579-591.

Campbell, M.J., Tonlaar, N.Y., Garwood, E.R., Huo, D.Z., Moore, D.H., Khramtsov, A.I., et al. (2011) 'Proliferating macrophages associated with high grade, hormone receptor negative breast cancer and poor clinical outcome', *Breast Cancer Research and Treatment*, vol. 128, no. 3, pp. 703-711.

Cannarile, M.A., Weisser, M., Jacob, W., Jegg, A.M., Ries, C.H. & Ruttinger, D. (2017) 'Colony-stimulating factor 1 receptor (CSF1R) inhibitors in cancer therapy', *Journal for Immunotherapy of Cancer*, vol. 5, no. 1, pp. 53.

Carapuca, E.F., Gemenetzidis, E., Feig, C., Bapiro, T.E., Williams, M.D., Wilson, A.S., et al. (2016) 'Anti-stromal treatment together with chemotherapy targets multiple signalling pathways in pancreatic adenocarcinoma', *Journal of Pathology*, vol. 239, no. 3, pp. 286-296.

Casazza, A., Laoui, D., Wenes, M., Rizzolio, S., Bassani, N., Mambretti, M., et al. (2013) 'Impeding Macrophage Entry into Hypoxic Tumor Areas by Sema3A/Nrp1 Signaling Blockade Inhibits Angiogenesis and Restores Antitumor Immunity', *Cancer Cell*, vol. 24, no. 6, pp. 695-709.

Chabner, B.A. & Roberts, T.G. (2005) 'Timeline - Chemotherapy and the war on cancer', *Nature Reviews Cancer*, vol. 5, no. 1, pp. 65-72.

Chacon, R.D. & Costanzo, M.V. (2010) 'Triple-negative breast cancer', *Breast Cancer Research*, vol. 12, no. 3, pp. 3.

Chang, H.Y., Chi, J.T., Dudoit, S., Bondre, C., van de Rijn, M., Botstein, D., et al. (2002) 'Diversity, topographic differentiation, and positional memory in human fibroblasts', *Proceedings of the National Academy of Sciences of the United States of America*, vol. 99, no. 20, pp. 12877-12882.

Chang, K. & Pastan, I. (1996) 'Molecular cloning of mesothelin, a differentiation antigen present on mesothelium, mesotheliomas, and ovarian cancers', *Proceedings of the*

National Academy of Sciences of the United States of America, vol. 93, no. 1, pp. 136-140.

Chang, L., Chiang, S.H. & Saltiel, A.R. (2004) 'Insulin signaling and the regulation of glucose transport', *Molecular Medicine*, vol. 10, no. 7-12, pp. 65-71.

Christofori, G. & Semb, H. (1999) 'The role of the cell-adhesion molecule E-cadherin as a tumour-suppressor gene', Trends in Biochemical Sciences, vol. 24, no. 2, pp. 73-76.

Claire, D., Marine, G., Aurelie, A., Olivier, T., Sandrine, O.T., Flora, P., et al. (2016) 'Heterogeneity of metastatic pancreatic adenocarcinoma: Lung metastasis show better prognosis than liver metastasis-a case control study', *Oncotarget*, vol. 7, no. 29, pp. 45634-45640.

Colegio, O.R., Chu, N.Q., Szabo, A.L., Chu, T., Rhebergen, A.M., Jairam, V., et al. (2014) 'Functional polarization of tumour-associated macrophages by tumour-derived lactic acid', *Nature*, vol. 513, no. 7519, pp. 559-563.

Condeelis, J. & Pollard, J.W. (2006) 'Macrophages: Obligate partners for tumor cell migration, invasion, and metastasis', *Cell*, vol. 124, no. 2, pp. 263-266.

Coniglio, S.J., Eugenin, E., Dobrenis, K., Stanley, E.R., West, B.L., Symons, M.H., et al. (2012) 'Microglial Stimulation of Glioblastoma Invasion Involves Epidermal Growth Factor Receptor (EGFR) and Colony Stimulating Factor 1 Receptor (CSF-1R) Signaling', *Molecular Medicine*, vol. 18, no. 3, pp. 519-527.

Conroy, T., Desseigne, F., Ychou, M., Bouche, O., Guimbaud, R., Becouarn, Y., et al. (2011) 'FOLFIRINOX versus Gemcitabine for Metastatic Pancreatic Cancer', *New England Journal of Medicine*, vol. 364, no. 19, pp. 1817-1825.

Cooper, C.L., O'Toole, S.A. & Kench, J.G. (2013) 'Classification, morphology and molecular pathology of premalignant lesions of the pancreas', *Pathology*, vol. 45, no. 3, pp. 286-304.

Costa, A., Kieffer, Y., Scholer-Dahirel, A., Pelon, F., Bourachot, B., Cardon, M., et al. (2018) 'Fibroblast Heterogeneity and Immunosuppressive Environment in Human Breast Cancer', *Cancer Cell*, vol. 33, no. 3, pp. 463-479.

Costea, D.E., Hills, A., Osman, A.H., Thurlow, J., Kalna, G., Huang, X.H., et al. (2013) 'Identification of Two Distinct Carcinoma-Associated Fibroblast Subtypes with Differential Tumor-Promoting Abilities in Oral Squamous Cell Carcinoma', *Cancer Research*, vol. 73, no. 13, pp. 3888-3901.

Dai, X.F., Li, T., Bai, Z.H., Yang, Y.K., Liu, X.X., Zhan, J.L., et al. (2015) 'Breast cancer intrinsic subtype classification, clinical use and future trends', *American Journal of Cancer Research*, vol. 5, no. 10, pp. 2929-2943.

Dal-Secco, D., Wang, J., Zeng, Z.T., Kolaczkowska, E., Wong, C.H.Y., Petri, B., et al. (2015) 'A dynamic spectrum of monocytes arising from the in situ reprogramming of CCR2(+) monocytes at a site of sterile injury', *Journal of Experimental Medicine*, vol. 212, no. 4, pp. 447-456.

Dangaj, D., Abbott, K.L., Mookerjee, A., Zhao, A.Z., Kirby, P.S., Sandaltzopoulos, R., et al. (2011) 'Mannose Receptor (MR) Engagement by Mesothelin GPI Anchor Polarizes Tumor-Associated Macrophages and Is Blocked by Anti-MR Human Recombinant Antibody', *Plos One*, vol. 6, no. 12, pp. e28386

Darby, I.A. & Hewitson, T.D. (2007) 'Fibroblast differentiation in wound healing and fibrosis', *International Review of Cytology - a Survey of Cell Biology, Vol 257*, vol. 257, pp. 143-179.

Davie, S.A., Maglione, J.E., Manner, C.K., Young, D., Cardiff, R.D., MacLeod, C.L., et al. (2007) 'Effects of FVB/NJ and C57Bl/6J strain backgrounds on mammary tumor phenotype in inducible nitric oxide synthase deficient mice', *Transgenic Research*, vol. 16, no. 2, pp. 193-201.

Davies, C., Pan, H.C., Godwin, J., Gray, R., Arriagada, R., Raina, V., et al. (2013a) 'Long-term effects of continuing adjuvant tamoxifen to 10 years versus stopping at 5 years after diagnosis of oestrogen receptor-positive breast cancer: ATLAS, a randomised trial', *Lancet*, vol. 381, no. 9869, pp. 805-816.

Davies, L.C., Jenkins, S.J., Allen, J.E. & Taylor, P.R. (2013b) 'Tissue-resident macrophages', *Nature Immunology*, vol. 14, no. 10, pp. 986-995.

Davison, Z., de Blacquiere, G.E., Westley, B.R. & May, F.E.B. (2011) 'Insulin-like Growth Factor-Dependent Proliferation and Survival of Triple-Negative Breast Cancer Cells: Implications for Therapy', *Neoplasia*, vol. 13, no. 6, pp. 504-515.

De Palma, M. & Lewis, C.E. (2013) 'Macrophage Regulation of Tumor Responses to Anticancer Therapies', *Cancer Cell*, vol. 23, no. 3, pp. 277-286.

De Palma, M., Venneri, M.A., Galli, R., Sergi, L.S., Politi, L.S., Sampaolesi, M., et al. (2005) 'Tie2 identifies a hematopoietic monocytes required for tumor lineage of proangiogenic vessel formation and a mesenchymal population of pericyte progenitors', *Cancer Cell*, vol. 8, no. 3, pp. 211-226.

DeNardo, D., Andreu, P. & Coussens, L.M. (2010) 'Interactions between lymphocytes and myeloid cells regulate pro- versus anti-tumor immunity', *Cancer and Metastasis Reviews*, vol. 29, no. 2, pp. 309-316.

DeNardo, D.G., Brennan, D.J., Rexhepaj, E., Ruffell, B., Shiao, S.L., Madden, S.F., et al. (2011) 'Leukocyte complexity predicts breast cancer survival and functionally regulates response to chemotherapy', *Cancer Discovery*, vol. 1, no. 1, pp. 54-67.

Denduluri, S.K., Idowu, O., Wang, Z., Liao, Z., Yan, Z., Mohammed, M.K., et al. (2015) 'Insulin-like growth factor (IGF) signaling in tumorigenesis and the development of cancer drug resistance', *Genes Dis*, vol. 2, no. 1, pp. 13-25.

Dexter, D.L., Kowalski, H.M., Blazar, B.A., Fligiel, Z., Vogel, R. & Heppner, G.H. (1978) 'Heterogeneity of tumor-cells from a single mouse mammary-tumor', *Cancer Research*, vol. 38, no. 10, pp. 3174-3181.

Duda, D.G., Sunamura, M., Lefter, L.P., Furukawa, T., Yokoyama, T., Yatsuoka, T., et al. (2003) 'Restoration of SMAD4 by gene therapy reverses the invasive phenotype in pancreatic adenocarcinoma cells', *Oncogene*, vol. 22, no. 44, pp. 6857-6864.

DuFort, C.C., DelGiorno, K.E. & Hingorani, S.R. (2016) 'Mounting Pressure in the Microenvironment: Fluids, Solids, and Cells in Pancreatic Ductal Adenocarcinoma', *Gastroenterology*, vol. 150, no. 7, pp. 1545-1557.

Dvorak, H.F., Flier, J. & Frank, H. (1986) Tumors - wounds that do not heal - similarities between tumor stroma generation and wound-healing', *New England Journal of Medicine*, vol. 315, no. 26, pp. 1650-1659.

Eguchi, T., Kodera, Y., Nakanishi, H., Yokoyama, H., Ohashi, N., Ito, Y., et al. (2008) 'The Effect of Chemotherapy against Micrometastases and Isolated Tumor Cells in Lymph Nodes: An In Vivo Study', *In Vivo*, vol. 22, no. 6, pp. 707-712.

Erkan, M., Weis, N., Pan, Z., Schwager, C., Samkharadze, T., Jiang, X., et al. (2010) 'Organ-, inflammation- and cancer specific transcriptional fingerprints of pancreatic and hepatic stellate cells', *Molecular Cancer*, vol. 9, pp. 88.

Fagan, D.H., Uselman, R.R., Sachdev, D. & Yee, D. (2012) 'Acquired Resistance to Tamoxifen Is Associated with Loss of the Type I Insulin-like Growth Factor Receptor: Implications for Breast Cancer Treatment', *Cancer Research*, vol. 72, no. 13, pp. 3372-3380.

Fantin, A., Vieira, J.M., Gestri, G., Denti, L., Schwarz, Q., Prykhozhij, S., et al. (2010) 'Tissue macrophages act as cellular chaperones for vascular anastomosis downstream of VEGF-mediated endothelial tip cell induction', *Blood*, vol. 116, no. 5, pp. 829-840.

Fantozzi, A. & Christofori, G. (2006) 'Mouse models of breast cancer metastasis', *Breast Cancer Research*, vol. 8, no. 4, pp. 1-11.

Farabaugh, S.M., Boone, D.N. & Lee, A.V. (2015) 'Role of IGF1R in breast cancer subtypes, sternness, and lineage differentiation', *Frontiers in Endocrinology*, vol. 6, p. 59.

Faris, J.E., Blaszkowsky, L.S., McDermott, S., Guimaraes, A.R., Szymonifka, J., Huynh, M.A., et al. (2013) 'FOLFIRINOX in Locally Advanced Pancreatic Cancer: The Massachusetts General Hospital Cancer Center Experience', *Oncologist*, vol. 18, no. 5, pp. 543-548.

Farmer, P., Bonnefoi, H., Anderle, P., Cameron, D., Wirapati, P., Becette, V., et al. (2009) 'A stroma-related gene signature predicts resistance to neoadjuvant chemotherapy in breast cancer (vol 15, pg 68, 2009)', *Nature Medicine*, vol. 15, no. 2, pp. 220-220.

Federici, M., Porzio, O., Zucaro, L., Fusco, A., Borboni, P., Lauro, D., et al. (1997) 'Distribution of insulin/insulin-like growth factor-I hybrid receptors in human tissues', *Molecular and Cellular Endocrinology*, vol. 129, no. 2, pp. 121-126.

Fedi, P., Tronick, S.R. & Aaronson, S.A. (1997) 'Growth factors in cancer medicine', J.F Holland, R.C Bast, D.L Morton, E Frei, D.W Kufe, R.R Weichselbaum (Eds.), Cancer Medicine, Williams and Wilkins, pp. 41–64.

Feig, C., Gopinathan, A., Neesse, A., Chan, D.S., Cook, N. & Tuveson, D.A. (2012) 'The Pancreas Cancer Microenvironment', *Clinical Cancer Research*, vol. 18, no. 16, pp. 4266-4276.

Forget, M.A., Voorhees, J.L., Cole, S.L., Dakhlallah, D., Patterson, I.L., Gross, A.C., et al. (2014) 'Macrophage Colony-Stimulating Factor Augments Tie2-Expressing Monocyte Differentiation, Angiogenic Function, and Recruitment in a Mouse Model of Breast Cancer', *Plos One*, vol. 9, no. 6, e98623

Freedman, G.M., Anderson, P.R., Li, T.Y. & Nicolaou, N. (2009) 'Locoregional Recurrence of Triple-negative Breast Cancer After Breast-conserving Surgery and Radiation', *Cancer*, vol. 115, no. 5, pp. 946-951.

Fridlender, Z.G., Kapoor, V., Buchlis, G., Cheng, G., Sun, J., Wang, L.C.S., et al. (2011) 'Monocyte Chemoattractant Protein-1 Blockade Inhibits Lung Cancer Tumor Growth by Altering Macrophage Phenotype and Activating CD8(+) Cells', *American Journal of Respiratory Cell and Molecular Biology*, vol. 44, no. 2, pp. 230-237.

Friedbichler, K., Hofmann, M.H., Kroez, M., Ostermann, E., Lamche, H.R., Koessl, C., et al. (2014) 'Pharmacodynamic and Antineoplastic Activity of BI 836845, a Fully Human IGF Ligand-Neutralizing Antibody, and Mechanistic Rationale for Combination with Rapamycin', *Molecular Cancer Therapeutics*, vol. 13, no. 2, pp. 399-409.

Friedman, S.L. (2000) 'Molecular regulation of hepatic fibrosis, an integrated cellular response to tissue injury', *Journal of Biological Chemistry*, vol. 275, no. 4, pp. 2247-2250.

Fuchs, C.S., Azevedo, S., Okusaka, T., Van Laethem, J.L., Lipton, L.R., Riess, H., et al. (2015) 'A phase 3 randomized, double-blind, placebo-controlled trial of ganitumab or placebo in combination with gemcitabine as first-line therapy for metastatic adenocarcinoma of the pancreas: the GAMMA trial', *Annals of Oncology*, vol. 26, no. 5, pp. 921-927.

Fukumura, D., Xavier, R., Sugiura, T., Chen, Y., Park, E.C., Lu, N.F., et al. (1998) 'Tumor induction of VEGF promoter activity in stromal cells', *Cell*, vol. 94, no. 6, pp. 715-725.

Furukawa, T., Sunamura, M. & Horii, A. (2006) 'Molecular mechanisms of pancreatic carcinogenesis', *Cancer Science*, vol. 97, no. 1, pp. 1-7.

Garcia-Closas, M., Brinton, L.A., Lissowska, J., Chatterjee, N., Peplonska, B., Anderson, W.F., Szeszenia-Dabrowska, N.,et al. (2006) 'Established breast cancer risk factors by clinically important tumour characteristics', *British Journal of Cancer*, vol. 95, no. 1, pp. 123-129

Gebski, V., Burmeister, B., Smithers, B.M., Foo, K., Zalcberg, J., Simes, J., et al. (2007) 'Survival benefits from neoadjuvant chemoradiotherapy or chemotherapy in oesophageal carcinoma: a meta-analysis', *Lancet Oncology*, vol. 8, no. 3, pp. 226-234.

Gibbings, S.L., Goyal, R., Desch, A.N., Leach, S.M., Prabagar, M., Atif, S.M., et al. (2015) 'Transcriptome analysis highlights the conserved difference between embryonic and postnatal-derived alveolar macrophages', *Blood*, vol. 126, no. 11, pp. 1357-1366.

Gibby, K., You, W.K., Kadoya, K., Helgadottir, H., Young, L.J.T., Ellies, L.G., et al. (2012) 'Early vascular deficits are correlated with delayed mammary tumorigenesis in the MMTV-PyMT transgenic mouse following genetic ablation of the NG2 proteoglycan', *Breast Cancer Research*, vol. 14, no. 2, pp. 67.

Gilman, A. (1963) 'The initial clinical trial of nitrogen mustard', *American Journal of Surgery*, vol. 105, no. 5, pp. 574-578.

Giovannucci, E. (2003) 'Nutrition, insulin, insulin-like growth factors and cancer', Hormone and Metabolic Research, vol. 35, no. 11-12, pp. 694-704.

Gocheva, V., Wang, H.W., Gadea, B.B., Shree, T., Hunter, K.E., Garfall, A.L., et al. (2010) 'IL-4 induces cathepsin protease activity in tumor-associated macrophages to promote cancer growth and invasion', *Genes & Development*, vol. 24, no. 3, pp. 241-255.

Gocheva, V., Zeng, W., Ke, D.X., Klimstra, D., Reinheckel, T., Peters, C., et al. (2006) 'Distinct roles for cysteine cathepsin genes in multistage tumorigenesis', *Genes & Development*, vol. 20, no. 5, pp. 543-556.

Gooch, J.L., Van Den Berg, C.L. & Yee, D. (1999) 'Insulin-like growth factor (IGF)-I rescues breast cancer cells from chemotherapy-induced cell death - proliferative and anti-apoptotic effects', *Breast Cancer Research and Treatment*, vol. 56, no. 1, pp. 1-10.

Gordon, S. & Martinez, F.O. (2010) 'Alternative Activation of Macrophages: Mechanism and Functions', *Immunity*, vol. 32, no. 5, pp. 593-604.

Gordy, C., Pua, H., Sempowski, G.D. & He, Y.W. (2011) 'Regulation of steady-state neutrophil homeostasis by macrophages', *Blood*, vol. 117, no. 2, pp. 618-629.

Goswami, S., Sahai, E., Wyckoff, J.B., Cammer, N., Cox, D., Pixley, F.J., et al. (2005) 'Macrophages promote the invasion of breast carcinoma cells via a colony-stimulating factor-1/epidermal growth factor paracrine loop', *Cancer Research*, vol. 65, no. 12, pp. 5278-5283.

Gradishar, W.J., Yardley, D.A., Layman, R., Sparano, J.A., Chuang, E., Northfelt, D.W., et al. (2016) 'Clinical and Translational Results of a Phase II, Randomized Trial of an Anti-IGF-1R (Cixutumumab) in Women with Breast Cancer That Progressed on Endocrine Therapy', *Clinical Cancer Research*, vol. 22, no. 2, pp. 301-309.

Greer, E.L. & Brunet, A. (2005) 'FOXO transcription factors at the interface between longevity and tumor suppression', *Oncogene*, vol. 24, no. 50, pp. 7410-7425.

Grivennikov, S.I., Greten, F.R. & Karin, M. (2010) 'Immunity, Inflammation, and Cancer', *Cell*, vol. 140, no. 6, pp. 883-899.

Guha, M. (2013) 'Anticancer IGF1R classes take more knocks', *Nature Reviews Drug Discovery*, vol. 12, no. 4, p. 250.

Gunderson, A.J., Kaneda, M.M., Tsujikawa, T., Nguyen, A.V., Affara, N.I., Ruffell, B., et al. (2016) 'Bruton Tyrosine Kinase-Dependent Immune Cell Cross-talk Drives Pancreas Cancer', *Cancer Discovery*, vol. 6, no. 3, pp. 270-285.

Guy, C.T., Cardiff, R.D. & Muller, W.J. (1992) 'Induction of mammary-tumors by expression of polyomavirus middle T-oncogene- a transgenic mouse model for metastatic disease', *Molecular and Cellular Biology*, vol. 12, no. 3, pp. 954-961.

Haddow, A., Kon, G.A.R. & Ross, W.C.J. (1948) Effects upon tumours of various haloalkylarylamines', *Nature*, vol. 162, no. 4125, pp. 824-825.

Haeusler, R.A., McGraw, T.E. & Accili, D. (2018) 'Biochemical and cellular properties of insulin receptor signalling', *Nature Reviews Molecular Cell Biology*, vol. 19, no. 1, pp. 31-44.

Hanahan, D. & Coussens, L.M. (2012) 'Accessories to the Crime: Functions of Cells Recruited to the Tumor Microenvironment', *Cancer Cell*, vol. 21, no. 3, pp. 309-322.

Hanahan, D. & Weinberg, R.A. (2000) 'The hallmarks of cancer', *Cell*, vol. 100, no. 1, pp. 57-70.

Hanahan, D. & Weinberg, R.A. (2011) 'Hallmarks of cancer: the next generation', *Cell*, vol. 144, no. 5, pp. 646-674.

Hansel, D.E., Kern, S.E. & Hruban, R.H. (2003) 'Molecular pathogenesis of pancreatic cancer', *Annual Review of Genomics and Human Genetics*, vol. 4, pp. 237-256.

Hart, P.A., Bellin, M.D., Andersen, D.K., Bradley, D., Cruz-Monserrate, Z., Forsmark, C.E., et al.(2016) 'Type 3c (pancreatogenic) diabetes mellitus secondary to chronic pancreatitis and pancreatic cancer', vol. 1, no. 3, pp. 226-237.

Hassan, R., Bera, T. & Pastan, I. (2004) 'Mesothelin: A new target for immunotherapy', *Clinical Cancer Research*, vol. 10, no. 12, pp. 3937-3942.

Hayes, D.F. & Schott, A.F. (2015) 'Neoadjuvant chemotherapy: what are the benefits for the patient and for the investigator?', *Journal of the National Cancer Institute Monographs*, vol. 2015, no. 51, pp. 36-39.

Hayflick, L. (1965) 'The limited in vitro lifetime of human diploid cell strains', Experimental cell research, vol. 37, no. 3, pp. 614-636.

Hayflick, L. (1997) 'Mortality and immortality at the cellular level. A review', Biochemistry-Moscow, vol. 62, no. 11, pp. 1180-1190.

Hezel, A.F., Kimmelman, A.C., Stanger, B.Z., Bardeesy, N. & DePinho, R.A. (2006) 'Genetics and biology of pancreatic ductal adenocarcinoma', *Genes & Development*, vol. 20, no. 10, pp. 1218-1249.

Hingorani, S.R., Petricoin, E.F., Maitra, A., Rajapakse, V., King, C., Jacobetz, M.A., et al. (2003) 'Preinvasive and invasive ductal pancreatic cancer and its early detection in the mouse', *Cancer Cell*, vol. 4, no. 6, pp. 437-450.

Hingorani, S.R., Wang, L.F., Multani, A.S., Combs, C., Deramaudt, T.B., Hruban, R.H., et al. (2005) 'Trp53(R172H) and KraS(G12D) cooperate to promote chromosomal instability and widely metastatic pancreatic ductal adenocarcinoma in mice', *Cancer Cell*, vol. 7, no. 5, pp. 469-483.

Ho, M., Bera, T.K., Willingham, M.C., Onda, M., Hassan, R., FitzGerald, D., et al. (2007) 'Mesothelin expression in human lung cancer', *Clinical Cancer Research*, vol. 13, no. 5, pp. 1571-1575.

Holohan, C., Van Schaeybroeck, S., Longley, D.B. & Johnston, P.G. (2013) 'Cancer drug resistance: an evolving paradigm', *Nature Reviews Cancer*, vol. 13, no. 10, pp. 714-726.

House, S.W., Warburg, O., Burk, D. & Schade, A.L. (1956) 'On respiratory impairment in cancer cells', *Science*, vol. 124, no. 3215, pp. 267-272.

Housman, G., Byler, S., Heerboth, S., Lapinska, K., Longacre, M., Snyder, N., et al. (2014) 'Drug Resistance in Cancer: An Overview', *Cancers*, vol. 6, no. 3, pp. 1769-1792.

Howell, A., Anderson, A.S., Clarke, R.B., Duffy, S.W., Evans, D.G., Garcia-Closas, M., Gescher, A.J., Key, T.J., Saxton, J.M. & Harvie, M.N. (2014) 'Risk determination and prevention of breast cancer', Breast Cancer Research, vol. 16, no. 5, pp. 446.

Hruban, R.H., Maitra, A., Kern, S.E. & Goggins, M. (2007) 'Precursors to pancreatic cancer', *Gastroenterology Clinics of North America*, vol. 36, no. 4, pp. 831-849.

Humphris, J.L., Johns, A.L., Simpson, S.H., Cowley, M.J., Pajic, M., Chang, D.K., et al. (2014) 'Clinical and Pathologic Features of Familial Pancreatic Cancer', *Cancer*, vol. 120, no. 23, pp. 3669-3675.

Huxley, J. (1958) Biological aspects of cancer, Allen and Unwin, Length: pp.1-156

Iacobuzio-Donahue, C.A., Fu, B., Yachida, S., Luo, M., Abe, H., Henderson, C.M., et al. (2009) 'DPC4 gene status of the primary carcinoma correlates with patterns of failure in patients with pancreatic cancer', *Journal of clinical oncology*, vol. 27, no. 11, p. 1806.

Iengar, P. (2012) 'An analysis of substitution, deletion and insertion mutations in cancer genes', Nucleic Acids Research, vol. 40, no. 14, pp. 6401-6413.

Inoue, S., Ding, H., Portilla-Arias, J., Hu, J.W., Konda, B., Fujita, M., et al. (2011) 'Polymalic Acid-Based Nanobiopolymer Provides Efficient Systemic Breast Cancer Treatment by Inhibiting both HER2/neu Receptor Synthesis and Activity', *Cancer Research*, vol. 71, no. 4, pp. 1454-1464.

Ireland, L., Santos, A., Ahmed, M.S., Rainer, C., Nielsen, S.R., Quaranta, V.,et al. (2016) 'Chemoresistance in Pancreatic Cancer Is Driven by Stroma-Derived Insulin-Like Growth Factors', Cancer Research, vol. 76, no. 23, pp. 6851-6863.

Ireland, L., Santos, A., Campbell, F., Figueiredo, C., Hammond, D., Ellies, L.G.,et al. (2018) 'Blockade of insulin-like growth factors increases efficacy of paclitaxel in metastatic breast cancer', Oncogene, vol. 37, no. 15, pp. 2022-2036.

Jenkins, S.J., Ruckerl, D., Cook, P.C., Jones, L.H., Finkelman, F.D., van Rooijen, N., et al. (2011) 'Local Macrophage Proliferation, Rather than Recruitment from the Blood, Is a Signature of T(H)2 Inflammation', *Science*, vol. 332, no. 6035, pp. 1284-1288.

Jenkins, S.J., Ruckerl, D., Thomas, G.D., Hewitson, J.P., Duncan, S., Brombacher, F., et al. (2013) 'IL-4 directly signals tissue-resident macrophages to proliferate beyond homeostatic levels controlled by CSF-1', *Journal of Experimental Medicine*, vol. 210, no. 11, pp. 2477-2491.

Jiang, H., Hegde, S. & DeNardo, D.G. (2017) 'Tumor-associated fibrosis as a regulator of tumor immunity and response to immunotherapy', *Cancer Immunology Immunotherapy*, vol. 66, no. 8, pp. 1037-1048.

Jiang, Y.J., Lee, C.L., Wang, Q., Zhou, Z.W., Yang, F., Jin, C., et al. (2014) 'Establishment of an orthotopic pancreatic cancer mouse model: Cells suspended and injected in Matrigel', *World Journal of Gastroenterology*, vol. 20, no. 28, pp. 9476-9485.

Jones, R.L., Kim, E.S., Nava-Parada, P., Alam, S., Johnson, F.M., Stephens, A.W., et al. (2015) 'Phase I Study of Intermittent Oral Dosing of the Insulin-like Growth Factor-1 and Insulin Receptors Inhibitor OSI-906 in Patients With Advanced Solid Tumors', *Clinical Cancer Research*, vol. 21, no. 4, pp. 693-700.

Joyce, J.A. & Pollard, J.W. (2009) 'Microenvironmental regulation of metastasis', *Nature Reviews Cancer*, vol. 9, no. 4, pp. 239-252.

Juneja, V.R., McGuire, K.A., Manguso, R.T., LaFleur, M.W., Collins, N., Haining, W.N., et al. (2017) 'PD-L1 on tumor cells is sufficient for immune evasion in immunogenic tumors and inhibits CD8 T cell cytotoxicity', *Journal of Experimental Medicine*, vol. 214, no. 4, pp. 895-904.

Junttila, M.R. & de Sauvage, F.J. (2013) 'Influence of tumour micro-environment heterogeneity on therapeutic response', *Nature*, vol. 501, no. 7467, pp. 346-354.

Kalbasi, A., Komar, C., Tooker, G.M., Liu, M.G., Lee, J.W., Gladney, W.L., et al. (2017) 'Tumor-Derived CCL2 Mediates Resistance to Radiotherapy in Pancreatic Ductal Adenocarcinoma', *Clinical Cancer Research*, vol. 23, no. 1, pp. 137-148.

Kalluri, R. (2003) 'Basement membranes: Structure, assembly and role in tumour angiogenesis', *Nature Reviews Cancer*, vol. 3, no. 6, pp. 422-433.

Kalluri, R. (2016) 'The biology and function of fibroblasts in cancer', *Nature Reviews Cancer*, vol. 16, no. 9, pp. 582-598.

Kalluri, R. & Zeisberg, M. (2006) 'Fibroblasts in cancer', *Nature Reviews Cancer*, vol. 6, no. 5, pp. 392-401.

Kau, P., Nagaraja, G. M., Zheng, H. Y., GizachewI, D., Galukande, M., Krishnan, S., et al. (2012) 'A mouse model for triple-negative breast cancer tumor-initiating cells (TNBC-TICs) exhibits similar aggressive phenotype to the human disease', *Bmc Cancer*, vol. 12, no. 120.

Keane, M.P., Strieter, R.M. & Belperio, J.A. (2005) 'Mechanisms and mediators of pulmonary fibrosis', *Critical Reviews in Immunology*, vol. 25, no. 6, pp. 429-463.

Khalil, N., Bereznay, O., Sporn, M. & Greenberg, A.H. (1989) 'Macrophage production of transforming growth factor-beta and fibroblast collagen-synthesis in chronic pulmonary inflammation', *Journal of Experimental Medicine*, vol. 170, no. 3, pp. 727-737.

Kim, M.P. & Gallick, G.E. (2008) 'Gemcitabine resistance in pancreatic cancer: Picking the key players', *Clinical Cancer Research*, vol. 14, no. 5, pp. 1284-1285.

Kindler, H.L., Richards, D.A., Garbo, L.E., Garon, E.B., Stephenson, J.J., Rocha-Lima, C.M., et al. (2012) 'A randomized, placebo-controlled phase 2 study of ganitumab (AMG 479) or conatumumab (AMG 655) in combination with gemcitabine in patients with metastatic pancreatic cancer', *Annals of Oncology*, vol. 23, no. 11, pp. 2834-2842.

King, H., Aleksic, T., Haluska, P. & Macaulay, V.M. (2014) 'Can we unlock the potential of IGF-1R inhibition in cancer therapy?', *Cancer Treatment Reviews*, vol. 40, no. 9, pp. 1096-1105.

Klastersky, J. & Paesmans, M. (2001) 'Response to chemotherapy, quality of life benefits and survival in advanced non-small cell lung cancer: review of literature results', *Lung Cancer*, vol. 34, no. 4, pp. S95-S101.

Kleeff, J., Korc, M., Apte, M., La Vecchia, C., Johnson, C.D., Biankin, A.V., et al. (2016) 'Pancreatic cancer', *Nature Reviews Disease Primers*, vol. 2. no. 16022.

Klei, T.R.L., Meinderts, S.M., van den Berg, T.K. & van Bruggen, R. (2017) 'From the Cradle to the Grave: The Role of Macrophages in erythropoiesis and erythrophagocytosis', *Frontiers in Immunology*, vol. 8. no. 73.

Klemm, F. & Joyce, J.A. (2015) 'Microenvironmental regulation of therapeutic response in cancer', *Trends in Cell Biology*, vol. 25, no. 4, pp. 198-213.

Kojima, T., Oheda, M., Hattori, K., Taniguchi, Y., Tamura, M., Ochi, N., et al. (1995) 'Molecular-cloning and expression of megakaryocyte potentiating factor cDNA', *Journal of Biological Chemistry*, vol. 270, no. 37, pp. 21984-21990.

Labori, K.J., Katz, M.H., Tzeng, C.W., Bjornbeth, B.A., Cvancarova, M., Edwin, B., et al. (2016) 'Impact of early disease progression and surgical complications on adjuvant chemotherapy completion rates and survival in patients undergoing the surgery first approach for resectable pancreatic ductal adenocarcinoma - A population-based cohort study', *Acta Oncologica*, vol. 55, no. 3, pp. 265-277.

Lawrence, T. & Natoli, G. (2011) 'Transcriptional regulation of macrophage polarization: enabling diversity with identity', *Nature Reviews Immunology*, vol. 11, no. 11, pp. 750-761.

LeBleu, V.S., Taduri, G., O'Connell, J., Teng, Y.Q., Cooke, V.G., Woda, C., et al. (2013) 'Origin and function of myofibroblasts in kidney fibrosis', *Nature Medicine*, vol. 19, no. 8, pp. 1047-1054.

Lee, E. & Muller, W.J. (2010) 'Oncogenes and Tumor Suppressor Genes', Cold Spring Harbor Perspectives in Biology, vol. 2, no. 10, a003236.

Leek, R.D., Lewis, C.E., Whitehouse, R., Greenall, M., Clarke, J. & Harris, A.L. (1996) 'Association of macrophage infiltration with angiogenesis and prognosis in invasive breast carcinoma', *Cancer Research*, vol. 56, no. 20, pp. 4625-4629.

Li, D.H., Xie, K.P., Wolff, R. & Abbruzzese, J.L. (2004) 'Pancreatic cancer', *Lancet*, vol. 363, no. 9414, pp. 1049-1057.

Lin, E.Y., Nguyen, A.V., Russell, R.G. & Pollard, J.W. (2001) 'Colony-stimulating factor 1 promotes progression of mammary tumors to malignancy', *Journal of Experimental Medicine*, vol. 193, no. 6, pp. 727-739.

Linde, N., Lederle, W., Depner, S., van Rooijen, N., Gutschalk, C.M. & Mueller, M.M. (2012) 'Vascular endothelial growth factor-induced skin carcinogenesis depends on recruitment and alternative activation of macrophages', *Journal of Pathology*, vol. 227, no. 1, pp. 17-28.

Liu, Y.H. (2006) 'Renal fibrosis: New insights into the pathogenesis and therapeutics', *Kidney International*, vol. 69, no. 2, pp. 213-217.

Liu, F.T. & Rabinovich, G.A. (2005) 'Galectins as modulators of tumour progression', Nature Reviews Cancer, vol. 5, no. 1, pp. 29-41.

Loberg, R.D., Ying, C., Craig, M., Day, L.L., Sargent, E., Neeley, C., et al. (2007) 'Targeting CCL2 with systemic delivery of neutralizing antibodies induces prostate cancer tumor regression in vivo', *Cancer Research*, vol. 67, no. 19, pp. 9417-9424.

Lobov, I.B., Rao, S., Carroll, T.J., Vallance, J.E., Ito, M., Ondr, J.K., et al. (2005) 'WNT7b mediates macrophage-induced programmed cell death in patterning of the vasculature', *Nature*, vol. 437, no. 7057, pp. 417-421.

Lodhia, K.A., Tienchaiananda, P. & Haluska, P. (2015) 'Understanding the key to targeting the IGF axis in cancer: a biomarker assessment', *Frontiers in Oncology*, vol. 5, p. 152.

Lu, X. & Kang, Y.B. (2009) 'Chemokine (C-C Motif) Ligand 2 Engages CCR2(+) Stromal Cells of Monocytic Origin to Promote Breast Cancer Metastasis to Lung and Bone', *Journal of Biological Chemistry*, vol. 284, no. 42, pp. 29087-29096.

Lu, Y.H., Zi, X.L., Zhao, Y.H., Mascarenhas, D. & Pollak, M. (2001) 'Insulin-like growth factor-I receptor signaling and resistance to trastuzumab (Herceptin)', *Journal of the National Cancer Institute*, vol. 93, no. 24, pp. 1852-1857.

Ma, C.X., Suman, V.J., Goetz, M., Haluska, P., Moynihan, T., Nanda, R., et al. (2013) 'A phase I trial of the IGF-1R antibody Cixutumumab in combination with temsirolimus

in patients with metastatic breast cancer', *Breast Cancer Research and Treatment*, vol. 139, no. 1, pp. 145-153.

Ma, J. C., Tang, W. K., Esser, L., Pastan, I. & Xia, D. (2012) 'Recognition of Mesothelin by the Therapeutic Antibody MORAb-009 Structural and mechanistics insights', *Journal of Biological Chemistry*, vol. 287, no. 40, pp. 33123-33131.

Madden, J.I. (2012) *Infinity reports update from phase 2 study of saridegib plus gemcitabine in patients with metastatic pancreatic cancer.*, http://phx.corporate-ir.net/phoenix.zhtml?c=121941&p=irolnewsArticle&ID=1653550.

Maglione, J.E., Moghanaki, D., Young, L.J.T., Manner, C.K., Ellies, L.G., Joseph, S.O., et al. (2001) 'Transgenic Polyoma middle-T mice model premalignant mammary disease', *Cancer Research*, vol. 61, no. 22, pp. 8298-8305.

Maitra, A., Adsay, N.V., Argani, P., Iacobuzio-Donahue, C., De Marzo, A., Cameron, J.L., et al. (2003) 'Multicomponent analysis of the pancreatic adenocarcinoma progression model using a pancreatic intraepithelial neoplasia tissue microarray', *Modern Pathology*, vol. 16, no. 9, pp. 902-912.

Mantovani, A. & Allavena, P. (2015) 'The interaction of anticancer therapies with tumor-associated macrophages', *Journal of Experimental Medicine*, vol. 212, no. 4, pp. 435-445.

Mantovani, A. & Sica, A. (2010) 'Macrophages, innate immunity and cancer: balance, tolerance, and diversity', *Current Opinion in Immunology*, vol. 22, no. 2, pp. 231-237.

Marquette, C. & Nabell, L. (2012) 'Chemotherapy-Resistant Metastatic Breast Cancer', *Current Treatment Options in Oncology*, vol. 13, no. 2, pp. 263-275.

Marsh, T., Pietras, K. & McAllister, S.S. (2013) 'Fibroblasts as architects of cancer pathogenesis', *Biochimica Et Biophysica Acta-Molecular Basis of Disease*, vol. 1832, no. 7, pp. 1070-1078.

Mass, E., Ballesteros, I., Farlik, M., Halbritter, F., Gunther, P., Crozet, L., et al. (2016) 'Specification of tissue-resident macrophages during organogenesis', *Science*, vol. 353, no. 6304, aaf4238

Massague, J. & Obenauf, A.C. (2016) 'Metastatic colonization by circulating tumour cells', *Nature*, vol. 529, no. 7586, pp. 298-306.

Massarweh, S., Osborne, C.K., Creighton, C.J., Qin, L., Tsimelzon, A., Huang, S., et al. (2008) 'Tamoxifen resistance in breast tumors is driven by growth factor receptor signaling with repression of classic estrogen receptor genomic function', *Cancer Research*, vol. 68, no. 3, pp. 826-833.

Mazzieri, R., Pucci, F., Moi, D., Zonari, E., Ranghetti, A., Berti, A., et al. (2011) 'Targeting the ANG2/TIE2 Axis Inhibits Tumor Growth and Metastasis by Impairing Angiogenesis and Disabling Rebounds of Proangiogenic Myeloid Cells', *Cancer Cell*, vol. 19, no. 4, pp. 512-526.

Meacham, C.E. & Morrison, S.J. (2013) 'Tumour heterogeneity and cancer cell plasticity', Nature, vol. 501, no. 7467, pp. 328-337.

McMillin, D.W., Negri, J.M. & Mitsiades, C.S. (2013) 'The role of tumour-stromal interactions in modifying drug response: challenges and opportunities', *Nature Reviews Drug Discovery*, vol. 12, no. 3, pp. 217-228.

McPherson, K., Steel, C.M. & Dixon, J.M. (2000) 'ABC of breast disease: Breast cancer-epidemiology, risk factors, and genetics', *British Medical Journal*, vol. 321, no. 7261, pp. 624-628.

Mielgo, A. & Schmid, M.C. (2013) 'Impact of tumour associated macrophages in pancreatic cancer', *Bmb Reports*, vol. 46, no. 3, pp. 131-138.

Mills, C.D. (2012) 'M1 and M2 Macrophages: Oracles of Health and Disease', *Critical Reviews in Immunology*, vol. 32, no. 6, pp. 463-488.

Mills, C.D., Lenz, L.L. & Harris, R.A. (2016) 'A Breakthrough: Macrophage-Directed Cancer Immunotherapy', *Cancer Research*, vol. 76, no. 3, pp. 513-516.

Mitchem, J.B., Brennan, D.J., Knolhoff, B.L., Belt, B.A., Zhu, Y., Sanford, D.E., et al. (2013) 'Targeting Tumor-Infiltrating Macrophages Decreases Tumor-Initiating Cells, Relieves Immunosuppression, and Improves Chemotherapeutic Responses', *Cancer Research*, vol. 73, no. 3, pp. 1128-1141.

Morris, J.P., Wang, S.C. & Hebrok, M. (2010) 'KRAS, Hedgehog, Wnt and the twisted developmental biology of pancreatic ductal adenocarcinoma', *Nature Reviews Cancer*, vol. 10, no. 10, pp. 683-695.

Morton, J.P., Timpson, P., Karim, S.A., Ridgway, R.A., Athineos, D., Doyle, B., et al. (2010) 'Mutant p53 drives metastasis and overcomes growth arrest/senescence in pancreatic cancer', *Proceedings of the National Academy of Sciences of the United States of America*, vol. 107, no. 1, pp. 246-251.

Murray, P.J. & Wynn, T.A. (2011) 'Protective and pathogenic functions of macrophage subsets', *Nature Reviews Immunology*, vol. 11, no. 11, pp. 723-737.

Nakasone, E.S., Askautrud, H.A., Kees, T., Park, J.H., Plaks, V., Ewald, A.J., et al. (2012) 'Imaging Tumor-Stroma Interactions during Chemotherapy Reveals Contributions of the Microenvironment to Resistance', *Cancer Cell*, vol. 21, no. 4, pp. 488-503.

Navegantes, K.C., Gomes, R.D., Pereira, P.A.T., Czaikoski, P.G., Azevedo, C.H.M. & Monteiro, M.C. (2017) 'Immune modulation of some autoimmune diseases: the critical role of macrophages and neutrophils in the innate and adaptive immunity', *Journal of Translational Medicine*, vol. 15, no. 1, p. 36.

Nielsen, S.R., Quaranta, V., Linford, A., Emeagi, P., Rainer, C., Santos, A., et al. (2016) 'Macrophage-secreted granulin supports pancreatic cancer metastasis by inducing liver fibrosis', *Nature Cell Biology*, vol. 18, no. 5, pp. 549-560.

Noy, R. & Pollard, J.W. (2014) 'Tumor-Associated Macrophages: From Mechanisms to Therapy', *Immunity*, vol. 41, no. 1, pp. 49-61.

O'Shea, J.J. & Murray, P.J. (2008) 'Cytokine signaling modules in inflammatory responses', *Immunity*, vol. 28, no. 4, pp. 477-487.

Oezdemir, B.C., Pentcheva-Hoang, T., Carstens, J.L., Zheng, X., Wu, C.-C., Simpson, T.R., et al. (2014) 'Depletion of Carcinoma-Associated Fibroblasts and Fibrosis Induces Immunosuppression and Accelerates Pancreas Cancer with Reduced Survival', *Cancer Cell*, vol. 25, no. 6, pp. 719-734.

Ohlund, D., Handly-Santana, A., Biffi, G., Elyada, E., Almeida, A.S., Ponz-Sarvise, M., et al. (2017) 'Distinct populations of inflammatory fibroblasts and myofibroblasts in pancreatic cancer', *Journal of Experimental Medicine*, vol. 214, no. 3, pp. 579-596.

Ohmura, E., Okada, M., Onoda, N., Kamiya, Y., Murakami, H., Tsushima, T., et al. (1990) 'Insulin-like growth factor-I and transforming growth factor-alpha as autocrine growth-factors in human pancreatic-cancer cell growth', *Cancer Research*, vol. 50, no. 1, pp. 103-107.

Olive, K.P., Jacobetz, M.A., Davidson, C.J., Gopinathan, A., McIntyre, D., Honess, D., et al. (2009) 'Inhibition of Hedgehog Signaling Enhances Delivery of Chemotherapy in a Mouse Model of Pancreatic Cancer', *Science*, vol. 324, no. 5933, pp. 1457-1461.
Olive, K.P., Tuveson, D.A., Ruhe, Z.C., Yin, B., Willis, N.A., Bronson, R.T., et al. (2004) 'Mutant p53 gain of function in two mouse models of Li-Fraumeni syndrome', *Cell*, vol. 119, no. 6, pp. 847-860.

Orkin, S.H. & Zon, L.I. (2008) 'Hematopoiesis: An evolving paradigm for stem cell biology', *Cell*, vol. 132, no. 4, pp. 631-644.

Outtz, H.H., Tattersall, I.W., Kofler, N.M., Steinbach, N. & Kitajewski, J. (2011) 'Notch1 controls macrophage recruitment and Notch signaling is activated at sites of endothelial cell anastomosis during retinal angiogenesis in mice', *Blood*, vol. 118, no. 12, pp. 3436-3439.

Pan, S., Chen, R., Crispin, D.A., May, D., Stevens, T., McIntosh, M.W., et al. (2011) 'Protein Alterations Associated with Pancreatic Cancer and Chronic Pancreatitis Found in Human Plasma using Global Quantitative Proteomics Profiling', Journal of Proteome Research, vol. 10, no. 5, pp. 2359-2376.

Pandol, S., Edderkaoui, M., Gukovsky, I., Lugea, A. & Gukovskaya, A. (2009) 'Desmoplasia of Pancreatic Ductal Adenocarcinoma', *Clinical Gastroenterology and Hepatology*, vol. 7, no. 11, pp. S44-S47.

Pandya, S. & Moore, R.G. (2011) 'Breast Development and Anatomy', *Clinical Obstetrics and Gynecology*, vol. 54, no. 1, pp. 91-95.

Pastan, I. & Hassan, R. (2014) 'Discovery of Mesothelin and Exploiting It as a Target for Immunotherapy', *Cancer Research*, vol. 74, no. 11, pp. 2907-2912.

Paulus, P., Stanley, E.R., Schafer, R., Abraham, D. & Aharinejad, S. (2006) 'Colony-stimulating factor-1 antibody reverses chemoresistance in human MCF-7 breast cancer xenografts', *Cancer Research*, vol. 66, no. 8, pp. 4349-4356.

Pollak, M. (2008) 'Insulin and insulin-like growth factor signalling in neoplasia', *Nature Reviews Cancer*, vol. 8, no. 12, pp. 915-928.

Pollak, M. (2012) 'The insulin and insulin-like growth factor receptor family in neoplasia: an update', *Nature Reviews Cancer*, vol. 12, no. 3, pp. 159-169.

Pollina, E.A., Legesse-Miller, A., Haley, E.M., Goodpaster, T., Randolph-Habecker, J. & Coller, H.A. (2008) 'Regulating the angiogenic balance in tissues - A potential role for the proliferative state of fibroblasts', *Cell Cycle*, vol. 7, no. 13, pp. 2056-2070.

Porta, M., Fabregat, X., Malats, N., Guarner, L., Carrato, A., de Miguel, A., et al. (2005) 'Exocrine pancreatic cancer: symptoms at presentation and their relation to tumour site and stage', vol. 7, no. 5, pp. 189-197.

Prasad, N.B., Biankin, A.V., Fukushima, N., Maitra, A., Dhara, S., Elkahloun, A.G., et al. (2005) 'Gene expression profiles in pancreatic intraepithelial neoplasia reflect the effects of hedgehog signaling on pancreatic ductal epithelial cells', Cancer Research, vol. 65, no. 5, pp. 1619-1626.

Priceman, S.J., Sung, J.L., Shaposhnik, Z., Burton, J.B., Torres-Collado, A.X., Moughon, D.L., et al. (2010) 'Targeting distinct tumor-infiltrating myeloid cells by inhibiting CSF-1 receptor: combating tumor evasion of antiangiogenic therapy', *Blood*, vol. 115, no. 7, pp. 1461-1471.

Pulaski, B.A. & Ostrand-Rosenberg, S. (1998) 'Reduction of established spontaneous mammary carcinoma metastases following immunotherapy with major histocompatibility complex class II and B7.1 cell-based tumor vaccines', *Cancer Research*, vol. 58, no. 7, pp. 1486-1493.

Pylayeva-Gupta, Y., Das, S., Handler, J.S., Hajdu, C.H., Coffre, M., Koralov, S.B., et al. (2016) 'IL35-Producing B Cells Promote the Development of Pancreatic Neoplasia', *Cancer Discovery*, vol. 6, no. 3, pp. 247-255.

Qian, B.Z., Li, J.F., Zhang, H., Kitamura, T., Zhang, J.H., Campion, L.R., et al. (2011) 'CCL2 recruits inflammatory monocytes to facilitate breast-tumour metastasis', *Nature*, vol. 475, no. 7355, pp. 222-225.

Qian, B.Z. & Pollard, J.W. (2010) 'Macrophage Diversity Enhances Tumor Progression and Metastasis', *Cell*, vol. 141, no. 1, pp. 39-51.

Qian, B.Z., Zhang, H., Li, J.F., He, T.F., Yeo, E.J., Soong, D.Y.H., et al. (2015) 'FLT1 signaling in metastasis-associated macrophages activates an inflammatory signature that promotes breast cancer metastasis', *Journal of Experimental Medicine*, vol. 212, no. 9, pp. 1433-1448.

Qiao, Y., Zhang, C., Li, A., Wang, D., Luo, Z., Ping, Y., et al. (2018) 'IL6 derived from cancer-associated fibroblasts promotes chemoresistance via CXCR7 in esophageal squamous cell carcinoma', *Oncogene*, vol. 37, no. 7, pp. 873-883.

Qiu, W.L., Sahin, F., Iacobuzio-Donahue, C.A., Garcia-Carracedo, D., Wang, W.M., Kuo, C.Y., et al. (2011) 'Disruption of p16 and Activation of Kras in Pancreas Increase Ductal Adenocarcinoma Formation and Metastasis in vivo', *Oncotarget*, vol. 2, no. 11, pp. 862-873.

Quail, D.F., Bowman, R.L., Akkari, L., Quick, M.L., Schuhmacher, A.J., Huse, J.T., et al. (2016) 'The tumor microenvironment underlies acquired resistance to CSF-1R inhibition in gliomas', *Science*, vol. 352, no. 6288.

Quail, D.F. & Joyce, J.A. (2013) 'Microenvironmental regulation of tumor progression and metastasis', *Nature Medicine*, vol. 19, no. 11, pp. 1423-1437.

Rakha, E.A., El-Sayed, M.E., Green, A.R., Lee, A.H., Robertson, J.F. & Ellis, I.O. (2007) 'Prognostic markers in triple-negative breast cancer', *Cancer*, vol. 109, no. 1, pp. 25-32.

Resnicoff, M., Burgaud, J.L., Rotman, H.L., Abraham, D. & Baserga, R. (1995) 'Correlation between apoptosis, tumorigenesis and levels of insulin-like growth-factor I receptors', *Cancer Research*, vol. 55, no. 17, pp. 3739-3741.

Rhim, A.D., Oberstein, P.E., Thomas, D.H., Mirek, E.T., Palermo, C.F., Sastra, S.A., et al. (2014) 'Stromal Elements Act to Restrain, Rather Than Support, Pancreatic Ductal Adenocarcinoma', *Cancer Cell*, vol. 25, no. 6, pp. 735-747.

Ritchie, M.E., Phipson, B., Wu, D., Hu, Y.F., Law, C.W., Shi, W. & Smyth, G.K. (2015) 'limma powers differential expression analyses for RNA-sequencing and microarray studies', Nucleic Acids Research, vol. 43, no. 7, p. e47.

Rivenbark, A.G., O'Connor, S.M. & Coleman, W.B. (2013) 'Molecular and Cellular Heterogeneity in Breast Cancer Challenges for Personalized Medicine', American Journal of Pathology, vol. 183, no. 4, pp. 1113-1124.

Rivlin, N., Brosh, R., Oren, M. & Rotter, V. (2011) 'Mutations in the p53 tumor suppressor gene: important milestones at the various steps of tumorigenesis', Genes & cancer, vol. 2, no. 4, pp. 466-474.

Robertson, J.F.R., Ferrero, J.M., Bourgeois, H., Kennecke, H., de Boer, R.H., Jacot, W., et al. (2013) 'Ganitumab with either exemestane or fulvestrant for postmenopausal women with advanced, hormone-receptor-positive breast cancer: a randomised, controlled, double-blind, phase 2 trial', *Lancet Oncology*, vol. 14, no. 3, pp. 228-235.

Robinson, B.W.S., Creaney, J., Lake, R., Nowak, A., Musk, A.W., de Klerk, N., et al. (2003) 'Mesothelin-family proteins and diagnosis of mesothelioma', *Lancet*, vol. 362, no. 9396, pp. 1612-1616.

Rock, J.R., Barkauskas, C.E., Cronce, M.J., Xue, Y., Harris, J.R., Liang, J.R., et al. (2011) 'Multiple stromal populations contribute to pulmonary fibrosis without evidence for epithelial to mesenchymal transition', *Proceedings of the National Academy of Sciences of the United States of America*, vol. 108, no. 52, pp. E1475-E1483.

Ronnovjessen, L. & Petersen, O.W. (1993) 'Induction of alpha-smooth muscle actin by transforming growth factor beta 1 in quiescent human breast gland fibroblasts -

Implications for myofibroblast generation in breast neoplasia', *Laboratory Investigation*, vol. 68, no. 6, pp. 696-707.

Ruffell, B., Affara, N.I. & Coussens, L.M. (2012) 'Differential macrophage programming in the tumor microenvironment', *Trends in Immunology*, vol. 33, no. 3, pp. 119-126.

Rump, A., Morikawa, Y., Tanaka, M., Minami, S., Umesaki, N., Takeuchi, M., et al. (2004) 'Binding of ovarian cancer antigen CA125/MUC16 to mesothelin mediates cell adhesion', *Journal of Biological Chemistry*, vol. 279, no. 10, pp. 9190-9198.

Sato, N., Fukushima, N., Maitra, A., Iacobuzio-Donahue, C.A., van Heek, N.T., Cameron, J.L., et al. (2004) 'Gene expression profiling identifies genes associated with invasive intraductal papillary mucinous neoplasms of the pancreas', American Journal of Pathology, vol. 164, no. 3, pp. 903-914.

Sanders, M.E., Schuyler, P.A., Dupont, W.D. & Page, D.L. (2005) 'The natural history of low-grade ductal carcinoma in situ of the breast in women treated by biopsy only revealed over 30 years of long-term follow-up', Cancer, vol. 103, no. 12, pp. 2481-2484.

Sappino, A.P., Skalli, O., Jackson, B., Schurch, W. & Gabbiani, G. (1988) 'Smooth-muscle differentiation in stromal cells of malignant and non-malignant breast tissues', *International Journal of Cancer*, vol. 41, no. 5, pp. 707-712.

Savill, J., Dransfield, I., Gregory, C. & Haslett, C. (2002) 'A blast from the past: Clearance of apoptotic cells regulates immune responses', *Nature Reviews Immunology*, vol. 2, no. 12, pp. 965-975.

Schmid, M.C., Avraamides, C.J., Dippold, H.C., Franco, I., Foubert, P., Ellies, L.G., et al. (2011) 'Receptor tyrosine kinases and TLR/IL1Rs unexpectedly activate myeloid cell PI3kgamma, a single convergent point promoting tumor inflammation and progression', *Cancer Cell*, vol. 19, no. 6, pp. 715-727.

Schmid, M.C., Franco, I., Kang, S.W., Hirsch, E., Quilliam, L.A. & Varner, J.A. (2013) 'PI3-kinase γ promotes Rap1a-mediated activation of myeloid cell integrin α4β1, leading to tumor inflammation and growth', *PloS one*, vol. 8, no. 4, p. e60226.

Schmittgen, T.D. & Livak, K.J. (2008) 'Analyzing real-time PCR data by the comparative C-T method', *Nature Protocols*, vol. 3, no. 6, pp. 1101-1108.

Schneider, B.P., Winer, E.P., Foulkes, W.D., Garber, J., Perou, C.M., Richardson, A., et al. (2008) 'Triple-negative breast cancer: risk factors to potential targets', *Clin Cancer Res*, vol. 14, no. 24, pp. 8010-8018.

Segara, D., Biankin, A.V., Kench, J.G., Langusch, C.C., Dawson, L.C., Skalicky, D.A., et al. (2005) 'Expression of HOXB2, a retinoic acid signaling target in pancreatic cancer and pancreatic intraepithelial neoplasia', Clinical Cancer Research, vol. 11, no. 9, pp. 3587-3596.

Sharon, E., Zhang, J.L., Hollevoet, K., Steinberg, S.M., Pastan, I., Onda, M., et al. (2012) 'Serum mesothelin and megakaryocyte potentiating factor in pancreatic and biliary cancers', Clinical Chemistry and Laboratory Medicine, vol. 50, no. 4, pp. 721-725.

Shee, K., Yang, W., Hinds, J.W., Hampsch, R.A., Varn, F.S., Traphagen, N.A., et al. (2018) 'Therapeutically targeting tumor microenvironment–mediated drug resistance in estrogen receptor–positive breast cancer', *Journal of Experimental Medicine*, vol. 215, no. 3, pp. 895-910.

Sherman, M.H., Yu, R.T., Engle, D.D., Ding, N., Atkins, A.R., Tiriac, H., et al. (2014) 'Vitamin d receptor-mediated stromal reprogramming suppresses pancreatitis and enhances pancreatic cancer therapy', *Cell*, vol. 159, no. 1, pp. 80-93.

Shi, C., Hruban, R.H. & Klein, A.P. (2009) 'Familial Pancreatic Cancer', *Archives of Pathology & Laboratory Medicine*, vol. 133, no. 3, pp. 365-374.

Shi, C. & Pamer, E.G. (2011) 'Monocyte recruitment during infection and inflammation', *Nature Reviews Immunology*, vol. 11, no. 11, pp. 762-774.

Shintani, Y., Fujiwara, A., Kimura, T., Kawamura, T., Funaki, S., Minami, M., et al. (2016) 'IL-6 Secreted from Cancer-Associated Fibroblasts Mediates Chemoresistance in NSCLC by Increasing Epithelial-Mesenchymal Transition Signaling', *Journal of Thoracic Oncology*, vol. 11, no. 9, pp. 1482-1492.

Shree, T., Olson, O.C., Elie, B.T., Kester, J.C., Garfall, A.L., Simpson, K., et al. (2011) 'Macrophages and cathepsin proteases blunt chemotherapeutic response in breast cancer', *Genes & Development*, vol. 25, no. 23, pp. 2465-2479.

Siegel, R.L., Miller, K.D. & Jemal, A. (2017) 'Cancer Statistics, 2017', *CA: A Cancer Journal for Clinicians*, vol. 67, no. 1, pp. 7-30.

Sindrilaru, A., Peters, T., Wieschalka, S., Baican, C., Baican, A., Peter, H., et al. (2011) 'An unrestrained proinflammatory M1 macrophage population induced by iron impairs wound healing in humans and mice', *Journal of Clinical Investigation*, vol. 121, no. 3, pp. 985-997.

Singh, N., Das, P., Gupta, S., Sachdev, V., Srivasatava, S., Gupta, S.D., et al. (2014) 'Plasma cathepsin L: A prognostic marker for pancreatic cancer', World Journal of Gastroenterology, vol. 20, no. 46, pp. 17532-17540.

Somoracz, A., Tatrai, P., Horvath, G., Kiss, A., Kupcsulik, P., Kovalszky, I. & Schaff, Z. (2010) 'Agrin immunohistochemistry facilitates the determination of primary versus metastatic origin of liver carcinomas', Human Pathology, vol. 41, no. 9, pp. 1310-1319.

Spanheimer, P.M., Cyr, A.R., Liao, J.L., Johlin, F.C., Hoshi, H., Howe, J.R., et al. (2014) 'Complications and survival associated with operative procedures in patients with unresectable pancreatic head adenocarcinoma', *Journal of Surgical Oncology*, vol. 109, no. 7, pp. 697-701.

Standring, S., Ellis, H., Healy, J., Johnson, D., Williams, A., Collins, P., et al. (2005) 'Gray's anatomy: the anatomical basis of clinical practice', *American Journal of Neuroradiology*, vol. 26, no. 10, p. 2703.

Stockmann, C., Doedens, A., Weidemann, A., Zhang, N., Takeda, N., Greenberg, J.I., et al. (2008) ' ', *Nature*, vol. 456, no. 7223, pp. 814-818.

Strutz, F., Okada, H., Lo, C.W., Danoff, T., Carone, R.L., Tomaszewski, J.E., et al. (1995) 'Identification and characterization of a fibroblast marker - FSP1', *Journal of Cell Biology*, vol. 130, no. 2, pp. 393-405.

Sugimoto, H., Mundel, T.M., Kieran, M.W. & Kalluri, R. (2006) 'Identification of fibroblast heterogeneity in the tumor microenvironment', *Cancer Biology & Therapy*, vol. 5, no. 12, pp. 1640-1646.

Tabernero, J., Chawla, S.P., Kindler, H., Reckamp, K., Chiorean, E.G., Azad, N.S., et al.(2015) 'Anticancer activity of the type I insulin-like growth factor receptor antagonist, ganitumab, in combination with the death receptor 5 agonist, conatumumab', *Targeted Oncology*, vol. 10, no. 1, pp. 65-76.

Tampe, B. & Zeisberg, M. (2014) 'Contribution of genetics and epigenetics to progression of kidney fibrosis', *Nephrology Dialysis Transplantation*, vol. 29, pp. 72-79.

Tape, C.J., Ling, S., Dimitriadi, M., McMahon, K.M., Worboys, J.D., Leong, H.S., et al. (2016) 'Oncogenic KRAS Regulates Tumor Cell Signaling via Stromal Reciprocation', *Cell*, vol. 165, no. 4, pp. 910-920.

Tarin, D. & Croft, C.B. (1969) 'Ultrastructural features of wound healing in mouse skin', *Journal of Anatomy*, vol. 105, no. 1, pp. 189-190.

Tchou, J., Wang, L.C., Selven, B., Zhang, H.T., Conejo-Garcia, J., Borghaei, H., et al. (2012) 'Mesothelin, a novel immunotherapy target for triple negative breast cancer', *Breast Cancer Research and Treatment*, vol. 133, no. 2, pp. 799-804.

Thayer, S.P., di Magliano, M.P., Heiser, P.W., Nielsen, C.M., Roberts, D.J., Lauwers, G.Y., et al. (2003) 'Hedgehog is an early and late mediator of pancreatic cancer tumorigenesis', *Nature*, vol. 425, no. 6960, pp. 851-856.

Tian, H., Callahan, C.A., DuPree, K.J., Darbonne, W.C., Ahn, C.P., Scales, S.J., et al. (2009) 'Hedgehog signaling is restricted to the stromal compartment during pancreatic carcinogenesis', *Proceedings of the National Academy of Sciences of the United States of America*, vol. 106, no. 11, pp. 4254-4259.

Tomasek, J.J., Gabbiani, G., Hinz, B., Chaponnier, C. & Brown, R.A. (2002) 'Myofibroblasts and mechano-regulation of connective tissue remodelling', *Nature Reviews Molecular Cell Biology*, vol. 3, no. 5, pp. 349-363.

Torres, M.P., Rachagani, S., Souchek, J.J., Mallya, K., Johansson, S.L. & Batra, S.K. (2013) 'Novel Pancreatic Cancer Cell Lines Derived from Genetically Engineered Mouse Models of Spontaneous Pancreatic Adenocarcinoma: Applications in Diagnosis and Therapy', *Plos One*, vol. 8, no. 11, p. e80580.

Turner, M.D., Nedjai, B., Hurst, T. & Pennington, D.J. (2014) 'Cytokines and chemokines: At the crossroads of cell signalling and inflammatory disease', *Biochimica Et Biophysica Acta-Molecular Cell Research*, vol. 1843, no. 11, pp. 2563-2582.

Tyanova, S., Temu, T., Sinitcyn, P., Carlson, A., Hein, M.Y., Geiger, T., Mann, M. & Cox, J. (2016) 'The Perseus computational platform for comprehensive analysis of (prote)omics data', Nature Methods, vol. 13, no. 9, pp. 731-740.

Vainio, H., Kaaks, R. & Bianchini, F. (2002) 'Weight control and physical activity in cancer prevention: international evaluation of the evidence', European journal of cancer prevention: the official journal of the European Cancer Prevention Organisation (ECP), vol. 11, pp. S94-100.

Valsecchi, M.E., McDonald, M., Brody, J.R., Hyslop, T., Freydin, B., Yeo, C.J., et al. (2012) 'Epidermal growth factor receptor and insulinlike growth factor 1 receptor expression predict poor survival in pancreatic ductal adenocarcinoma', *Cancer*, vol. 118, no. 14, pp. 3484-3493.

van de Laar, L., Saelens, W., De Prijck, S., Martens, L., Scott, C.L., Van Isterdael, G., et al. (2016) 'Yolk Sac Macrophages, Fetal Liver, and Adult Monocytes Can Colonize an Empty Niche and Develop into Functional Tissue-Resident Macrophages', *Immunity*, vol. 44, no. 4, pp. 755-768.

Vincent, A., Herman, J., Schulick, R., Hruban, R.H. & Goggins, M. (2011) 'Pancreatic cancer', *Lancet*, vol. 378, no. 9791, pp. 607-620.

Vincent, A.M. & Feldman, E.L. (2002) 'Control of cell survival by IGF signaling pathways', *Growth Hormone & Igf Research*, vol. 12, no. 4, pp. 193-197.

Virchow, R. (1858) Die Cellularpathologie in ihrer Begrundung auf physiologische und pathologische Gewebelehre, Berlin: Verlag von August Hirschwald, length: 478.

Von Hoff, D.D., Ramanathan, R.K., Borad, M.J., Laheru, D.A., Smith, L.S., Wood, T.E., et al. (2011) 'Gemcitabine Plus nab-Paclitaxel Is an Active Regimen in Patients With Advanced Pancreatic Cancer: A Phase I/II Trial', *Journal of Clinical Oncology*, vol. 29, no. 34, pp. 4548-4554.

Wahba, H.A. & El-Hadaad, H.A. (2015) 'Current approaches in treatment of triple-negative breast cancer', *Cancer Biol Med*, vol. 12, no. 2, pp. 106-116.

Wake, K. & Sato, T. (1993) 'Intralobular heterogeneity of perisinusoidal stellate cells in porcine liver', *Cell and Tissue Research*, vol. 273, no. 2, pp. 227-237.

Warburg, O.H. & Dickens, F. (1930) *The metabolism of tumours: investigations from the Kaiser Wilhelm Institute for Biology, Berlin-Dahlem*, London: Constable & Co. Ltd. 40 s. net. British Journal of Surgery, vol 19, pp. 168–168.

Weigelt, B., Peterse, J.L. & van't Veer, L.J. (2005) 'Breast cancer metastasis: Markers and models', *Nature Reviews Cancer*, vol. 5, no. 8, pp. 591-602.

Weinberg, R.A. (1995) The retinoblastoma protein and cell-cycle control, Cell, vol. 81, no. 3, pp. 323-330.

Weizman, N., Krelin, Y., Shabtay-Orbach, A., Amit, M., Binenbaum, Y., Wong, R.J., et al. (2014) 'Macrophages mediate gemcitabine resistance of pancreatic adenocarcinoma by upregulating cytidine deaminase', *Oncogene*, vol. 33, no. 29, pp. 3812-3819.

Wenes, M., Shang, M., Di Matteo, M., Goveia, J., Martin-Perez, R., Serneels, J., et al. (2016) 'Macrophage Metabolism Controls Tumor Blood Vessel Morphogenesis and Metastasis', *Cell Metabolism*, vol. 24, no. 5, pp. 701-715.

Williams, C.B., Yeh, E.S. & Soloff, A.C. (2016) 'Tumor-associated macrophages: unwitting accomplices in breast cancer malignancy', *NPJ Breast Cancer*, vol. 2, p. 15025

Workman, P., Aboagye, E.O., Balkwill, F., Balmain, A., Bruder, G., Chaplin, D.J., et al (2010) 'Guidelines for the welfare and use of animals in cancer research', British Journal of Cancer, vol. 102, no. 11, pp. 1555-1577.

Wyckoff, J.B., Wang, Y., Lin, E.Y., Li, J.F., Goswami, S., Stanley, E.R., et al. (2007) 'Direct visualization of macrophage-assisted tumor cell intravasation in mammary tumors', *Cancer Research*, vol. 67, no. 6, pp. 2649-2656.

Wynn, T.A., Chawla, A. & Pollard, J.W. (2013) 'Macrophage biology in development, homeostasis and disease', *Nature*, vol. 496, no. 7446, pp. 445-455.

Xu, Q.H., Li, P., Chen, X., Zong, L., Jiang, Z.D., Nan, L.G., et al. (2015) 'miR-221/222 induces pancreatic cancer progression through the regulation of matrix metalloproteinases', Oncotarget, vol. 6, no. 16, pp. 14153-14164.

Yachida, S., Jones, S., Bozic, I., Antal, T., Leary, R., Fu, B.J., et al. (2010) 'Distant metastasis occurs late during the genetic evolution of pancreatic cancer', *Nature*, vol. 467, no. 7319, pp. 1114-1117.

Yamaguchi, N., Hattori, K., Oheda, M., Kojima, T., Imai, N. & Ochi, N. (1994) 'A novel cytokine exhibiting mekaryocyte potentiating activity from a human pancreatic tumor-cell line', *Journal of Biological Chemistry*, vol. 269, no. 2, pp. 805-808.

Yamamoto, S., Tomita, Y., Hoshida, Y., Nagano, H., Dono, K., Umeshita, K., et al. (2004) 'Increased expression of valosin-containing protein (p97) is associated with lymph node metastasis and prognosis of pancreatic ductal adenocarcinoma', Annals of Surgical Oncology, vol. 11, no. 2, pp. 165-172.

Yamazaki, K., Takamura, M., Masugi, Y., Mori, T., Du, W.L., Hibi, T.,et al. (2009) 'Adenylate cyclase-associated protein 1 overexpressed in pancreatic cancers is involved in cancer cell motility', Laboratory Investigation, vol. 89, no. 4, pp. 425-432.

Yang, C.X., He, L.Y., He, P.Q., Liu, Y.W., Wang, W.J., He, Y.Q., et al. (2015) 'Increased drug resistance in breast cancer by tumor-associated macrophages through IL-10/STAT3/bcl-2 signaling pathway', *Medical Oncology*, vol. 32, no. 2, p. 352.

Yauch, R.L., Gould, S.E., Scales, S.J., Tang, T., Tian, H., Ahn, C.P., et al. (2008) 'A paracrine requirement for hedgehog signalling in cancer', *Nature*, vol. 455, no. 7211, pp. 406-410.

Yin, Y., Yao, S., Hu, Y., Feng, Y., Li, M., Bian, Z., et al. (2017) 'The Immune-microenvironment Confers Chemoresistance of Colorectal Cancer through Macrophage-Derived IL6', *Clinical Cancer Research*, vol. 23, no. 23, pp. 7375-7387.

Yona, S., Kim, K.W., Wolf, Y., Mildner, A., Varol, D., Breker, M., et al. (2013) 'Fate Mapping Reveals Origins and Dynamics of Monocytes and Tissue Macrophages under Homeostasis', *Immunity*, vol. 38, no. 1, pp. 79-91.

Yu, K.H., Barry, C.G., Austin, D., Busch, C.M., Sangar, V., Rustgi, A.K., et al. (2009) 'Stable Isotope Dilution Multidimensional Liquid Chromatography-Tandem Mass Spectrometry for Pancreatic Cancer Serum Biomarker Discovery', Journal of Proteome Research, vol. 8, no. 3, pp. 1565-1576.

Zeisberg, E.M. & Zeisberg, M. (2013) 'The role of promoter hypermethylation in fibroblast activation and fibrogenesis', *Journal of Pathology*, vol. 229, no. 2, pp. 264-273.

Zervos, E., Agle, S., Freistaedter, A.G., Jones, G.J.B. & Roper, R.L. (2016) 'Murine mesothelin: characterization, expression, and inhibition of tumor growth in a murine model of pancreatic cancer', Journal of Experimental & Clinical Cancer Research, vol. 35, no. 39.

Zha, J.P. & Lackner, M.R. (2010) 'Targeting the Insulin-like Growth Factor Receptor-1R Pathway for Cancer Therapy', *Clinical Cancer Research*, vol. 16, no. 9, pp. 2512-2517.

Zhang, H.F., Xie, C.H., Yue, J., Jiang, Z.Z., Zhou, R.J., Xie, R.F., et al. (2017) 'Cancer-associated fibroblasts mediated chemoresistance by a FOXO1/TGF1 signaling loop in esophageal squamous cell carcinoma', *Molecular Carcinogenesis*, vol. 56, no. 3, pp. 1150-1163.

Zhang, X.H.F., Jin, X., Malladi, S., Zou, Y.L., Wen, Y.H., Brogi, E., et al. (2013) 'Selection of Bone Metastasis Seeds by Mesenchymal Signals in the Primary Tumor Stroma', *Cell*, vol. 154, no. 5, pp. 1060-1073.

Zhang, Y.H., Moerkens, M., Ramaiahgari, S., de Bont, H., Price, L., Meerman, J., et al. (2011a) 'Elevated insulin-like growth factor 1 receptor signaling induces

antiestrogen resistance through the MAPK/ERK and PI3K/Akt signaling routes', *Breast Cancer Research*, vol. 13, no. 3, p. R52.

Zhang, Y.J., Chertov, O., Zhang, J.L., Hassan, R. & Pastan, I. (2011b) 'Cytotoxic Activity of Immunotoxin SS1P Is Modulated by TACE-Dependent Mesothelin Shedding', *Cancer Research*, vol. 71, no. 17, pp. 5915-5922.

Zheng, C., Jia, W., Tang, Y., Zhao, H., Jiang, Y. & Sun, S. (2012) 'Mesothelin regulates growth and apoptosis in pancreatic cancer cells through p53-dependent and -independent signal pathway', Journal of Experimental & Clinical Cancer Research, vol. 31, p. 83.

Zheng, H.C. (2017) 'The molecular mechanisms of chemoresistance in cancers', *Oncotarget*, vol. 8, no. 35, pp. 59950-59964.

Zhu, Y., Herndon, J.M., Sojka, D.K., Kim, K.W., Knolhoff, B.L., Zuo, C., et al. (2017) 'Tissue-Resident Macrophages in Pancreatic Ductal Adenocarcinoma Originate from Embryonic Hematopoiesis and Promote Tumor Progression', *Immunity*, vol. 47, no. 2, pp. 323-338.

Zhu, Y., Knolhoff, B.L., Meyer, M.A., Nywening, T.M., West, B.L., Luo, J.Q., et al. (2014) 'CSF1/CSF1R Blockade Reprograms Tumor-Infiltrating Macrophages and Improves Response to T-cell Checkpoint Immunotherapy in Pancreatic Cancer Models', *Cancer Research*, vol. 74, no. 18, pp. 5057-5069.